Tribological Investigation of Articular Cartilage Substitution in the Medial Compartmental Knee

Laura McCann BEng (Hons)

Submitted in accordance with the requirements for the degree of

Doctor of Philosophy

The University of Leeds

School of Mechanical Engineering

March 2009

Acknowledgements

The decision to undertake my PhD studies in the University of Leeds was difficult but now as the end draws near, I can see that it was, without a doubt, the right choice. First and foremost, I would like to thank Professor John Fisher, Professor Zhongmin Jin and Professor Eileen Ingham, for offering me the chance to study within the iMBE. The outstanding support and guidance I received from you all has been invaluable and very important for the completion of this work.

I greatly appreciate the help I received from Simon, Jay and Ewen during the initial months of my project, and a special thank you to Jay for leading the cartilage substitution group within the iMBE and for generally being a great source of ideas and advice. Sainath thanks for your help with FE modelling. Manyi, thank you for your help with the MRI studies, particularly the tedious validations! I'd like to thank all of the iMBE laboratory technicians, particularly Phil, Lee and Adrian. Tom and Stacey, my microbiology friends, I'd like to thank you for all the training and help you gave me in Eileen's lab and sorry for the few mishaps (fire alarms etc!).

Thanks to everyone in the iMBE for making my experiences so memorable – sports days, bowling nights, Christmas parties, drinks after work for no particular reason, the lake district...the list goes on! All of these experiences have definitely enhanced my experiences in Leeds, made me laugh, and really enjoy myself!! Not forgetting the great room that is 442c – thanks to everyone that has passed through, for the great camaraderie, the friendly and sometimes lively atmosphere, the jokes and the pranks! I was very sad when Debra moved me next door.

I'd like to thank my friends from Ireland, for the visits, emails and calls! Don't forget, I'm still in Leeds, so you know where to go for your shopping sprees! I'd like to say a special thanks to Nicola, my most frequent visitor, caller and emails everyday! A huge thank you to Mark. You're so great always, but a particular thanks for the last few months during my write up, when I sat in the corner of the living room with my back to you! I'd like to thank my brothers and sister, David, Grainne and Kieran. And a huge, special thank you to Mam and Dad. You're so encouraging of everything we do – we couldn't ask for more love and support.

Abstract

In the development of any cartilage substitution device, an understanding of the tribological response of the natural joint, as well as the treated joint is of upmost importance. Many previous studies have investigated the tribology of potential cartilage substitution therapies, using small scale pin on plate experiments. The aim of the current study was to develop an anatomical and physiological simulation of the medial compartmental bovine knee joint and to use this simulation to investigate a number of cartilage substitution therapies for damaged or diseased knee joints.

A pendulum friction simulator was used to apply physiological loading and motion to medial compartmental knees. The wear of the cartilage was characterised following the experiments using three different techniques: surface topography analysis, volumetric wear quantification using μMRI scans and histological assessment. Three main interventions were investigated using this novel anatomical simulation - the tribological response of meniscectomy, the effect of conformity of tibial hemiarthroplasty designs, and finally, a number of potential cartilage substitution materials were investigated as osteochondral repair devices in the femoral condyle.

In the first two studies, the removal of the meniscus and a decrease of tibial hemiarthroplasty conformity, resulted in an elevation of the coefficient of friction, contact stress, friction shear stress and subsequently the wear and degradation of cartilage. In the defect repair study, biphasic defect repair materials (hydrogels) had a superior tribological performance to non-compliant single phase materials (stainless steel). Across the three studies, the use of non-biphasic materials and/or the loss of joint congruity resulted in a more rapid decrease of cartilage interstitial fluid pressurisation and biphasic fluid load support, resulting in increased cartilage solid-solid contact and increased wear.

This tribological simulation can be used to investigate many potential knee joint intervention, from uni- or hemi-arthroplasty, cartilage defect repair, meniscus substitutes or tissue engineered substitutes. This simulation can be used to further our understanding of the tribological characteristics of more satisfactory and conservative therapies for damaged and diseased synovial joints.

Table of Contents

List of Figures

List of Tables

Abbreviations

AC	Articular cartilage
ACI	Autologous chondrocyte implantation
AFM	Atomic force microscopy
AS	Articular surface
BSAL	Biphasic surface amorphous layer
CD	Collagen disruption
CG	Collagen gaps
CT	Collagen tearing
CMM	Coordinate measuring machine
CoC	Ceramic-on-ceramic
COD	Composite osteochondral device
C-SEM	Cryo-scanning electron microscopy
DTI	Diffusion tensor imaging
ECM	Extracellular matrix
EHL	Elasto-hydrodynamic lubrication
ESEM	Environmental scanning electron microscopy
FA	Fractional anisotropy
FCD	Fixed charge density
FSS	Friction shear stress
GAG	Glycosaminoglycan
HA	Hyaluronic acid
H&E	Haemotoxylin and Eosin
Hgel	Hydrogel

LCS	Low Contact Stress (DePuy knee design)
LPG-1	Lubricating glycoprotein
LVDT	Linear variable differential transformer
MRI	Magnetic resonance imaging
μCT	Micro computed topography
μMRI	Micro magnetic resonance imaging
MSME	Multi spin multi echo
NBF	Neutral buffered formalin
NMR	Nuclear magnetic resonance
OA	Osteoarthritis
OC	Osteochondral
PBS	Phosphate buffered saline
PL	Peak load
PMMA	Polymethyl-methacrylate
PoP	Pin-on-plate
PU	Polyurethane
PVA	Poly(vinyl alchohol)
Ra	Arithmetic mean of absolute departures of roughness profile from the mean line
SAL	Surface amorphous layer
SDS	Sodium dodecyl sulphate
SEM	Scanning electron microscopy
SoD	Sphere-on-disc
SS	Stainless steel
STZ	Superficial tangential zone

TE	Echo time
TEM	Transmission electron microscopy
TKA	Total knee arthroplasty
TR	Relaxation time
UKA	Unicompartmental knee arthroplasty
WLI	White light interferometry

Nomenclature

z	Sommerfeld number
η	viscosity
u	entraining velocity
R_1	radius
W	applied load
f	friction factor
FSS	friction shear stress
F_F	friction force
A	contact area
T	frictional torque
μ	coefficient of friction
σ	contact stress
Ha	aggregate modulus
k	permeability
R_x	radius in x-direction
d	cartilage thickness
E_{eq}	Combined elastic modulus
h	film thickness

Chapter 1. Introduction and Literary Review

"Cartilages are spread on some parts of bones, such as the joints, to make them smooth, and Nature also uses cartilages occasionally as moderately yielding bodies... Cartilage serves as a grease for the joints....Nature has again searched out a double remedy, first covering each member of the joint with cartilage and then pouring over the cartilages themselves a sort of oily substance, a greasy, glutinous fluid, which gives every joint an easy movement and protection against wear." This is the first documented description of articular cartilage, described by Galen in 175 AD (Benedek, 2006). Perhaps it was also the first documentation of synovial joint tribology, although Galen himself may not have been aware.

Throughout the centuries many anatomists and physicians documented the presence and function of articular cartilage, many of which are reported in Benedek's review of the historical development of the understanding of articular cartilage (Benedek, 2006). In this paper Benedek described the work of William Hunter, an anatomist and surgeon from London who discussed the anatomy and pathology of articular cartilage, a study considered to be the first scientific study of cartilage. Since then the scientific understanding of the lubrication mechanisms in natural joints has been investigated extensively. Many different treatment options have been developed for degenerated joints, from non-invasive interventions, to minimally invasive surgery, to total joint replacement. However, studies to gain a more in-depth understanding of cartilage tribology and synovial joint lubrication continues, as well as the mission to increase patient comfort and satisfaction by increasing the efficacy and longevity of current and future treatments.

The development of effective cartilage substitution therapies not only requires the quantification of wear and tribological performance of the implant but also that of the surrounding and opposing cartilage surfaces. Of upmost importance in the development of cartilage substitution therapies, is an in-depth understanding of the tribological properties of the natural synovial joint as well as joints treated by hemiarthroplasty or cartilage substitution therapies. The aim of this study is to create a tribological simulation of the medial compartment of the natural bovine knee, in order to examine the friction and wear properties of natural and treated (meniscectomy, hemiarthroplasty and cartilage substitution) joints.

1.1 Synovial Joints

The joints of the human body can be classified into three groups: fibrous, cartilaginous and synovial. Fibrous joints (synarthroses) are those in which the bony surfaces have very little relative motion, the bones in the skull being the prime example. Cartilaginous joints are those in which the bony surfaces have a little more relative motion such as the joint between two adjacent vertebrae (facet joints). The third type are synovial (or diarthrodial) joints, for example the knee joint, which is the joint of interest in this research.

1.1.1 Geometry and Structure of the Knee Joint

The bones forming the knee joint are the condyles of the femur, the head of the tibia and the patella anteriorly. The bearing surfaces are covered with articular cartilage, lined by synovial membrane and connected together by ligaments, some of which are present on the exterior of the joint, while others occupy the interior of the joint.

The human knee joint is not a simple hinge. When the individual stands upright, the rounded cartilage ends of the femur, called the condyles, roll to make contact with the flattened tibia. The menisci fit comfortably between the two bones ensuring smooth movement between what would otherwise be two very incongruous surfaces, so the condyles articulate with both the flattened top of the tibial plateau and the menisci as shown in Figure 1-1a. As the knee flexes, the rounded condyles roll anteriorly along the tibial plateau and menisci. A knee in flexion is shown in Figure 1-1b, where the shiny cartilage surfaces of the two rounded condyles are more visible, as well as the notch between them.

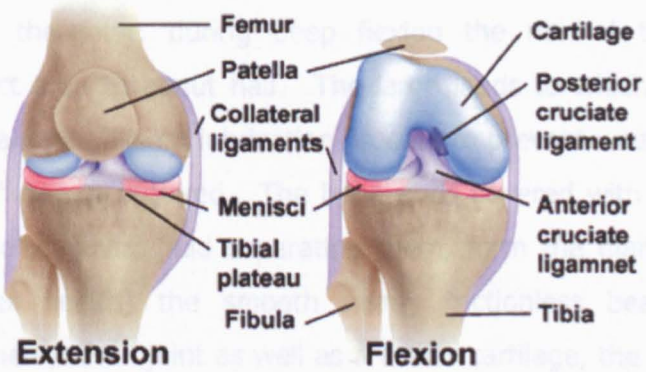

Figure 1-1: The anatomy of the knee (a) in extension and (b) in flexion. Image taken from http://www.yoursurgery.com/ProcedureDetails.cfm?BR=5&Proc=30

1.1.2 Loading and Motion in the Knee

The knee joint is subject to large mechanical loads during daily activity caused by a number of mechanical factors. It has a large range of motion and it is located below the centre of gravity of the body which results in large loads acting through the joint. Coupled with this, it is not a highly conforming joint which means loads are distributed over relatively small areas and stresses can be large. However, this very complex joint has anatomical features, mainly the menisci discussed in Section 1.3, which help to distribute the loads, increase stability and aid in the lubrication of the joint.

The knee is a superficial joint which allows for a large range of flexion, a fact which increases its vulnerability to injury and trauma. During daily movements a large range of flexion is required at the knee. For level walking, flexion of about 70° is required, to stand from a chair, flexion of about 100° and for a very low chair or stool this increases to 120°. Greater degrees of flexion are required for more strenuous activities such as squatting or kneeling (Dowson and Wright, 1981). This large range of motion required of the knee is the reason for its non-conforming surfaces.

Deep knee flexion imposes large loads on the knee joint. In a study by Nagura *et al.*, four deep flexion movements were analysed: double leg rise (starts from deep kneeling position, then lifting knees to squat position and then standing using both legs); double leg descend (the reverse of double leg rise); single leg rise (using one leg only) and single leg descend (the reverse of single leg rise). It was shown that the knee joint experienced maximum flexion moments and loads during deep flexion activities (Figure 1-2), in comparison to walking or stair-climbing (Nagura *et al.*, 2001).

Large loads in deep flexion may affect some articular injuries if the loads are applied very frequently to the joint; during deep flexion the normal tibio-femoral joint decreases its contact area to about half. The large loads to which the knee joint is subject, mean that a very efficient lubrication process to prevent wear and degradation of the cartilage surfaces, is required. The bone ends covered with articular cartilage and the thin layer of synovial fluid separating them, form the diarthrodial joint that provides (in normal health) the smooth nearly frictionless bearing mechanism. Synovial fluid and the synovial joint as well as articular cartilage, the main focus of this thesis, will be discussed in more detail in subsequently.

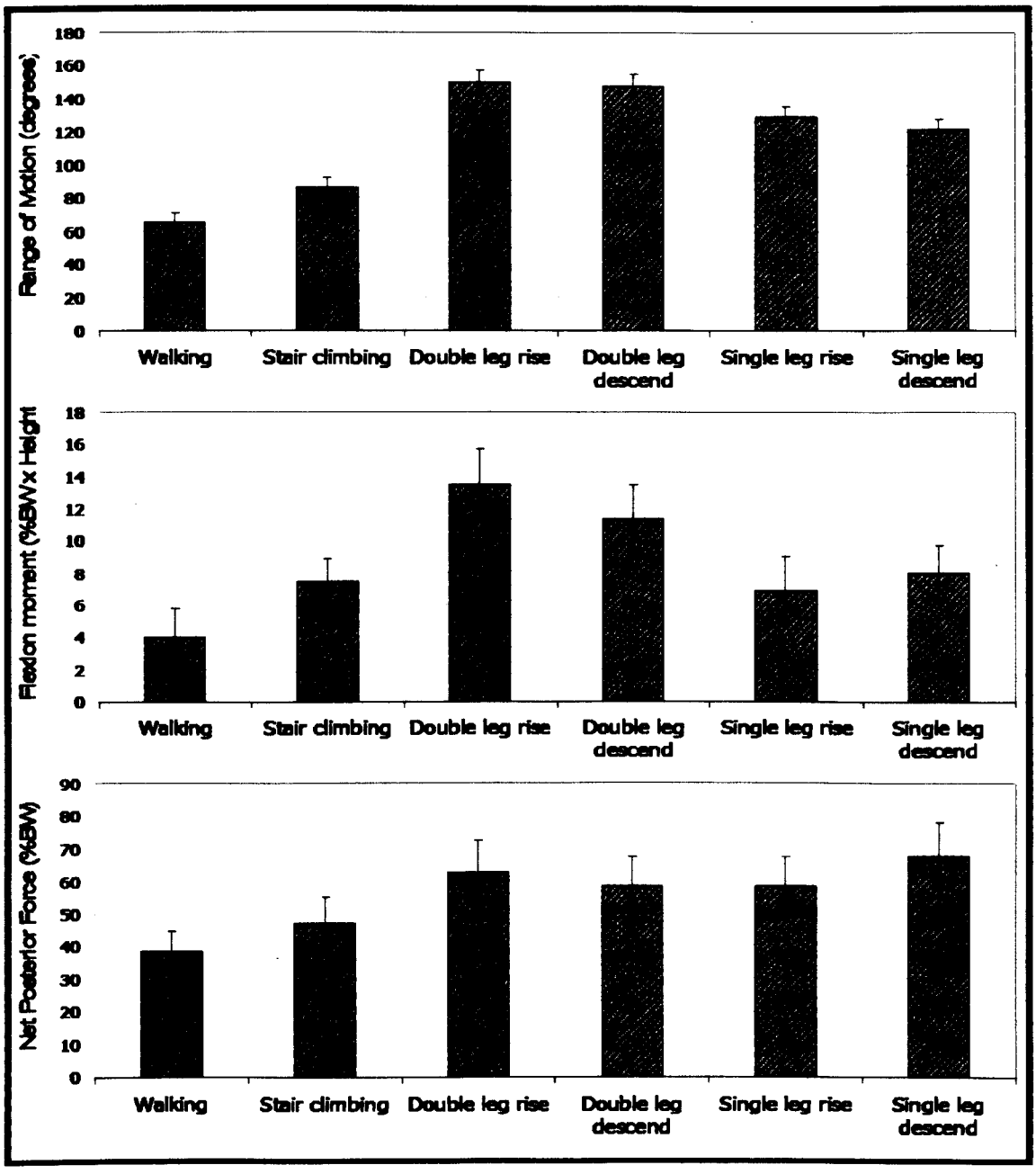

Figure 1-2: Knee kinematics and kinetics during normal daily activities. Activities include walking, stair climbing, double leg rise, double leg descend, single leg rise and single leg descend (Mean ± SD). Adapted from Nagura et al. (2001).

1.1.3 Synovial Fluid and the Synovial Joint

Synovial joints allow a large degree of relative motion between contacting bones, while minimising the inevitable penalties of friction and wear as a result of load carriage. A high level of lubrication is offered in which sliding friction coefficients can be as low as 0.005 (Stachowiak *et al.*, 1994). A strong fibrous capsule surrounds the joint. The inner surfaces of the joint capsules are lined with a metabolically active tissue, the synovium,

which secretes synovial fluid and the nutrients required by the tissues of the joint (Figure 1-3).

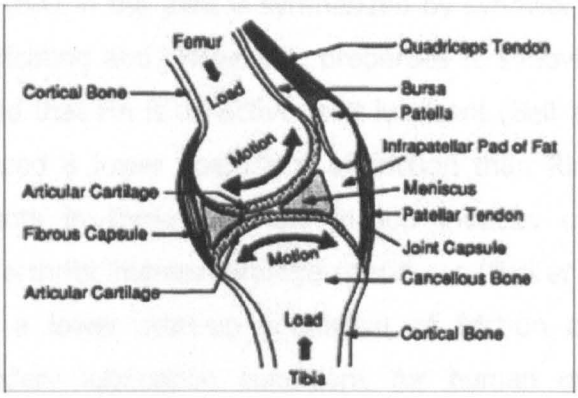

Figure 1-3: Schematic representation of the knee joint. The image shows the important anatomic features for mechanical functioning, including the joint capsule which contains synovial fluid (Mow *et al.*, 2005).

The synovium is also responsible for the absorption of the metabolic waste products of cellular activities from intra-articular tissues. The bone ends of diarthrodial joints are lined with articular cartilage. These two linings, the synovium and the articular cartilage, form the joint cavity that contains the synovial fluid. The synovial fluid, articular cartilage and bone form the most spectacular wear resistant bearing system of the body (Mow *et al.*, 2005). Tendons and ligaments play a vital role in providing joint stability, guiding the position of the bones during motion and transmitting muscle forces.

Synovial fluid shows non-Newtonian flow properties including an elastic effect, a shear thinning effect and a normal stress effect. These flow properties are similar to those evident in other bio-macromolecular solutions such as solutions of proteoglycans. For example, in the knee joint the apparent viscosity of synovial fluid has been shown to decrease nonlinearly from 10 to 0.02 N-sec/ m^2 as the shear rate increases from 0.1 to 1000s^{-1} (Ateshian and Mow, 2005). Synovial fluid is a clear or a yellowish fluid which comprises of a dialysate of blood plasma without clotting factors, blood cells or haemoglobin. It contains hyaluronate, (an extended glycosaminoglycan (GAG) chain), lubricating glycoproteins and wear retarding phospholipids (Ateshian and Mow, 2005). These synovial fluid constituents have been the subject of much debate over the past few decades, with respect to identifying the primary component of synovial fluid responsible for boundary lubrication. The following sections describe the various components that make up synovial fluid which are proposed as boundary lubricants.

Hyaluronic Acid (HA)

The flow properties of synovial fluid are believed to be related to the HA content of the fluid. Hyaluronic acid (HA) in the joint is synthesized by synoviocytes (Mazzucco *et al.*, 2004). It endows lubricating and viscoelastic properties to synovial fluid. Many *in vitro* studies have confirmed that HA is an active joint lubricant (Bell *et al.*, 2006; Forsey *et al.*, 2006). HA produced a lower coefficient of friction than Ringer's solution, when compared as lubricants in three different friction models, using healthy bovine, damaged bovine and arthritic human cartilage specimens (Bell *et al.*, 2006). In another study, HA produced a lower start-up coefficient of friction compared to Ringer's solution under boundary lubrication conditions for human osteoarthritic cartilage (Forsey *et al.*, 2006).

Lubricin

Some studies in the 1970's and 1980's examined a glycoprotein isolated from bovine and human synovial fluid, which they found to provide boundary lubrication properties (Radin *et al.*, 1970; Swann *et al.*, 1984; Swann *et al.*, 1985). This synovial fluid constituent was called lubricating glycoprotein (LGP-I), or as it's more commonly known, lubricin. In the study by Radin *et al.* hyaluronate was separated from synovial fluid using centrifugation techniques. Using the same technique protein was separated. Friction testing of bovine metatarsal-phalangeal joints, comparing normal synovial fluid as the lubricant with and three test lubricants: one containing no hyaluronate; a second containing all the hyaluronate from the original synovial fluid; and a third contained most of the protein present in the original synovial fluid and was hyaluronate free. Buffer was used as the positive control lubricant. The first two test lubricants showed improvement in friction coefficients over buffer, however using the third test lubricant had the same levels of coefficient of friction were achieved as when using whole synovial fluid. This indicated that the active boundary lubricant was a protein or glycoprotein (Radin *et al.*, 1970). Swann *et al.* investigated the lubricating properties of two lubricin preparations of different concentration (65 μg/ml and 100 μg/ml), in a rotating cartilage on glass friction apparatus. Normal synovial fluid and Veronal buffer were used as the positive and negative controls, respectively. The 100mg/ml lubricin preparation showed equivalent frictional responses to the whole synovial fluid. However, at the lower concentration, and in particular at lower speeds, the friction values increased.

Surface-active Phospholipids

The phospholipid content of synovial fluid has led to the idea that synovial fluid could be the transport mechanism for phospholipids between the synovium and articulating joint surfaces (Hills and Butler, 1984; Kobayashi *et al.*, 1995; Kobayashi *et al.*, 1996; Hills and Crawford, 2003). Hills and Butler argued that the methods used by Swann *et al.* to extract lubricin, were unlikely to have excluded phospholipids as contaminants in their lubricin. Hills and Butler demonstrated that phospholipids were readily adsorbed to hydrophilic solids whose surfaces then became hydrophobic and concluded that if these phospholipids (surfactants) had the potential act as boundary lubricants, if they could be adsorbed to cartilage surfaces *in vivo*, in the same manner that they were adsorbed during the *in vitro* experiment. In another study, Schwarz and Hills, isolated lubricin from bovine synovial fluid following the original procedure of Swann *et al.* (Swann *et al.*, 1981). Following analysis of the lipid extract by thin-layer chromatography as well as phosphorous quantification, it was demonstrated that a phospholipid component of 11.1% was present in lubricin. Schwarz and Hills concluded that lubricin was indeed an active constituent of synovial fluid, but that because it is a large water-soluble molecule, it functions as a carrier for the very insoluble surface-active phospholipids and that it is the phospholipids which lubricate, rather than the lubricin (Schwarz and Hills, 1998).

Chondroitin Sulphate

Chondroitin Sulphate is a glycosaminoglycan present in small quantities (in the μg/ml) in synovial fluid which may have boundary lubricating abilities, however, to date it has received little attention in comparison to the other constituents of synovial fluid. Katta *et al.* has demonstrated that when used as a lubricant, chondroitin sulphate produced a lower coefficient of friction than PBS, in a cartilage pin on cartilage plate, *in vitro* experiment (Katta *et al.*, 2008a). However, more *in vitro* studies are required, under different tribological conditions and with normal and degenerative cartilage, to determine the potential of chondroitin sulphate as a lubricant

Summary

The aforementioned studies suggest that all the components of synovial fluid may have some role to play as boundary lubricants, and it is not possible to identify one single synovial fluid constituent, as the lubricant responsible for boundary lubrication in synovial joints. The combined effect of all of these constituents working together may well be the reason synovial fluid is such an ideal joint lubricant.

1.2 Articular Cartilage

Articular cartilage and meniscus are vital to the function of healthy knee joints and they are both involved in joint degeneration leading to the well-known disease called osteoarthritis (OA). They can withstand very large loads while providing smooth, lubricating bearing materials with minimal friction and wear. Articular cartilage can be described as a multiphasic material. It comprises of two major phases: a fluid phase containing water and dissolved electrolytes and a solid phase composed of collagen, proteoglycans, other proteins, glycoproteins and chondrocytes. The third phase, which is important in the understanding of cartilage swelling is the dissolved electrolytes within the interstitial fluid. The solid phase is also charged. Each phase plays a role in the mechanical and physiochemical functions. The main components of cartilage in each of the two major phases and their percentage wet weight are shown in Table 1-1.

Phase	Components	% Wet Weight
Solid Phase	Collagen	10%-20%
	Proteoglycans	5%-10%
	Chondrocytes	<10% of tissue volume
Fluid Phase	Water	60%-85%
	Inorganic salts; proteins	Very small quantities

Table 1-1: Percentage weight of components of articular cartilage (Mow *et al.*, 2005).

Many models have been developed in an attempt to describe the behaviour of cartilage. In the early days the tissue was assumed to be isotropic and linearly elastic. Although these models can describe the mechanical behaviour of soft hydrated tissue under static or equilibrium conditions they lack the ability to demonstrate the time-dependent creep and stress-relaxation behaviours (Sokoloff, 1969; Lipiello *et al.*, 1985). Following these earlier models, a variety of viscoelastic models were introduced in an attempt to describe the creep and stress-relaxation behaviours. These models were limited in that they had some difficulty in representing the effects of interstitial fluid flow (Hayes and Mockros, 1971).

The most successful models to date are those developed by Mow and his colleagues. Named by Mow, the biphasic theory models the cartilage tissue as a composite material consisting of two intrinsically incompressible phases: a solid phase and a fluid phase which are separate and immiscible (Mow *et al.*, 1984a). The biphasic theory was later developed into a triphasic theory (Lai *et al.*, 1989a; Lai *et al.*, 1989b) which takes into consideration a third phase, an ionic phase, which generates an osmotic pressure effect, ion transport through the tissue and other streaming potential and electro-kinetic effects. These theories will be discussed in more detail subsequently.

1.2.1 Cartilage Macrostructure

The extracellular matrix (ECM) of cartilage is a fibre-reinforced composite solid consisting of a dense stable network of collagen II fibres embedded in a very high concentration of proteoglycan gel, which itself is also a viscoelastic network. The composition and structure of articular cartilage are inhomogeneous within the tissue and vary with depth (Mow *et al.*, 2005). The density of collagen, proteoglycans and water also vary with depth. In the superficial tangential zone (STZ), which makes up 10%-20% of the total thickness, there is the highest content of water (75%-85%) and the highest content of collagen (85% dry weight) and the collagen is orientated parallel to the surface. The concentration of proteoglycans in this layer is low in comparison to deeper layers (Figure 1-4).

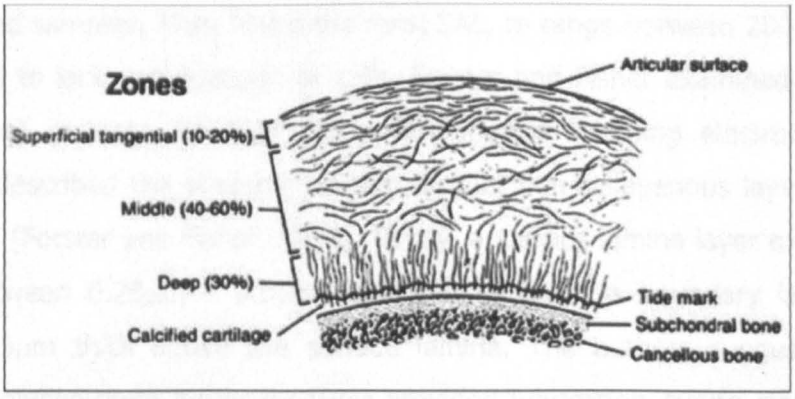

Figure 1-4: Layered structure of articular cartilage showing three distinct regions (Mow *et al.*, 1990).

The middle zone represents 40%-60% of the total thickness. In this zone, the collagen content decreases compared to the STZ and is more randomly orientated. The proteoglycan content is at a maximum in the middle zone and the water content decreases with depth. Finally, the deep zone comprises about 30% of the total thickness. In this layer, the collagen density is fairly consistent with the middle zone

but fibres appear to be woven together forming large bundles, which insert into the calcified cartilage and subchondral bone, thus securely attaching the uncalcified tissue to the bone (Mow *et al.*, 2005).

1.2.2 The Surface Amorphous Layer (SAL)

Evidence has been presented in the past describing the presence of a soft, amorphous layer, which covers the surface of healthy articular cartilage surfaces (Kobayashi *et al.*, 1995; Jurvelin *et al.*, 1996; Kobayashi *et al.*, 1996; Sasada, 2000; Sawae *et al.*, 2000). This thin layer appears directly from the STZ but is void of any collagen and contains glycosaminoglycans/glycoproteins. It is believed to enhance fluid/gel film between the articulating surfaces in a loaded joint, contributing to the exceptional lubrication and also to protect the underlying collagen from direct contact and interfacial wear.

Recent advances in microscopic techniques have allowed in-depth investigation of the presence of this layer and its role in load bearing and lubrication. Koyabashi *et al.* examined cartilage from porcine medial tibial plateaus (portion beneath meniscus), using cryo-scanning electron microscopy (C-SEM) and found this SAL to range between 2μm-200μm (Kobayashi *et al.*, 1995). Jurvelin *et al.* used atomic force microscopy (AFM) to image the 3-D surface and sub-surface morphology of fresh bovine humeral head cartilage, maintained in phosphate buffered solution (PBS) (Jurvelin *et al.*, 1996). Ultrastructural data was obtained using transmission electron microscopy (TEM) of cryo-processed samples. They found the most SAL, to range between 200nm-500nm in thickness and to lack any collagen or cells. Forster and Fisher examined bovine distal femoral (knee) cartilage by TEM and environmental scanning electron microscopy (ESEM) and described the presence of two distinct non-collagenous layers, extending from the STZ (Forster and Fisher, 1999). Firstly, a surface lamina layer extending from the STZ, between 0.25μm – 0.5μm thick and secondly a boundary layer between 0.03μm – 0.5μm thick above the surface lamina. The authors suggested that the phospholipid/glycoprotein boundary layer provided lubrication during close contact of the articulating cartilage surfaces, the surface lamina prevented fibrillation of the collagen fibres beneath and that both layers may contribute to the time dependency of the frictional response of cartilage. Kumar *et al.* found that the thickness of SAL in porcine patella ranged between 800nm – 2μm, when examining the tissue using AFM (Kumar *et al.*, 2001).

While all of the aforementioned studies confirm the presence of a fourth SAL extending from the STZ, there is some variation between the studies, in the reported thickness of this layer. This can probably be attributed to the different species and different cartilaginous regions examined.

Since the confirmation that the SAL exists, some studies have investigated its function. Krishnan investigated the role of the SAL in regulating the frictional response of articular cartilage (Krishnan *et al.*, 2004a). They carried out unconfined compression tests with sliding of cartilage (plugs from bovine shoulder) against glass in PBS. Friction tests were carried out before and after removal of a layer approximately 100μm in thickness from the surface and two levels of applied load were used (4.4N and 22.2N). It was found that there was no change in minimum friction coefficient before and after removal of this layer, at either level of loading but long-term friction coefficient decreased dramatically upon removal. They concluded that the SAL produces no significant change in the minimum friction coefficient, which is achieved immediately after loading. A second test was carried out in which the cartilage surface was removed as far as the deep zone, which further decreased the friction coefficients by 60% when tested under the same conditions. The authors did not propose any explanation for their findings. However, the issue of whether SAL plays a role in reducing wear at the articular surface was never addressed, nor was the potential interaction between the SAL and synovial fluid. In the second part of the study in which they removed cartilage as far as the deep layer, they failed to investigate the likely effects of matrix component concentration, such as glycosaminoglycans (GAGs) on decreasing the frictional coefficient, which are known to increase in content towards the deep zone.

Kumar and colleagues found the non-fibrous surface layer to be resistant to digestion by hyaluronidase, partially digested with chondroitinase ABC (protease free) and completely digested by alkaline protease, which suggests that the layer is either glycoprotein and/or protein in composition (Kumar *et al.*, 2001). High frictional coefficients were found for cartilage samples digested with chondroitinase ABC, which was attributed to loss of some lubrication activity at the surface, most probably the GAG activity. In boundary lubrication hyaluronic acid and some proteins are known to be important. In this study, at a low sliding speed of 1mm/s the coefficient of friction was low between pyrex and untreated cartilage, as well as between hyaluronidase

digested specimens, suggesting that the surface layer of cartilage is probably composed of absorbed molecules forming a gel film on the articulating surface.

In a finite element study Graindorge *et al.* modelled the effect of a thin, soft, biphasic surface amorphous layer (BSAL) on the frictional response of articular cartilage in unconfined compression, particularly focusing on the implications for joint lubrication (Graindorge *et al.*, 2005). The response of the BSAL was investigated during compression and stress-relaxation. The SAL was modelled as a biphasic tissue similar to the bulk cartilage. The results of the study indicated that the BSAL significantly altered the load carriage of the underlying cartilage, reducing friction and improving lubrication. Graindorge *et al.* suggested that such a surface layer may not only play an important role in the lubrication, but also in protecting the underlying cartilage, particularly during sudden impact loads and other transient motions.

In another study by Graindorge *et al.* the effect of the SAL-deprived cartilage (10% sodium dodecyl sulphate (SDS) in water was used to remove SAL) on the friction properties in a cartilage-on-cartilage pin on plate configuration was investigated, in comparison to healthy cartilage (Graindorge *et al.*, 2006). Morphology characterisation techniques used were ESEM, TEM, white light interferometry (WLI) and biochemical analysis. SAL-deprived cartilage was found to be significantly rougher than healthy cartilage. However, there was no difference found in the static or dynamic frictional coefficients between the healthy and SAL-deprived samples, indicating that there was some replenishment of the SAL during loading. Considering potential mechanisms for SAL replenishment, Graindorge highlighted that as the test configuration did not contain any mechanism of biochemical activation, since the cells were not kept viable, SAL replenishment must have resulted from the motion and loading between the cartilage pin and plate surfaces and the resultant hydraulic pressures generated within the cartilage. Referring back to Krishnan's work mentioned above, a similar mechanism may account for why there was no increase in frictional coefficient after manually removing the uppermost 100μm of the STZ. In other words, this SAL replenishment may not be confined to the articular surface. Upon qualitative biochemical analysis of the deliberately regenerated SAL, it was found that it contained high levels of sulphated GAGs however proteins were not detected. Another explanation was that these sulphated GAGs could have been derived from the break up of the larger proteoglycan molecules near the surface, due to the induced surface damage during loading.

Although, the composition and functional properties of the SAL are not completely understood, the aforementioned studies show that the SAL plays an important role in the lubrication between cartilage surfaces by possibly having the capability to transfer applied loads to the fluid phase, reducing the frictional coefficient at contact zones.

1.2.3 Cartilage Microstructure

In the following Sections the main constituents of the fluid and solid phases of cartilage will be discussed: water, collagen, proteoglycans and chondrocytes. It must be noted however, that other quantitatively minor components exist, including hyaluronan, smaller proteoglycans and cartilage matrix proteins. Although these are not major components in terms of mass, some of them may serve important biological regulatory functions, which may not yet have been accounted for.

Interstitial Water

Water is the most abundant component of articular cartilage. Water distribution varies, making up 65% of wet weight at the deep zone and 80% at the surface. Water exists in two compartments within the cartilage: intrafibrillar (within the collagen fibres) and extrafibrillar. Approximately 30% of the total water resides within the intrafibrillar spaces of collagen. The amount of water within the intrafibrillar compartment is modulated by the swelling pressure of the "fixed charge density" (FCD) of the surrounding proteoglycans. It is thought that most of this intrafibrillar water is not available for transport under mechanical loading. This exclusion effectively raises the density of the fixed charges within the tissue, thus raising the interstitial osmotic pressure and the charge-charge repulsion. On the other hand, there is a significant increase of water content in degenerating articular cartilages (Mow and Hayes, 1997). This is due to disruption of the collagen network, which allows additional swelling and water uptake. This process of additional water uptake is known as hyperhydration.

Most of the water in cartilage is loosely bound in the form of a proteoglycan-collagen gel and is freely exchangeable with synovial fluid. This extrafibrillar water may be moved freely throughout the tissue under the action of hydraulic and osmotic pressure gradients and mechanical consolidation of the solid matrix. This water allows the cartilage to deform by moving in and out in response to stress applied on the surface. The amount of interstitial fluid within the tissue is regulated by a number of factors: the concentration of proteoglycans; the collagen organisation and the ability of the collagen network to resist proteoglycan swelling (Mow *et al.*, 2005). The collagen

fibres form a fine network which traps large proteoglycan aggregates within the interfibrillar space. This composite forms a fibre-reinforced solid matrix, which has been shown to be porous and permeable (Gu *et al.*, 1993). When a load is applied to cartilage, the fluid is responsible for up to 90% of initial load-bearing and over time, when the fluid is exuded out, the load is transferred on to the solid phase. The viscous drag forces generated during this exudation of fluid through the pores of the ECM, provide a mechanism for energy dissipation (Mow *et al.*, 1980). This mechanism results in lower levels of stress on the solid matrix.

Water content has been shown to increase by approximately 9% in osteoarthritic joints due to disruption of the collagen network (Mankin and Thrasher, 1975). This increase in water content results in an increase in the permeability of the tissue and a reduction in strength.

Collagen

The ECM of cartilage is a fibre-reinforced composite solid consisting of a dense stable network of collagen fibres embedded in a very high concentration of proteoglycan gel. Articular cartilage is mainly composed of collagen type II, with smaller amounts of Type V, VI, IX and XI. Tropocollagen is the basic structural unit of collagen II and it is composed of three $\alpha 1$ polypeptide chains, coiled into left-handed helices, which are further coiled into right-handed triple helices. These molecules further polymerise into larger collagen fibrils, which range from 10-300nm in diameter. Intermolecular and intramolecular covalent crosslinks are present between the polypeptide chains, which result in a strong collagen network. These bonds contribute to the capability of collagen to resist the swelling pressure caused by the charged proteoglycans present in the ECM as well as stresses induced due to loading in situ (Mow and Hayes, 1997).

As previously described, the collagen content is highest in the superficial zone, where collagen fibres are densely packed and orientated parallel to the surface. Moving through the middle towards the deep zone, the collagen fibres increase in size, become randomly orientated and then perpendicularly orientated in the deep zone, where they are woven into bundles. These bundles cross what is known as the tidemark to insert into the calcified cartilage and subchondral bone, thus firmly anchoring the uncalcified tissue to the bone ends (Mow and Hayes, 1997).

Proteoglycans

The charged nature of the extracellular matrix (ECM) derives from the proteoglycans. These molecules are very large and have very complex molecular organisations. Each proteoglycan monomer is composed of a single protein core, to which are attached numerous glycosaminoglycan (GAG) chains (bottle brush like structures) (Figure 1-5). The dimeric units of these GAGs are usually chondroitin sulfate and keratan sulphate and have sulphate and carboxyl groups. The proteoglycan monomers are noncovalently attached, via a link protein, to a hyaluronate chain, forming a supra-macromolecular structure.

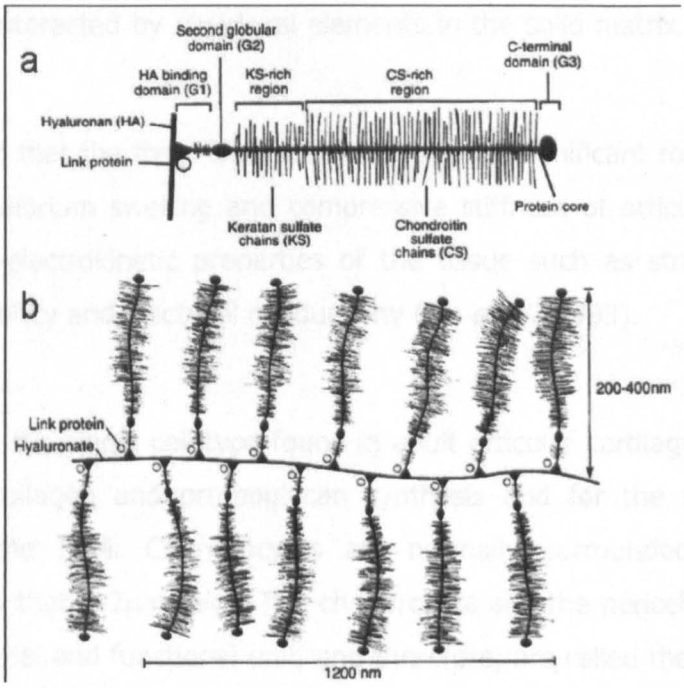

Figure 1-5: (a) Schematic representation of an aggregating proteoglycan monomer (aggrecan). It is composed of keratan sulfate and chondroitin sulphate chains bound covalently to a protein core molecule. (b) A proteoglycan aggregate that is composed of aggrecans noncovalently attached to hyaluronan with stabilizing link proteins.

Within the interstitial fluid, at physiological pH and ionic strength the sulphate and carboxyl groups are ionised. These negative charges are thus firmly fixed onto the porous permeable solid ECM and are known as fixed charges. The ECM of articular cartilage is thus negatively charged and hydrated. Under normal physiological conditions, the fixed negative charge in the ECM is electrically neutralised by mobile cations and anions contained in the synovial fluid. Thus, the total ion concentration inside the tissue is greater than the ion concentration in the external solution (synovial

fluid). This imbalance of ions gives rise to a pressure in the interstitial fluid that is higher than the ambient pressure in the external bath. This is known as the Donnan osmotic pressure. This osmotic pressure is one of the causes of cartilage swelling and maintenance of hydration (Mow *et al.*, 2005).

In the ECM, is approximated that the proteoglycans are restricted to 20% of their original volume in a free solution. As a result, the charge groups fixed along the GAG chains are in close proximity, causing large charge-charge repulsive forces to be exerted on each other (Mow *et al.*, 2005). At equilibrium, the swelling pressure, which consists of the Donnan osmotic pressure and a charge-charge expansion stress within the tissue, is counteracted by structural elements in the solid matrix (Wu and Herzog, 2002).

It is hypothesised that the fixed charge density plays a significant role not only in the governing of equilibrium swelling and compressive stiffness of articular cartilage, but also in mechano-electrokinetic properties of the tissue such as streaming potential, hydraulic permeability and electrical conductivity (Gu *et al.*, 1993).

Chondrocytes

Chondrocytes are the single cell type found in adult articular cartilage. These cells are responsible for collagen and proteoglycan synthesis and for the maintenance and remodelling of the ECM. Chondrocytes are normally surrounded by a layer of pericellular matrix that is 2μm thick. The chondrocyte and the pericellular matrix seem to act as a structural and functional unit, and therefore, are called the chondron (Poole *et al.*, 1987).

The chondrocytes only occupy a very small proportion of the total volume (1% - 10%), however, the cells are responsible for the synthesis and organisation of the ECM, as well as for the maintenance of homeostasis. Articular cartilage can be thought of as a strongly woven network of collagen fibres with proteoglycans and chondrocytes distributed inconsistently throughout the network and swelled up with interstitial water. Chondrocytes vary in size, shape, orientation and biosynthetic activity in the different zones of the tissue. In the superficial zone, the cells are flattened and lie parallel to the surface. In this zone, chondrocytes synthesise an ECM that is high in collagen and low in proteoglycans and they also turn over proteoglycans more rapidly. The cell density decreases into the middle and deep zones. In the middle zone, chondrocytes are more rounded. They synthesise a matrix with a greater concentration of proteoglycans and

larger-diameter collagen fibrils. In the deep zone, the chondrocytes are normally lined up in columns, perpendicular to the collagen surface (Mow *et al.*, 2005).

Since cartilage does not have a blood supply, chondrocytes have been reported to receive their nutrients mainly through synovial fluid. The transport of solutes from synovial fluid into cartilage has been demonstrated (McKibbin and Holdsworth, 1966; Honner and Thompson, 1971). Nutritional supply from the underlying subchondral bone is another obvious route. Many investigators in the past have ignored this possibility, based on the fact that the densely calcified basal zone of normal cartilage would provide an impassable barrier to solute and fluid diffusion. However, it has been shown that a nutritional route may exist between articular cartilage and subchondral bone (Malinin and Ouellette, 2000). Malinin and Ouellette observed the progress of two types of autologous osteochondral transplants, implanted in vascularised, viable cancellous bone wells in baboon femoral heads, over three years. Half of the transplants were coated in methylmethacrylate, preventing any contact between the implant and the host bone. This interruption of contact between the transplant and the underlying bone, resulted in degenerative changes comparable with OA after three years. The cartilage of the transplants without the methylmethacrylate coating appeared very similar to that of the normal condyles, smooth and glistening. The edges of these grafts had adhered well with the surrounding bone. Although this study supports the theory that subchondral bone plays a role in cartilage nutrition, the relative importance of these two modes of nutrition has yet to be determined.

Collagen-Proteoglycan Interactions

In order for articular cartilage to function as a stress reducing layer in a joint, it must allow an appropriate amount of deformation to achieve load-spreading while remaining structurally coherent (Broom and Silyn-Roberts, 1990). The interactions between the proteoglycan and collagen molecules are very important for this but to date poorly understood. The extremely varied distribution of collagen network and proteoglycan aggregates in each of the cartilage layers may lead to many mechanical interactions. Although poorly understood, the interaction is thought to be primarily frictional in nature. The proteoglycans, possessing a high density of fixed negative charges, enables cartilage to exhibit a significant Donnan osmotic pressure effect. This osmotic pressure leads to the swelling pressure caused by the fixed charge density inflating the collagen network and maintaining the ECM organisation. The other component of the total swelling pressure is derived from the repulsive force exerted by the closely spaced

negative charged groups along the proteoglycan molecules (Mow *et al.*, 1992; Mow *et al.*, 2005).

The interaction of the collagen and proteoglycan matrix provides a mechanism, which enables the tissue to resist tension. The swollen state enables the collagen network to sustain tensile loads and thus provides shear stiffness to the ECM (Mow *et al.*, 2005). In a recent study (Schmidt *et al.*, 2005) it was found that the physical restraints imposed on the collagen by the bulk of proteoglycan in the cartilage tissue retarded fibrillar reorganization and alignment under tensile loading. This prevented sudden extension of the collagen network and protected the joint when exposed to sudden impact forces.

1.3 The Meniscus

The menisci are fibrous structures, semi-lunar in shape which sit between the femoral condyles and tibial surface of the knee, as shown in Figure 1-1 and Figure 1-3. In each knee there are two menisci – a medial and lateral. The menisci are extensions of the tibia, which serve to extend the articular surfaces of the tibial plateau in order to provide a more congruous bearing for the femoral condyles. Each meniscus is thickest at its outer rim, where it is convex in shape and attached to the joint capsule via connective tissues. It tapers to a thin free edge towards the centre. The proximal surfaces of the menisci are concave and in contact with the condyles. The distal surfaces are flat and sit on the tibial plateau. Each meniscus is attached to the tibial plateau at the intercondylar fossa via ligaments called the meniscal horns (Arnoczky, 1990).

The meniscus is a fibrocartilaginous tissue composed primarily, of an interlacing network of collagen fibres and cells. In addition to collagen the ECM contains elastin, proteoglycans and glycoproteins (Arnoczky, 1990). The articulating surface of the meniscus is composed of fine fibrils in a random mesh-like woven matrix. The collagen fibres are primarily arranged in bundles in the circumferential direction, while smaller radial fibres appear to reinforce the structure by tying the larger circumferential fibres together (Mow *et al.*, 2005).

The menisci appear white, glossy and smooth. The smoothness of the articulating surface of the meniscus is due to a covering by a synovial membrane. The meniscus plays a key role in knee joint biomechanics. Scientists have been compiling evidence of

the important role of the menisci since the 1930's, before which the meniscus was thought to be a functionless part of the knee (King, 1936).

1.3.1 Protective Role of Meniscus

Total meniscectomy has been shown to induce osteoarthritic changes in the underlying cartilage, providing evidence that the menisci have a protective role in the knee, preventing degeneration caused by joint forces (Fairbank, 1948; DiStefano, 1980; Klompmaker *et al.*, 1992; McDermott *et al.*, 2006). The menisci provide congruity between otherwise very incongruous joint surfaces. They allow load bearing and transmission of forces in the knee joint, even when undergoing a wide range of motions. Damage or removal of part of the meniscus causes degeneration of the underlying cartilage in the form of joint space narrowing, roughening and fibrillation (King, 1936; Fairbank, 1948; Johnson *et al.*, 1974; Abdel-Hamid *et al.*, 2005).

1.3.2 Contact area and pressure distribution

Many studies have investigated the contact area and pressure distribution in the human cadaveric knee, with both menisci intact, as well as with one or both menisci removed. Techniques have included casting methods, pressure sensitive transducers and films, as well as roentgenographic methods (Kettlekamp and Jacobs, 1972; Seedhom *et al.*, 1974; Walker and Erkman, 1975; Krause *et al.*, 1976; Ahmed and Burke, 1983; Baratz *et al.*, 1986; Ihn *et al.*, 1993; Seedhom and Hargreaves, 1979a; Seedhom and Hargreaves, 1979b). These studies have shown that in a loaded situation, at least 50% of the body's weight is transmitted through the menisci and this is related proportionally to the meniscal coverage of the tibial tray (Seedhom *et al.*, 1974; Krause *et al.*, 1976; Ahmed and Burke, 1983; Cole *et al.*, 2002) and this load has been reported to be as high as 90% (Seedhom and Hargreaves, 1979b). The medial meniscus was found to transmit 50% of the joint load in the medial compartment and the lateral meniscus was found to transmit 70% of the joint load in the lateral compartment (Walker and Erkman, 1975). In the same study, Walker and Erkman used a casting method, while applying loads of 150 kg to cadaveric knees, with flexion varied from 0° - 90°. It was found that the load-bearing contacting area decreased following meniscectomy from $6cm^2$ to $2cm^2$ on each condyle. (Walker and Erkman, 1975). This decrease in contacting area resulted in elevated contact stresses on the cartilage surfaces. The meniscus has a load bearing function and a linear correlation has been found in a number of studies, between the increase in peak stresses on the

joint surface of the tibia and the amount of meniscal tissue removed (Burke *et al.*, 1978; Baratz *et al.*, 1986).

1.3.3 Shock absorber

The meniscus also functions as a shock absorber. Krause *et al.* (1976), reported the energy absorbing function of the menisci in the knee joint using load deflection and load contact area studies, with both menisci intact, after removing the medial meniscus and after removing both menisci (Krause *et al.*, 1976). Stress acting across the knee joint increased significantly following medial meniscectomy and again following excision of both menisci, indicating the load bearing role of the menisci. Hoshino and Wallace (1987), reported on the impact absorbing properties of the human knee using a falling weight onto a transacted proximal femur and the force transmitted through the knee was measured using a load transducer. Peak force was found to increase sequentially as menisci were damaged (both menisci were cut radially and vertically) or removed (both menisci excised). Removal of the menisci caused an increase in impact force by 21% compared to the native knee (Hoshino and Wallace, 1987). This work was supported by Proctor's study, which demonstrated, using compression testing that the medial meniscus has a combination of low compressive stiffness and permeability in comparison to cartilage. The meniscus thus acts as a very efficient medium to absorb and dissipate energy exerted on the knee (Proctor *et al.*, 1989).

1.3.4 Lubrication

Finally the menisci play an important role in joint lubrication (King, 1936, Schumacher *et al.*, 2005, Sun *et al.*, 2006). It has been shown that lubricin is secreted by bovine meniscal cells. Lubricin has been found associated with synoviocytes cells of the meniscal surfaces as well as cells along tie and circumferential collagen fibres. Lubricin has been reported to have boundary lubrication properties and aids movement of the synovial joint (Jay, 1992). However, the biphasic nature of menisci and its effect on tribology has not been studied in detail. One study did look at the frictional properties of the meniscus articulating with a flat cobalt chrome surface, and found it to have an increased frictional coefficient compared with native cartilage (Pickard *et al.*, 1998b).

1.4 Mechanical Properties of Articular Cartilage

Articular cartilage shows inhomogeneous and anisotropic mechanical behaviour owing to the varying structural organisation of the collagen and proteoglycans, through the

depth of the tissue, both at a macroscopic and microscopic level. The variation of the collagen fibrils in size, density and orientation, as well as the proteoglycan distribution are perhaps the most important factors leading to this inhomogeneous behaviour.

During joint articulation, forces at the joint surface can vary from almost zero to several times body weight and so cartilage, under physiological loading conditions is a highly stressed material. To understand how cartilage performs under these high loading conditions, its intrinsic mechanical properties in compression, tension and shear must be understood.

1.4.1 Tensile Properties

Cartilage exhibits different tensile strengths when tested parallel to the predominant fibre direction and perpendicular to it. Tensile strength is always higher in the direction parallel to the collagen fibrils at the cartilage surface (split line direction), than in the corresponding perpendicular direction. The stress-strain curve for articular cartilage, tested under a constant low strain-rate condition is shown in Figure 1-6. It shows the same j-shaped curve as other soft tissues such as ligaments and tendons, as it tends to stiffen with increasing strain when the strain becomes large.

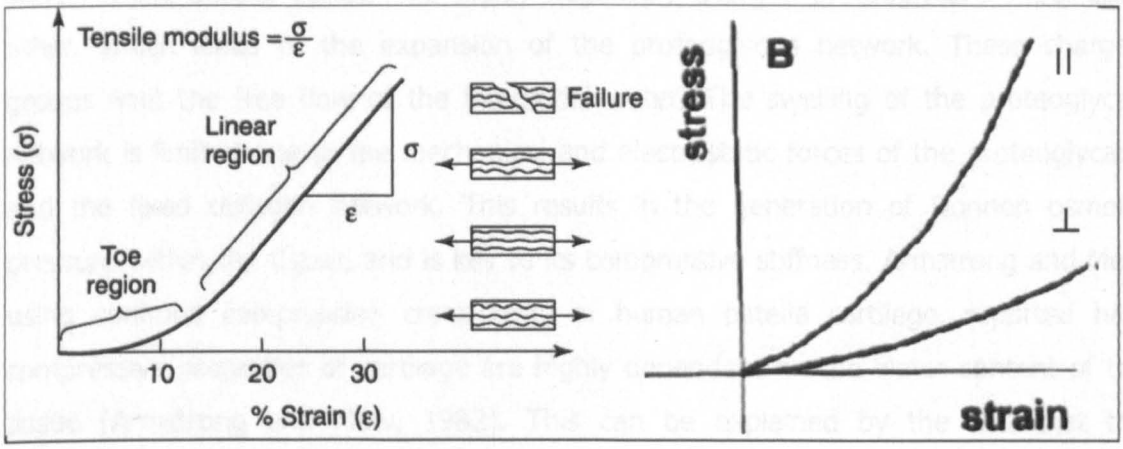

Figure 1-6: Tensile properties of articular cartilage. (a) The fibre-recruitment model for the non-linear tensile behaviour of cartilage showing the typical toe and linear regions and (b) the non-linear and anisotropic behaviour of cartilage when tested parallel (| |) and perpendicular (⊥) to the split lines. Specimens are stiffer in parallel direction (Mow *et al.*, 1992).

At up to 6% strain in tension, the Young's modulus of articular cartilage cannot be described by one value. For large strains, the curve has an initial toe region, in which the collagen fibres undergo realignment or "uncrimping", during the initial phase of

tensile stress. The linear region is caused by stretching of the straightened collagen fibres. Failure occurs when all the collagen fibres contained within the specimen are broken (Ozkaya and Nordin, 1999; Nordin and Frankel, 2001). As shown in Figure 1-6b, the tensile modulus of the cartilage specimen is higher when the specimens are aligned parallel to the split line, in comparison to specimens aligned perpendicular (Mow and Ateshian, 1997). This shows that there is a preferential alignment of fibres at the surfaces, providing the joint with a tough wear-resistant "skin".

Due to the random orientation of collagen fibres in the deeper layers compared to the parallel uniformity at the surface, the tensile modulus decreases with increasing depth from the surface. This pattern indicates that the surface fibres are designed to resist more tensile stress parallel to the split lines than those in deeper zones (Nordin and Frankel, 2001; Ozkaya and Nordin, 1999).

1.4.2 Compressive Properties

Compressive properties vary with the zone tested and in particular, with the proteoglycan and interstitial fluid content. When the proteoglycan concentration increases so too does the compressive stiffness of the tissue meaning that cartilage is stiffer in the deeper zones. The highly negatively charged proteoglycans repel each other, which leads to the expansion of the proteoglycan network. These charged groups limit the free flow of the interstitial water. The swelling of the proteoglycan network is limited due to the mechanical and electrostatic forces of the proteoglycans and the fixed collagen network. This results in the generation of Donnon osmotic pressure within the tissue, and is key to its compressive stiffness. Armstrong and Mow using confined compression creep tests of human patella cartilage, reported how compressive properties of cartilage are highly dependent on the water content of the tissue (Armstrong and Mow, 1982). This can be explained by the fact that the resistance to deformation and fluid flow through the tissue depends on the amount of collagen-proteoglycan solid matrix per unit volume. The STZ of articular cartilage plays the least important role in compression resistance and the deeper zones, with their greater proteoglycan concentration, play a more important role (Nordin and Frankel, 2001).

1.4.3 Viscoelasticity

The most important physical mechanism affecting the time dependent response of cartilage is the frictional drag caused by interstitial fluid flow through the porous-

permeable solid matrix. The viscoelastic properties of articular cartilage are mainly associated with the movement of water in the tissue. Fluid flow is proportional to pressure gradients in the pore water and is described by the coefficient of hydraulic permeability. The higher the pressures and compressive strains, the less permeable cartilage becomes. The areas in which the concentration of proteoglycans is highest are the areas in which the frictional drag (inverse of hydraulic permeability) is the highest. However, the cartilage matrix itself also behaves in a viscoelastic manner which is known as flow-independent viscoelastic behaviour. To establish this intrinsic viscoelastic behaviour, a small strain, pure shear test must be performed. When these conditions are met, no volumetric change or hydrodynamic pressures are generated in the tissue, allowing no interstitial fluid flow and the associated frictional dissipation to occur in the cartilage specimen. By performing a stress-relaxation test, with pure shear conditions, the equilibrium shear modulus can be obtained (Mow *et al.*, 1992; Mow *et al.*, 2005). Mow *et al.* found the shear modulus for cartilage to range between 0.2 MPa and 0.40 MPa, by studying the response of cartilage to an applied torsional shear deformation (Mow *et al.*, 1992).

The dynamic shear properties of cartilage were investigated by Zhu *et al.* using torsional shear conditions, under low strain over a physiological range of frequencies (0.01-20 Hz). The values of the shear modulus varied from 0.2 MPa to 2.5 MPa for bovine cartilage. As there was no volumetric change during the experiment, there was no relative interstitial fluid flow within the collagen-proteoglycan matrix and the viscoelastic shear response of the cartilage was primarily as a result of intrinsic or flow-independent viscoelasticity of the matrix components (Zhu *et al.*, 1993).

When a volume of cartilage is exposed to shear deformation, the fluid remains in the tissue while the solid components deform. This may put collagen fibrils under tension and move the proteoglycans in such a way as to increase the overall resistance to deformation (Figure 1-7).

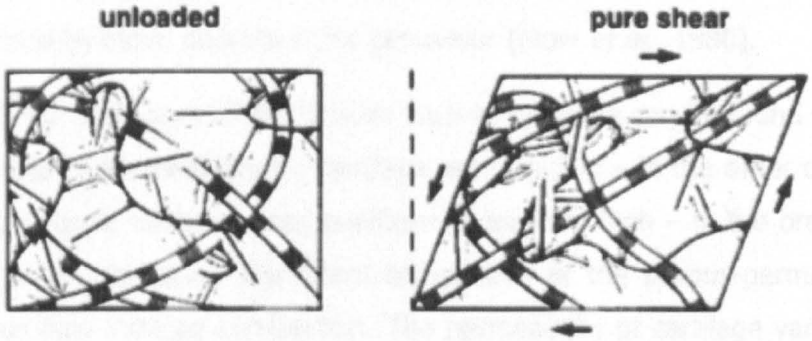

Figure 1-7: Diagram of articular cartilage unloaded and in pure shear (Mow and Proctor, 1989).

The collagen network plays an important mechanical role in contributing to the shear stiffness and energy storage in cartilage. When a torsional load is applied to the cartilage the tension in the collagen fibres provides the shear stiffness. In the same study by Zhu *et al.* the contributions of collagen and proteoglycan to the shear stiffness were examined, by examining the biochemical composition in comparison to mechanical properties. They found a strong correlation between the shear modulus and collagen content, suggesting collagen has an important role in the shear stiffness of cartilage (Zhu *et al.*, 1993)

Woo and colleagues examined canine medial collateral ligaments, which are mainly composed of collagen, and found that the energy dissipation of these ligaments in tension was very slight, with a phase-shift angle (angle between the sinusoidal displacement input and torque output) of only about 3.6° (Woo *et al.*, 1980). In similar studies, of high concentration pure proteoglycan solutions, the phase shift angle was found to range between 50° and 70° (Mow *et al.*, 1984a; Hardingham *et al.*, 1987; Mow *et al.*, 1989b; Zhu *et al.*, 1991). These studies underline the ability of collagen to resist tension and provide strength for the matrix when in shear. The proteoglycans help to maintain the collagen fibrils in proper spatial orientation, providing the overall tissue with strength and stiffness in shear (Mow *et al.*, 2005).

1.4.4 Biphasic Viscoelasticity

In the previous Section the flow-independent properties of cartilage have been discussed. The most dominant physical mechanism affecting the time-dependent response of cartilage is the frictional drag, caused by the flow of interstitial fluid flow

through matrix. These are the fluid-dependent properties of the tissue. The biphasic theory proposed by Mow, describes this behaviour (Mow *et al.*, 1980).

The permeability coefficient of soft tissues such as cartilage can be found using Darcy's Law. The values of permeability for cartilage are very low – in the order of 10^{-15} to 10^{-16} $m^4N^{-1}s$. As a result, diffusive drag coefficients are very high – in the order of 10^{15} to 10^{16} Nsm^{-4}, which can cause significant compaction of the porous-permeable matrix, also known as flow-induced compaction. The permeability of cartilage varies with both applied pressure and compressive strain. The non-linearity of the strain dependent permeability of cartilage, is very important during loading, particularly sudden impact loading. It regulates the transient compressive responses of cartilage in dispersing energy and it prevents rapid and excessive fluid exudation from the tissue during compression (Mow *et al.*, 2005). Soltz and Ateshian found the permeability coefficient of cartilage from bovine carpometacarpal joints to range between $2.9x10^{-16}$ $m^4N^{-1}s$ and $3.6x10^{-16}$ $m^4N^{-1}s$, using stress relaxation and creep tests with a contact stress of 0.13MPa (Soltz and Ateshian, 1998).

The creep and stress-relaxation behaviour of cartilage is due to the balance of stresses between that supported by the drag forces of the interstitial fluid flow and that carried by the solid matrix.

Creep experiments

The compressive creep behaviour of cartilage has been widely investigated (Mow *et al.*, 1980; Lai *et al.*, 1981; Mow *et al.*, 1984b; Holmes *et al.*, 1985; Kwan *et al.*, 1989; Mow *et al.*, 1989a). In cartilage creep experiments, a cylindrical cartilage plug is loaded (constant load function) against a rigid porous plate, within a confined chamber which stops lateral fluid flow and radial deformation of the tissue. As pressure is applied, fluid flow from the tissue can occur in an unimpeded manner, but only across the cartilage surface and porous plate surface, since the chamber prevents any lateral flow. As the load is applied to, and constantly maintained, on the cartilage specimen, exudation of the interstitial fluid begins immediately. As fluid leaves the tissue, compressive creep deformation occurs. A typical creep curve is shown in Figure 1-8.

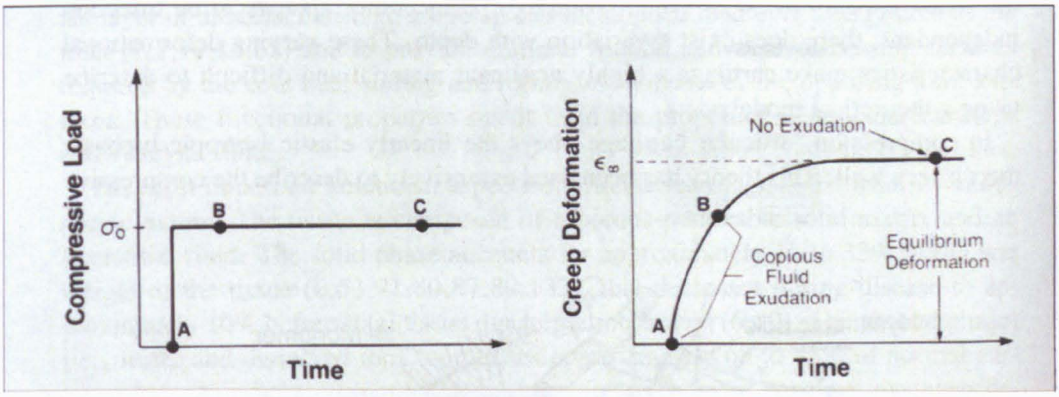

Figure 1-8: Creep response of cartilage under a constant compressive load (Mow *et al.*, 1980).

When the load is initially applied, exudation of fluid occurs at a rapid rate, leading to high rates of deformation. The rate of deformation decreases gradually as the flow ceases (Figure 1-8). At equilibrium, fluid flow ceases and the applied load is completely supported by the collagen-proteoglycan matrix (Mow *et al.*, 1980). The initial rate of creep is controlled by the rate of fluid exudation, so it can be used to determine the permeability of the tissue. Also, after fluid flow has ceased, the final equilibrium deformation can be used to determine the aggregate modulus of the solid matrix.

Unconfined compression tests of articular cartilage have been used to determine biomechanical properties (aggregate modulus, Poisson's ratio and permeability) and electrochemical properties (fixed charge density) simultaneously, using the osmotic pressure predictions of the triphasic theory (Lu *et al.*, 2004).

Stress relaxation experiments

Stress relaxation of cartilage can be examined using the same set-up as creep tests but instead of applying a constant load, a constant displacement is applied. The tissue is compressed at a constant rate with the porous plate, causing an initial fluid efflux and matrix compaction, fluid redistribution and before finally reaching equilibrium as shown in Figure 1-9.

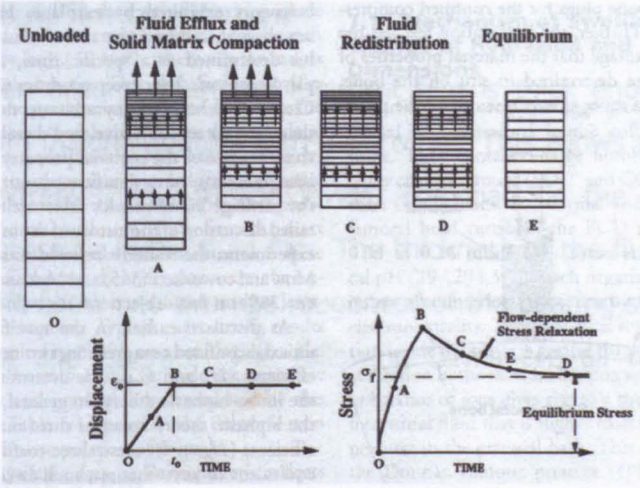

Figure 1-9: Fluid efflux and redistribution within cartilage during a compression stress-relaxation experiment. The horizontal bars in the upper figures indicate distribution of strain in the tissue. The lower right-hand graph shows the stress response during compression (O-A-B) and relaxation (B-C-D-E) (Mow *et al.*, 2005).

Fluid exudation occurs across the surface. Due to the large frictional drag properties, large loads are needed to compress the tissue. Initially, during displacement application, stress levels increase in the cartilage solid matrix due to the forced fluid exudation. During the relaxation phase the compressive strain is held constant, no fluid exudation occurs and the compressive stress at the surface decays with time as solid compaction at the surface is relieved. This results in transfer of stress away from the surface in the form of fluid redistribution and dissipation of hydrostatic pressure developed during compression.

1.5 Lubrication of Diarthroidal Joints

The natural synovial joint is an outstanding bearing mechanism. It can function for many decades, transmitting dynamic loads of quite large magnitude and allowing a wide range of movement. The healthy synovial joint performs these movements with high efficiency and with coefficients of friction as low as 0.005 (Dowson and Wright, 1981). Synovial joints appear to function with a mixture of engineering modes of lubrication (and perhaps some novel ones), rather than a single mode. In the following sections, the different modes of lubrication are discussed, bearing in mind that one mode alone cannot account for the excellent lubrication properties of synovial joints.

1.5.1 Fluid Film Lubrication

Fluid film lubrication occurs when the lubricant film is thick enough to prevent the opposing solids from making contact with each other. This allows motion between the two surfaces at extremely low friction levels. The load on the bearing surfaces is supported by the pressure in the fluid film. The thickness of the fluid film should be at least three times the combined average roughness of the bearing surfaces for fluid film lubrication to exist and operate. The following terms are all related to fluid film lubrication:

Hydrodynamic lubrication

This is a form of lubrication in which substantial load-carrying pressures are generated by high-speed motion of the bearing surfaces relative to one another. As the surfaces move relative to one another at speed, a layer of viscous synovial fluid is dragged though a narrowing wedge-shaped gap. This action creates a hydrodynamic pressure in the fluid separating the two surfaces and supporting the load. However, synovial joints still manage to operate with low friction at low sliding speeds, indicating that hydrodynamic lubrication alone does not account for the lubrication regime in synovial joints (Mow *et al.*, 1980; Ateshian and Mow, 2005).

Squeeze film lubrication

Squeeze film lubrication affords protection to bearing surfaces separated by a film of lubricant during normal motion. Viscous fluids show a remarkable resistance to lateral flow between closely separated solids, subjected to large forces trying to close the gap. The fluid pressure generated as a result has the ability to bear load and keeps the articulating surfaces apart. This mechanism is important for dynamically loaded bearings and under start-up and stopping conditions (Ateshian and Mow, 2005).

Elasto-hydrodynamic lubrication (EHL)

EHL occurs where the contacting bearing surfaces are elastic in nature, and the bearing surfaces become deformed under pressure for the maintenance of the fluid film. Micro-EHL lubrication is an extension of EHL which describes the local EHL action, deformation and smoothing of asperities on cartilage surfaces at a macro level during articulation (Dowson and Jin, 1986). Transient-EHL was described by Medley *et al.* This extension of EHL described the entrainment of synovial fluid into the contact by the motion of the surfaces. As a result of joint loading, a film pressure is generated which opposes the fluid entrainment and a balance is achieved at a particular film thickness.

The deformation of the surfaces reduces this film pressure, allowing an increase in the fluid entrainment and fluid film thickness. Therefore, during normal variations in loading, motion and velocity, a dynamic variation in film thickness results (Medley *et al.*, 1984).

Boosted lubrication

Boosted lubrication is a lubrication mechanism in which the applied loads force low molecular weight components of the synovial fluid into the cartilage surfaces, leaving highly viscous hyaluronic acid (HA) and protein filtrates on the cartilage surface with load bearing abilities (Mow and Hayes, 1997; Dowson and Wright, 1981).

1.5.2 Boundary Lubrication

Boundary lubrication takes effect when the combined surface roughness of the opposing surfaces is greater than the lubricant thickness. Contact takes place over an area similar to that which develops in dry contact. In such a case it is the physical and chemical properties of thin surface films of molecular proportions, which govern the contact characteristics. Hyaluronic acid, glycoproteins (lubricin) and surface amorphous phospholipids have all been proposed as the lubricants responsible for boundary lubrication in cartilage. The properties of the bulk lubricant are of lesser importance in this case and the friction coefficient is independent of viscosity (Dowson and Wright, 1981).

Many studies have investigated the influence of these boundary lubricants on cartilage friction, often in conjunction with the important role played by interstitial fluid pressurisation, on the low frictional coefficient of cartilage. Krishnan *et al.* believe, based on their recent study (Krishnan *et al.*, 2004b), that boundary lubricants complement the role of interstitial fluid pressurisation. Studies which have compared the frictional response of articular cartilage using synovial fluid versus saline have shown in general a lower minimum friction with synovial fluid. Forster and Fisher tested a cartilage pin articulating on a steel plate, using both synovial fluid and Ringer's solution as lubricants and found that synovial fluid provided statistically significantly lower coefficients of friction ($p < 0.05$; Student t-test), than Ringer's solution (Forster and Fisher, 1999). This indicates that boundary lubricants supplement the primary role of interstitial fluid pressurization and reduces further the friction coefficient.

1.5.3 Mixed Lubrication

Mixed lubrication is a combination of fluid film and boundary lubrication regimes (Figure 1-10). In full fluid-film lubrication separation of the opposing solids is complete. In boundary lubrication, the coefficient of friction is independent of load, speed and apparent contact area. When the lubricating film breaks down due to extreme loading or intermittent motions, the bearing surfaces come into contact, boundary lubrication comes into the play to maintain minimal friction and wear of the articulating surfaces (Dowson and Wright, 1981; Mow and Hayes, 1997).

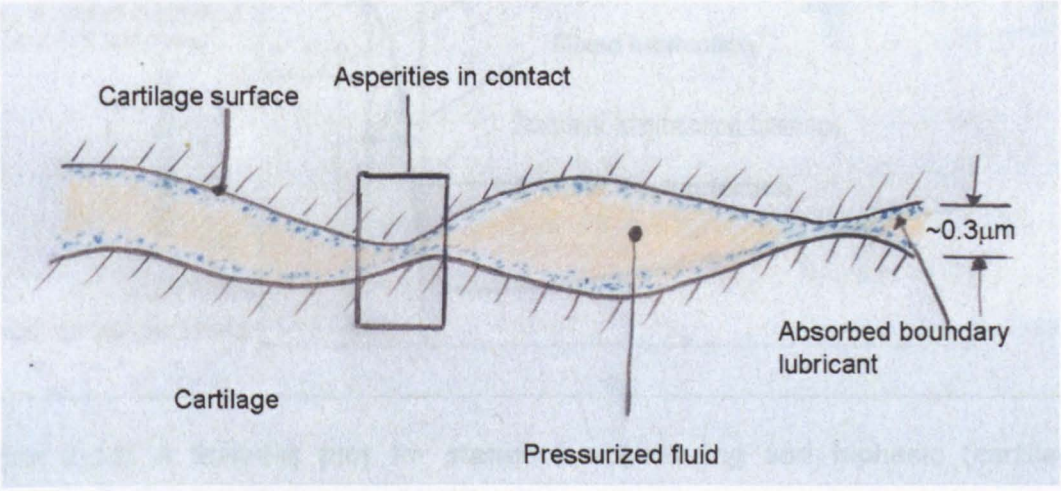

Figure 1-10: Mixed lubrication operating in a synovial joint. Boundary lubrication occurs when the asperities of the surfaces come into contact and fluid-film lubrication takes place in areas with more widely separated surfaces. Adapted from (Woo and Buckwalter, 1988).

The Sommerfeld Number (z) is a dimensionless parameter given by,

$$Z = \eta u R_1 / W$$

where (η) is the viscosity of the lubricant, and (u) is the entraining velocity of the bearing surfaces, (R_1) is the radius of curvature and (W) is the applied load. A classic approach in tribology, is the use of the Stribeck plot to determine the mode of lubrication in operation, by plotting the friction factor against the Sommerfeld number. A typical Stribeck plot for a standard engineering bearing (black line) and a biphasic cartilage bearing (red line) is shown in Figure 1-11. Biphasic materials such as articular cartilage operate under a highly complex lubrication regime known as biphasic lubrication, which will be discussed in more detail in the next section. It means that very low levels of friction are maintained over a period of time (as depicted by the red

horizontal line in Figure 1-11). However, if constant loading is maintained for long periods of time, the fluid load support within in the tissue decays, and the mode of lubrication shifts towards boundary lubrication (as depicted by the red vertical arrows in Figure 1-11). As a result, the time dependent response of biphasic lubrication is independent of the Sommerfeld number and dependent on the level of fluid pressurisation within the tissue, specifically the proportion of the load supported by the fluid phase, rather than the solid matrix constituents.

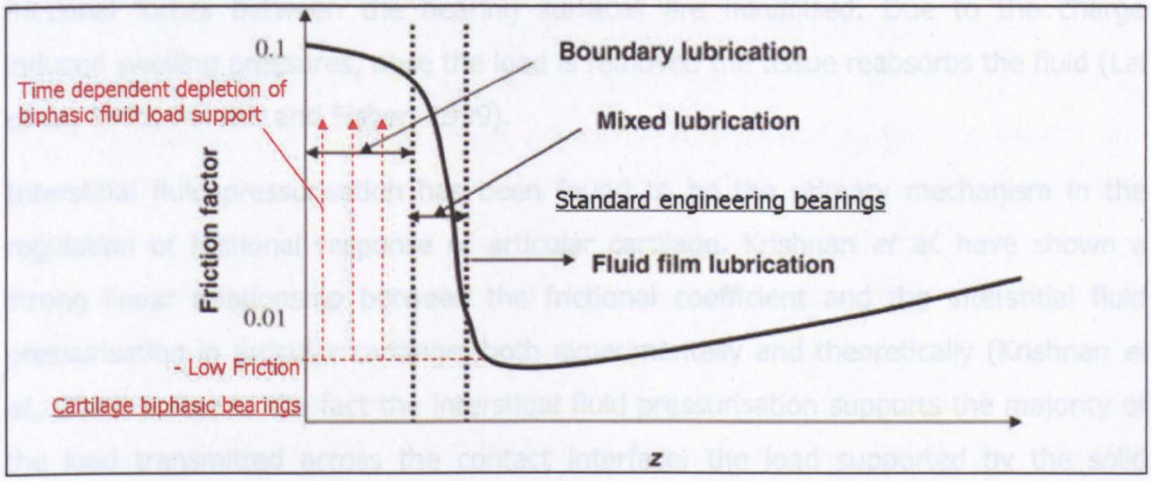

Figure 1-11: A Stribeck plot for standard engineering and biphasic (cartilage) materials, indicating the mode of lubrication.

It is generally thought that synovial joints generally act under mixed lubrication regimes, under normal physiological loading and motion and that they change to more specific modes of lubrication during different activities, based on the loading and/or motion of the activity. Fluid film, boundary and mixed modes of lubrication operate within the synovial joint and are influenced by the materials between the articulating surfaces and the composition of the articulating surfaces. The very important lubrication regime which operates in synovial joints, biphasic lubrication, will be discussed in detail in the following Section. Biphasic lubrication, is largely inherent to the cartilage tissue and plays an important load bearing within the tissue and subsequently, within the synovial joint.

1.5.4 Biphasic Lubrication

The classic biphasic theory assumes cartilage to comprise of two separate, immiscible and incompressible phases – the interstitial fluid phase and the solid matrix phase (Mow *et al.*, 1980; Mow *et al.*, 1990). This biphasic theory is quite similar to the weeping lubrication mechanism proposed by McCutcheon (McCutchen, 1959;

McCutchen, 1962). As the joint takes up load and the cartilage surfaces are compressed, fluid is exuded from loaded to unloaded areas and into the joint capsule itself (McCutchen, 1959; McCutchen, 1962; Mow *et al.*, 1984b; Forster and Fisher, 1996). This exudation of fluid through the solid matrix results in the generation of pressure gradients in the form of interstitial fluid pressurisation. This interstitial fluid pressurisation means the fluid phase acts as a load bearing structure, and the solid matrix is exposed to a much lesser load than would otherwise be expected and frictional forces between the bearing surfaces are minimised. Due to the charge induced swelling pressures, once the load is removed the tissue reabsorbs the fluid (Lai *et al.*, 1991; Forster and Fisher, 1999).

Interstitial fluid pressurisation has been found to be the primary mechanism in the regulation of frictional response of articular cartilage. Krishnan *et al.* have shown a strong linear relationship between the frictional coefficient and the interstitial fluid pressurisation in articular cartilage, both experimentally and theoretically (Krishnan *et al.*, 2004b). Due to the fact the interstitial fluid pressurisation supports the majority of the load transmitted across the contact interface, the load supported by the solid matrix is reduced, which significantly reduces the coefficient of friction between the surfaces. As long as the interstitial fluid pressurisation remains elevated, the effective frictional coefficient is small. As the fluid pressure reduces to zero, the contact force increasingly moves onto the solid matrix and as a result the coefficient of friction begins to rise.

The biphasic properties of cartilage, in conjunction with its elastic nature mean that joint lubrication is a combination of EHL, biphasic and boundary lubrication. The transition between these modes of lubrication is not completely understood and so synovial joints *in vivo* are often described as operating under a "mixed lubrication" regime, described in Section 1.5.3.

An extension of the biphasic theory, the triphasic theory was proposed by (Lai *et al.*, 1991). This modelled a mixture of three phases: the incompressible solid and fluid phases from the biphasic theory and an ion phase of two species (cations and anions) of a single salt (Na^+ and Cl^-). This theory included both the physio-chemical aspects of cartilage swelling as well as the biphasic aspects of solid matrix deformation and interstitial fluid flow. This triphasic mechano-electrochemical theory by Lai has been shown to be able to describe the Donnan osmotic pressure for cartilage and is an extension of Mows biphasic theory (Gu *et al.*, 1993). The addition of this third ionic

phase increased the accuracy of the model predictions of cartilage tissue deformational response during equilibrium free swelling and confined compression. However, the ionic phase played a very small role in comparison to the solid and fluid phases of cartilage. For most tribological studies of cartilage, the biphasic theory is referred to and the small role of the ionic phase is deemed negligible.

1.6 Cartilage Wear

Wear is defined as the progressive loss of material from contact surfaces due to mechanical action between them. There are many contributing factors to the wear of articular cartilage due to its complex nature, and in particular, the mechanical and biochemical relationships within its structure. Cartilage wear can be split into mechanical wear and biochemical degradation. In general cartilage wear is considerably low when compared to any engineered bearing mechanism, owing to the very effective lubrication of synovial joints and potential regenerating capacity. However, the rate of wear can increase as the superficial lubrication layer is diminished by normal aging, excessive loading or disease (Mow and Hayes, 1997). The following sections will discuss the two main types of cartilage wear: mechanical wear which can be discussed in terms of fatigue wear or interfacial wear and biochemical wear.

1.6.1 Fatigue Wear

The cyclic stresses and strains generated within the material and the accumulation of any small microscopic wear debris present in the joint due to repetitive loading lead to what is known as fatigue wear. It can cause collagen fibres to buckle or loosen, which affects the ECM interactions and changes how the cartilage reacts under loading. Furthermore, this collagen disruption can result in decreased stiffness and increased tissue permeability hence increasing the water content of cartilage abnormally, similar to that found in osteoarthritic cartilage. Fatigue wear can also occur if there is insufficient time for internal fluid redistribution to relieve high stress in the compacted region of cartilage tissue during high impact loads. This type of wear is independent of lubrication or surface contact area (Mow and Hayes, 1997).

1.6.2 Interfacial Wear

Interfacial wear occurs when there is direct solid-solid contact between two articulating surfaces and it can be classified into two types: adhesive wear and abrasive wear. Adhesive wear occurs when surface fragments adhere to one another due to strong

cohesive bonds and are then torn from the surface during relative motion (Dowson and Wright, 1981). Abrasive wear is the displacement of material by hard particles and protuberances, in other words a harder material may cut into a softer material when they come into contact with one another. The addition of debris to the joint capsule leads to an increase in surface to surface contact and an increase in all types of wear (Ateshian and Mow, 2005).

1.6.3 Biochemical Degradation

Articular cartilage often shows some changes with age, and those changes can be somewhat different in the different cartilage zones. There is much evidence that chondrocytes senesce with age. Hickery and colleagues found that cell yields from cartilage samples from donors older than 40 years were much lower than from younger donors. Rates of proliferation in culture were decreased in cells from donors older than 30 years (Hickery *et al.*, 2003). In the same study it was shown that proliferation rates of chondrocytes in culture were nearly equal after the addition of growth factors, but that the GAG content of the cultures was increased by growth factors only in the cells from younger donors. This implies that the response of chondrocytes to growth factors may differ with donor age, which may mean that cell age has a role to play in the progression of aging cartilage towards wear and disease.

Chondrocyte apoptosis is influenced by several factors, including altered ECM components, cytokines, nitric oxide and mechanical injury. Apoptosis increases in aging joint cartilage and may contribute to the increased risk of OA. Further studies are required to clarify to what extent chondrocyte death is due to aging (Adams and Horton, 1998). Chondrocyte apoptosis is also increased in OA and this is associated with depletion of matrix proteoglycans. This means that cell death and a consequent inability to maintain the cartilage matrix may be important in the development of OA in aging and after injury. Furthermore, the presence of chondrocyte-derived apoptotic bodies in the tissue may contribute to pathologic cartilage calcification associated with aging, OA, and other joint diseases (Hashimoto *et al.*, 1998).

The non-vascularised ECM provides the local milieu for the articular chondrocyte and it is known that matrix changes occur in cartilage with age. The matrix is responsible for the biomechanical properties of cartilage. Changes in matrix composition or configuration with age could potentially influence the chondrocyte. Equally, diminished chondrocyte function would be expected to alter the ability of cartilage to withstand

mechanical stress. In addition, the ECM acts as a reservoir for growth factors. Therefore, age-related alterations in the matrix may affect the bioavailability of various factors upon which the chondrocyte depends, leading to further decline in tissue integrity and possibly to disease (Carrington, 2004).

1.7 Cartilage Degeneration and Current Treatments

OA is a painful and debilitating disease of synovial joints, which involves abnormal wearing of cartilage. Articular cartilage has limited healing potential due to its avascular and aneural nature (Dorotka *et al.*, 2004). OA can be divided into primary and secondary forms. Primary OA has no apparent initiating factor. It is related to the aging process and typically occurs in older individuals. Secondary OA refers to degradation of synovial joints which results from trauma to the joint causing damage to ligaments, meniscus, cartilage and/or subchondral bone or it can be secondary to the natural aging of other tissues. Secondary OA often occurs in relatively young patients.

In the earlier stages of disease the structural damage to cartilage is often defined as matrix disruption, partial thickness defects or full thickness defects. In the case of matrix disruption the ECM is damaged but not beyond repair in many cases. It has been suggested that a reduction in proteoglycan content may be due to increased degradation of the molecules or decreased synthesis. Considerable reductions in matrix proteoglycan content decreases cartilage stiffness and increases its hydraulic permeability. When subjected to impact loading, other distortions, ruptures or partial degradation of the collagen fibril meshwork may occur, as well as disruptions to the collagen-proteoglycan relationship (Buckwalter and Mow, 1992). These disruptions may cause increased loading of the remaining macro-molecular framework increasing the vulnerability of the tissue to more damage from impact loading or even normal joint use. Chondrocytes are thought to have the ability to sense changes in the matrix composition and synthesise new molecules making it possible to repair damage to the macromolecular framework. However, chondrocytes can only do so under certain conditions: if the loss of matrix proteoglycans does not exceed that which the cells could rapidly produce; if the collagen meshwork remains intact; and if there are sufficient living chondrocytes (Buckwalter, 1996). However, in cases where these conditions are not met, it is possible that the cells would be unable to restore the

matrix, damage would continue with joint activity and lead to articular cartilage degeneration and osteoarthritis.

Partial thickness defects involve disruption of the cartilage surface (in the form of fissures), but this does not extend to the subchondral bone. Following the injury or trauma causing the defect, cells begin to proliferate. However, for reasons not yet understood, cellular attempts to fill and repair the defect site cease before the defect is completely repaired (Temenoff and Mikos, 2000).

Full thickness cartilage defects arise from injury or trauma which penetrates the entire cartilage depth as well as the subchondral bone. The defect is filled with a fibrin clot and a wound healing response initiates (Temenoff and Mikos, 2000). Unlike with the partial thickness defect, there is access to progenitor cells from the bone marrow which can migrate to fill the defect (Buckwalter, 1998). These cells tend to initiate the formation of a cartilage-like tissue – a tissue between articular and fibrocartilage. However, the stiffness and permeability properties of this cartilage-like tissue are inferior to those of normal articular cartilage, which can cause its deterioration over time (Buckwalter, 1998).

Cartilage does not self-repair and it is believed that this is because it is avascular and has a limited number of cells (Beris *et al.*, 2005). Depending on the severity of joint disease there are a broad spectrum of treatment options for arthritic joints from non-invasive, to minimally invasive surgery to total joint replacement. In the next sections, cartilage repair techniques and joint replacement will be briefly discussed. Following this, in Sections 1.8 and 1.9, hemiarthroplasty and cartilage defect repair, two of the main subjects of this thesis, will be discussed in more detail.

1.7.1 Pharmacologic Treatments

Current pharmacologic treatments for OA aim to relieve pain and restore function. OA often has an inflammatory component, however there is little evidence to suggest that anti-inflammatory drugs which are commonly used in OA treatment provide more relief than simple analgesics (Pinals, 1992). It has been suggested that NSAIDs are more efficacious (Sarzi-Puttini *et al.*, 2005). Different pharmacologic treatments work using different mechanisms: inhibition of chondrocyte-derived degenerative enzymes; stimulation of matrix synthesis; enhancement of synovial fluid lubrication.

1.7.2 Viscosupplementation

Viscosupplementation is a procedure which involves injecting a preparation of hyaluronic acid (HA) or any other therapeutic lubricant into the affected joint. HA is a naturally occurring substance (a charged linear polymer carbohydrate) found in synovial fluid and it is believed to be the most important component of synovial fluid involved in joint lubrication. HA is the most commonly tested viscosupplement, however glucosamine and chondroitin sulphate have also been utilised but their benefits are still debateable (McAlindon *et al.*, 2000). Viscosupplementation can be an attractive therapy since it is less invasive and traumatic than surgical treatments and the hospitalisation time is significantly shorter. However, there is some controversy surrounding this therapy, related to turnover rate of these supplements and their degradation within the joint capsule.

1.7.3 Arthroscopic Repair Techniques

There are a number of widely used cartilage arthroscopic techniques. Arthroscopic lavage is used to wash out any blood, fluid or loose debris from inside the joint space in order to alleviate irritation in the knee. Debridement is the meticulous removal of all unstable cartilage in an effort to improve lubrication and reduce friction in the joint. Debridement is commonly carried out in conjunction with arthroscopic lavage. Abrasion arthroplasty involves reshaping the joint by grinding down the damaged surface with a rotating burr and then allowing a new joint surface to form by itself.

1.7.4 Autologous Chondrocyte Implantation

This is a two-stage procedure: the first in which healthy chondrocyte cells are harvested from an unloaded part of the joint. After culturing in the laboratory, these cells are implanted (Figure 1-12). The damaged area is debrided, a piece of the periosteum is harvested and sewn over the defect and then the cells from the lab are injected behind the fibrous covering, where they start to grow into cartilage cells (Beris *et al.*, 2005; Smith *et al.*, 2005), although it is debatable whether this cartilage is normal hyaline or the fibrocartilage type.

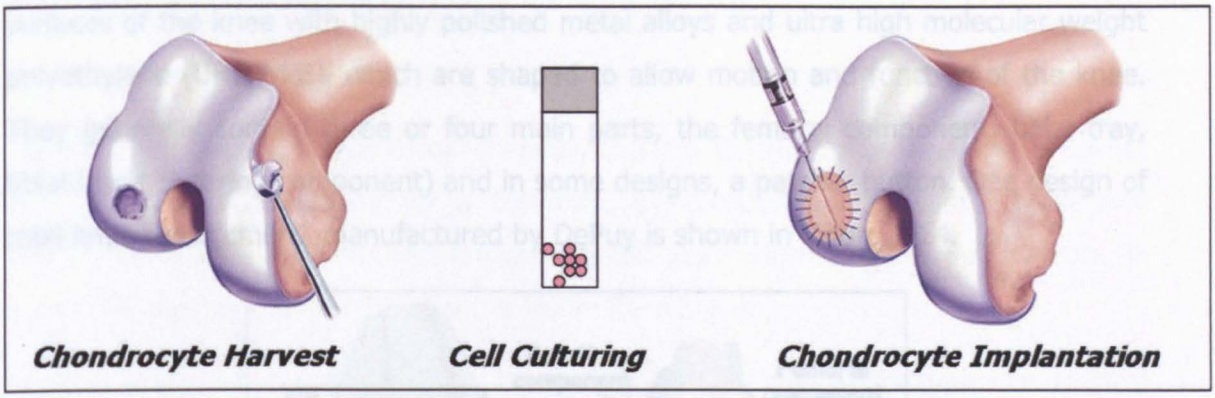

Figure 1-12: Schematic representation of autologous chondrocyte implantation (ACI). Image adapted from http://www.wnycrc.buffalo.edu/autulogous.html

1.7.5 Mosaicplasty

Mosaicplasty, also known as osteochondral transplantation is widely used for the repair of osteochondral defects. Osteochondral plugs are taken from non-weight bearing areas of articular cartilage, with a cylindrical cutting device, and used to fill a cartilage defect (Figure 1-13). The plugs are usually harvested from the peripheries of both femoral condyles at the level of the patello-femoral joint and introduced as a mosaic to fill the defect. It is a one stage procedure and does not carry the risk of an immunological graft rejection (Smith *et al.*, 2005).

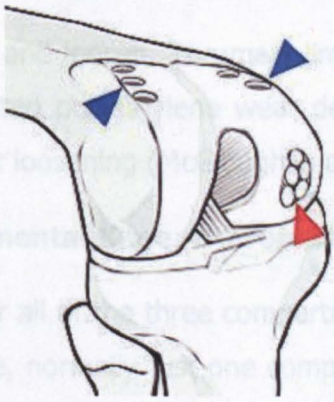

Figure 1-13: Schematic representation of mosaicplasty. Image taken from http://www.pathology.unibe.ch/Forschung/osteoart/osteoart.htm

1.7.6 Total Knee Arthroplasty

Total knee arthroplasty (TKA) is generally considered the end-stage treatment option, when there is severe damage to the cartilage and subchondral bone and no other treatment option is suitable. TKA involves replacing the diseased and painful joint

surfaces of the knee with highly polished metal alloys and ultra high molecular weight polyethylene (UHMWPE), which are shaped to allow motion and function of the knee. They generally contain three or four main parts, the femoral component, tibial tray, tibial insert (bearing component) and in some designs, a patellar button. One design of total knee replacement, manufactured by DePuy is shown in Figure 1-14.

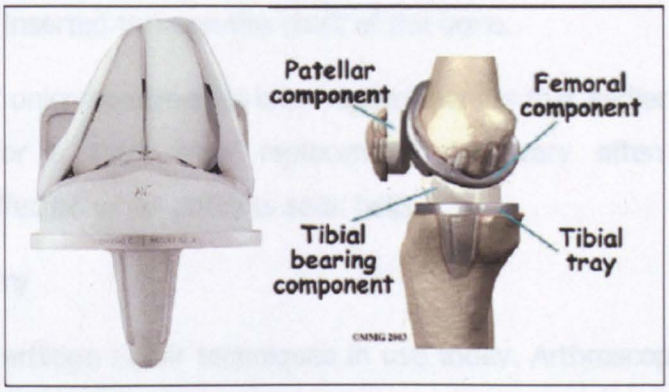

Figure 1-14: DePuy Low Contact Stress (LCS) Mobile Bearing Total Knee.

The LCS mobile bearing allows the important rotation component to human knee motion, which is not included in many other fixed bearing designs. In most designs, the tibial components of the prosthesis are fixed together and this puts additional stress on the polyethylene spacer component and underlying bone. In the LCS total knee, the metal tibial tray allows the tibial bearing component (the polyethylene spacer) to rotate within, as the femoral component rotates.

Over time, implants can wear and loosen. The main limiting factor to the longevity of TKA's is wear, as the associated polyethylene wear debris may produce an adverse tissue reaction and subsequent loosening (McGloughlin and Kavanagh, 2000).

1.7.7 Unicompartmental Knee Arthroplasty

Osteoarthritis can affect any or all of the three compartments of the knee joint. During the early stages of the disease, normally just one compartment is affected. Symptoms may not be severe enough to justify surgical intervention, but if they are it is an attractive option to merely replace the damaged part and leave the healthy compartments alone (Newman, 2000). This may prevent the onset of multi-compartmental arthritis. Unicompartmental knee arthroplasty (UKA) is advantageous in terms of shorter recovery times and overall function and range of movement obtained (Newman *et al.*, 1998). In a study by Murray and colleagues the results of a ten year follow-up showed that with a congruent mobile bearing UKA, 97%

survivorship was obtained (Murray *et al.*, 1998). This result compares favourably with the best survivorship studies of total knee replacements (Newman, 2000).

The tibial component is made from polyethylene and the femoral component is usually metallic, made from cobalt chrome. Generally, the components are fixed in place with cement but occasionally designs are constrained using long-stemmed components, in which the stem is inserted through the shaft of the bone.

A disadvantage of unicompartmental knee replacement is that earlier detection of OA is required, than for a total knee replacement and very often more than one compartment is affected when patients seek help.

1.7.8 Summary

There are many cartilage repair techniques in use today. Arthroscopic techniques, ACI and mosaicplasty are all used in clinical practice for the treatment of chondral injuries. Continuous review and modifications to these techniques are made and there are always two main factors to be considered with cartilage repair techniques: the first one is filling the defect with a material that is similar in mechanical properties to articular cartilage; the second consideration is how to consolidate the material with the native articular cartilage. Even when the defect is very small, failure to fill it adequately will lead to further degeneration, which is likely to lead to OA (Beris *et al.*, 2005).

Lately, researchers have been keen to produce a tissue with hyaline cartilage properties, with the ability to consolidate in the native surrounding articular cartilage. The formation of hyaline cartilage may be achieved in the future with the use of autologous cultured cells in conjunction with an appropriate scaffold. The fast developing area of tissue engineering may provide promising solutions for the treatment of chondral defects in the future. Possibilities include mesenchymal stem cells, embryonic stem cells, resorbable biomaterials and growth factors. It is necessary to develop methods to detect and monitor slight changes in cartilage metabolism and identify the joint changes which occur prior to articular cartilage loss. This will make it possible to detect the early signs of OA, when tissue engineering and biological therapies may be most beneficial and have the greatest potential for preventing progression of disease (Buckwalter *et al.*, 2000).

However, in the meantime TKA can offer patients remarkable relief from pain and improved mobility and functionality, albeit it is not a life-long solution and revisions are

rarely as successful or as simple as the primary. UKA is an attractive option where only one compartment of the knee is diseased.

Hemiarthroplasty and cartilage defect repair with synthetic biomaterials, are two potential cartilage substitution therapies that may be particularly beneficial for the younger patient. These therapies will be focused on throughout this project and therefore, they will be discussed separately, and in more detail in Sections 1.8 and 1.9.

1.8 Hemiarthroplasty

The treatment of knee osteoarthritis (OA) in the young and active patient poses a difficult problem. OA is a progressive, irreversible disease which normally requires surgical intervention. Unicompartmental knee arthroplasty (UKA) and total knee arthroplasty (TKA) are commonly performed therapies in patients aged 65 years and above. The treatment of patients in their fifties and younger poses a very difficult problem, since TKA and UKA are contraindicated for patients below 65 years of age because the implants generally have a limited life-span in comparison to that of younger patients. Furthermore, higher activity levels amongst younger patients add to the demands on the prostheses. While TKA and UKA offer relief from pain and can restore function, they often compromise the results of future revisions in the longer term, and revision would be inevitable for most young patients. It is clear that there is an alarming lack of options for the young and active osteoarthritic patient.

Alternatives to UKA and TKA are hemiarthroplasty and knee spacer technology (Figure 1-15), which preserve more bone stock for potential revisions and are thus more suited to the younger patient. However, there has been varied success with these interventions to date.

The McKeever metallic hemiarthroplasty is one such prosthesis, made from Vitallium, with a shape that roughly simulates that of the tibial plateau, with a slightly concave and very polished superior surface. There were some promising results with this prosthesis in the 1980's. In two separate studies good to excellent results were reported in 70% and 72% of knees, at an average follow up period of 8 years and 5 years, respectively (Emerson and Potter, 1985; Scott *et al.*, 1985). In a more recent study, Springer and colleagues concluded that the McKeever tibial hemiarthroplasty was a reasonable surgical option for patients where osteotomy, UKR and TKR were contraindicated due to patients being too young, active or obese (1% of patients). Out

of a total of 24 knees, 13 were revised at an average of 8 years follow-up (0.5 to 17 years). All failed implants were successfully revised to a UKA or TKA, without complication, due to the preservative nature of the hemiarthroplasty. The authors concluded that due to the bone-sparing nature of tibial hemiarthroplasty it is an attractive, although perhaps temporary treatment option for suitable patients (Springer *et al.*, 2006). In the three aforementioned studies degeneration of the opposing femoral cartilage and onset of OA in other compartments was the most common cause of failure. Additionally, some clinical studies of hip hemiarthroplasty have shown that erosion of the opposing articular cartilage (AC) is a considerable late complication (D'Arcy and Devas, 1976; Amstutz *et al.*, 1994).

Figure 1-15: The McKeever and UniSpacer tibial hemiarthroplasty protheses (a) The McKeever hemiarthroplasty design, which is made from Vitallium and comes in thicknesses ranging from 2 mm to 15 mm. (b) The UniSpacer design, which is a cobalt-chrome self-centred tibial spacer device.

The UniSpacer™ is a cobalt-chrome self-centred tibial hemiarthroplasty device (or spacer), used in the treatment of isolated medial compartmental knee OA. This design has been the subject of much debate. A study reported short-term success (21% revision rate at 1 year) with this design (Hallock and Fell, 2003), while others have found little success and do not recommend this device to patients (Sisto and Mitchell, 2005; Bailie *et al.*, 2008).

1.9 Cartilage Defect Repair

Although ACI (Section 1.7.4) and mosaicplasty (Section 1.7.5) are commonly performed clinically with good success rates, they are not without disadvantages. ACI

involves two incisions and two surgeries, which increases the risk of infection and mosaicplasty can have complications associated with harvest site degeneration. Interest has begun to shift towards synthetic substitutes to replace damaged cartilage. Similar to cylindrical osteochondral plugs used to fill cartilage defects, the implantation of synthetic plugs is a possible approach to treat damaged cartilage, in the hope of preventing further degeneration and OA. When designing a biomaterial or tissue engineered plug for cartilage replacement, there are several important factors to consider: biocompatibility; osseointegration; wear and fatigue resistance; friction and lubrication properties; and mechanical properties. One such device to recently arrive on the US market is called OsteoBiologics (Agrawal and Stinson, 2007).

Despite its potential in the future, tissue engineering of articular cartilage is a relatively recent area of interest and its long-term performance has yet to be investigated. However, there have been many animal studies and a few clinical trials investigating biomaterial cartilage substitutes. These therapies are discussed in the following sections.

1.9.1 Tissue Engineered Cartilage

There is considerable interest in the development of techniques to regenerate or reconstruct damaged articular cartilage. The three primary constituents of a tissue-engineering approach are cells, a scaffold for delivering and/or retaining cells and bioactive factors. The main design considerations include how to integrate with the surrounding surfaces, the biomechanical properties and durability of the tissue, biocompatibility and how to align the construct with the surface of the native healthy tissue (Reinholz *et al.*, 2004).

The ultimate success for tissue-engineered cartilage would be the complete replication of the embryonic development of an articular surface. However, the required environment for this (growth factor cytokine milieu and mechanical stimulus) is no longer present in the adult joint. Furthermore, the precise sequence of events which leads to the formation of articular cartilage is not completely understood, which means it is not possible to completely duplicate the process *in vitro.* It is critical that tissue engineered cartilage has similar biomechanical and tribological properties to native cartilage. Furthermore, tissue engineered cartilage should have other important characteristics of cartilage incorporated such as surface integrity and the ability to integrate with the host tissue. Some recent *in vitro* experiments have shown that the

friction and wear characteristics of tissue engineered cartilage were inferior to that of native cartilage (Reinholz *et al.*, 2004; Morita *et al.*, 2006; Plainfosse *et al.*, 2007).

One challenge which has been highlighted as one of the causes of these inferior mechanical properties, is that the isolated chondrocytes grown in culture usually do not amass enough extracellular matrix, resulting in a weak matrix compared to native tissue. Waldman *et al.* found that chondrocytes stimulated with intermittent compression or shear, during culture were markedly thicker and had accumulated more extracellular matrix compared with the unstimulated controls. However, shear stimulation had a greater effect than compression and was recommended by the authors for future chondrocyte culture experiments (Waldman *et al.*, 2003). This finding was supported by another study, in which surface motion during culture increased the expression of surface zone proteins and hyaluronan (Grad *et al.*, 2005). In this same study, axial compression had no effect.

1.9.2 Biomaterial Defect Repair - Animal Studies

Several animal studies have examined different biomaterials and designs for cartilage defect repair. Kawalec *et al.* evaluated the response of surgically created defects to pyrolytic carbon and cobalt chromium alloy plug-like implants, when implanted in the femoral condyle of adult beagles for one year. There were no adverse inflammatory responses and there was increased subchondral bone formation and fibrocartilage regeneration beneath the defect, for both implants. However, on the opposing tibial surface, histological analysis showed surface cracks on 14% of those articulating with the pyrolytic carbon and on 100% of those articulating with the stainless steel (Kawalec *et al.*, 1998). In a similar study, extensive damage to the opposing tibial surface was found after only four weeks, when using cobalt chromium and oxidised zirconium plug-like implants in the femoral condyles of rabbits (Custers *et al.*, 2007b).

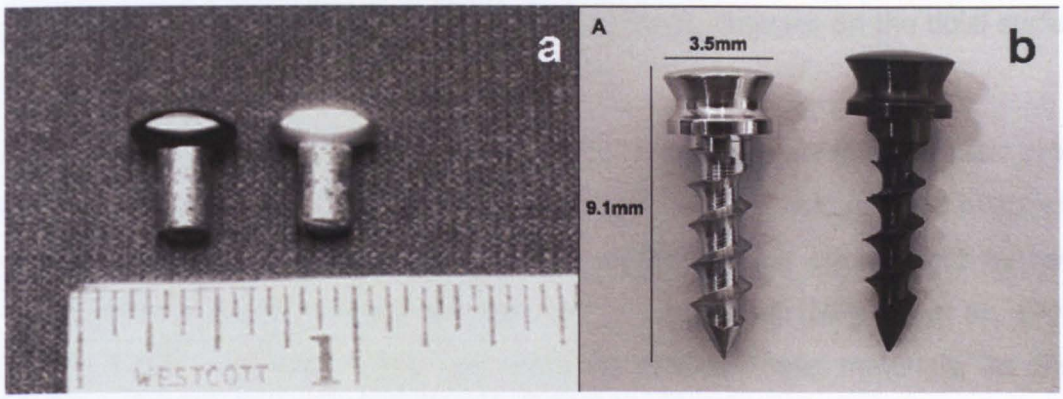

Figure 1-16: Metal defects used as articular cartilage substitutes (a) pyrolytic carbon and cobalt-chromium alloy implants with polished heads and stems coated in porous, commercially pure titanium (Kawalec *et al.*, 1998); (b) cobalt chromium (left) and oxidised zirconium (right) tack implants (Custers *et al.*, 2007b).

Undoubtedly, the damage to the opposing tibial surface in these studies was due to articulation with the metal plugs. This damage was probably accelerated because the substitute materials were single-phase materials and the overall biphasic and lubrication properties of the natural joint were compromised leading to degeneration of the cartilage. The stiff surface properties and high friction coefficients associated with these materials would have led to cartilage degeneration.

Other studies have looked at composite osteochondral devices (CODs), which comprise of two different biomaterials to substitute the cartilage and subchondral bone, in an attempt to match the properties of each. A COD used in a study by Ushio *et al.* was composed of polyvinyl alcohol hydrogel acting as artificial cartilage and a titanium fibre mesh acting as porous artificial bone. This COD was used for partial hemiarthroplasty in canine femoral heads for one year. Control implants made from UHMWPE and alumina ceramics, of the same geometry were implanted. After one year, the COD device demonstrated superior ability compared to the control implants, both in terms of preserving the opposing acetabular cartilage and its quick osseointegration (Ushio *et al.*, 2003). Chang *et al.* investigated the osseointegration and shock-absorbing properties of a COD (also consisting of a titanium fibre mesh and PVA hydrogel) implanted in canine femoral condyles and in a second study they examined the time dependent changes of the tibial surfaces (Chang *et al.*, 1997; Chang *et al.*, 1998a). They found abundant subchondral bone penetration through the open-pore structures, resulting in restoration of the shock-absorbing function. They found no damage to the opposing tibial cartilage after 24 weeks. In contrast, COD's made from harder materials

(alumina and titanium) showed significant pathologic changes on the tibial surface and meniscus at only 8 weeks (Chang *et al.*, 1997).

PVA hydrogels are known for their high water content, they display biphasic properties and are biocompatible. The mechanical properties of PVA hydrogels are relatively close to those of cartilage and these relatively new materials are thought to have the potential to be a very suitable cartilage defect substitution (Noguchi *et al.*, 1991; Oka *et al.*, 2000). However, work continues to develop these materials, as they are generally weaker than natural cartilage, the permeability is often too high and their biphasic properties are inadequate in comparison to healthy cartilage.

1.9.3 Salucartilage™ - Clinical Trials

Salucartilage™ is a biocompatible synthetic substitute made from Salubria® (hydrogel containing water in proportions similar to natural articular cartilage), designed to replace defective cartilage. It contains water in similar proportions to native articular cartilage. Material characterisation testing found Salucartilage™ to withstand normal and shear loading forces typical of those experienced by human cartilage in the knee and as a biphasic material, it recovered to nearly original form after load removal. Coefficients of friction between plates of Salucartilage™ and cadaveric condyles were found to be 0.065 ± 0.029, which was within range found by McCutchen for cadaveric cartilage (0.02-0.35) (McCutchen, 1962).

Figure 1-17: Salucartilage™, a synthetic substitute designed to replace defected cartilage. Image from Salumedica patient guide: http://www.salumedica.com

However, only short-term success was noted in some clinical trials using this implant and implant dislocation was reported at less than 1 year follow-up (Falez and Sciarretta, 2005; Meyer *et al.*, 2005; Lange *et al.*, 2006). Inadequate connection to the bone, with a high risk of dislocation was indicated as a serious risk with this implant (Lange *et al.*, 2006) and Meyer *et al.* concluded that this device and method was not fully developed (Meyer *et al.*, 2005).

1.10 Tribological Testing of Articular Cartilage

As discussed in Section 1.5 synovial joints operate under a highly complex lubrication regime. Biphasic lubrication plays an important role as well as conventional engineering hydrodynamic and boundary surface lubrication mechanisms. Additionally, synovial joints are subjected to a range of loading conditions during normal daily activities. Loads passing through the knee and hip can reach several times body weight, particularly during more strenuous activities such as stair-climbing or stumbling (Bergmann *et al.*, 1993). In the design of a hemiarthroplasty or cartilage defect repair implant, it is crucial to understand the tribology of the natural joint as well as that of the hemiarthroplasty bearing.

The wear and degradation of the biomaterial/cartilage interface is very important in the development of hemiarthroplasty or cartilage defect repair. Numerous studies have investigated the friction and wear of articular cartilage (native and treated) articulating against itself and against different biomaterials, with different loading conditions and with different lubricants/viscosupplements. These experiments have mainly been simple geometry pin-on-plate or sphere-on-disc geometries (Freeman *et al.*, 2000; Park *et al.*, 2003; Krishnan *et al.*, 2005; Katta *et al.*, 2007; Northwood and Fisher, 2007; Northwood *et al.*, 2007; Katta *et al.*, 2008d). In order to develop a hemiarthroplasty or defect repair it is important to gain an in-depth understanding of how this implant would function tribologically in the natural joint.

Bell *et al.* demonstrated that HA could be an effective lubricant, reducing static friction, under continuous loading which caused a depletion of the intrinsic biphasic lubrication mechanism (Bell *et al.*, 2006). The frictional response of cartilage pins articulating on cartilage plates (from skeletally mature bovine patella-femoral grove), under static conditions was investigated with and without (control) the addition of HA to the lubricant (PBS). In the second part of this study, HA was found to be less effective under dynamic conditions. It should be noted that under dynamic conditions using the control lubricant the friction was low due to replenishment of the biphasic lubrication mechanism. With the addition of HA to the lubricant the friction was slightly higher. It is possible that the HA was dynamically displaced from the small contact region or could not support the load (Bell *et al.*, 2006). This highlights the need for anatomical whole joint simulations to allow testing with more physiologically relevant geometries, as well as loading and motion.

Forster and Fisher examined the frictional response of cartilage pins (from bovine condyles and patella-femoral groves), against a metal plate under mixed lubrication conditions. Pins with diameters of 9 mm and 3 mm were tested under a load of 30 N, resulting in contact stresses of 0.5 MPa and 4.0 MPa respectively. It was found that the coefficient of friction was slightly smaller at 4 MPa (3 mm pin), than at 0.5 MPa (9 mm pin), after 45 minutes of loading (Forster and Fisher, 1996). In a similar tribological study of bovine cartilage pins articulating with cobalt chromium plate, tested at 3.5 N and 30 N, higher frictional coefficients were found at the lower level contact stress (Pickard *et al.*, 1998a). In these two studies however, a cartilage pin articulated against a metallic plate, meaning the pin was constantly loaded and there was no replenishment of biphasic properties. However, had the plate been a cartilage counterface, rehydration would have taken place during unloading, resulting in a much lower frictional coefficient. Furthermore, in Pickards study, degradation of the articular cartilage had no effect on the frictional properties of the cartilage, showing that altering the biphasic properties of the tissue did not necessarily alter its frictional response under the conditions considered. The complex biphasic biotribology of articular cartilage makes it difficult to predict the effect of the changes in the tribological conditions on subsequent degradation and wear of articular cartilage. Katta *et al.* studied the frictional response of a cartilage against cartilage contact in a pin on plate experiment, under both static and dynamic conditions. In both cases, it was found that the frictional coefficient decreased, when the applied contact stress was increased from 0.2 MPa, to 0.3 MPa and to 0.4 MPa (Katta *et al.*, 2007). The experimental rig used in Katta's study, however, was limited to a maximum applied contact stress of 0.4 MPa, when using a 9 mm cartilage pin. It has yet to be investigated if this decrease in friction continues when the contact stress is increased above 0.4 MPa, or at what physiologically relevant levels of stress does this trend stop?

It is generally known that the coefficient of friction decreases with increasing load in compliant bearings. Gong and Osada found this trend of decreasing friction with load, using non-biological polymer gels. They found that the frictional force and its dependency on load, differed substantially depending on the surface properties of the articulating surfaces (Gong and Osada, 2002). However, for biphasic bearings, there are two further possible explanations for this decrease in frictional coefficient, upon increasing the applied contact stress. Firstly, the application of higher levels of contact stress may result in the flattening of surface asperities, increasing the smoothness of

the articulation, hence reducing the friction. Ateshian offered this as a possible reason for decreasing friction in a study of cartilage plugs against a glass plate, under increasing load (Ateshian *et al.*, 2003). A second explanation is that boundary lubricant molecules which enhance frictional properties between cartilaginous surfaces are squeezed into the contact zone under the applied load, by a weeping mechanism (McCutchen, 1959; McCutchen, 1962). The amount of these molecules exuded into the contact zone may be dependent on the magnitude of the applied load. Lewis and McCutchen used flame photometry to measure the amount of fluid exuded from cartilage surfaces onto filter paper, when pressed with a glass slide. Where only slight contact was made, the amount of fluid was insignificant, with larger loads the amount of fluid collected increased and when physiologically relevant loads were applied, the amount of fluid collected was calculated to be sufficient enough to form a layer between 15-30 μm in thickness over the contact area (Lewis and McCutchen, 1959). It is likely that with increasing applied load, both surface smoothening and boundary lubricant exudation play a role in the reduced frictional coefficient, however, it is not yet clear which explanation plays the most important role or in what proportions? It is important to note that while the coefficient of friction decreases with increasing load, the actual friction force (shear stress on the interface) increased with increasing load. Intuitively, this was expected. However, in these cartilage models, the friction shear stress did not increase proportionally to increased load as is expected for rough dry engineering surfaces (with a constant coefficient of friction). In future, when load is a variable it is important to consider friction force as well as frictional coefficient.

Krishnan *et al.* measured the frictional coefficient and the interstitial fluid support simultaneously, while sliding bovine cartilage against glass. An inverse linear correlation was found between the frictional coefficient of interstitial fluid support, showing fluid load support to be a primary mechanism in the regulation of the frictional response of cartilage (Krishnan *et al.*, 2004b).

Other studies have looked at the tribology of cartilage and potential cartilage substitution materials, mainly hydrogels. Freeman *et al.* looked at the friction and wear of stainless steel spheres reciprocating on flat poly(HEMA) (hydrogel) disks. No correlation was found between friction and wear. The data fell into different categories: low wear and high friction; low friction and low wear; moderate friction and low wear; and high friction and low wear. However, for the different test variables (applied load, lubrication, hydrogel cross-linking density, hydrogel hydration) a sample

size of only two was used. Furthermore, the lack of physiological relevance in this study must be noted, neither bearing material was biological and water was used as the lubricant (Freeman *et al.*, 2000).

Northwood *et al.* investigated the friction and wear of cartilage substitution biomaterials against articular cartilage, using a simple geometry pin on plate rig, with cartilage pins loaded against a range of single-phase and biphasic materials. All of the single-phase materials showed a steady rise in friction which was dependent on the loss of interstitial fluid load support from the opposing cartilage. The biphasic materials produced a marked reduction in frictional coefficient, probably due to the ability of these materials to maintain an element of fluid load support by rehydration during the unloaded periods, however, it was not as low as native cartilage. There was less damage to the pins articulating with the biphasic materials, than to the pins articulating with the single phase materials (Northwood *et al.*, 2007). This study demonstrated the importance of biphasic properties of potential cartilage substitution biomaterials and provided an understanding of the tribological properties of these materials in comparison to native cartilage and single-phase materials. However, whole joint simulations are required to examine other important aspects of cartilage substitution such as how the substitute operates in the anatomical environment, under physiological loads and motion, as well as examining different fixation methods, graft heights and the use of composites to incorporate the mechanical properties of bone.

In summary, simple geometry tribological tests are valuable in many ways. They can give a good understanding of the tribological properties of cartilage and cartilage substitution biomaterials, allow the measurement of cartilage against known engineering materials and wear debris analyses and biochemical assays are easily performed following wear testing. However, there are a number of important questions which cannot be answered by such experiments, related to key tribological and biomechanical system variables, which are crucially important in a clinical application:

1. How much wear or degradation would a biomaterial implant impose on the opposing cartilage surface? How would the biomaterial interact with the meniscus in the knee, a very important structure biomechanically but often ignored in tribological experiments?

2. How will the implant perform under physiological loads and motions? What are the effects on stress and tribology when using different implant geometries?

3. What type of fixation methods are required to ensure the implant is not disrupted or dislocated?

Many of these questions could be answered using an anatomical joint simulator. The development and use of a tribological simulation of the medial compartmental knee will be the main focus of this thesis.

1.11 Wear Analysis of Articular Cartilage

Wear is generally measured as either the mass or volume of material removed from the interacting surfaces. However, it is very difficult to measure the wear of biological tissues such as cartilage due to their high water content and swelling properties. Most biotribology research to date has focused on determining the lubrication mechanisms of synovial joints and in comparison very few studies have focused on joint wear. Greater knowledge of wear mechanisms and the initiating factors of osteoarthritis are required, both clinically and in research. The following sections discuss the methodologies which have been implemented to measure wear of articular cartilage to date as well as some potential future methods.

1.11.1 Biochemistry and Histology

Biochemical assays can be used to quantify the amount of collagen or GAGs in the lubricant before and after wear experiments (Lipshitz *et al.*, 1975). Lipshitz *et al.* measured the wear and wear rates of cartilage by measuring the collagen and hydroxyproline content of the lubricant and solid wear debris, after in vitro wear tests performed with cartilage plugs rubbing with stainless steel plates, under varying levels of load, with PBS used as the lubricant. Wear rates were found to increase with increasing levels of load and at all levels of loading, the wear rate was found to be higher initially, decreasing with time and finally reaching a steady state.

A non-quantitative variation of this is histological assessment, in which various staining techniques can be used to visualise collagen, GAGs or chondrocytes. Surface damage or alterations can be identified. However, this method is destructive and non-quantitative.

1.11.2 Wear debris analysis

Wear debris analysis involves the filtration of wear debris from the lubrication medium and subsequently analysing the composition, mass or volume of the filtrate. SEM or

ESEM can be employed to analyse the composition or physical features of the wear particles (Graindorge and Stachowiak, 2000). Numerical techniques have also been employed by Stachowiak to characterise the shape of wear particles using boundary fractal dimension, shape factor and convexity (Stachowiak et al., 2006). The morphology of wear particles in a mechanical or biological system reflects wear processes involved in their formation. Hence, information about wear processes occurring in joints can be obtained through the studying wear particle morphology.

Although wear debris analysis is a straightforward and useful technique, it may not be useful where cartilage wear is purely biochemical or in situations where cartilage material is displaced, rather than removed.

1.11.3 Surface topography analysis

The use of contact and non-contact (laser) profilometers and coordinate measuring machines (CMM) are often successful methods for testing changes in surface topography as well optical microscopy techniques (such as SEM, ESEM, TEM and AFM) (Forster and Fisher, 1996; Jurvelin *et al.*, 1996; Kumar *et al.*, 2001; Krishnan *et al.*, 2004a; Park *et al.*, 2004; Northwood *et al.*, 2007; Northwood and Fisher, 2007).

1.11.4 Imaging

There have been a number of imaging modalities used in the clinic for the last few decades such as computed tomography (CT), ultra-sound imaging and magnetic resonance imaging (MRI). In recent years, some imaging techniques have been developed and refined, making it possible to achieve very high resolutions, particularly on small-sized samples. This is becoming increasingly useful in research, both for *in vitro* laboratory studies and small animal studies. One of the most commonly used imaging modalities clinically and recently in research is MRI. Some recent research on MRI and micro-MRI will be discussed in more detail in the following section and in later Chapters, applications of micro-MRI will be discussed.

1.12 MRI and Micro-MRI

MRI is probably the most widely used and accepted clinical imaging/diagnostic tool for osteoarthritis. MRI is based on the natural magnetisation that is induced in the human body when it is placed in a scanner. Human tissues including bone and cartilage contain plentiful hydrogen nuclei or protons, which are aligned with the main field of

the scanner (known as z-direction). When a radio frequency electromagnetic pulse excites these protons, they acquire energy (transverse magnetisation) and resonance. When the pulse ceases the protons return to their pre-excited state; this is the T_1 relaxation time measured as the recovery time (TR). The T_2 relaxation time refers to the time for the transverse magnetisation to disappear, represented by the echo time (TE). Moving protons in the tissue generate an electric current that is measured as the MR signal and the strength of the magnetisation depends on the proton density of the tissues (Conaghan, 2006; McRobbie *et al.*, 2003).

Achieving high-quality MRI images depends the choice of pulse sequence and the timing choices (TR and TE). The sequence contains radiofrequency pulses and gradient pulses which have carefully controlled durations (McRobbie *et al.*, 2003). As the scan duration is so critical for patient health and safety, sometimes contrast agents are used to effectively change the image intensity (and hence contrast between the tissues) and improve the specificity of MRI scans (Burstein and Gray, 2003; McRobbie *et al.*, 2003). Commonly used magnets in the clinical field are between 1.0 - 3.0 Tesla in strength. Clinical MRI studies of osteoarthritis have mainly been confined to assessing cartilage volume and thickness and have not really been able to assess the health of the cartilage. Recently high resolution MRI scanners, with strengths between 7.0 – 11.0 Tesla have been developed, which have allowed extensive studies of cartilage morphology, composition and function (Burstein and Gray, 2003; Mosher and Dardzinski, 2004; Nieminen *et al.*, 2004; Nissi *et al.*, 2004) and a number of techniques have been used.

The orientation of collagen fibres influences the T_2 relaxation parameter, as does the amount of collagen and its molecular structure. As collagen is the most abundant macromolecule in cartilage, it is the main determinant of T_2 relaxation (Burstein and Gray, 2003). Mosher and Dardzinski distinguished between the appearance of the diffuse increase in T_2 in aging cartilage and the focally increased T_2 observed in damaged cartilage (Mosher and Dardzinski, 2004).

One of the most widely used contrast agents is Gd-DTPA^{2-}, commercially known as Magnevist® (Berlex, Wayne, New Jersey). This agent is negatively charged. GAG's in cartilage possess negatively charged carboxyl and sulphate group side chains. Therefore, when Gd-DTPA^{2-} penetrates into cartilage, it distributes in higher concentration in areas of cartilage where the GAG concentration is low, so the concentration of Gd-DTPA^{2-} is inversely proportional to the amount of GAG's. By

determining the distribution of Gd-DTPA^{2-}, the GAG concentration can be quantified. This technique is known as dGEMRIC (delayed Gadolinium Enhanced MRI of Cartilage). The dGEMRIC technique to measure GAG concentration has been shown to correspond well with the more traditional and standardised techniques to measure GAGs, biochemistry (Bashir *et al.*, 1999) and histology (Trattnig *et al.*, 1999).

Proteoglycan- and collagen-sensitive MRI parameters (T_2, T_1 and Gd-DTPA-enhanced T_1 mapping) have been found to correlate well with structural and compositional properties of healthy and degenerated bovine articular cartilage, as well as with mechanical properties of degenerated bovine cartilage (Nieminen *et al.*, 2004, Nissi *et al.*, 2004). Despite the fact that some of these studies have been performed at higher field strengths than is clinically possible, these *in vitro* experiments provide new information that is close to cartilage degeneration *in vivo*. These studies allow quantification of GAG and collagen content, which cannot yet be obtained from clinical scans. In the future perhaps after further human *in vitro* and human *in vivo* studies, it may be possible to apply these techniques in the clinic, with appropriate sensitivity and specificity.

One of the most noteworthy recent developments is diffusion tensor imaging (DTI), which is a technique that quantifies the restricted diffusion of water in samples. In articular cartilage the diffusion of water in the very ordered collagen fibres is anisotropic, predominately along the fibre axis. In tissues such as cartilage, in which diffusion is anisotropic, the self-diffusion of water protons must be characterised tensor, which is a 3 x 3 matrix that describes the magnitude and direction of the diffusion in a 3-dimensional space (Meder *et al.*, 2006). The fractional anisotropy (FA), a scalar measure of the degree of anisotropy, can be calculated from this tensor and the principal direction of diffusion is given by its eigenvector. Filidoro *et al.* used DTI to analyse the structure of articular cartilage in a 9.4 Tesla MRI scanner. The mean diffusivity, FA and eigenvector projection maps (images) showed variations through the depth of the cartilage, which agreed well with the known macrostructure of cartilage. Eigenvectors were found to be promising for characterising the zonal structure of cartilage, and the tangential and radial zones and a zone of transition were depicted, suggesting that eigenvector analysis correlates well with the alignment of collagen fibres (Filidoro *et al.*, 2005). Potentially, this technique could be very important clinically in the early detection of OA, but as mentioned before, these experiments were performed using a magnet too strong for clinical application.

(Helmer *et al.*, 2006) subjected rabbit tendons to tensile loading and observed the water movements using NMR. The distribution of the internal water in the tendons was measured with the use of a one-dimensional proton-density map, which was collected along a radial line oriented transverse to the tendon's long axis. To directly observe the deformation and fluid flux in cartilage under an axial dynamic load would be a very useful technique.

1.13 Research Scope

Cartilage substitution techniques such as hemiarthroplasty and cartilage defect repair are very attractive treatment options for the young and active patient. These treatment options could prevent or at least delay the need for a total knee replacement affording the patient improved comfort, functionality and satisfaction. To date there has been varied success with hemiarthroplasty and little to no success with synthetic cartilage defect repairs. It is not clear if these interventions reduce the local biomechanics and biotribology necessary for the normal joint to function. Developing these treatments also requires the development of *in vitro* models to evaluate their biomechanical, tribological and biochemical effects in natural joints.

1.13.1 Aims and Objectives

This project is designed to explore the biomechanical and tribological effects of cartilage substitution techniques. As mentioned previously, although a lot of research has been conducted in the area of cartilage substitution biomaterials, very little information exists about *in vitro* functionality of these materials using whole joints and physiological loads and motion. This project aimed to develop a tribological simulation of the medial compartmental bovine knee joint, employing a pendulum friction simulator to apply physiologically relevant loading and motion. This tribological simulation will be used to explore a number of treatment options:

1. The model will be used to examine the effects of meniscectomy on friction and wear of cartilage, in comparison with that of the intact, healthy medial compartmental knee.

2. To examine the effect of hemiarthroplasty the entire tibial surface will be replaced with a stainless steel plate. The effect of conformity of the hemiarthroplasty bearings on contact stress, and hence friction and wear, will be examined by varying the conformity (radius) of the stainless steel plates.

3. The tribology of cartilage defect repair will be examined by removing a defect or plug of cartilage-bone from the femoral condyle and replacing it with a cartilage-bone plug (negative control), a stainless steel pin (positive control) and hydrogel pins of differing material properties.

This thesis is divided into chapters based on these aims, except for the next chapter which describes the commonly used materials and methods used in the project, and the final chapter which provides an overall discussion of the results of each study, limitations associated with the work and potential areas of future work.

Chapter 2. Materials and Methods

This chapter will describe the general materials, methodologies and equipment used throughout this PhD thesis, as well as calibration and validation procedures. Specific information will be presented in corresponding chapters.

2.1 Materials

2.1.1 Phosphate Buffered Saline

Phosphate buffered saline (PBS) was used throughout this project for storage of cartilage specimens and irrigation during dissection procedures. PBS tablets were purchased from MP Biomedicals (www.mpbio.com). PBS was prepared as per the manufacturers instructions: one tablet was dissolved in 100 ml of distilled water. The PBS tablets were composed of inorganic salts as shown in Table 2-1.

Component Inorganic Salts	Concentration (mg/litre)	Mol. Wt. (DA)	Molarity (mM)
Potassium chloride [KCl]	200.00	74.55	2.68
Potassium phosphate monobasic [KH_2PO_4]	200.00	136.09	1.47
Sodium chloride [NaCl]	8000.00	58.44	136.89
Sodium phosphate dibasic [Na_2HPO_4]	1150.00	141.96	8.10

Table 2-1: Formulation of PBS.

2.1.2 Bovine Serum

Newborn calf serum was purchased from Harlan Bioproducts for Science (Catalogue number BT-9501-500). It had low hemoglobin, low endotoxin levels and excellent growth-stimulating properties. The protein concentration of this newborn calf serum is shown in Table 2-2.

Protein Profile	Concentration (grams/deci-litre)
Total Protein	5.0-8.5
Albumin	~4
α-Globulin	~0.7
β-Globulin	~0.6
γ-Globulin	~0.7

Table 2-2: Protein composition in newborn calf serum.

For all friction experiments 25% (v/v) bovine serum in PBS was used as the lubricant, because of its similar protein concentration (16 – 18 mg/ml) to normal synovial fluid (approximately 20 mg/ml) (Wang *et al.*, 1998). In a large container 0.5 litres of newborn calf serum was mixed with 1.5 litres of PBS. After stirring thoroughly, the 25% (v/v) serum in PBS was divided into 100 ml containers and frozen at -20° C until required.

2.1.3 PMMA bone cement

PMMA bone cement, from Acrylic Denture Materials, was used for fixing cartilage-bone specimen in jigs for the friction simulator. It was purchased from WHW Plastics (Hull, UK) in the form of a powder (Cold Cure) and a liquid monomer (Rapid Repair Liquid), which were prepared as per the manufacturers instructions, with a powder to liquid ratio of 2:1. The mixing and curing of the cement was carried out in a fume cupboard.

2.2 Harvesting of the Femoral Condyle

All experiments were performed using bovine femoral condyles from skeletally mature 18-24 month old animals. Skinned bovine femurs were obtained from a local abattoir, between 24-48 hours after slaughter. Almost whole medial femoral condyles were dissected from the bovine femur. The joint capsule, ligaments, tendons and the patella were carefully removed using a scalpel and tweezers. Next, the femur was examined to ensure that the medial condyle was both free from damage and

"normal" in appearance. Normal was defined as white in colour, glossy, and firm to touch, without any signs of visible damage. Any joints not meeting these criteria were disposed of. At all times during the dissection procedure the cartilage was kept hydrated with PBS. The femur was mounted in a specially made clamp so that the condyles were facing upward as shown in Figure 2-1.

Figure 2-1: Photograph of a condyle clamped with the femoral condyles facing upwards during dissection. A saggital section was cut with a hacksaw.

The medial condyle was harvested by making two separate cuts in an approximately saggital plane, approximately 15-20 mm apart and spanning the crown of the condyle Figure 2-1. The cuts was made to a depth of at least 70 mm as shown in Figure 2-2a.

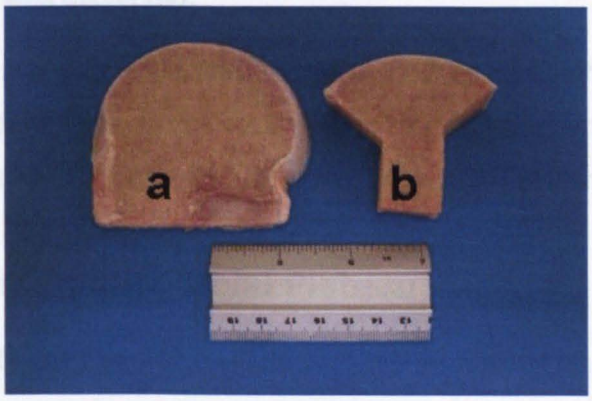

Figure 2-2: Photograph of a saggital section cut from the condyle. (a) shows the initial cut, which is 70mm from cartilage surface to cut surface and 15-20mm in thickness. (b) a wedge-shaped specimen is cut from the initial specimen, for potting in the friction simulator jigs.

The large condylar specimen was then cut into the wedge shape shown in Figure 2-2b, using a hacksaw and a vice grips. It was useful to mark the cut out shape into the bone. To accurately cut the wedge shape the condyle was firstly matched by eye

to a series of CAD templates of known radius (Figure 2-3) to identify a section of the flexion facet of the condyle crown that was a true circle and to determine the approximate radius of curvature (say ±1 mm). Perspex® templates were then used to select and mark, using a scalpel, an arc of between 90°-110°. The wedge specimen extended approximately 20 mm below the centre of curvature and the width of the stem was approximately 22 mm. The wedge shaped specimen was then cut using a vice grips and a hack-saw.

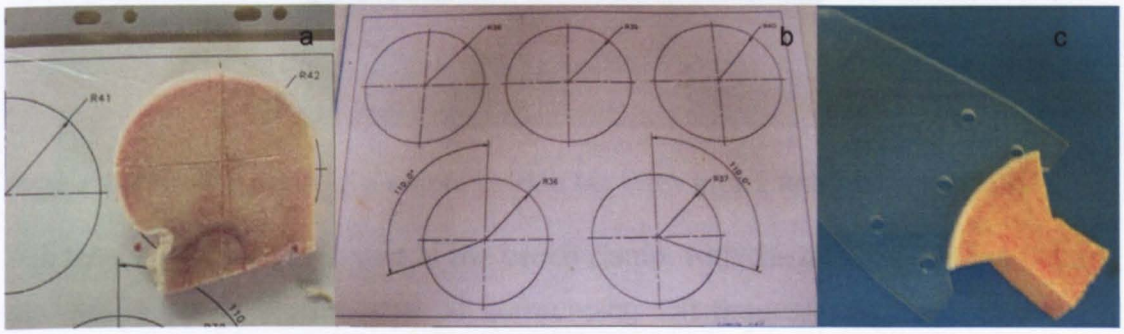

Figure 2-3: Photographs of CAD templates and Perspex radii used during dissection of condyles. (a) Femoral condyle was matched to CAD templates of known radius to determine the approximate radius and to find a portion of the flexion facet which was an approximate circle. (b) CAD templates had radii ranging between 38 mm and 42 mm. (c) Perspex templates (with radii between 38-42 mm) were also used to determine approximate radius and to ensure an approximate circle was dissected.

Femoral specimens were labelled and stored in PBS at 4° C when testing occurred promptly following dissection. When testing did not immediately follow dissection the specimens were stored in PBS at -20° C for no longer than one month.

2.3 Harvesting of the Tibial Plateau

In some experiments the femoral condyle was tested against its corresponding tibial plateau with the meniscus and its meniscal horns intact, as well as some of the circumferential connective tissue between the meniscus and tibia. These experiments simulated the natural medial compartment and were the negative control study, for all other experiments. Tibial specimen were obtained from the local abattoir, with the femur attached and the joint capsule intact as shown in Figure 2-4. The joint capsule and cruciate ligaments were carefully dissected using a scalpel and tweezers to separate the two bones. Care was taken not to scratch any medial cartilage or

meniscal surfaces. Both the medial tibial and medial femoral surfaces were inspected to ensure they were suitable for testing as per criteria described in Section 2.2.

Figure 2-4: Photograph of a whole bovine leg with intact knee joint capsule.

The tibial bones were clamped to the bench clamp, with the lateral side lying flat and the medial side facing upwards. All surrounding soft tissues were removed carefully using a scalpel, except the meniscus and its meniscal horns. The tibial surface was cut transversely as thinly as possible, using a hacksaw. A guide mark was made before sawing around the edge of bone, with a scalpel. The cut was made no more than 2 mm from top of the tibia and it extended transversely the whole way beneath the medial tibial surface, trying to maintain the cut close to, and in line with, the tibial surface. Finally a saggital cut was made between the medial and lateral sides of the tibial surface to remove the specimen. Extreme care was taken while making this saggital cut, so that the meniscal horns remained intact Figure 2-5.

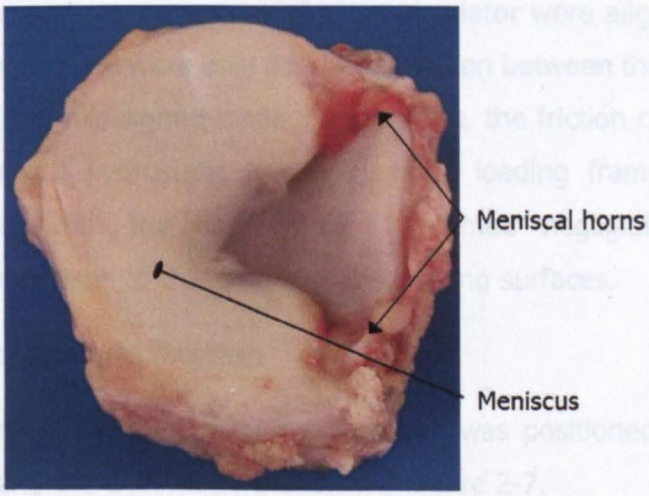

Figure 2-5: Dissected tibial plateau with meniscus and meniscal horns intact.

2.4 Fixation of specimen with PMMA bone cement

PMMA bone cement was used to reinforce the specimen in the appropriate jig for the friction simulator. The jigs are shown in Figure 2-6.

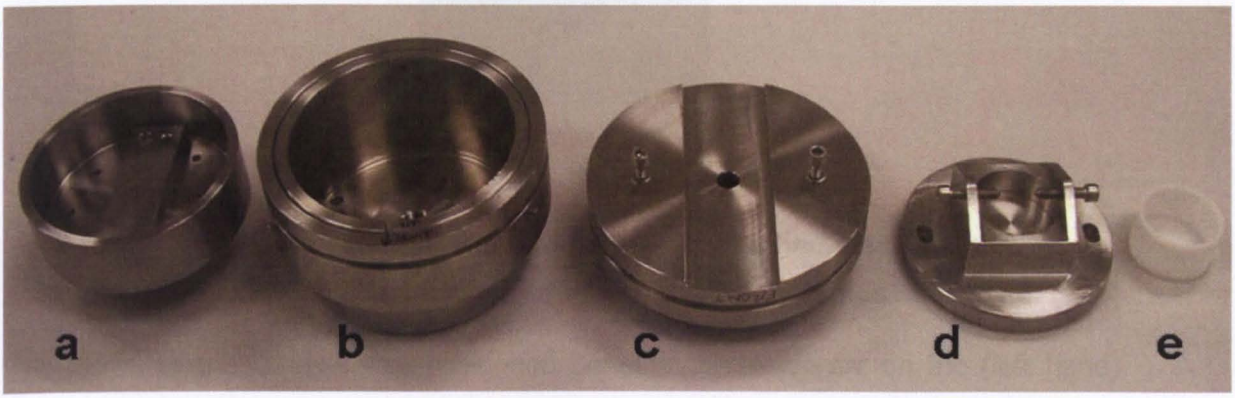

Figure 2-6: Jigs for the friction simulator. (a) Tibial specimen holder with flat SS plate attached (b) Tibial base component including clamping rings (c) femoral base component (d) femoral specimen holder (e) delrin pot which fitted in femoral specimen holder and held the specimen and cement.

Due to the variable nature of natural specimens, an allowance and height adjustment was built into the tibial specimen holder, which was height adjustable within the friction simulator. The height of the tibial holder stipulated the height of the centre of rotation of the femoral component. Alignment rods could be inserted through the centre of rotation of the friction simulator. Then the height of tibial holder and subsequently, the femoral component were adjusted to ensure that the centres of rotation of the femoral component and friction simulator were aligned. This ensured that the measured torques were only due to the friction between the bearing surfaces and not as a result of misaligned loads. Furthermore, the friction carriage sat on two externally pressurised hydrostatic bearings and a loading frame. Therefore, any friction associated with the carriage was assumed negligible (by orders of magnitude) in comparison to that between the bearing surfaces.

2.4.1 Femoral condyle fixation

Before mixing the cement the femoral component was positioned accurately in the femoral holder using the delrin fixture shown in Figure 2-7.

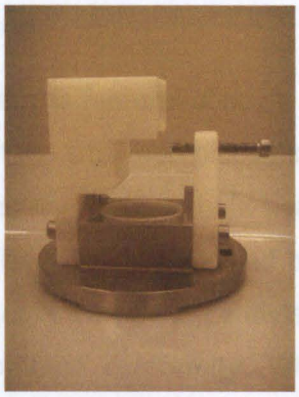

Figure 2-7: Femoral specimen holder with delrin jig attached. The jig was used to maintain position of condyle during potting and determine radius of condyle.

The crown of the condyle was positioned beneath the inside arc on the (left hand) delrin fixture, with one side of the condyle against the flat face, whilst the long flat-faced screw maintained this position from the right-hand side. Slip gauges were used when necessary to raise the height of the delrin fixture, when the radius, R >38 mm. The radius was limited to between 38 mm and 42 mm, due to height restrictions within the friction simulator.

When the correct position was obtained, the powder and liquid monomer were mixed and quickly drawn into a 20 ml syringe, while the cement was still in its most viscous state. Then the cement was injected into the delrin pot and left to set for 15-20 minutes.

Once cured, a second quantity of cement was prepared and left to cure for about 5 minutes in the mixing glass. During this time, the delrin fixtures were removed and screws were placed through holes in the femoral specimen holder. These screws held the specimen in place during testing and eliminated micro-motion. The cement was added around the specimen as shown in Figure 2-8.

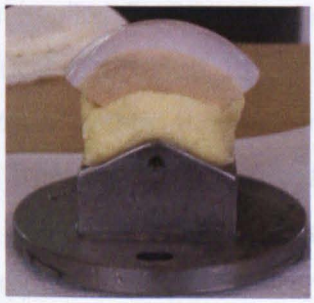

Figure 2-8: Femoral specimen potted in specimen holder using PMMA bone cement.

2.4.2 Tibial surface fixation

Before potting the tibial surface, the femoral condyle was potted and set it up in the friction simulator. The tibial surface was then placed in its specimen holder (shown in Figure 2-6) in the simulator and the femoral bulk head was lowered so the condyle and tibia came into contact. The tibia was allowed to shift into position, under the weight of the bulk-head and guidance of the condyle. By doing this the articulating surfaces found the position of best conformity. When the tibia had shifted into position, the bulk-head was raised again and a permanent marker was used to draw around the base of the tibial specimen, so its outline was on the specimen holder. Then the specimen was removed from the simulator and taken to the fume hood for cementing.

The cement was mixed as described in Section 2.4 and immediately drawn into a syringe (or two). A very thin layer of cement was injected on the bottom of specimen holder, just enough that the outlines were still visible. The specimen was pressed down and positioned according to the outline. Then cement was injected around the sides of the specimen.

2.5 Experimental Methods – Pendulum Friction Simulator

The ProSim Friction Simulator (Figure 2-9 and Figure 2-10), manufactured by Simulation Solutions (Manchester, UK), is a single-station servo-hydraulic machine, controlled by a PC via a graphic user interface which can apply a dynamic loading cycle similar to that of the knee. It has a fixed frame which consists of a friction measuring carriage, sitting on two externally pressurised hydrostatic bearings and a loading frame. All the measured frictional torque can be assumed to be between the bearing surfaces, as the friction in the carriage is negligible (by orders of magnitude) in comparison. A motion arm applies flexion-extension motion in the case of the knee. A piezoelectric transducer connected to the front of the friction carriage determines the frictional torque within the system, by measuring the forces transferred between the fixed frame and the carriage. Load and displacement are applied through the femoral component via the loading frame and motion arm respectively. The tibial holder contained the lubricant and the femoral component was lowered and its centre of rotation and that of the simulator were aligned as described in Section 2.4.

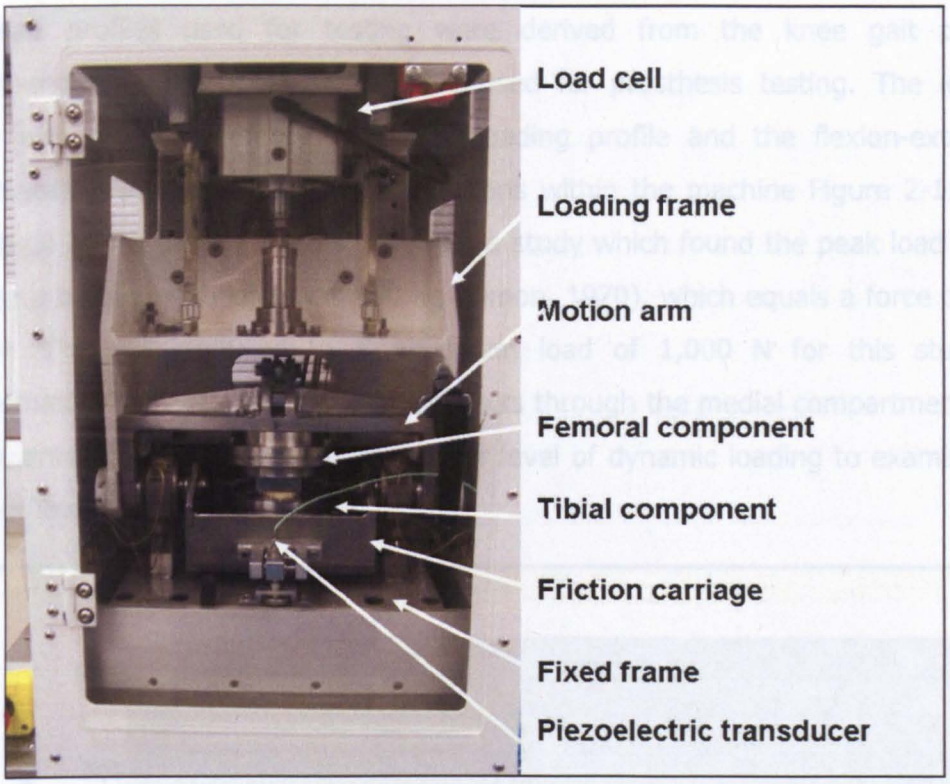

Figure 2-9: Labelled photograph of the ProSim Pendulum Friction Simulator.

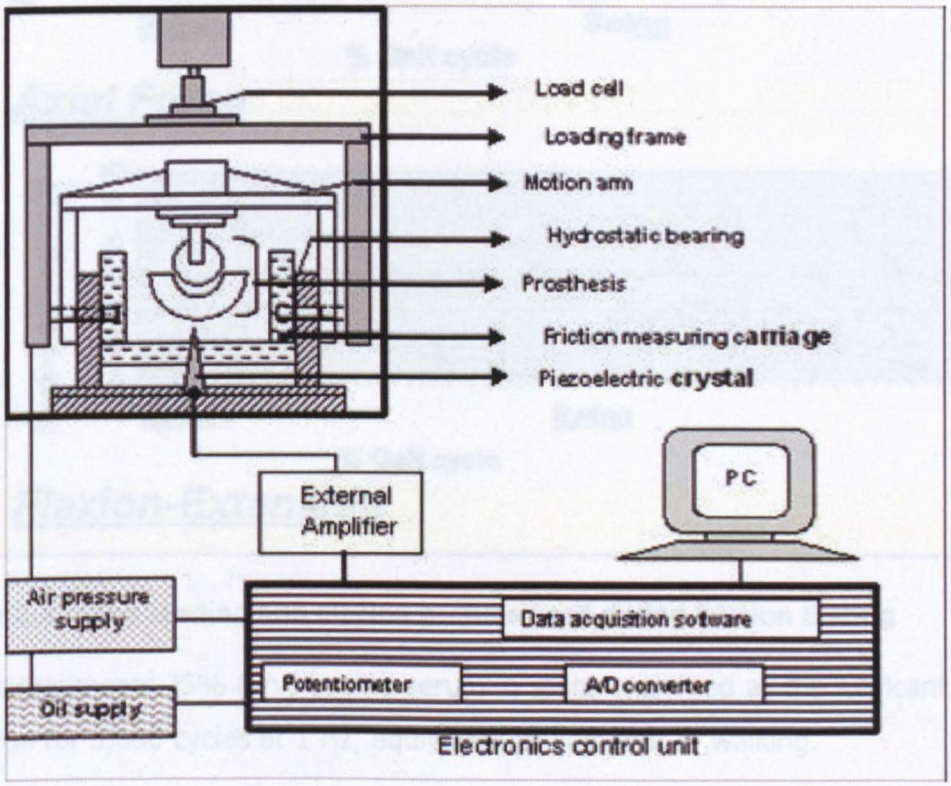

Figure 2-10: Schematic representation of the friction simulator hardware and software

The load profiles used for testing were derived from the knee gait profiles recommended in BS 14243-3:2004 and used for prosthesis testing. The loading profile was simplified to a single peak loading profile and the flexion-extension motion was limited to 25°, due to limitations within the machine Figure 2-11. The magnitude of the peak load was based on a study which found the peak load acting through a bovine knee joint was 190 kg (Simon, 1970), which equals a force of over 1,800N. This was reduced to a maximum load of 1,000 N for this study as approximately 60% of the knee joint load acts through the medial compartment. The experiments were also repeated at a lower level of dynamic loading to examine the effect of lower contact stress.

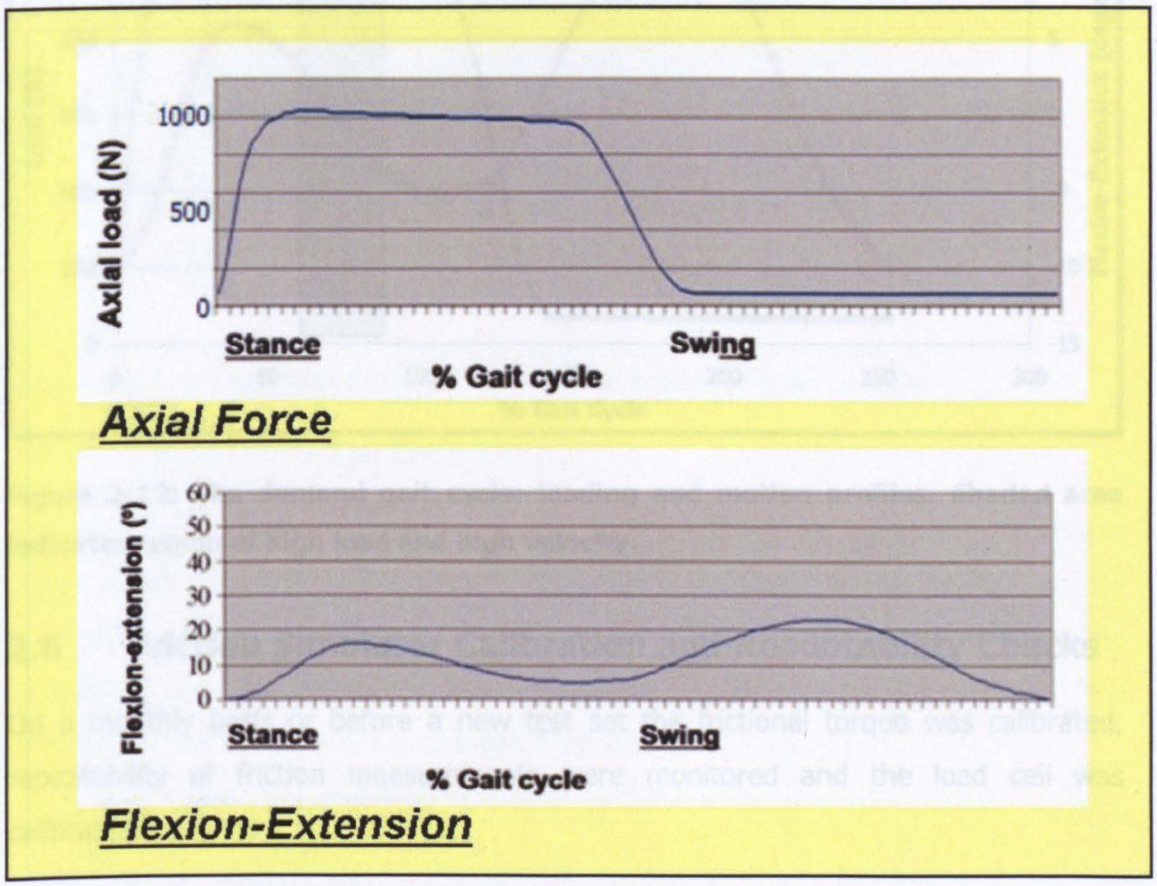

Figure 2-11: The loading and motion profiles used during friction testing

In all experiments 25% (v/v) bovine serum in saline was used as the lubricant. Tests were run for 3,600 cycles at 1 Hz, equivalent to one hour of walking.

Values recorded at the high load, high velocity phase of the cycle can be used to calculate the friction factor (*f*), using the following formula:

$$f = T \div (R_1 \times W)$$

where R_1 is the radius of the femoral condyle, T is the frictional torque measured by the piezoelectric transducer, and W is the applied load. This friction factor can be used to compare the effect of different variables, and also indicates the mode of lubrication. This high load, high velocity region of the cycle is shown in the shaded area in Figure 2-12, where data points were recorded every twenty cycles for the full duration of the test. It should be noted that the terms friction factor and coefficient of friction were used interchangeably throughout this thesis.

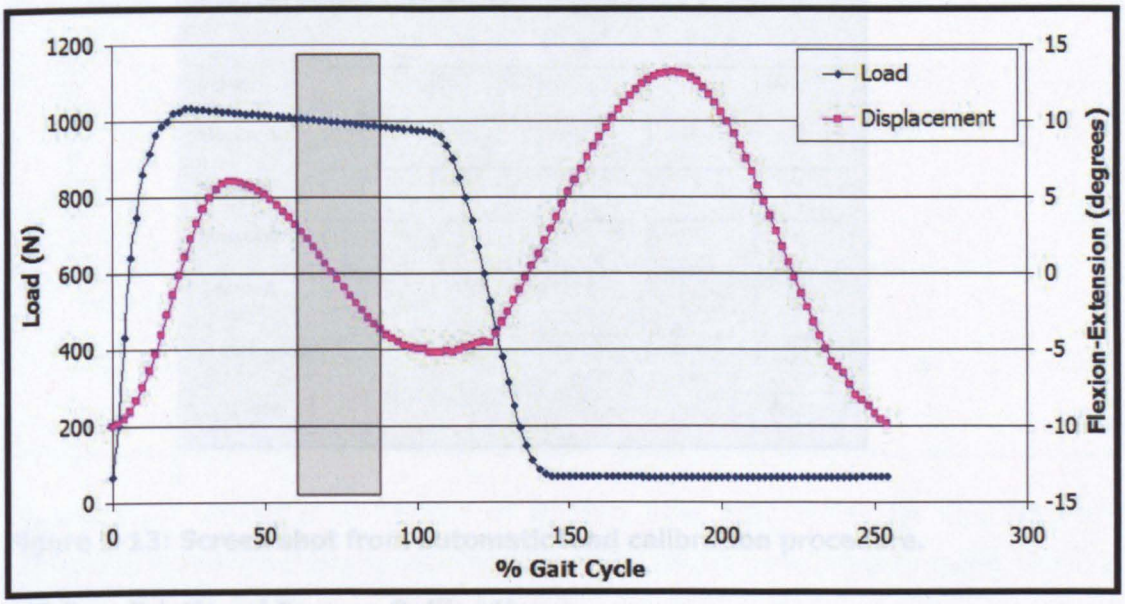

Figure 2-12: The demand gait cycle: loading and motion profiles. Shaded area indicates region of high load and high velocity.

2.6 Friction Simulator Calibration and Repeatability Checks

On a monthly basis or before a new test set the frictional torque was calibrated, repeatability of friction measurements were monitored and the load cell was calibrated.

2.6.1 Load Cell Calibration

The automatic load calibration facility in the software (Figure 2-13), was used to compute the calibration constants to relate the measured force against a known loadcell. The load transmitted though a standard bearing (a ceramic-on-ceramic (CoC) femoral head and acetabulum) was measured by a load cell mounted in the loading frame. During the calibration procedure, the air pressure valve in the friction simulator was opened through five positions equally spaced between zero (fully closed) and 250, causing the simulator to apply a pressure through the load cell. The

valve has a range between zero and 255 (full load). A test loadcell was used to record the actual force measured at each valve setting, and this value was entered into the calibration program. The calibration constant calculated by the program was used in the test system to correct the demand load applied by the simulator, hence ensuring the load applied in the test was the load specified.

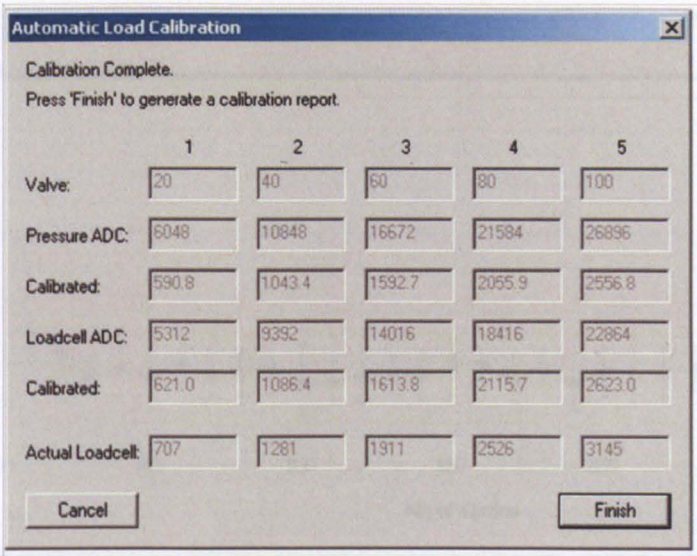

Figure 2-13: Screen shot from automatic load calibration procedure.

2.6.2 Frictional Torque Calibration

The frictional torque measurement was calibrated using an automatic calibration option in the software. Calibrated weights were placed one at a time, on the loading arm which sits on the friction carriage, as shown in Figure 2-14, and after the addition of each weight the frictional torque was measured and entered into the software, which calculated the calibration constant.

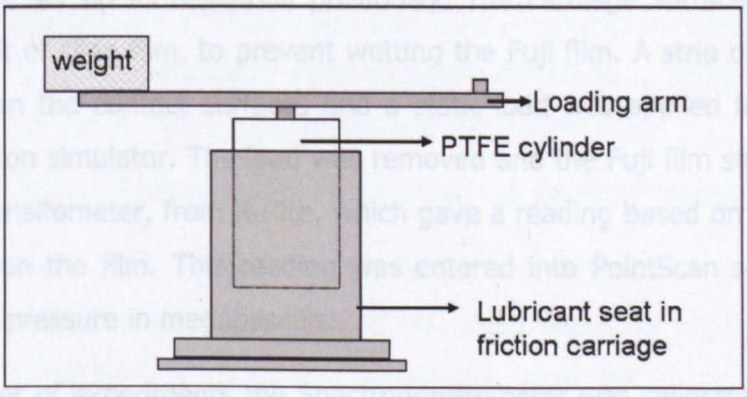

Figure 2-14: Schematic diagram of frictional torque calibration arm.

2.6.3 Reproducibility of the Friction Measurements

The standard ceramic-on-ceramic bearing was used to determine the repeatability of the frictional coefficient data. These tests were performed for 300 cycles with a peak load of 2 kN, a swing phase load of 100 N, and a frequency of 1 Hz. 25% (v/v) bovine serum in PBS was used as the lubricant. Typical results are shown in Figure 2-15.

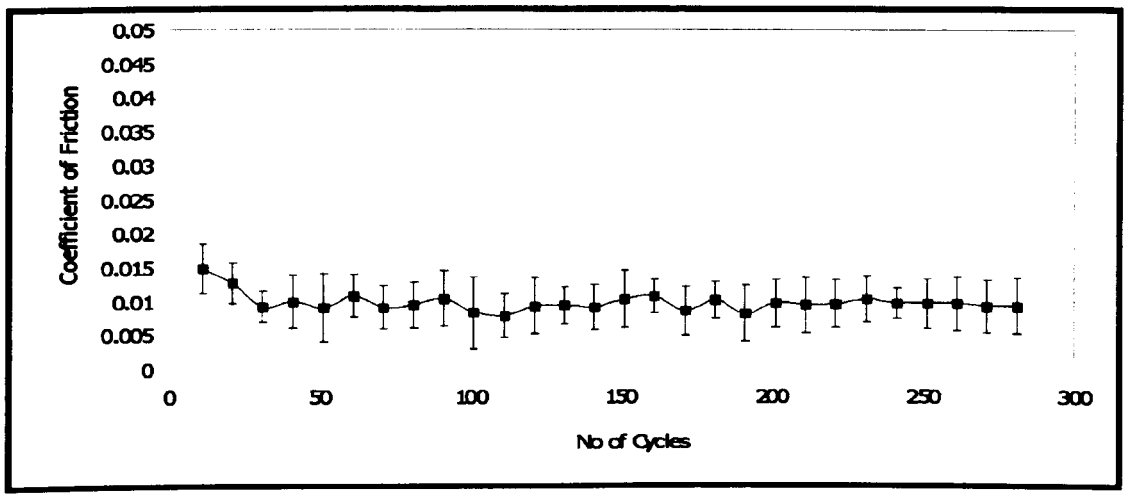

Figure 2-15: Average coefficient of friction over 300 cycles for the standard ceramic femoral head and acetabular cup. Results are presented as mean (n=4) ± 95% confidence intervals.

2.7 Contact Stress Measurement

To measure the contact stress between the bearing surfaces, pressure sensitive Fuji film called PressureX film, from Sensor Products LLC, USA, was used and the pendulum friction simulator applied the required load. The friction simulator and specimen were set up as described previously. The cartilage surfaces were sealed with one sheet of cling film, to prevent wetting the Fuji film. A strip of Fuji film was placed between the contact surfaces and a static load was applied for 30 seconds using the friction simulator. The load was removed and the Fuji film strip was placed in a Spectrodensitometer, from X-Rite, which gave a reading based on the density of colour (pink) on the film. This reading was entered into PointScan software which calculated the pressure in megapascals.

Before each set of experiments the Spectrodensitometer was calibrated by using its built-in automatic calibration option and measuring a standard white test patch, which was supplied by X-Rite.

2.8 Surface Roughness Measurements

The Ra value is a surface roughness parameter defined as the arithmetic mean of absolute departures of the roughness profile from the mean line. The Ra value of cartilage specimen was measured using a Talysurf 5 model from Taylor Hobson, UK. This machine operates by traversing a diamond tipped stylus over the surface area. This generates electrical signals proportional to the vertical movements of the stylus, which are then digitally processed to generate the roughness measurements and profile of the surface. The Talysurf 5 model has a vertical resolution of 20 nm and a traverse speed of 0.5 mm/s. A Gaussian cut-off filter equal to 0.8 mm was deemed suitable for assessing the variety of surface textures within this study.

When measuring the roughness of cartilage, it was decided to make replicas of the surfaces using Silicon rubber and measure the replica, rather than measuring the cartilage surface directly with the stylus. The reason for this was that there were subsequent methods of wear characterisation (μMRI and histology) to be completed after surface profilometry and dehydration of the cartilage surface during this first procedure was not desirable.

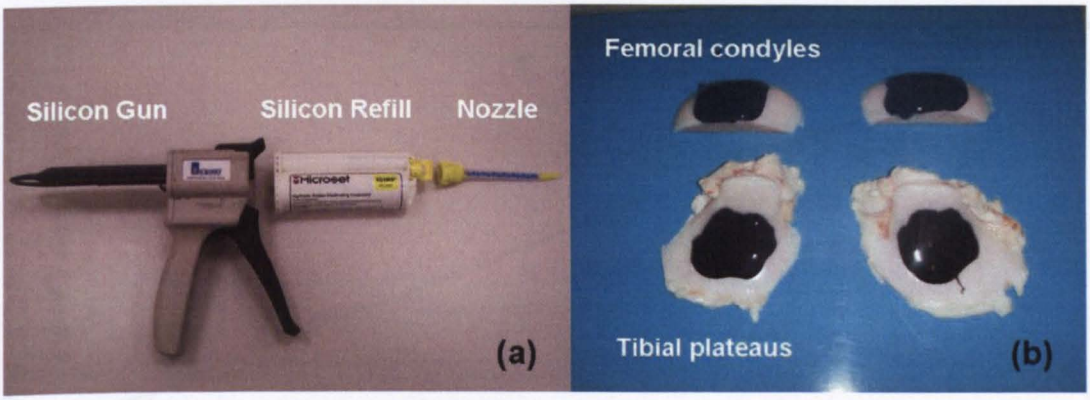

Figure 2-16: Photographs of Silicon gun and Silicon replicas on cartilage surfaces. (a) Silicon gun, refill and nozzle used to apply silicon to cartilage surfaces (b) Silicon rubber curing on two condylar and two tibial specimen.

2.8.1 Validation of Silicon Replica Method for Surface Roughness

Silicon replicas were made of the following surfaces. The surface roughness of each was measured using Talysurf. The surface roughness value, Ra (arithmetic mean of the absolute departures of the roughness profile from the mean line), was an average of data collected over six traces (between 10 mm and 18 mm in length) drawn on the sample surface (Gaussian Filter; 0.8 mm cut-off). Three different

materials, including cartilage, were used in this validation, as well as different methods of manually roughening each (Table 2-3). This was to ensure that a range of Ra values was measured and that the method was sensitive at each value.

Material	Quantity	Roughness
Aluminium	1	Manually roughened with emery paper
Polymer	1	Manually roughened with emery paper
Cartilage	2	Manually roughened with a blade
Cartilage	1	Untreated

Table 2-3: The materials used in validation of surface roughness measurements using silicon replicas and the treatments used to vary the roughness of each.

During the roughening, the preparation of moulds and the measurement of the cartilage surfaces, hydration with PBS was maintained. Excellent agreement was found between the two methods. Using silicon replicas was determined to be an appropriate method to measure the surface roughness of cartilage.

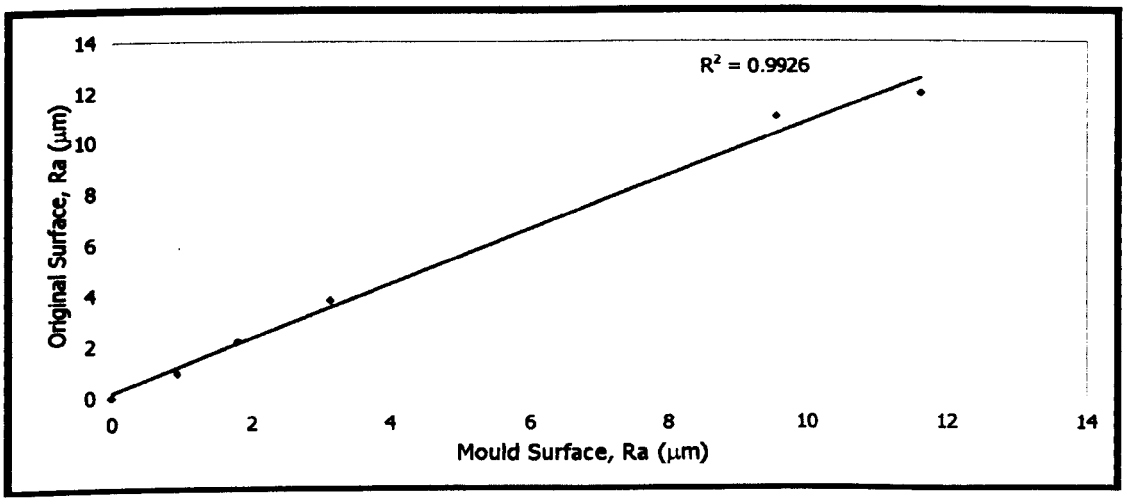

Figure 2-17: Correlation between surface roughness measurements of the real and silicon replicated surfaces. Graphs shows excellent correlation (R^2 = 0.9926) between the surface roughness measurements for the real and silicon replicated surfaces.

This method was adopted throughout this thesis as it prevented any dehydration to cartilage samples during roughness measurements. Dehydration effects would have compromised roughness results as well as subsequent wear analysis methodologies – MRI scanning and histology.

2.9 Micro-MRI

A Bruker Avance™ II 400 MHz 9.4 Tesla Nuclear Magnetic Resonance (NMR) scanner was used to scan the cartilage specimens after friction testing. Initially in a series of trial scans, various standard MR imaging sequences were used. It was found that the multi spin multi echo (MSME) sequence produced the highest quality delineation of cartilage morphology, the best signal to noise ratio as well as the most acceptable scanning duration. The scanning parameters used are shown in Table 2-4.

Imaging sequence	MSME
Echo Number	8
Repetition Time (TR)	4843.1 ms
Echo Time (TE)	10.5 – 14.0 ms
Number of Averages	1
Slice Thickness	1 mm
In plane pixel resolution	0.078 mm/pixel

Table 2-4: MR scanning parameters.

The in plane pixel resolution for all wear analyses was 0.078 mm/pixel. Depending on the size of the specimen the field of view varied between 20 mm and 25mm in the x- and y-directions (horizontal and vertical directions). To maintain the same resolution in both directions, the matrix size was varied between 256 and 295 pixels in the x- and y-directions. A higher resolution of 0.02 mm^2/pixel was also achieved and used for samples showing no wear at 0.078 mm^2/pixel, to establish if wear was detectable at this higher resolution.

After friction testing, the condyles were cut to a smaller size retaining the contacting surface, which fitted into the specimen tube for the NMR scanner (Figure 2-18). During the initial trial scans it was found that scanning cartilage-bone specimens in PBS produced very poor contrast and signal-to-noise. As a result, specimens were placed in the tube, directly from PBS so the surfaces were moist, some drops of PBS were placed in the bottom of the tube and it was immediately sealed. Using the parameters shown in Table 2-4, scan times were approximately 23 minutes and upon removal the cartilage surfaces appeared to have remained moist. Any dehydration

effects were not desirable as specimens were used for histological analysis after MRI scanning.

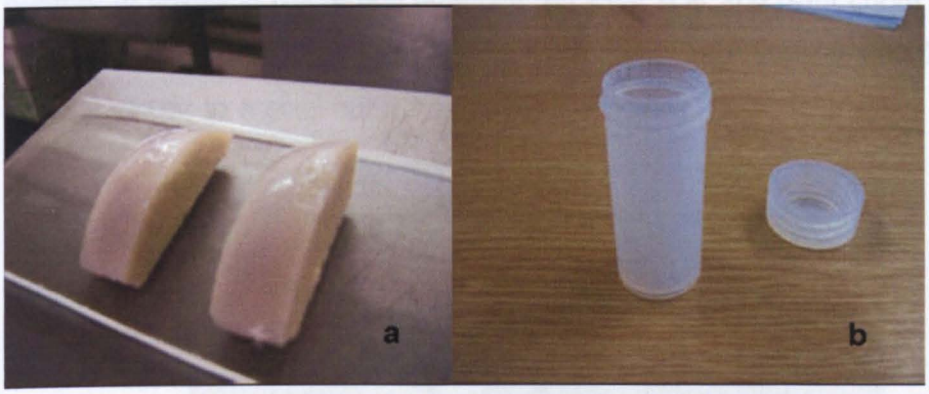

Figure 2-18: Femoral condyles before scanning and the MR specimen tube. (a) Cartilage-bone specimens were cut to smaller size for scanning to fit in imaging tube (b) imaging tube used to hold specimen during scanning.

A typical MR image of an undamaged sample at low and high resolution and a damaged sample at a low resolution are shown in Figure 2-19.

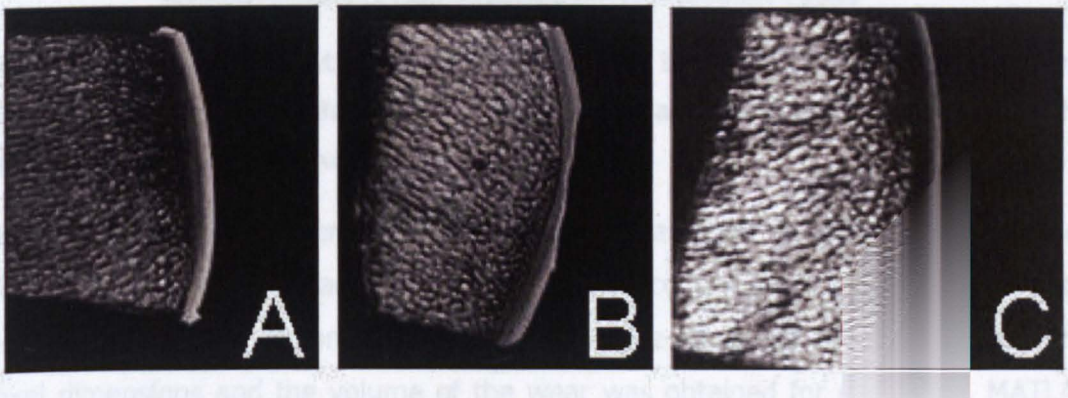

Figure 2-19: Typical MRI images (a) An unworn sample scanned with a resolution of 0.078 mm/pixel (b) a damaged sample scanned at a resolution of 0.078 mm/pixel and (c) an unworn sample scanned at the higher resolution f 0.02 mm/pixel.

2.9.1 Quantification of Wear

As this was a new wear analysis technique, two methods of quantifying the volume of cartilage lost during testing were developed, for comparative purposes and to assess this methodology.

The first method utilised commercial ANALYZE™ software (Mayo Clinic, USA). Wear volumes were quantified on a slice by slice basis. Each slice was loaded into

ANALYZE™ individually. A geometry tool was used to fit a properly-sized oval, matching the margin of the cartilage surface to refit the original curve. Then the number of voxels in the region between the wear scar and re-fit curve was calculated and the wear volume was obtained. The volume of each voxel was 6.08×10^{-3} mm^3. A voxel is similar to a pixel but it has three dimensions.

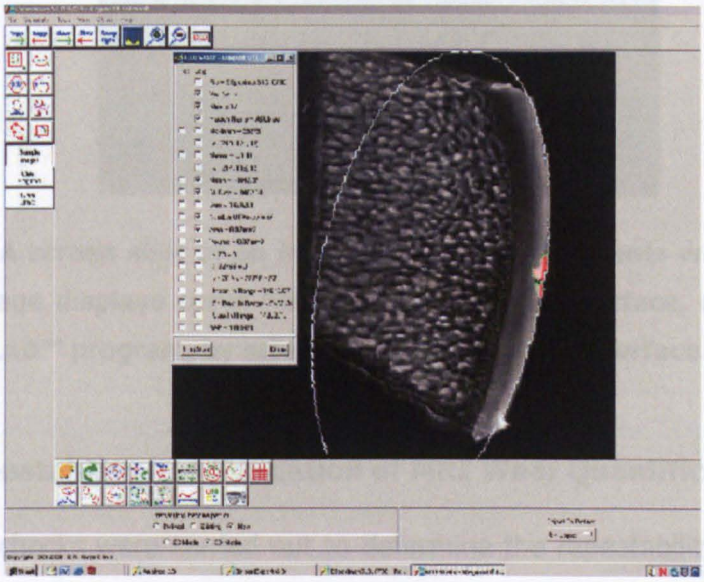

Figure 2-20: A screen shot of an MR image loaded in ANALYZE™. An oval matching the curvature of the cartilage surface was drawn and the number of voxels in the red region (worn region) was obtained.

Secondly, a custom written MATLAB™ program was used to read the MRI images slice by slice and to surface-fit the original surface curvature as shown in Figure 2-21. Next the worn region was selected. The code prompted the user to input the voxel dimensions and the volume of the wear was obtained for each slice. MATLAB functions such as *spline* and *polyarea* were employed to perform the curve-fitting and area calculations.

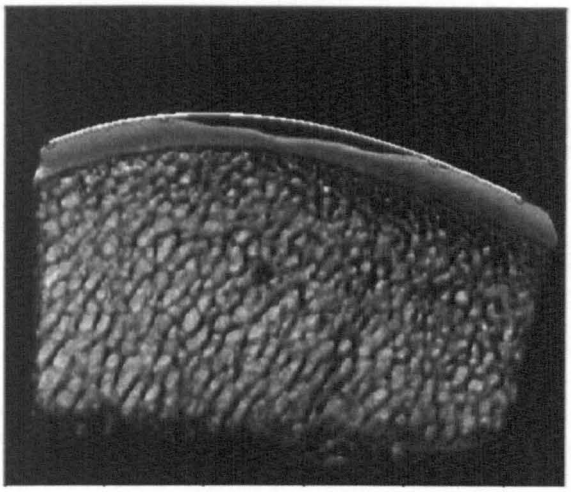

Figure 2-21: A screen shot of an image during measurements with the MATLAB™ program. Image displays curve fitting to the cartilage surface, using the custom written MATLAB™ program, by selecting points along the surface either side of the wear scar.

2.9.2 Repeatability and Validation of MRI Wear Quantification

A number of checks were carried out to determine the repeatability and accuracy of the new methodology, using micro-MRI scans to quantify the volume of cartilage lost during wear testing:

1. The results from the two methodologies were compared
2. Inter- and intra-person validation were carried out
3. A validation was carried out where the volume of a removed piece of tissue was measured using a pycnometer and the remaining void in the cartilage surface was measured from the MRI scans

1. Comparison ANALYZE™ and MATLAB™ Methods

Excellent correlation was found between the wear volumes calculated using the ANALYZE™ and MATLAB™, as shown in Figure 2-22.

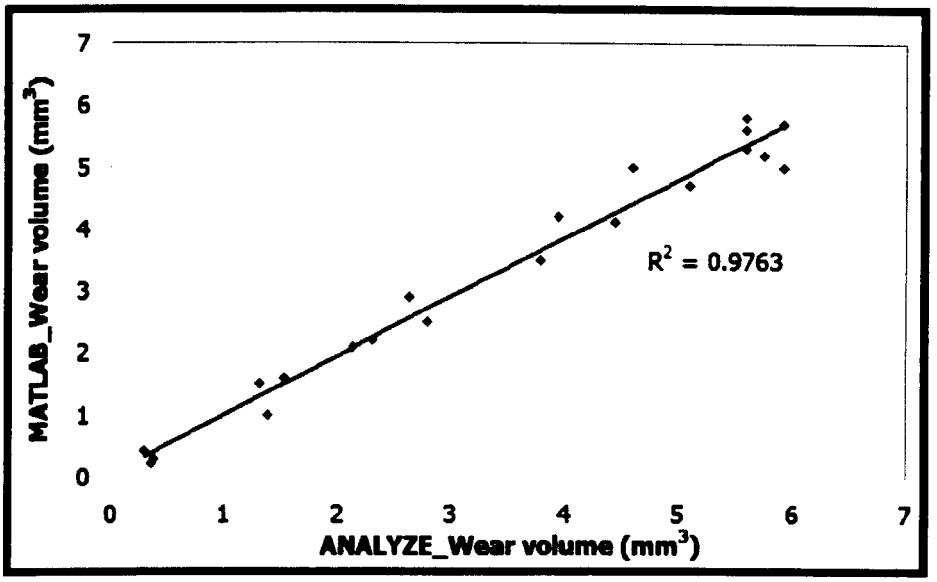

Figure 2-22: Graph demonstrating the excellent correlation (R^2 = 0.9763) found between MATLAB and ANALYZE techniques to calculate cartilage wear volumes. R^2 values were obtained using a regression analysis in Microsoft Excel.

2. Inter-person and Intra-person validation

Using the ANALYZE™ technique, good agreement was found between the wear volumes obtained by two different individuals for four different worn specimens, as shown in Figure 2-23.

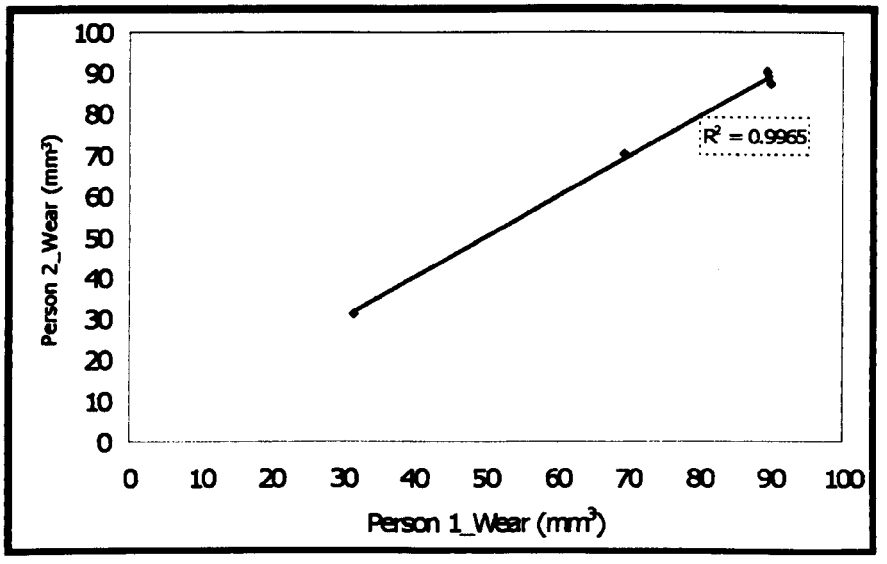

Figure 2-23: Inter-person validation of MRI wear quantification method. Good agreement between two individuals' measurements of wear volume for four damaged cartilage surfaces, using ANALYZE™ method. R^2 values were obtained using a regression analysis in Microsoft Excel.

Two intra-person investigations were carried out. Two individuals measured the wear volumes of four damaged samples on two occasions. The correlations found are shown in Figure 2-24 and Figure 2-25.

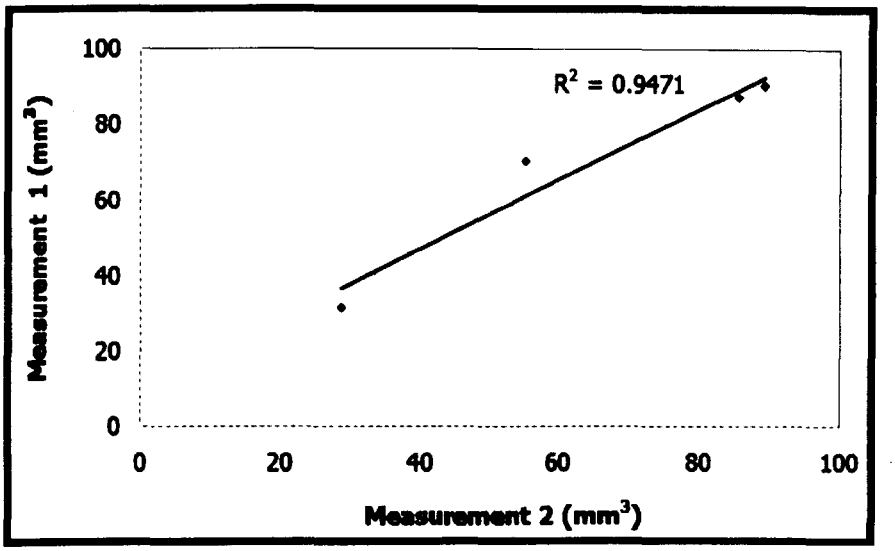

Figure 2-24: Intra Person validation of MRI wear quantification methods - Person 1. Wear volumes were obtained for four damaged samples, on two occasions by the same individual. R^2 values were obtained using a regression analysis in Microsoft Excel.

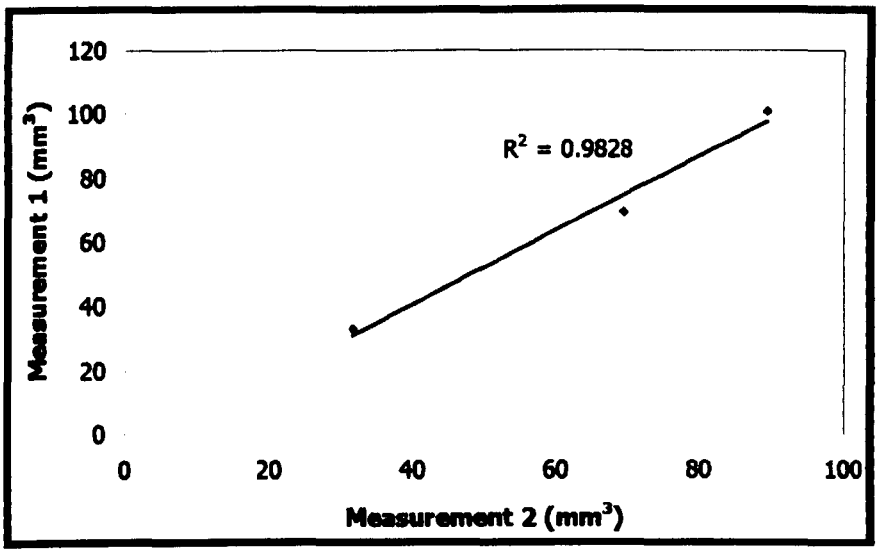

Figure 2-25: Intra Person validation of MRI wear quantification methods - Person 2. Wear volumes were obtained for four damaged samples, on two occasions by a second individual. R^2 values were obtained using a regression analysis in Microsoft Excel.

3. Validation using pycnometer

The ACCUPyc 1330 Pycnometer (Figure 2-26) is a fast, fully automatic density analyser that provides high-speed, high-precision volume and density measurements on a wide variety of materials. It was used to measure the volume of cartilage pieces removed from a cartilage-bone surface and the volume of the remaining void was measured using MRI scans and the MATLAB technique.

Figure 2-26: Image of ACCUPyc 1330 gas displacement pycnometer.

The AccuPyc works by measuring the amount of displaced gas (helium). The pressures observed upon filling the sample (cell) chamber and then discharging it into a second empty chamber (expansion chamber) allow computation of the sample volume. The schematic diagram in Figure 2-27 also appears on the pycnometer above the keypad and indicates system status during a measurement. The indicators (LED's) show the current status of fill, expansion and vent valves. The indicator is lit when the valve is open.

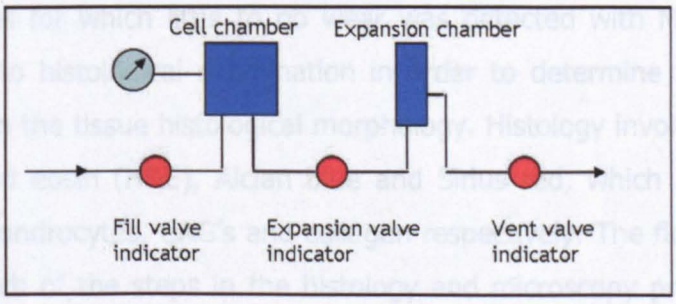

Figure 2-27: Schematic diagram of the ACCUPyc 1330.

Calibration of the pycnometer was performed on a daily basis prior to taking measurements. Stainless steel spheres of known density and volume are placed in the cell chamber, a calibration test is performed, after which the cell and expansion chamber volumes are automatically stored in set-up parameters.

Using the AccuPyc to measure the volume of a removed segment of tissue and the MRI scans and MATLAB program to measure the resulting void in the cartilage surface, good agreement was found between the two methods, as shown in Figure 2-28.

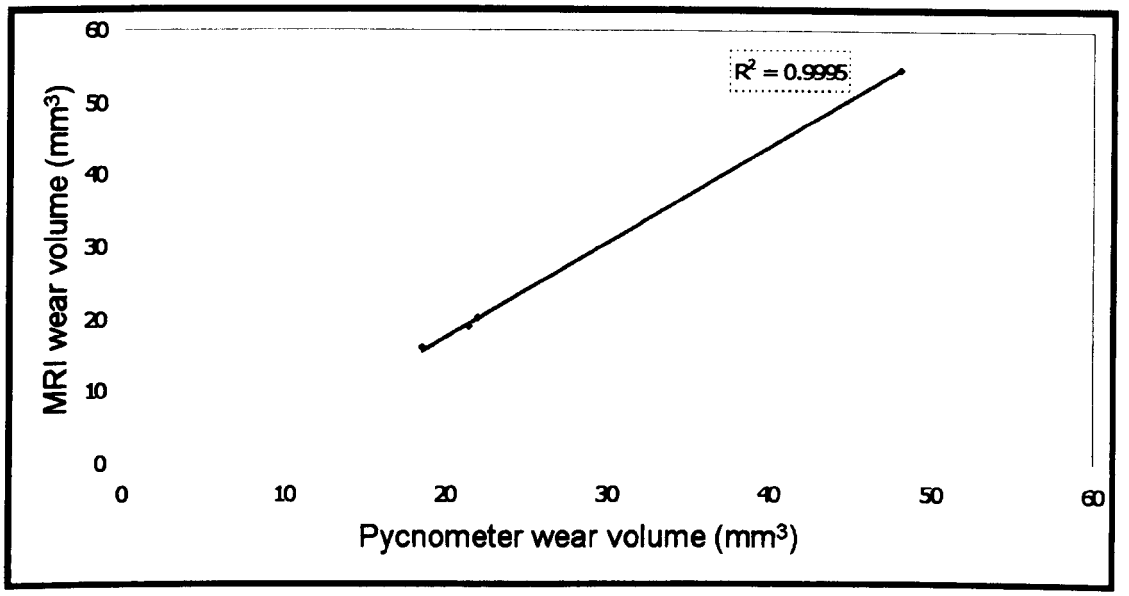

Figure 2-28: Volume measurements of void in cartilage surface using MRI compared with using the AccuPyc gas displacement pycnometer to measure the volume of the removed piece of cartilage. Excellent agreement was found between the two methods. R^2 values were obtained using a regression analysis in Microsoft Excel.

2.10 Microscopy and Histology

Cartilage samples for which little to no wear was detected with MRI and Talysurf, were subjected to histological examination in order to determine if friction testing had any effect on the tissue histological morphology. Histology involved staining with haematoxylin and eosin (H&E), Alcian blue and Sirius red, which stained for basic structure and chondrocytes, GAG's and collagen respectively. The flowchart in Figure 2-29 outlines each of the steps in the histology and microscopy process. Each step will be described in the following sections.

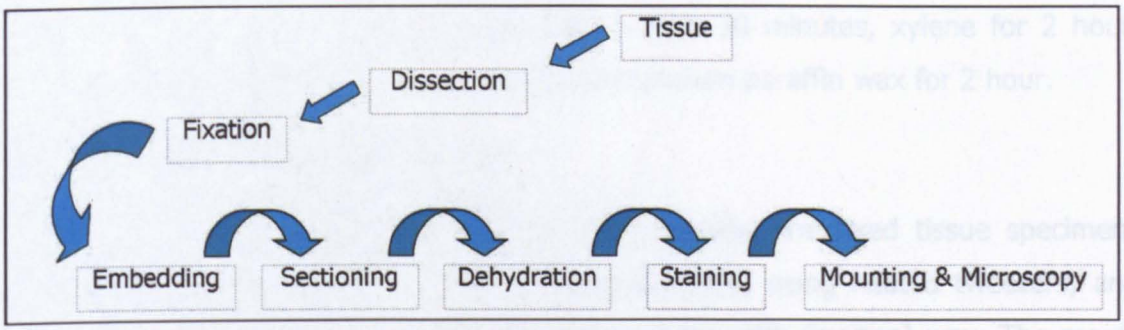

Figure 2-29: Flowchart outlining the histology and microscopy procedure.

2.10.1 Tissue Dissection

Using a surgical scalpel a small square piece of cartilage tissue was cut from the bulk surface, approximately 6 mm by 6 mm in length and from the surface to tidemark region in depth. Each sample was placed in a plastic histology embedding cassette (Histosette®) and labelled.

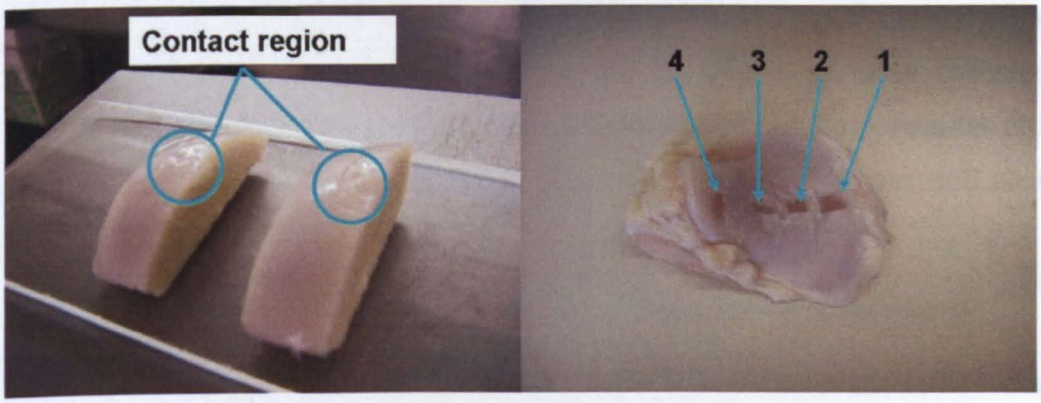

Figure 2-30: Histology sections taken from contact regions on condyle and tibia.

2.10.2 Tissue Fixation

Prior to paraffin wax embedding all tissue was fixed in 10% (v/v) neutral buffered formalin (NBF). The purpose of fixation was to prevent autolysis and bacterial degradation as well as to retain the morphology of the tissue throughout the remaining procedures. Furthermore, fixation helped to protect the tissues against the harmful effects of dehydration and embedding procedures, while it improved the optical differentiation of the tissues and allowed clear staining of tissue sections.

Automated tissue processing was then used to immerse the cassettes sequentially in 70% (v/v) ethanol for 1 hour, 90% (v/v) ethanol for 1 hour, absolute ethanol for 2 hour 20 minutes, absolute ethanol for 3 hour 20 minutes, absolute ethanol for 4 hour

20 minutes, xylene for 1 hour, xylene for 1 hour 30 minutes, xylene for 2 hour, molten paraffin wax for 1 hour 30 minutes and molten paraffin wax for 2 hour.

2.10.3 Paraffin Wax Embedding

Once the automated tissue processing was complete, the fixed tissue specimens were immediately taken from the histology cassettes, using heated tweezers, and they were orientated in metal moulds partially filled with (molten) wax. The mould was placed on an ice pack to assist wax solidification and fixation of specimen orientation. The histology cassettes were placed on top of the mould, which were then filled with wax. Moulds were cooled on the ice pack until the wax had fully solidified at which point the block was removed.

2.10.4 Sectioning

The wax-embedded tissue sections were cut from the paraffin blocks, to a thickness of 6μm, using a microtome. Using a forceps these sections were carefully transferred to a water bath heated to 40°C. The wax sections were then collected on to Superfrost Plus microscope slides and fixed by heating for twenty minutes at 55°C on a hot plate to dry. The hot plate also assisted in melting the wax and allowed the tissue to fix more firmly to the slide.

2.10.5 Dewaxing and Rehydrating of Wax Embedded Sections

Prior to staining, paraffin sections were de-waxed by immersion in two changes of xylene for 10 minutes each, followed by rehydration through three pots of graded ethanol for 2, 1 and 1 minutes respectively, dipped in 70% (v/v) ethanol for 30 seconds and finally rinsed with distilled water.

2.10.6 Staining: Haematoxylin and Eosin

Slides were immersed into:

- Haemotoxylin for 1 min
- Scott's water (Distilled water with 2% (w/v) $MgSO_4$ and 0.35% (w/v) $NaHCO_3$) for 3 mins
- 1% (w/v) Eosin for 3 minutes

with washing under running tap water between each step. Finally sections were dehydrated using an ethanol gradient, consisting of four separate glass troughs

containing different concentrations of ethanol, from 70% up to 100% (v/v). Slides were left in each trough for one minute. The slides were placed into two changes of xylene for ten minutes each.

2.10.7 Staining: Alcian Blue

Alcian blue stains GAGs. Slides were immersed into:

3% (v/v) acetic acid for a few seconds

Alcian blue for 5 minutes

Each section was blotted dry and rinsed with distilled water. Again, slides were dehydrated back through graded alcohols and cleared with xylene.

2.10.8 Staining: Sirius Red

Sirius red stains collagen within tissue sections and can distinguish damaged collagen from normal. Slides were immersed in 0.1% (w/v) Sirius red for 1 hour. Each slide was washed in 0.01 M hydrochloric acid for two minutes. Slides were dehydrated back through graded alcohols and cleared with xylene.

2.10.9 Mounting and Microscopy

After each of the above staining procedures, the slides were mounted with DePex mountant and glass coverslips. Following staining, the slides were inspected under light microscopy (Olympus IX71) and images were captured digitally.

2.11 Native Cartilage Histology Controls

Representative histological images of normal untested cartilage stained with H&E, Alcian blue and Sirius red are shown in Figures 2-31 to 2-33. Cartilage sections were taken from the medial condyle, the patella-femoral groove and from two regions on the tibial plateau – the region protected by the meniscus as well as the exposed, contacting regions. The staining procedures were performed as described in the previous Section. The articular surface (AS) is highlighted on all images in which the whole depth of the tissue is pictured.

H&E was used to stain for tissue architecture and cell nuclei. In the H&E images of the medial condyle and patella femoral groove, the surface architecture appeared to be intact and free from any damage (Figure 2-31, a-d). The darker region along the

surface is the collagen fibres running parallel to the surface in the superficial tangential zone. Similarly, the structure of some of the tibial surface in the protected zone appeared to be intact (Figure 2-31 e) but some surface irregularities were visible on one section (Figure 2-31, f). The collagen fibres running parallel to the surface were less visible on the cartilage sections taken from the exposed tibial surface (Figure 2-31, g-h). This lack of collagen may be due to the fact that this region was in constant contact with the femur *in vivo* and some matrix breakdown was induced. Conversely, perhaps the region was not loaded sufficiently to stimulate collagen synthesis and some form of degeneration had begun *in vivo*.

Sirius red allows visualisation of collagen fibres. In the Sirius red images of the medial condyle, the patella femoral groove and the protected tibial cartilage, a darker red band of collagen fibres can be seen along the surface (Figure 2-32, a-d). Similar to the H&E stained cartilage, the collagen fibres running parallel to the surface were less visible on the cartilage sections taken from the exposed tibial surface (Figure 2-32, g-h).

Alcian blue stains for GAG's. In general, the concentration of blue colouration was uniform throughout the tissue as shown in Figure 2-33, indicating that the distribution of GAG's was uniform. However, in one of the unprotected and one of the exposed tibial specimens, there was evidence of regions of GAG depletion close to the articular surface (Figure 2-33, f & h).

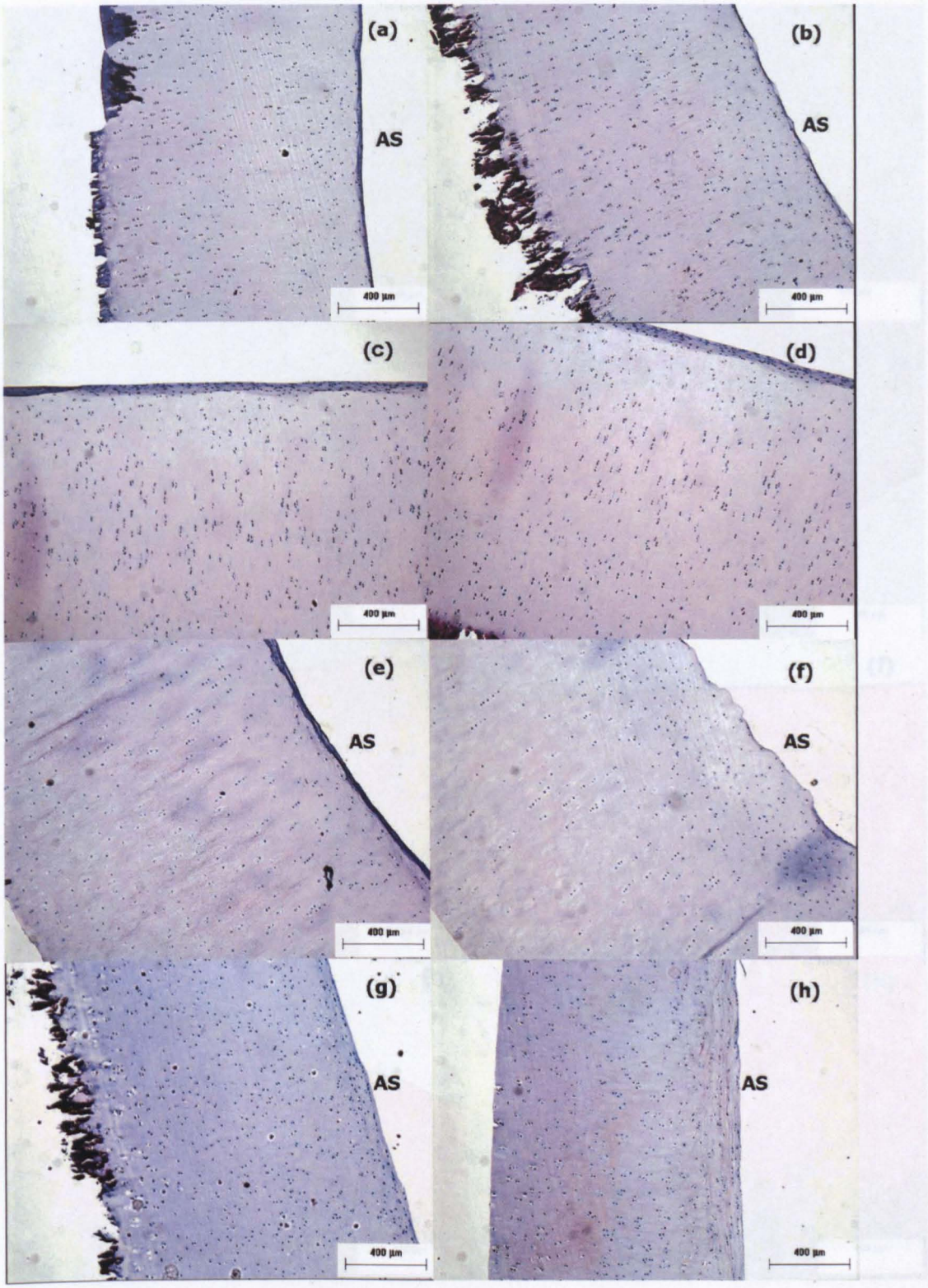

Figure 2-31: Representative images of H&E stained cartilage from control specimens. All images are at a magnification of 40x. Cartilage was taken from the contact region of the medial condyle (a-b), the patella-femoral grove (c-d), the protected (e-f) and exposed (g-h) regions of the tibial surface.

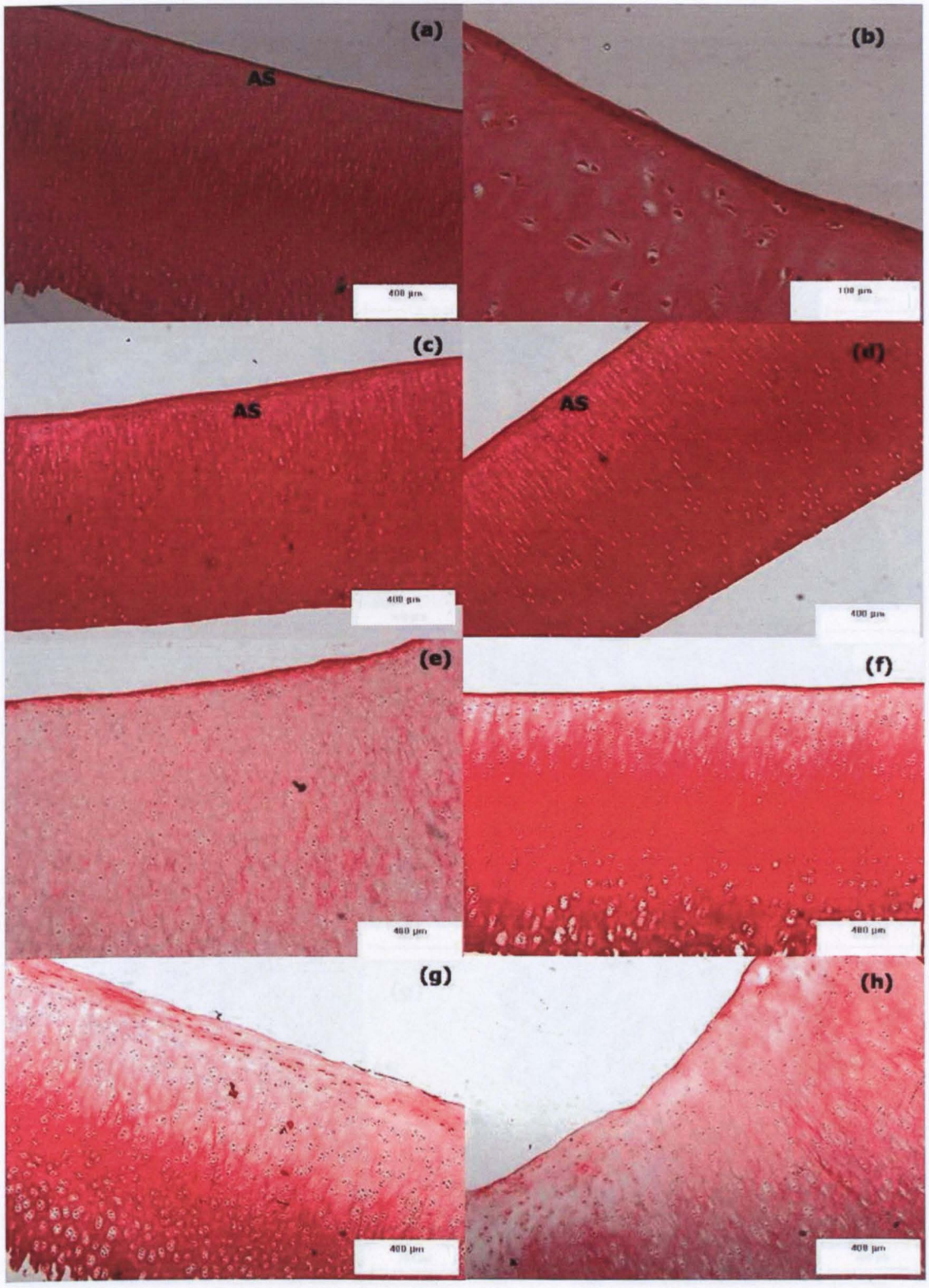

Figure 2-32: Representative images of Sirius red stained cartilage from control specimens. Images are at a magnification of 40x and Image (b) is at a magnification of 200x. Cartilage was taken from the contact region of the medial condyle (a-b), the patella-femoral grove (c-d), the protected (e-f) and exposed (g-h) regions of the tibial surface.

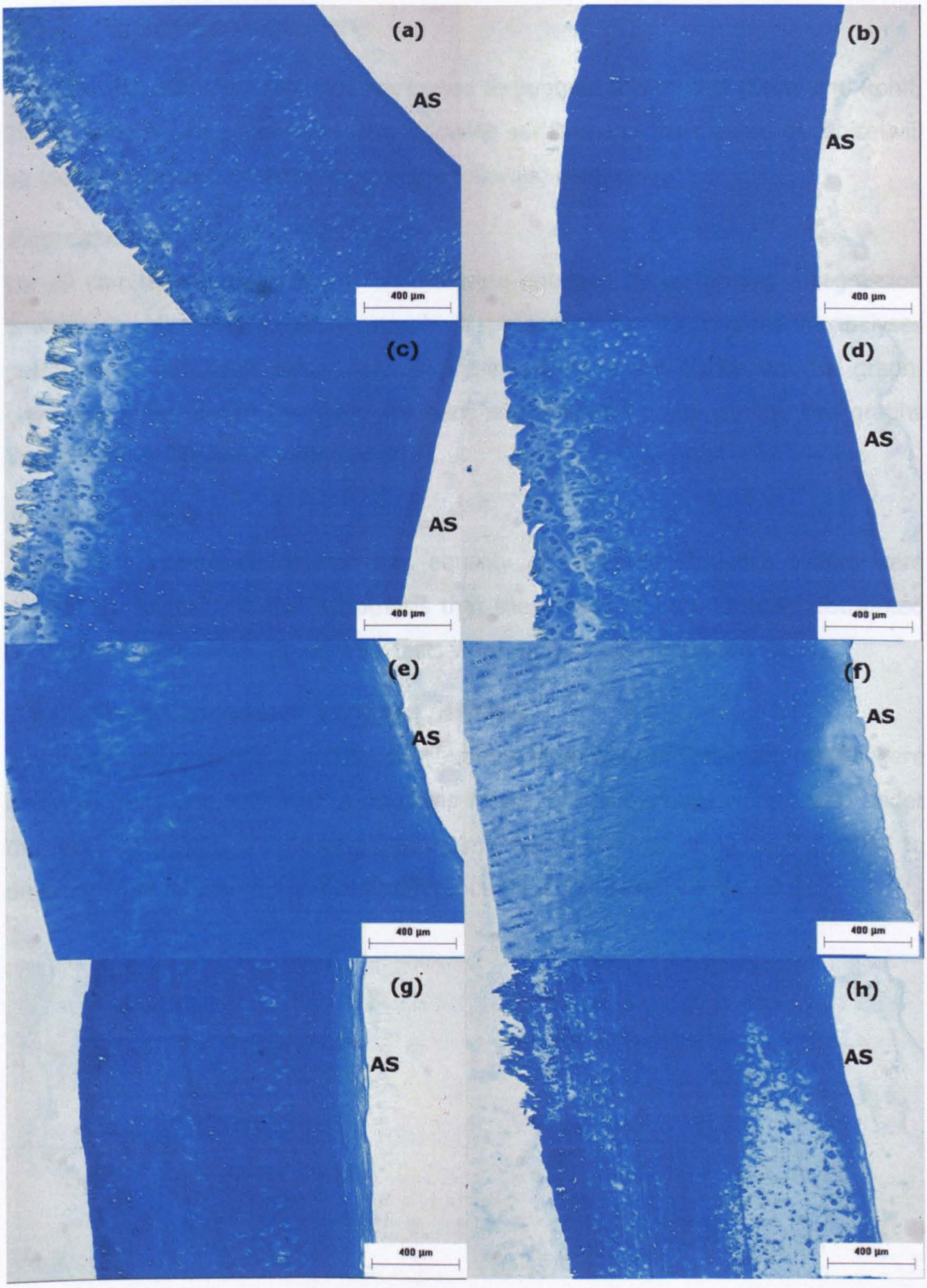

Figure 2-33: Representative images of Alcian blue stained cartilage from control specimens. All images are at a magnification of 40x. Cartilage was taken from the contact region of the medial condyle (a-b), the patella-femoral grove (c-d), the protected (e-f) and exposed (g-h) regions of the tibial surface.

2.12 Statistical analysis

The following statistical methods were used throughout this project (Sokal and Rohlf, 2005). They will be described in the following sections and the method of choice will be identified in each case throughout the following chapters.

Regression Analysis

For all correlations presented, R^2 values were obtained by performing a regression analysis in Microsoft Excel. A graph is presented for all regression analyses performed. The mean value only is presented, to allow clarity on the graph. However, 95% CI can be found for each experimental group, in the bar graphs preceding the regression analyses.

Student's t-test

Assuming a normal distribution and equality of variances student's t-tests were performed, to test the null hypothesis that the means of two normally distributed populations were equal. Student's t-tests were performed in Microsoft Excel.

Single Factor Analysis of Variance (ANOVA)

Assuming independence, a normal distribution and equality of variances, results were analysed using one way ANOVA, in cases where different groups were tested under the same conditions. Individual group means were compared using the T-method to determine the minimum significant difference (MSD) at $p<0.05$ and $p<0.01$.

Chapter 3. Tribological Response of Meniscectomy

3.1 Introduction

Total meniscectomy (removal of the meniscus) has been shown to induce osteoarthritic changes in the underlying cartilage and bone in the natural knee joint (Fairbank, 1948; Klompmaker *et al.*, 1992; McDermott *et al.*, 2006), indicating that the meniscus plays an important protective role in the load carrying capacity. Previous biomechanical studies have shown that the meniscus acts to make the knee joint more conforming or congruent, distributing the forces across the joint onto a larger area of articular cartilage hence reducing contact stress (Kettlekamp and Jacobs, 1972; Seedhom *et al.*, 1974; Walker and Erkman, 1975; Krause *et al.*, 1976; Seedhom and Hargreaves, 1979b). Studies have shown that at least 50% (Seedhom *et al.*, 1974), and up to 90% (Seedhom and Hargreaves, 1979b), of the load across the joint is transmitted through the meniscus, and removal of the meniscus has been shown to increase stress in the tibial cartilage and subchondral bone (Walker and Erkman, 1975). This elevation of stress is believed to contribute to subsequent osteoarthritic changes. Currently, damaged menisci are repaired if at all possible.

Recent fundamental studies of the tribology of articular cartilage have indicated that both the frictional force and degradation and wear are dependent on the loading period and contact stresses. The relationships are, however, complex due to the biphasic nature of articular cartilage and the time dependency of the tribological responses (Forster and Fisher, 1996; Forster and Fisher, 1999; Krishnan *et al.*, 2004b; Bell *et al.*, 2006; Carter *et al.*, 2007; Katta *et al.*, 2007; Northwood and Fisher, 2007; Northwood *et al.*, 2007). The tribological response of the whole natural knee as a biomechanical system cannot be predicted from simple geometry cartilage specimen tests. Determination of friction and wear in the whole natural joint *in vitro* or *in vivo* is technically difficult and the tribological effect of meniscectomy has not been previously studied in an articulating knee joint.

3.1.1 Hypothesis and Aims of the Study

It was hypothesised that removing of the meniscus from the medial compartment of the knee, in our *in vitro* experimental simulation, would substantially deplete the biphasic lubrication mechanism. Increased contact stresses arising from the reduced contact areas, as well as the increased friction, would lead to direct surface

degradation and wear of cartilage in the short term. An understanding of the mechanisms of degradation of articular cartilage and the time course of degradation following meniscectomy is important in research and development of interventional therapies for damaged menisci, whether they be direct biomechanical, surgical or biological interventions.

The aim of the investigation described in this chapter, was to study the tribological response (friction and wear) of the medial compartment of the natural knee joint, with and without the intact meniscus, under physiologically relevant, dynamic loading and motion. The pendulum friction simulator was used to apply this dynamic loading and motion, representative of the walking cycle.

The experimental simulation of the natural medial compartment (with the intact meniscus), formed the negative control group of this study. A flat stainless steel plate, simulating a tibial hemiarthroplasty, formed the positive control group. In this chapter the tribological response of meniscectomy is investigated, and compared with the positive and negative control groups.

3.2 Materials and Methods

Medial femoral condyles and the medial side of tibial plateaus were harvested from bovine knees, as described in Sections 2.2 and 2.3 and they were set-up in jigs for the friction simulator as described in Section 2.4. The effect of meniscectomy was examined by removing the meniscus, leaving the tibial plateau exposed to articulate with the femoral condyle. The meniscus was removed using a scalpel and all other dissection and set-up procedures were carried out, as described in Sections 2.3 and 2.4.

The pendulum friction simulator was used to apply a dynamic axial force, as described in Section 2.5. Two levels of loading were used, a physiologically relevant load, based on Simon's calculations of bovine knee joint loads (Simon, 1970) and a reduced level of loading to examine the effects of reduced contact stress. The higher dynamic load ranged between 66 N during swing phase to a maximum peak load of just over 1,000 N during stance. The lower dynamic load ranged between 16 N during swing phase to a peak load of 250 N during stance. For the remainder of this study, only the stance phase load or the maximum peak load (PL) will be referred to for simplicity.

There were six test groups performed for this study as outlined in Table 3-1. The negative control group for this study, as well as for the remaining studies of this thesis, was the simulation of the natural medial compartment – the femur articulating with the tibia and meniscus. The positive control group was the worst-case hemiarthroplasty simulation - the femur articulating with a flat stainless steel. The fluid film thickness was predicted for the positive control group, based on a study by Jin *et al.*, in which the transient lubrication in knee prosthesis with compliant layers, was considered (Jin *et al.*, 1998). The methodology and results of this fluid film prediction can be found in Appendix I. Fluid film predictions including the meniscus would be very complex and to the best of the authors knowledge, have not been reported before.

Load (N)	Bearing	Acronym
1,000	Femoral condyle vs tibia and meniscus	AC-vs-AC+meniscus
250		
1,000	Femoral condyle vs tibia with meniscectomy	AC-vs-AC_meniscectomy
250		
1,000	Femoral condyle vs stainless steel flat plate	AC-vs-SSFP
250		

Table 3-1: Six test groups for meniscectomy study. The table shows the three different bearings used in this study, the loads they were tested at and the acronym used to describe each throughout this chapter.

For each test group six specimens were tested. Tests ran for 3,600 cycles at 1 Hz, equivalent to one hour of walking. Following testing in the friction simulator, specimens were allowed to recover for 24 hours in PBS solution before making silicon rubber replicas of each condyle and tibial surface. Then specimens were stored in PBS solution and frozen at -20°C until MRI scanning. In cases where it was impossible to detect any wear from the MRI scans, histology sections were dissected from the cartilage surfaces and preparation and staining was carried out, as described in Section 2.10.

Throughout Section 3.3 results were analysed using single factor ANOVA. Where individual differences between group means were discussed throughout the text, the T-method was used, unless otherwise stated.

3.3 Results

3.3.1 Friction Measurements

The coefficient of friction against loading time for the three bearings (AC-vs-AC+meniscus; AC-vs-SSFP and AC-vs-AC_meniscectomy) is shown in Figure 3-1 and Figure 3-2, tested at applied peak loads (PL) of 250 N and 1,000 N, respectively. At both levels of loading, the coefficient of friction increased upon removal of the meniscus and the AC-vs-SSFP had the highest frictional coefficient of the three groups. Following testing at the PL of 250 N, there was some surface fibrillation visible on the femoral condyles articulating with the SSFP. The articulating surfaces from the AC-vs-AC+meniscus and AC-vs-AC_meniscectomy groups showed no signs of surface damage upon visual inspection following testing, at this lower level of loading.

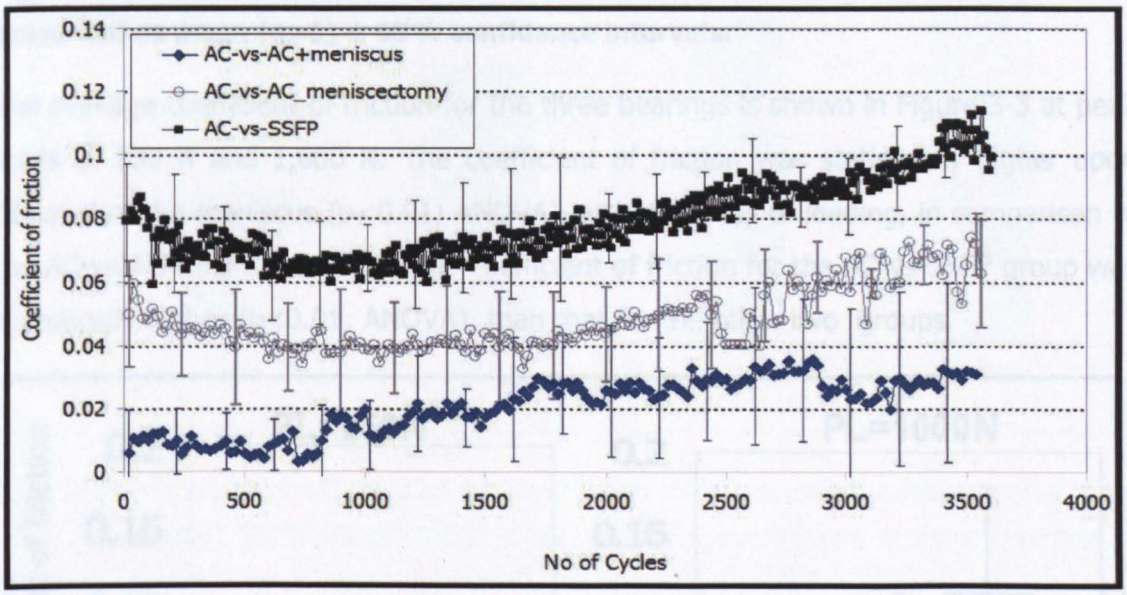

Figure 3-1: Coefficient of friction over 3,600 cycles at a peak load of 250 N. Data presented as mean (n=6) ± 95% confidence intervals.

During friction testing at the PL of 1,000 N, the condyles from the AC-vs-SSFP group displayed catastrophic wear of the cartilage through to the underlying bone after less than 300 cycles, at which point the test was discontinued. The AC-vs-AC+meniscus and AC-vs-AC_meniscectomy groups were tested successfully for the full 3,600 cycles, at this higher load. Some surface fibrillation was found on the condyles from the AC-vs-AC_meniscectomy group but there was no damage visible on any of the surfaces from the AC-vs-AC+meniscus group.

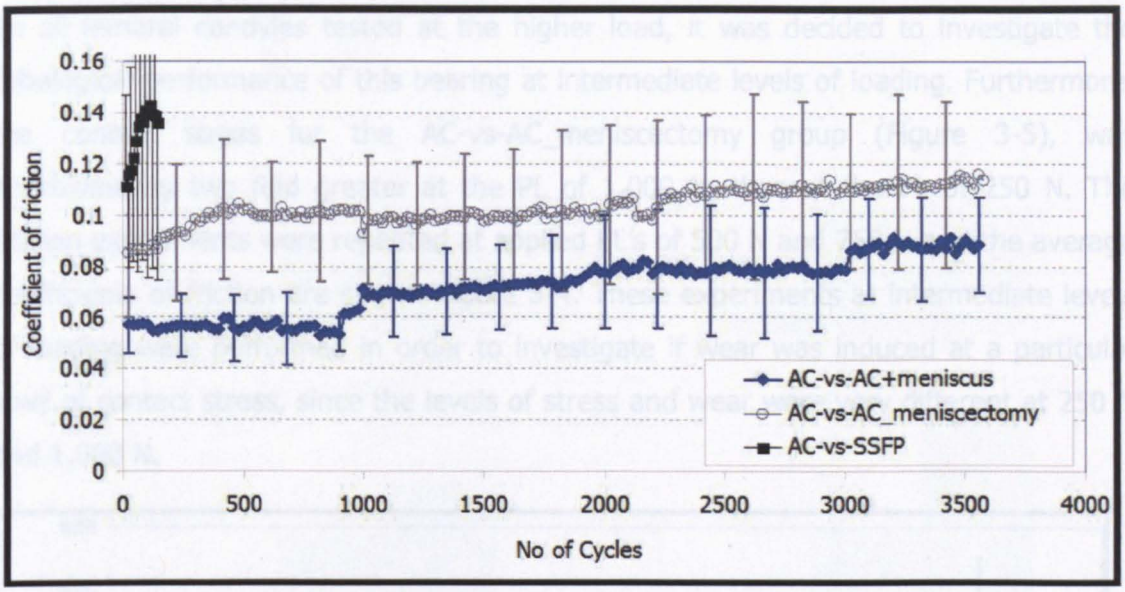

Figure 3-2: Coefficient of friction over 3,600 cycles at a peak load of 1,000 N. Data presented as mean (n=6) ± 95% confidence intervals.

The average coefficient of friction for the three bearings is shown in Figure 3-3 at peak loads of 250 N and 1,000 N. The coefficient of friction was statistically higher upon removal of the meniscus ($p<0.01$; ANOVA), at both levels of loading, in comparison to the AC-vs-AC+meniscus group. The coefficient of friction for the AC-vs-SSFP group was statistically higher ($p<0.01$; ANOVA), than that for the other two groups.

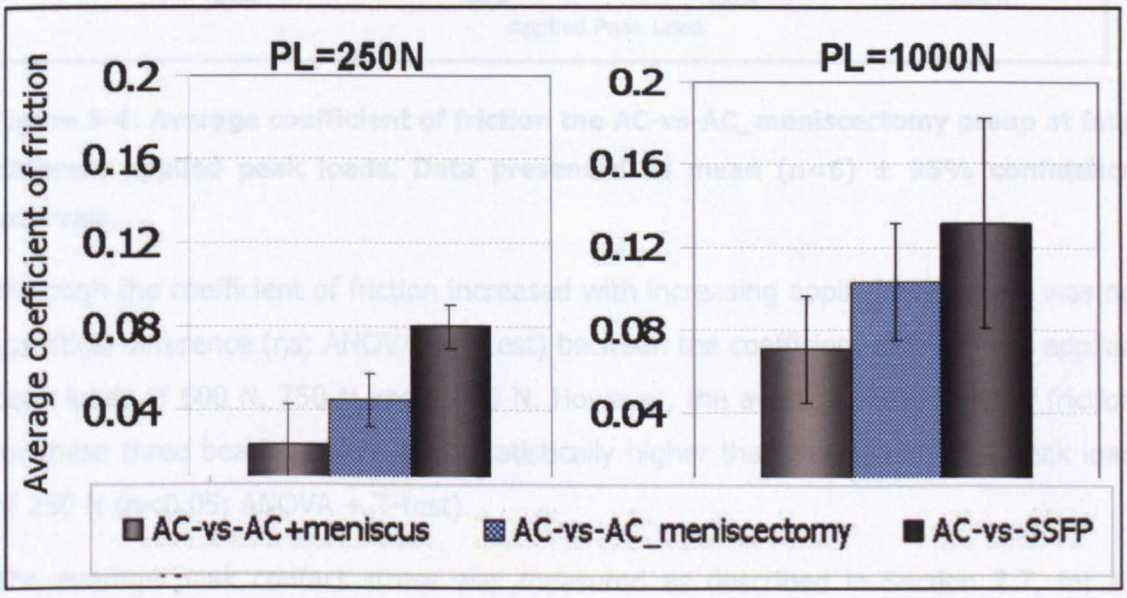

Figure 3-3: Average coefficient of friction for each bearing, at peak loads of 250 N and 1,000 N. Data presented as mean (n=6) ± 95% confidence intervals.

Due to the fact that there was no detectable wear on any of the surfaces from the AC-vs-AC_meniscectomy group tested at the lower load, but surface fibrillation was visible

on all femoral condyles tested at the higher load, it was decided to investigate the tribological performance of this bearing at intermediate levels of loading. Furthermore, the contact stress for the AC-vs-AC_meniscectomy group (Figure 3-5), was approximately two fold greater at the PL of 1,000 N, than at the PL of 250 N. The friction experiments were repeated at applied PL's of 500 N and 750 N and the average coefficients of friction are shown Figure 3-4. These experiments at intermediate levels of loading were performed in order to investigate if wear was induced at a particular level of contact stress, since the levels of stress and wear were very different at 250 N and 1,000 N.

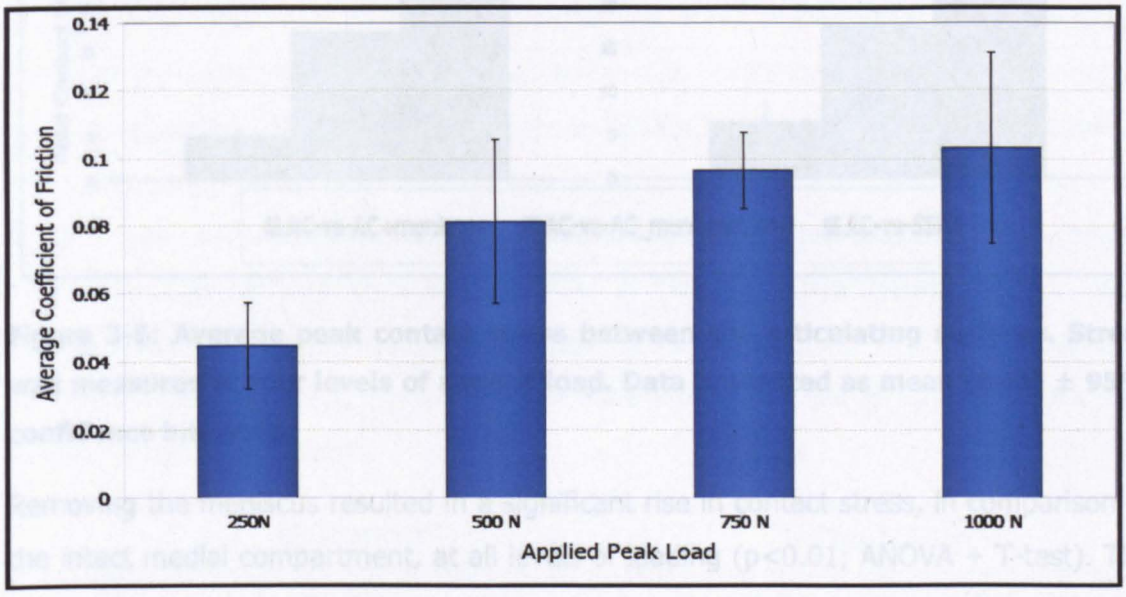

Figure 3-4: Average coefficient of friction the AC-vs-AC_meniscectomy group at four different applied peak loads. Data presented as mean (n=6) ± 95% confidence intervals.

Although the coefficient of friction increased with increasing applied load, there was no statistical difference (ns; ANOVA + T-test) between the coefficient of friction at applied peak loads of 500 N, 750 N and 1,000 N. However, the average coefficients of friction for these three bearings were each statistically higher than the friction at a peak load of 250 N ($p<0.05$; ANOVA + T-test).

The average peak contact stress was measured as described in Section 2.7, for all three bearings at applied peak loads of 250 N, 500 N, 1,000 N and 1,500 N as shown in Figure 3-5.

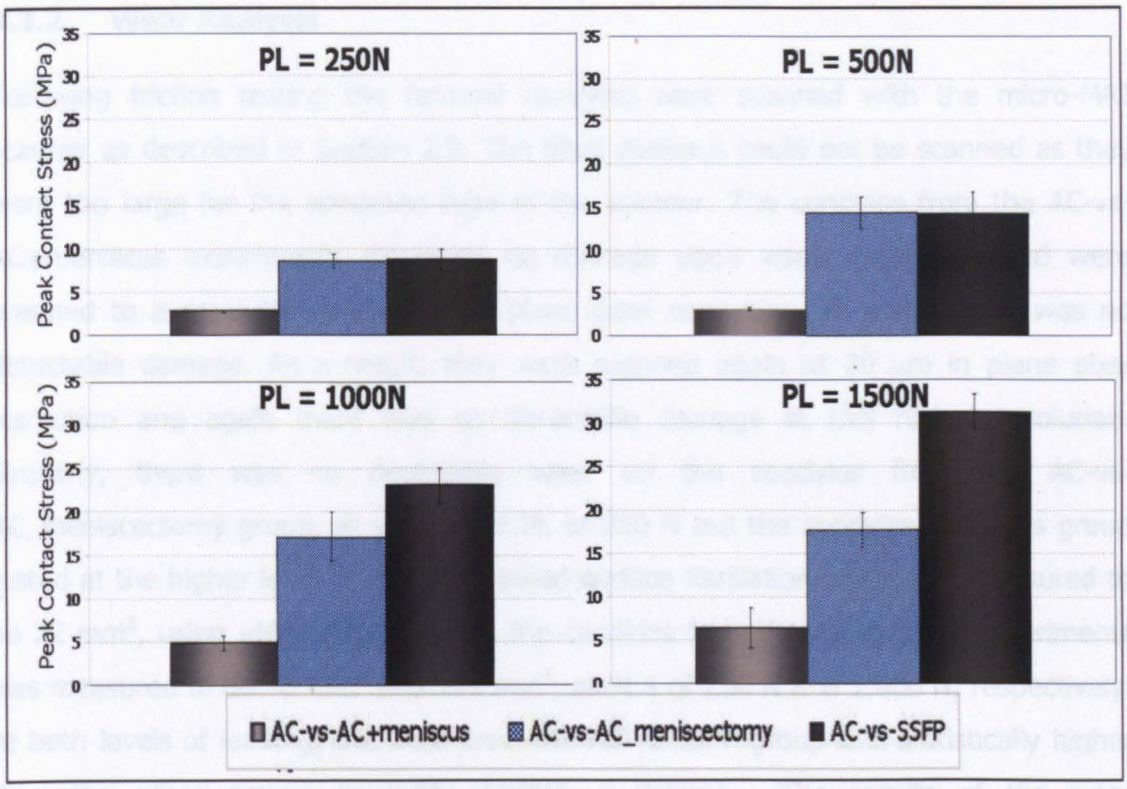

Figure 3-5: Average peak contact stress between the articulating surfaces. Stress was measured at four levels of applied load. Data presented as mean (n=6) ± 95% confidence intervals.

Removing the meniscus resulted in a significant rise in contact stress, in comparison to the intact medial compartment, at all levels of loading ($p<0.01$; ANOVA + T-test). The large proportion of joint forces which normally acted through the meniscus, passed through the very incongruous cartilage surfaces of the femoral condyle and tibial plateau. This very incongruous articulation meant that joint forces passed through relatively small contact areas, resulting in larger contact stresses. Even at an applied PL of 1,500 N, the contact stress for the AC-vs-AC+meniscus group was only 6.4 MPa, which was lower than for the AC-vs-AC_meniscectomy group at an applied PL of 250 N (8.6 MPa).

At the two lower levels of loading there was no significant difference (ns; ANOVA + T-test) between the contact stresses for the AC-vs-AC_meniscectomy and the AC-vs-SSFP groups. However, when the applied PL was increased to 1,000 N and 1,500 N, the contact stresses for the AC-vs-SSFP group were statistically higher ($p<0.01$; ANOVA + T-test) than both of the other two bearings. The contact stresses were as high as 23.1 MPa and 31.3 MPa, at PL's of 1,000 N and 1,500 N respectively.

3.3.2 Wear Analysis

Following friction testing the femoral condyles were scanned with the micro-MRI scanner as described in Section 2.9. The tibial plateaus could not be scanned as they were too large for the specimen tube in the scanner. The condyles from the AC-vs-AC+meniscus experiments displayed no damage upon visual inspection and were scanned to a resolution of 78 μm in plane pixel resolution, at which there was no detectable damage. As a result, they were scanned again at 20 μm in plane pixel resolution and again there was no detectable damage at this higher resolution. Similarly, there was no detectable wear on the condyles from the AC-vs-AC_meniscectomy group, at an applied PL of 250 N but the condyles from this group tested at the higher level of loading showed surface fibrillation which was measured to be 72 mm^3, using μMRI. The wear on the condyles from the AC-vs-SSFP experiments was measured to be 46 mm^3 and 191 mm^3, at PL's of 250 N and 1,000 N, respectively. At both levels of loading, the wear from the AC-vs-SSFP group was statistically higher than the other groups ($p<0.01$; ANOVA + T-test). The results of the wear measurements are shown in Figure 3-6. Due to the repeatability of this methodology, described in Section 2.9.2, any variation in the results was deemed to be primarily due to inter-specimen variation.

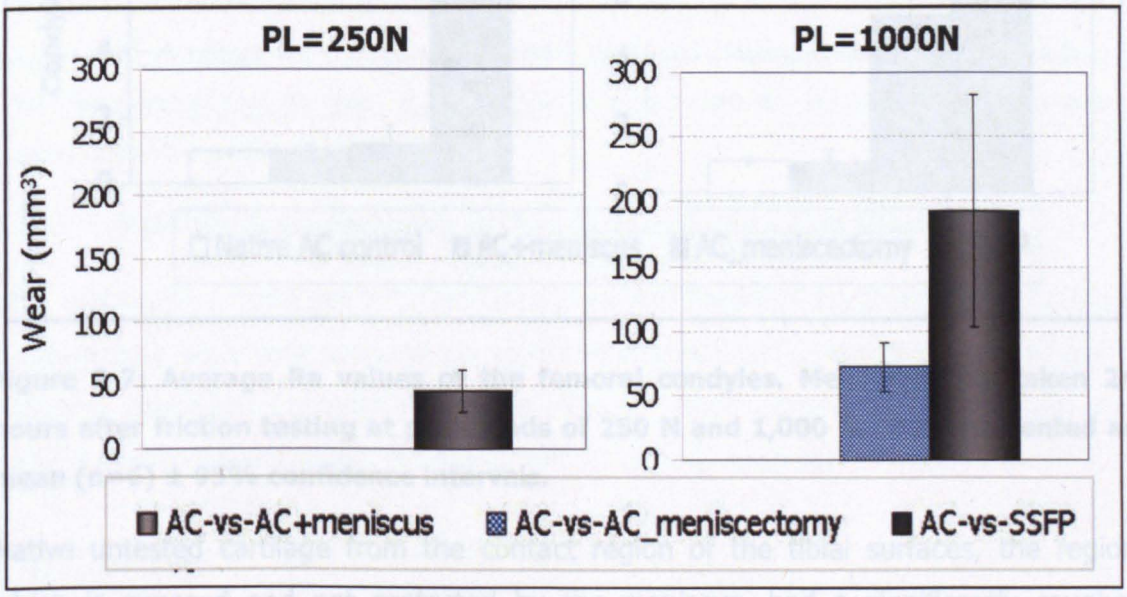

Figure 3-6: Average volume of cartilage removed from the femoral condyles during testing. There was no wear detectable on the condyles from the AC-vs-AC+meniscus group at either load or on those from the AC-vs-AC_meniscectomy at low load. Data presented as mean (n=6) ± 95% confidence intervals.

The surface roughness (Ra value) was measured using Talysurf as described in Section 0. The Ra values of the femoral condyles and tibial surfaces are shown in Figure 3-7 and Figure 3-8, respectively. Native, untreated cartilage taken from the contact regions on the femoral condyles and tibial surfaces was also measured as a control.

The Ra values of the condyles from the AC-vs-AC+meniscus group tested at both levels of loading, and the Ra value condyles from the AC-vs-AC_meniscectomy group tested at the PL of 250 N, were approximately 1 μm and not statistically different (ns; ANOVA + T-test) from the native cartilage control. However, the condyles from the AC-vs-AC_meniscectomy group had a significantly greater ($p<0.01$; ANOVA + T-test) Ra value of 5.3 μm following testing at the higher PL of 1,000 N. The condyles from the AC-vs-SSFP group had a significantly greater Ra value than either of the natural bearings ($p<0.01$; ANOVA + T-test). It was measured to be 8 μm and 10 μm, after testing at the PL of 250 N and 1,000 N, respectively.

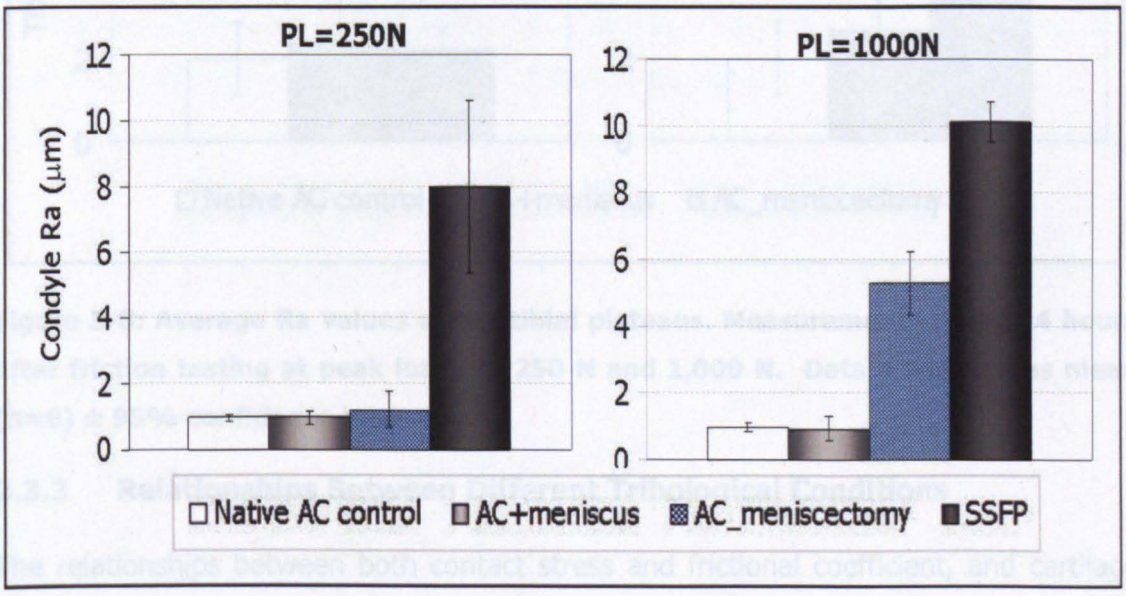

Figure 3-7: Average Ra values of the femoral condyles. Measurements taken 24 hours after friction testing at peak loads of 250 N and 1,000 N. Data presented as mean (n=6) ± 95% confidence intervals.

Native untested cartilage from the contact region of the tibial surfaces, the region which is exposed and not protected by the meniscus, had a significantly rougher surface ($p<0.04$; Students t-test) than the cartilage from the femoral condyles. This was evident upon visual inspection during dissection. The cartilage in this region of the tibia was softer to the touch and very often surface cracks were visible.

The Ra values for the tibial cartilage is shown in Figure 3-8. After testing at the PL of 250 N, the tibial surface Ra values for both groups were approximately 2 μm, not statistically different (ns; ANOVA + T-test) from the native tibial cartilage control.

Following testing at a PL of 1,000 N, there was a slight increase in the tibial surface Ra value for the AC-vs-AC+meniscus group to 2.7 μm but it was not statistically different from the control (ns; ANOVA + T-test). However, the Ra value for the AC-vs-AC_meniscectomy group increased significantly to 8.7 μm ($p<0.01$; ANOVA + T-test).

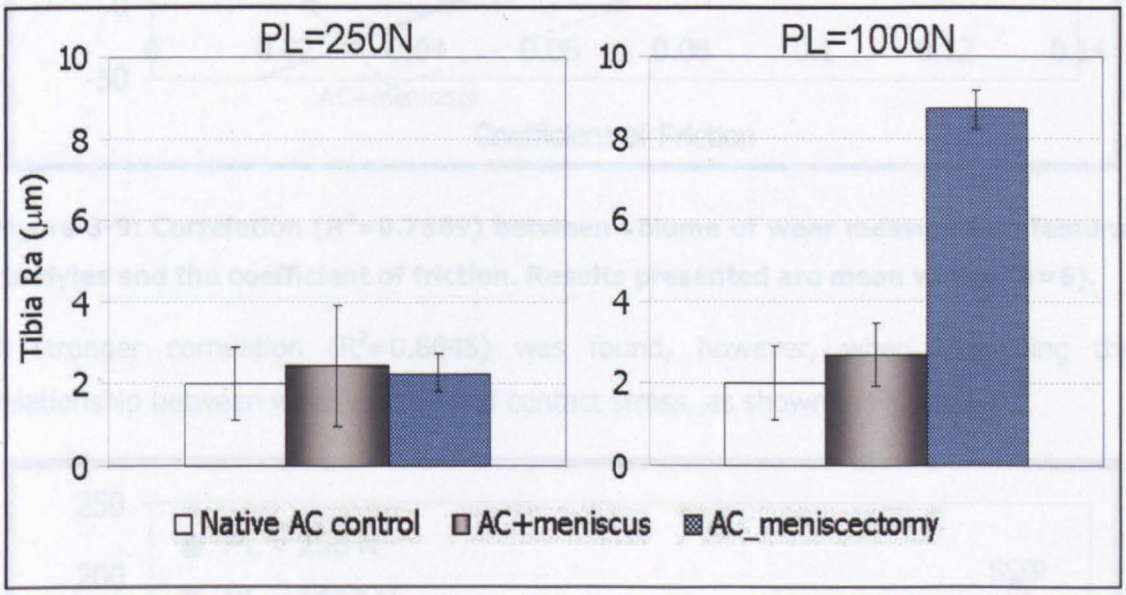

Figure 3-8: Average Ra values of the tibial plateaus. Measurements taken 24 hours after friction testing at peak loads of 250 N and 1,000 N. Data presented as mean (n=6) ± 95% confidence intervals.

3.3.3 Relationships Between Different Tribological Conditions

The relationships between both contact stress and frictional coefficient, and cartilage degeneration were examined, to try to determine at what levels of contact stress or frictional coefficient cartilage wear was induced. Good correlation ($R^2=0.7809$) was found between wear volume and coefficient of friction, as shown in Figure 3-9.

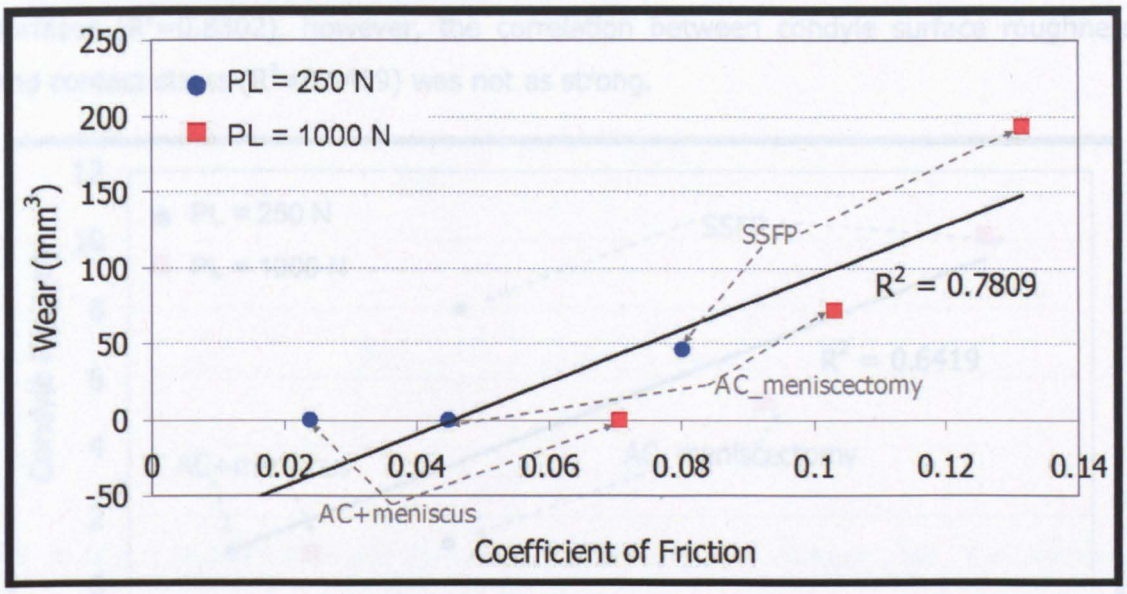

Figure 3-9: Correlation (R^2=0.7809) between volume of wear measured on femoral condyles and the coefficient of friction. Results presented are mean values (n=6).

A stronger correlation (R^2=0.8645) was found, however, when examining the relationship between wear volume and contact stress, as shown in Figure 3-10.

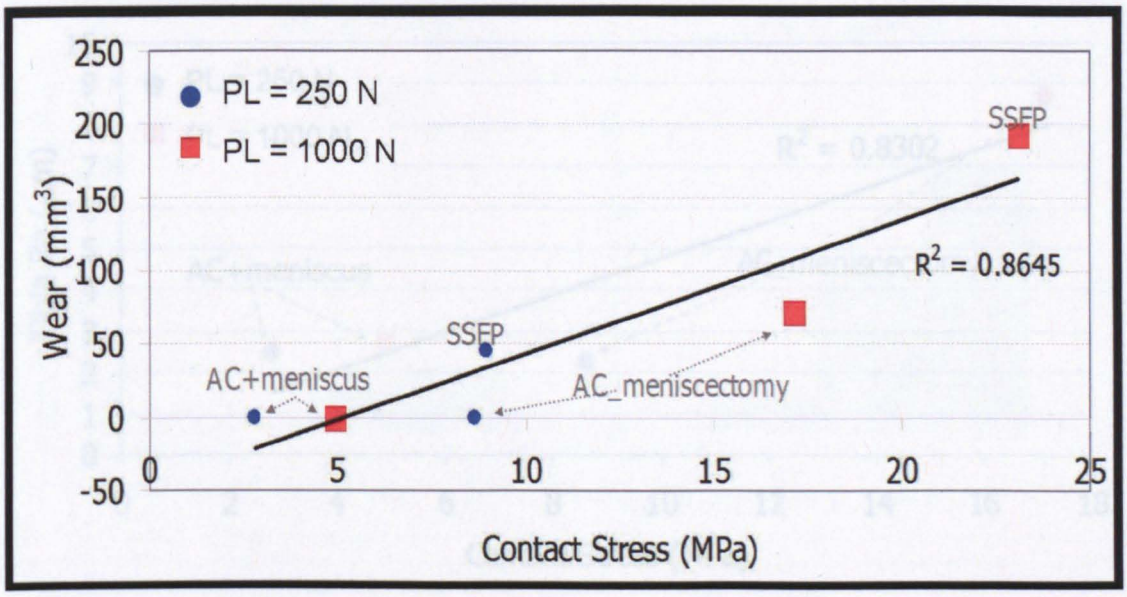

Figure 3-10: Correlation (R^2=0.8645) between volume of wear measured on the femoral condyles and measured peak contact stress. Results presented are mean values (n=6).

The correlations between surface roughness and contact stress, are shown in Figure 3-11 and Figure 3-12, for the femoral condyles and tibial surfaces, respectively. A good correlation was found between contact stress and the surface roughness of the tibial

surfaces (R^2=0.8302), however, the correlation between condyle surface roughness and contact stress (R^2=0.6419) was not as strong.

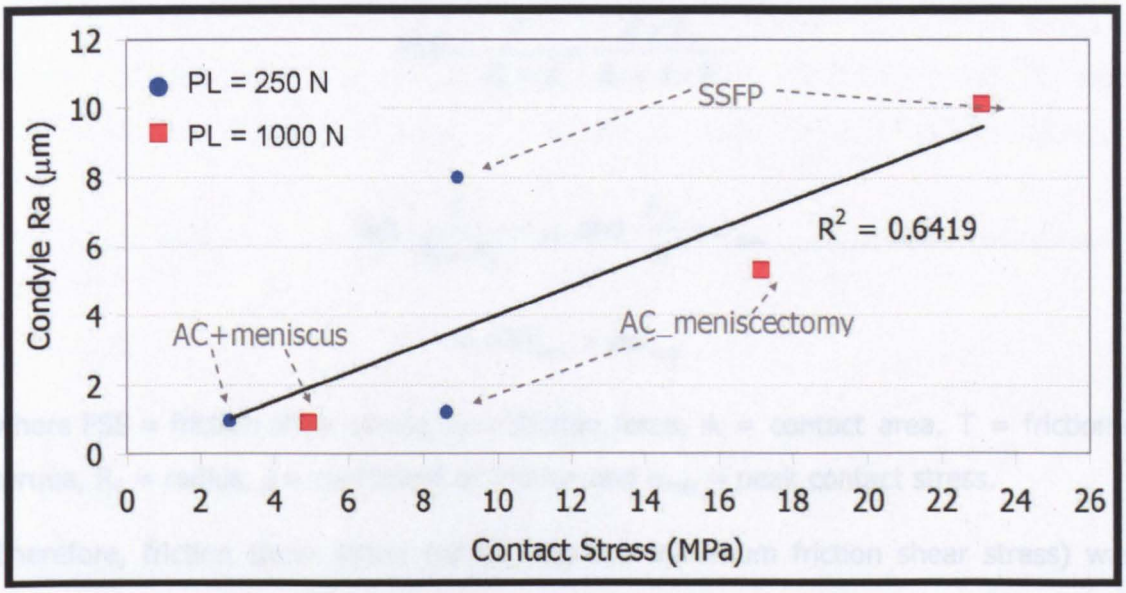

Figure 3-11: Correlation (R^2=0.6419) between Ra value of femoral condyles and measured peak contact stress. Results presented are mean values (n=6).

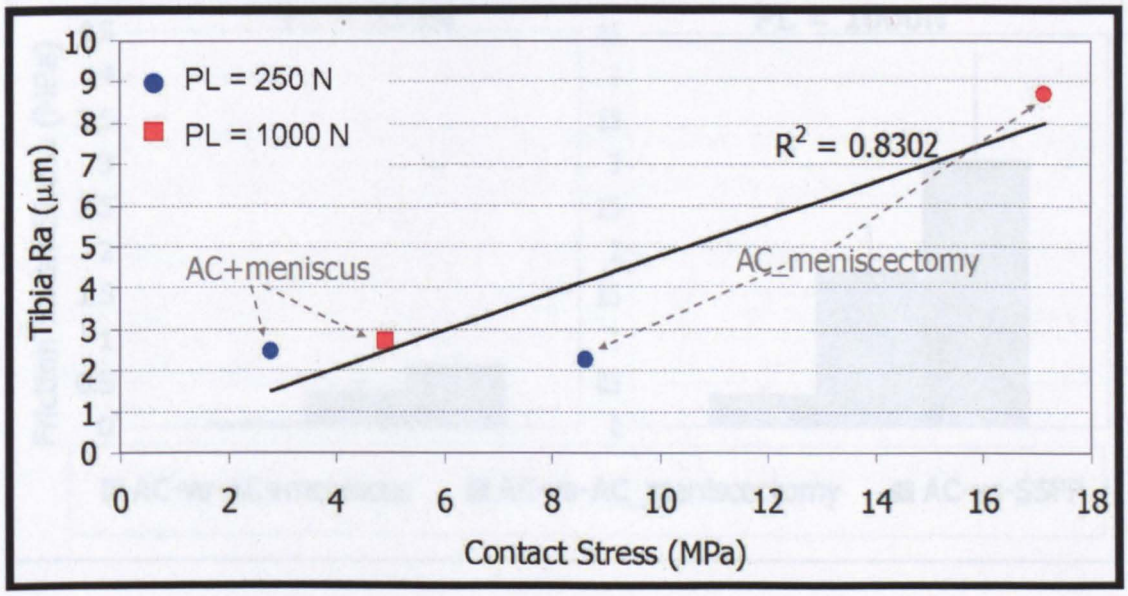

Figure 3-12 Correlation (R^2=0.8302) between Ra value of tibial plateaus and measured peak contact stress. Results presented are mean values (n=6).

Although the coefficient of friction can give a good indication of cartilage degeneration, wear of cartilage and coefficient of friction do not always have a linear relationship. The complex nature of its biphasic composite structure may provide only low resistance to shear stress at the articular surface and it is possible that the degradation and wear

of cartilage is dependent on the shear stress at the articular surface, the friction shear stress (FSS).

$$FSS = \frac{T}{R_1 \times A} = \frac{T \times F_F}{R_1 \times A \times F_F}$$

$$\text{But } \frac{T}{R_1 \times F_F} = \mu \text{ and } \frac{F_F}{A} = \sigma_{max}$$

$$\Rightarrow FSS_{max} = \mu\sigma_{max}$$

where FSS = friction shear stress, F_F = friction force, A = contact area, T = frictional torque, R_1 = radius, μ = coefficient of friction and σ_{max} = peak contact stress.

Therefore, friction shear stress (which was the maximum friction shear stress) was obtained by computing the product of peak contact stress and frictional coefficient. The average friction shear stress for each bearing is shown in Figure 3-13.

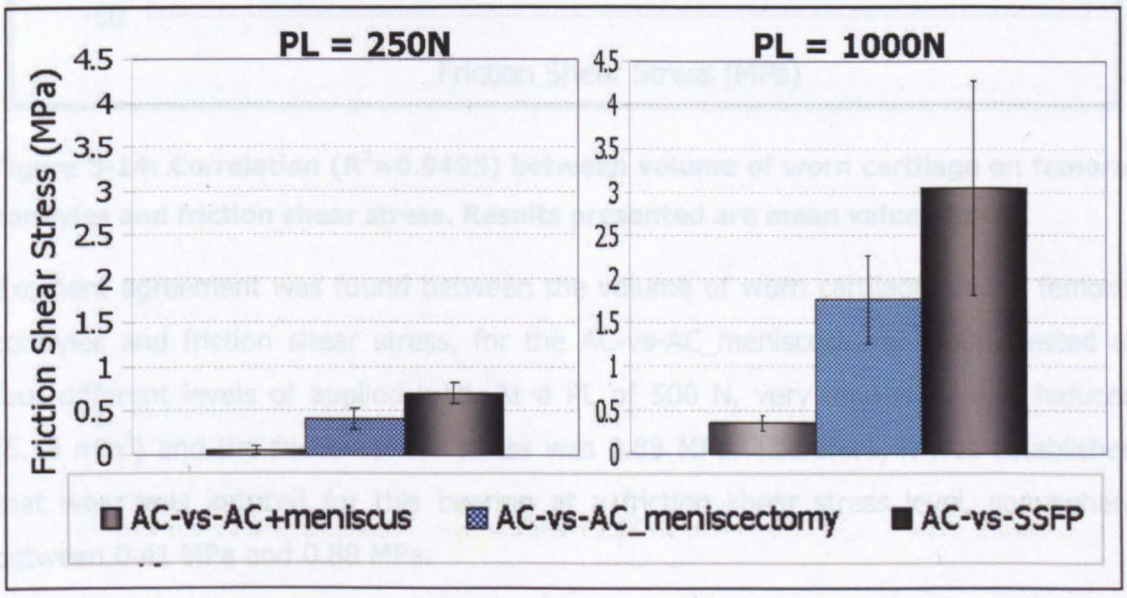

Figure 3-13: Average friction shear stress at applied peak loads of 250 N and 1,000 N. Data presented as mean (n=6) ± 95% confidence intervals.

Removing the meniscus had an impact on the levels of friction shear stress at both applied peak loads. The friction shear stress for the AC-vs-AC_meniscectomy, was statistically higher than that for the AC-vs-AC+meniscus ($p<0.01$; ANOVA + T-test). Replacing the tibial plateau with a hard material such as stainless steel, simulating a

hemiarthroplasty situation, resulted in a further significant increase ($p<0.01$; ANOVA + T-test) in the levels of friction shear stress.

The relationship between the volume of cartilage wear and friction shear stress is shown in Figure 3-14, where excellent correlation ($R^2=0.9495$) was found. No wear was detected on any bearing surfaces, in which the friction shear stress was below 0.5 MPa.

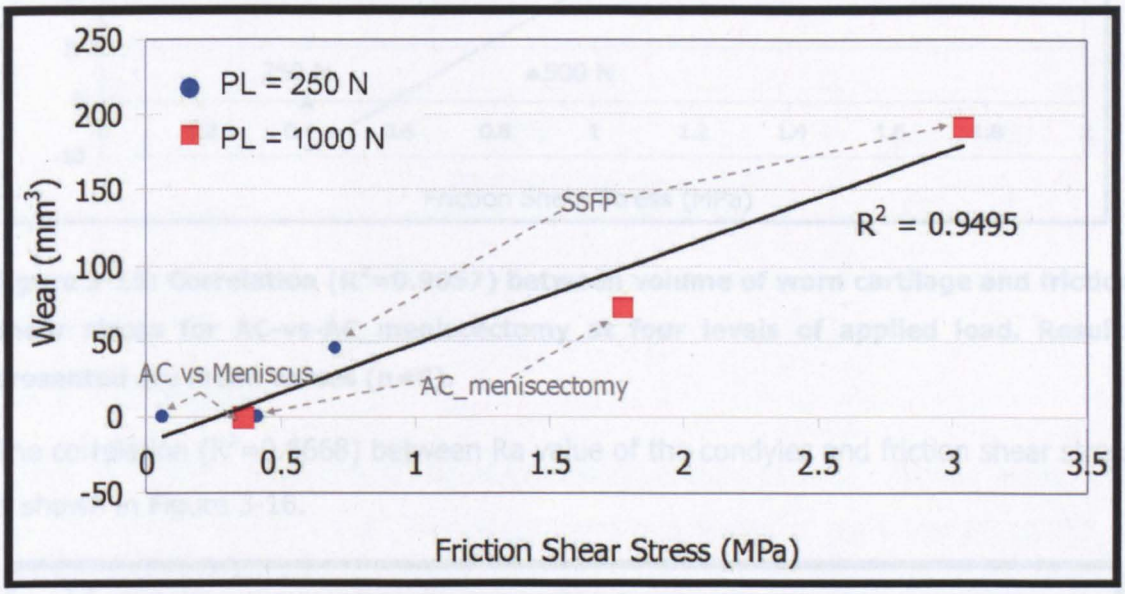

Figure 3-14: Correlation ($R^2=0.9495$) between volume of worn cartilage on femoral condyles and friction shear stress. Results presented are mean values (n=6).

Excellent agreement was found between the volume of worn cartilage on the femoral condyles and friction shear stress, for the AC-vs-AC_meniscectomy group, tested at four different levels of applied load. At a PL of 500 N, very little wear was induced (5.19 mm^3) and the friction shear stress was 0.88 MPa. Therefore, it was established that wear was induced for this bearing at a friction shear stress level, somewhere between 0.41 MPa and 0.88 MPa.

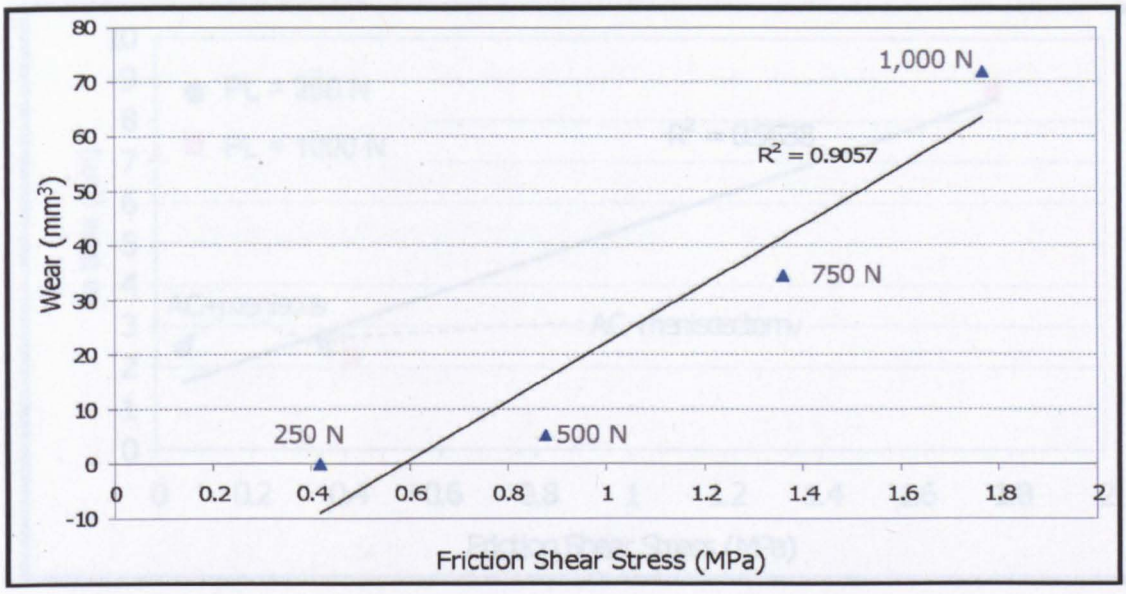

Figure 3-15: Correlation (R^2=0.9057) between volume of worn cartilage and friction shear stress for AC-vs-AC_meniscectomy at four levels of applied load. Results presented are mean values (n=6).

The correlation (R^2=0.6668) between Ra value of the condyles and friction shear stress is shown in Figure 3-16.

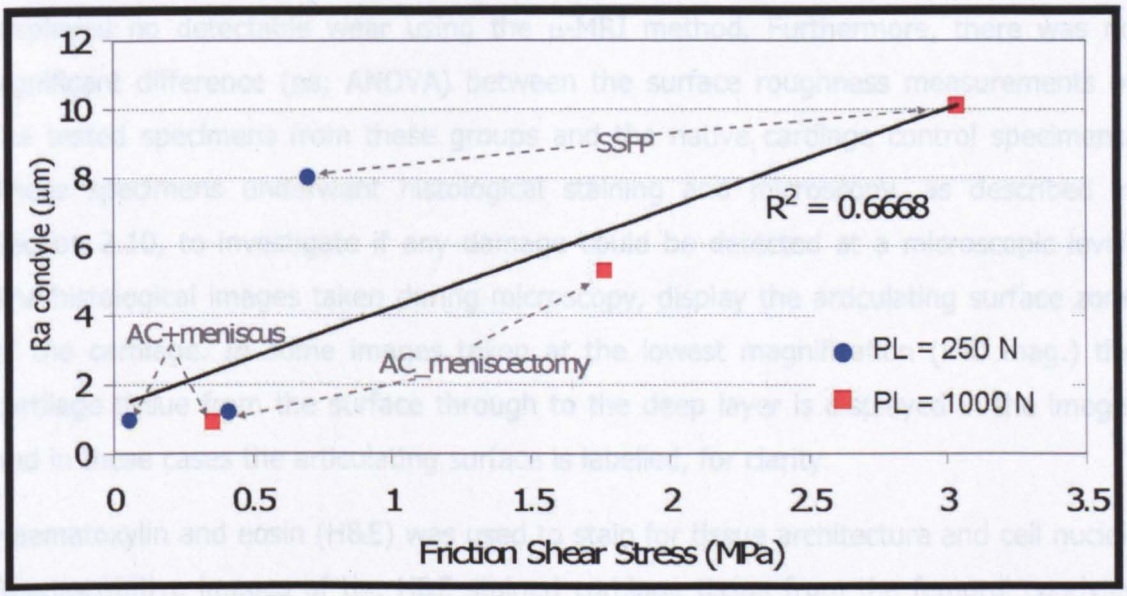

Figure 3-16: Correlation (R^2=0.6668) between Ra value on femoral condyles and friction shear stress. Results presented are mean values (n=6).

The relationship between tibial plateau surface roughness and friction shear stress is shown in Figure 3-17, where a strong correlation (R^2=0.9538) was found.

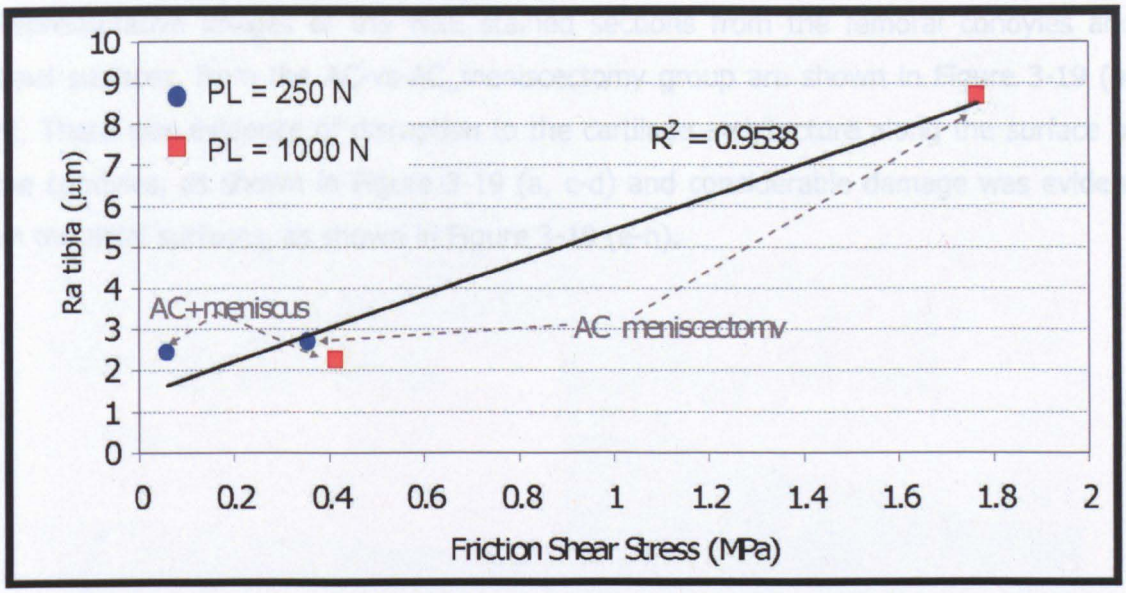

Figure 3-17: Correlation (R^2=0.9538) between Ra value on tibial plateaus and friction shear stress. Results presented are mean values (n=6).

3.3.4 Histology

Tested specimens from the AC-vs-AC+meniscus groups (at both applied loads) and specimens from the AC-vs-AC_meniscectomy group tested at the lower PL of 250 N, displayed no detectable wear using the μ-MRI method. Furthermore, there was no significant difference (ns; ANOVA) between the surface roughness measurements of the tested specimens from these groups and the native cartilage control specimens. These specimens underwent histological staining and microscopy, as described in Section 2.10, to investigate if any damage could be detected at a microscopic level. The histological images taken during microscopy, display the articulating surface zone of the cartilage. In some images taken at the lowest magnification (x40 mag.) the cartilage tissue from the surface through to the deep layer is displayed in the image, and in these cases the articulating surface is labelled, for clarity.

Haematoxylin and eosin (H&E) was used to stain for tissue architecture and cell nuclei. Representative images of the H&E stained cartilage tissue from the femoral condyles and tibial surfaces, from the AC-vs-AC+meniscus group are shown in Figure 3-18. The surface architecture of the condyles appeared to be intact and free from any damage, as can be seen in Figure 3-18 (a-d). Similarly, the structure of the tibial surface appeared intact Figure 3-18 (e-d) but some surface irregularities were visible (Figure 3-18 (h)).

Representative images of the H&E stained sections from the femoral condyles and tibial surfaces, from the AC-vs-AC_meniscectomy group are shown in Figure 3-19 (a-h). There was evidence of disruption to the cartilage architecture along the surface of the condyles, as shown in Figure 3-19 (a, c-d) and considerable damage was evident on the tibial surfaces, as shown in Figure 3-19 (e-h).

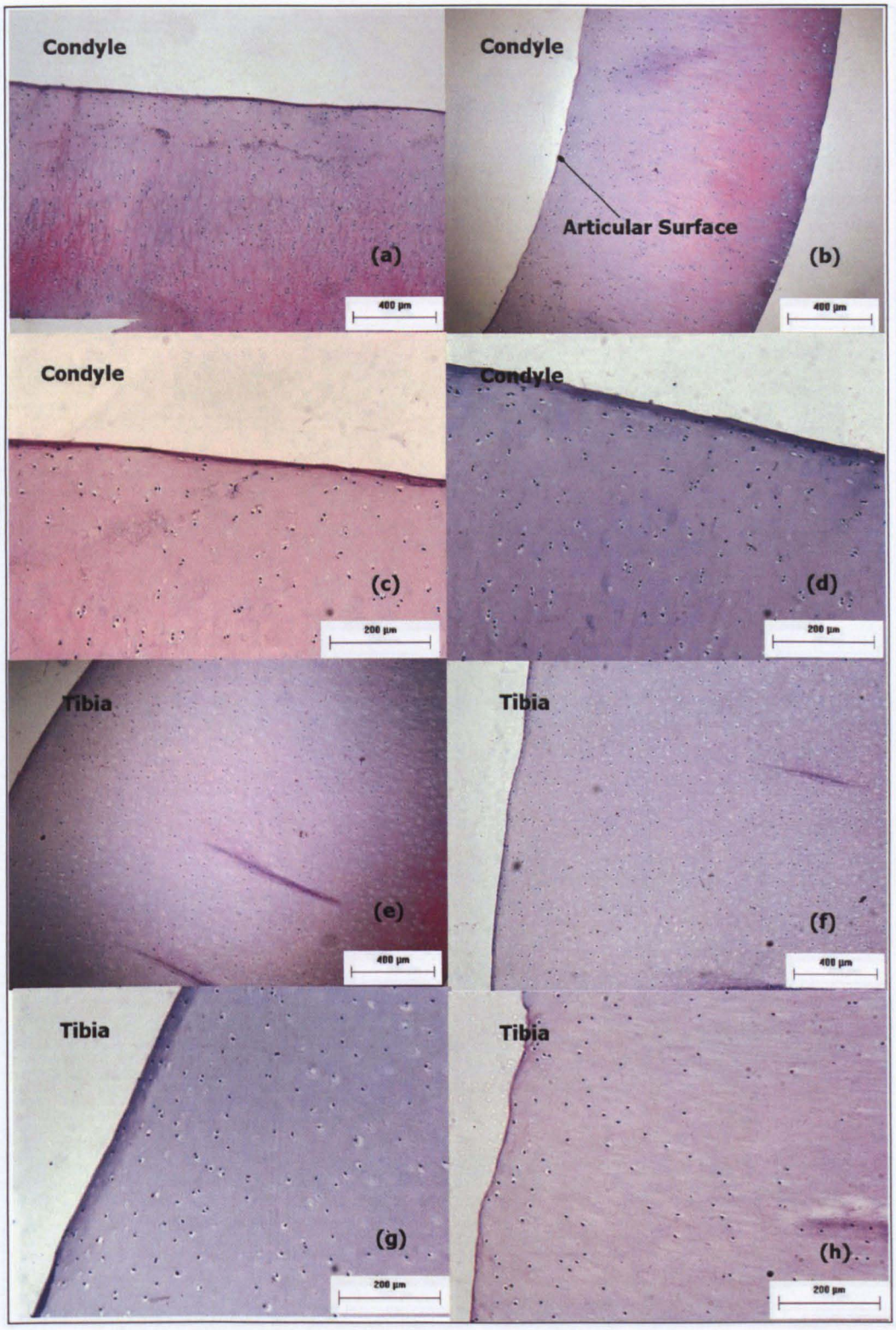

Figure 3-18: H&E stained cartilage from AC-vs-AC+meniscus group: Cartilage from contact region of femoral condyle (a & b) x40 mag. and (c & d) x100 mag. Cartilage from contact region of tibial surface (e & f) x40 mag. and (g & h) x100 mag.

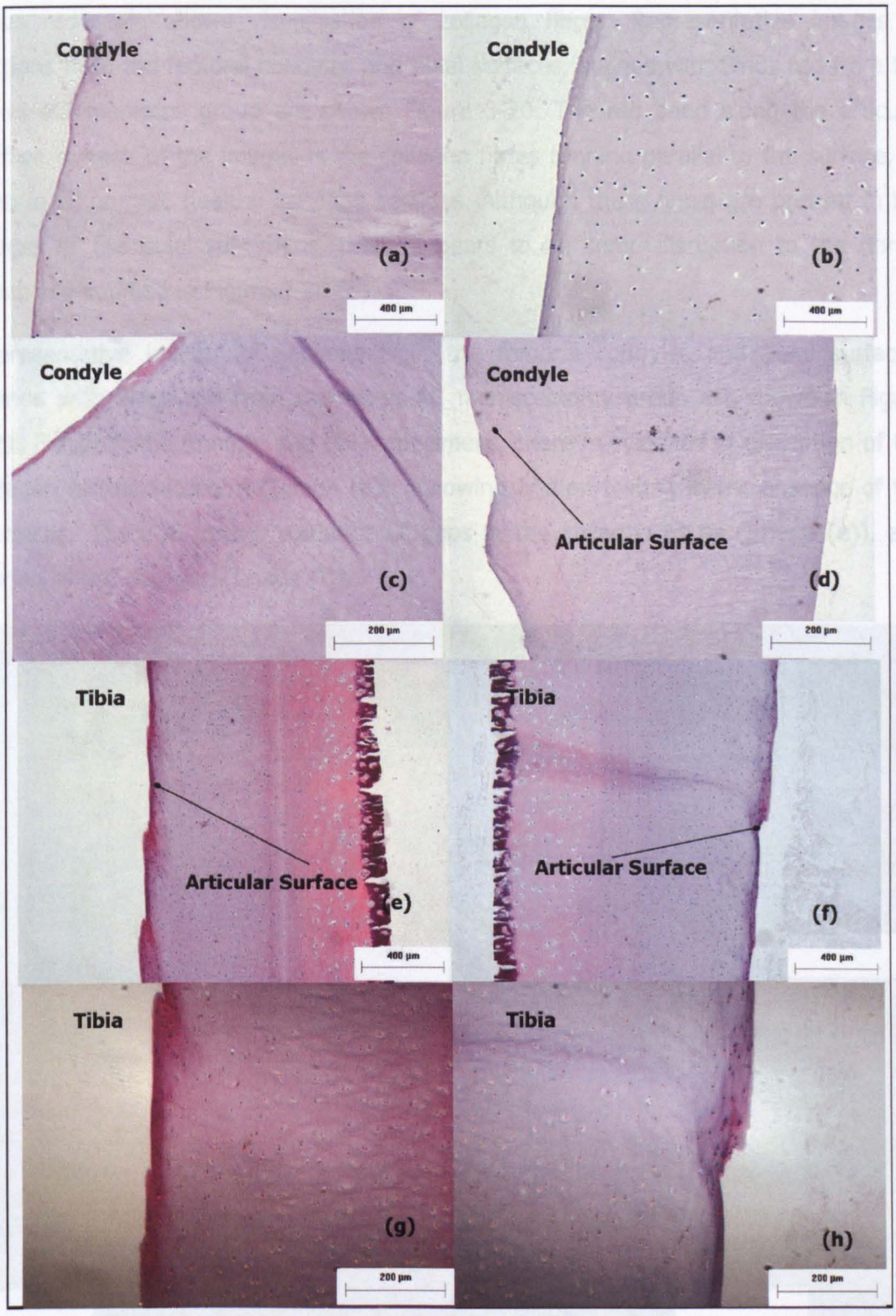

Figure 3-19: H&E stained cartilage from AC-vs-AC_meniscectomy group. Cartilage from contact region of femoral condyle (a & b) x40 mag. and (c & d) x100 mag. Cartilage from contact region of tibial surface (e & f) x40 mag. and (g & h) x100 mag.

Sirius red stain allows visualisation of collagen fibres. Representative images of sections from the femoral condyles and tibial surfaces, stained with Sirius red from the AC-vs-AC+meniscus group are shown Figure 3-20. The red band along the articular surface in each of the images is the collagen fibres running parallel to the surface, as seen in all normal, healthy cartilage sections. Although these fibres are present in the images of the tibial specimens, there appears to be some disruption to the fibres, which are outlined in Figure 3-20 (d).

Representative images of sections from the femoral condyles and tibial surfaces, stained with Sirius red from the AC-vs-AC_meniscectomy group are shown in Figure 3-21. For both the femoral and tibial specimens, there is evidence of disruption of the collagen histoarchitecture (Image (b)), following friction testing in the absence of the meniscus. There is further evidence of gaps in the collagen fibres (Image (e)), and tearing of the collagen (Image (f)).

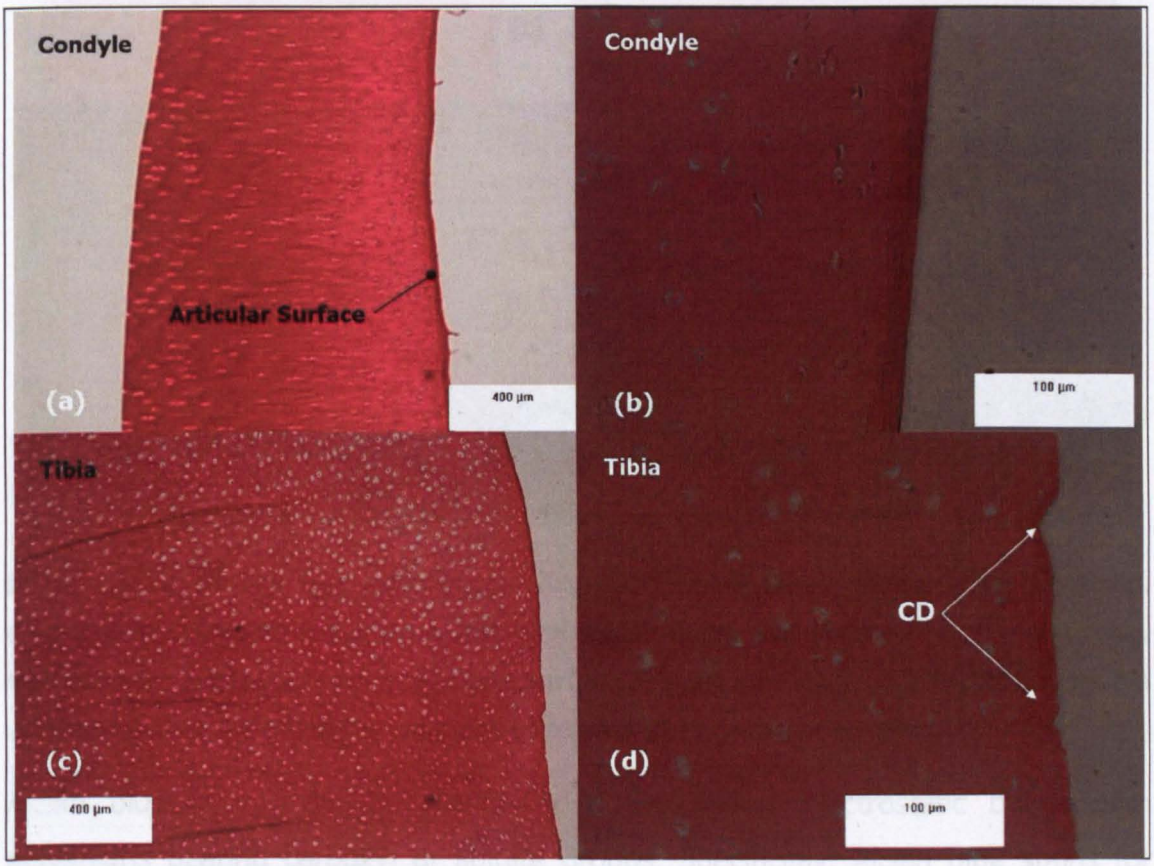

Figure 3-20: Sirius red stained cartilage from AC-vs-AC+meniscus group: Cartilage from the contact region of femoral condyle (a) x40 mag. and (b) x200 mag. Cartilage from the contact region of tibial surface (c) x40 mag. and (d) x200 mag. CD (collagen disruption) denotes areas of possible disruption to the collagen fibres running parallel to the articular surface.

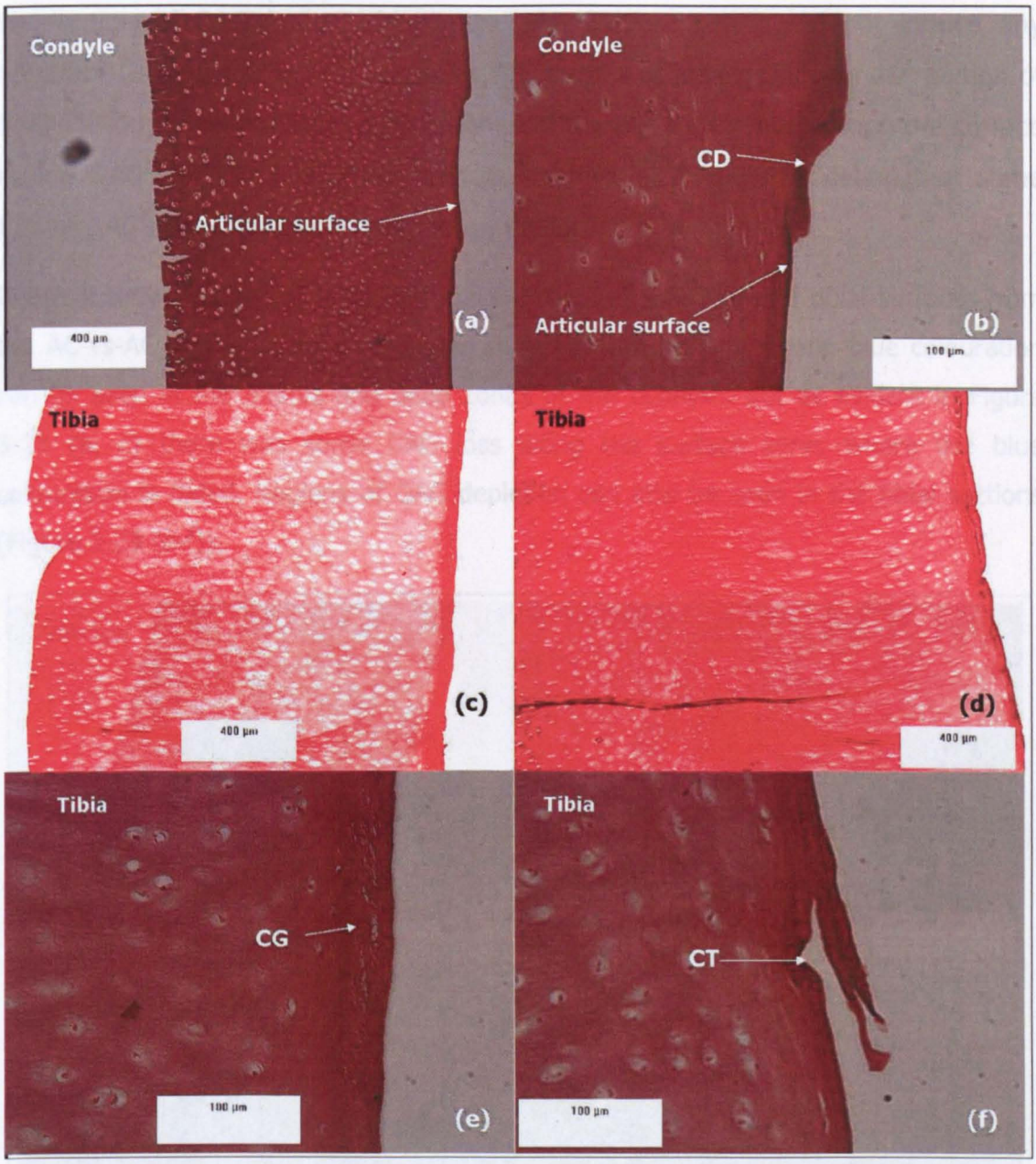

Figure 3-21: Sirius red stained cartilage from AC-vs-AC_meniscectomy group. Cartilage from contact region of femoral condyle (a) x40 mag. and (b) x200 mag. Cartilage from contact region of tibial surface (c & d) x40 mag. (e & f) x200 mag. CD = collagen disruption; CG = collagen gaps and CT = collagen tearing.

Alcian blue is a positively charged dye that forms electrostatic bonds with polyanions bearing carboxyl or sulfate groups. Specifically, Alcian blue stains for GAG's. Representative images of sections from the femoral condyles and tibial surfaces from the AC-vs-AC+meniscus group, are shown in Figure 3-22. On examining the femoral condyle sections, the concentration of blue colour was uniform throughout the tissue as shown in Figure 3-22 (a-b), indicating that the

distribution of GAG's was uniform and the friction testing did not induce any apparent GAG loss. The tibial surfaces displayed a relatively uniform distribution of GAG's through the middle and deep zones of the tissue, however, along the surface region GAG staining was greatly reduced Figure 3-22 (c-d), indicating that some loss of GAG's may have occurred during testing.

Representative images of sections from the femoral condyles and tibial surfaces from the AC-vs-AC_meniscectomy group are shown Figure 3-23. A strong blue colouration can be seen in the middle and deep zones of the condyles but as evident in Figure 3-23 (a, c) there was some GAG loss along the surface zone, where the blue colouration is faded. Regions of GAG depletion can also be seen in the tibial sections (Figure 3-23 (e-f)).

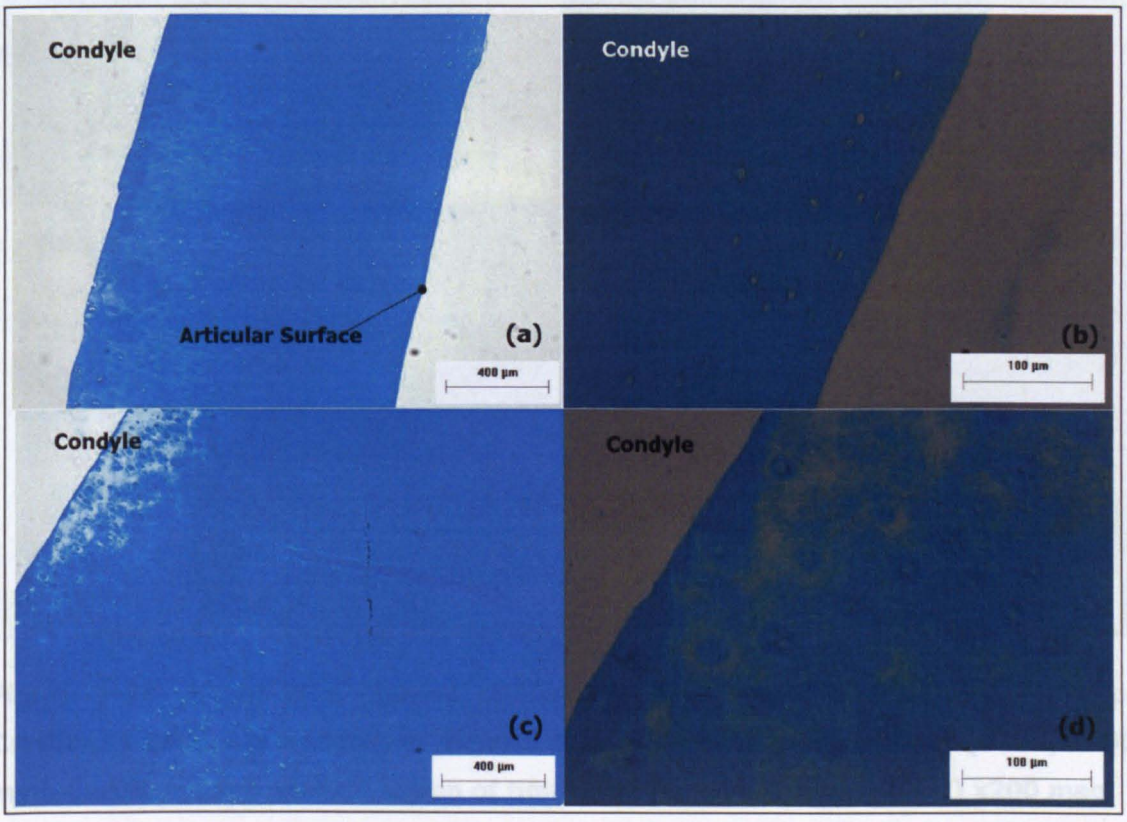

Figure 3-22: Alcian blue stained cartilage from AC-vs-AC+meniscus group: Cartilage from contact region of femoral condyle (a) x40 mag. and (b) x200 mag. Cartilage from contact region of tibial surface (c) x40 mag. and (d) x200 mag.

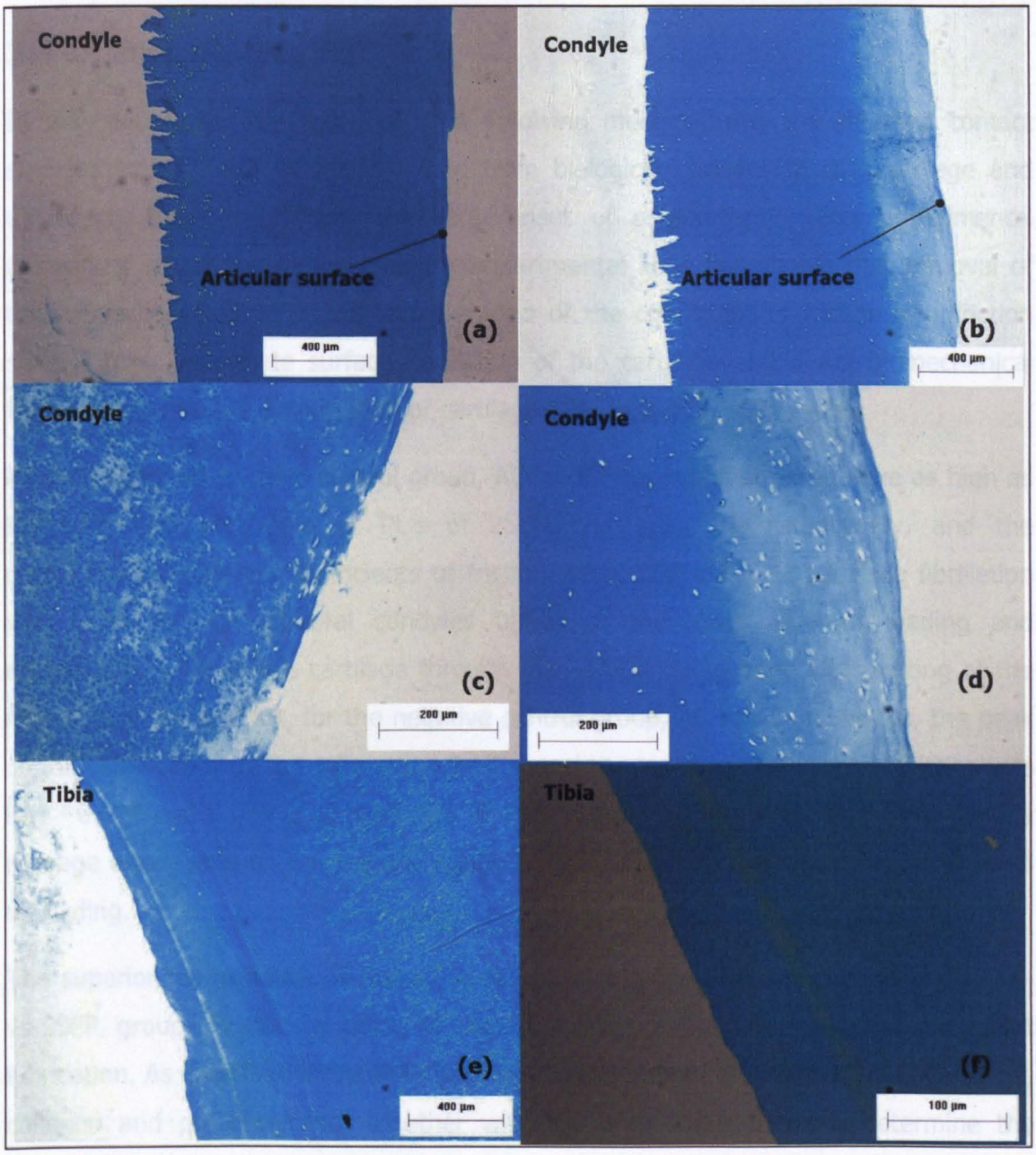

Figure 3-23: Alcian blue stained cartilage from AC-vs-AC_meniscectomy group. Cartilage from contact region of femoral condyle (a & b) x40 mag. and (c & d) x100 mag. Cartilage from contact region of tibial surface (e) x40 mag. and (f) x200 mag.

3.4 Discussion

It has been previously described that following meniscectomy the elevated contact stresses in the cartilage lead to long term biological changes in the cartilage and underlying bone, and thus, the early onset of osteoarthritis. This experimental tribological simulation of the medial compartmental knee has shown that removal of the meniscus, resulted in a direct elevation of the coefficient of friction and friction shear stress, immediate surface fibrillation of the cartilage and direct biomechanical wear and permanent deformation of cartilage after less than 3600 cycles.

When testing the positive control group, AC-vs-SSFP, contact stresses were as high as 8.9 MPa and 23.1 MPa at PL's of 250N and 1,000 N, respectively, and the corresponding average coefficients of friction were 0.08 and 0.13. Surface fibrillation was found on the femoral condyles tested at the lower level of loading and catastrophic wear of the cartilage through to the underlying bone after testing at the higher load. In contrast, for the negative control group, AC-vs-AC+meniscus, the peak contact stresses were 2.4 MPa and 4.9 MPa, and the average coefficient of friction was low - 0.024 and 0.071 at applied PL's of 250 N and 1,000 N, respectively. No surface damage was visible on the femoral condyles, menisci or tibial surfaces, at either level of loading.

The superior performance of the AC-vs-AC+meniscus group in comparison to the AC-vs-SSFP group, is due in part, to the vital role cartilage plays in synovial joint lubrication. As described in detail in Section 1.2, the structural components of cartilage, collagen and proteoglycans, together with the high water content, determine the biomechanical behaviour of cartilage and make it an exceptional bearing material. Under loading cartilage expels interstitial fluid into its unloaded areas and into the joint capsule. During this exudation process, the pressure differences produced in the fluid phase that cause the flow, also carry varying amounts of the load, effectively reducing the load carriage and stresses in the solid matrix and thus the frictional forces between opposing surfaces are minimised. When the load is removed the tissue recovers the lost water, due to its inherent swelling pressure (McCutchen, 1959; McCutchen, 1962; Mow *et al.*, 1980; Mow *et al.*, 1984b; Forster and Fisher, 1996). Many studies (Forster and Fisher, 1996; Krishnan *et al.*, 2004b; Carter *et al.*, 2007; Katta *et al.*, 2007; Northwood *et al.*, 2007) have shown the importance of the level of contact stress and

the nature of the loading-unloading cycle and the subsequent ability of cartilage to rehydrate during unloading (Bell *et al.*, 2006).

In addition to the role cartilage plays in synovial joint lubrication, the lack of wear and lower frictional coefficient with the AC-vs-AC+meniscus group, can be attributed to the conformity of the natural knee, provided by the meniscus. The superior concave surface conforms to the femoral condyle, while the flatter inferior surface conforms with the tibial plateau. Additionally, the wedge-shape of the meniscus facilitates joint stabilisation (Kawamura *et al.*, 2003). The protective role of the meniscus has been recognised by many (Fairbank, 1948; DiStefano, 1980; McDermott *et al.*, 2006). The lack of wear and low frictional coefficient with the intact medial compartment is thought to be due to this protective role played by the meniscus, the joint congruency the meniscus provides and the subsequent reduction in contact stress.

The meniscus absorbs over 50% of the load acting through the joint (Seedhom *et al.*, 1974; Krause *et al.*, 1976; Cole *et al.*, 2002). On removal of the meniscus this load passes through the cartilage surfaces. The congruity of the joint is decreased without the meniscus, and these larger loads must pass through smaller contacting areas. Furthermore, the meniscus is a biphasic material, without which the overall biphasic properties of the joint are compromised. The contact stress in this study increased by approximately 350% upon removal of the meniscus. At contact stresses of 17.1 MPa, surface fibrillation was found on the femoral condyles. However, there was no detectable wear or degradation at the lower level of loading where contact stress was 8.9 MPa. Significantly higher ($p<0.01$; ANOVA) frictional coefficients were also observed upon removal of the meniscus.

In previous studies, increase in friction was the result of loss of fluid support and increased direct solid-to-solid contact due to the unique biphasic nature of articular cartilage (Forster and Fisher, 1996; Northwood and Fisher, 2007). Other studies have indicated that the frictional force and wear are dependent on the loading cycle and contact stress (Bell *et al.*, 2006; Katta *et al.*, 2007). In the current study, when comparing the frictional response of each bearing, at the two levels of applied load, it was shown that at the lower load (with artificially reduced contact stress), the coefficient of friction was reduced in comparison to the coefficient of friction at the higher, more physiologically relevant load. Furthermore, there was a significant difference between the friction shear stress at the high and low levels of loading, for the AC-vs-AC+meniscus group ($p<0.0007$; Student's t-test) and the AC-vs-

AC_meniscectomy group ($p<0.001$; Student's t-test). It is possible that under higher physiological load and contact stress, there would be more solid-to-solid contact causing higher friction due to the biphasic nature of cartilage (Forster and Fisher, 1996). Consequently, wear increased as a result of direct solid-to-solid contact.

Meniscectomy can cause cartilage damage and fibrillation in the short term as well as in the long term osteoarthritis. A number of animal studies have reported that the tibiofemoral joint shows degenerative changes such as permanent displacement of matrix material, cartilage softening and cartilage lesions shortly after a total meniscectomy (Bruns *et al.*, 1998; Kohn *et al.*, 1992; Szomor *et al.*, 2000). In the current study, wear was observed following meniscectomy at an applied PL of 1,000 N, where the contact stress was 17.1 MPa. The volume of cartilage lost was measured to be 72 mm^3. The surface roughness was measured to be 5.3 μm and 8.7 μm for the condyle and tibial cartilage, respectively, in comparison to ~1 μm and ~2 μm on the native cartilage control specimens. Under the same two loading conditions, the wear volume and surface roughness of the condyles articulating with the SSFP positive control, were statistically higher ($p<0.01$; ANOVA). This showed that even in the absence of the meniscus, the biphasic fluid load support was maintained between the cartilage-cartilage articulation for some time, reducing contact stress, friction and wear. However, for the AC-vs-AC+meniscus group, this fluid support was maintained for longer, due to the conformity of the articulation and subsequent lower contact stress. Due to the applied loads acting through smaller contacting areas following meniscectomy, it is likely there was a more rapid decrease of the fluid load support, increased direct solid-to-solid contact, and cartilage degradation, as seen at the higher level of loading.

The relationships between both contact stress and frictional coefficient, and cartilage degradation were examined, to try to determine at what levels of contact stress or frictional coefficient cartilage wear was induced. The relationship between wear volume (on femoral condyles) and coefficient of friction is shown in Figure 3-9, where an R^2 value of 0.7772 was found. Coefficient of friction can be a good indication of cartilage degradation, but friction and wear do not always have a linear relationship when testing biological tissues such as cartilage (Forster and Fisher, 1996; Pickard *et al.*, 1998b; Katta *et al.*, 2007; Katta *et al.*, 2008c). Coefficient of friction does not, however, represent stresses acting locally on the cartilage.

The correlation between wear volume and contact stress (R^2 = 0.8645) is shown in Figure 3-10. Although good agreement was found between wear and contact stress, it is evident that the relationship did not apply under all circumstances. At an applied PL of 250 N, the contact stress for AC-vs-SSFP and AC-vs-AC_meniscectomy groups were very similar (8.9 and 8.6 MPa). There was no surface damage on the condyles, from the AC-vs-AC meniscectomy experiments, however, surface fibrillation was found on all condyles from the AC-vs-SSFP group, and the wear volume was measured to be 46 mm^3. Although, the contact stress for these two bearings was similar, the nature of the cartilage against the single-phase stainless steel articulation, resulted in a more rapid breakdown of the fluid phase load support (on the cartilage side) which induced wear on the femoral condyle. The more rapid decrease of fluid load support for cartilage articulating with hard bearings has been reported in many simple geometry experiments (Forster and Fisher, 1996; Forster and Fisher, 1999; Kumar *et al.*, 2001; Basalo *et al.*, 2005; Krishnan *et al.*, 2005; Northwood *et al.*, 2007; Northwood and Fisher, 2007). On the other hand, in the cartilage against cartilage articulation the cartilages had the ability to rehydrate during the unloaded phase of the cycle, minimising wear and the biphasic, porous nature of cartilage increased the lubricity of the contact area, reducing friction and degradation.

The correlation between the condyle surface roughness and contact stress is shown in Figure 3-11, where an R^2 value of 0.6419 was found. Similar to the previous correlation, at the same level of applied load and contact stress (8.5 - 9 MPa), the Ra value of the condyles from the AC-vs-AC_meniscectomy group were very different to those from the AC-vs-SSFP group. There was no significant difference between the Ra value of the control samples and the AC-vs-AC_meniscectomy condyles, but those from the AC-vs-SSFP experiments had an Ra value of ~8 μm. Again the differences in material properties, specifically the biphasic nature of cartilage in comparison to the single phase nature of stainless steel explain these differences.

All specimens for which an increase in surface roughness was found, a loss of cartilage volume was also found in the μMRI scans, and vice-versa, meaning one method of wear analysis was not more sensitive than the other. However, the wear volumes obtained through MRI, correlated better with contact stress than the surface roughness. It is possible that although cartilage wear in the form of surface fibrillation does tend to cause an increase in surface roughness, there may be some flattening of surface asperities during loading, resulting in a smoother surface than would otherwise

be expected. Ateshian *et al.* speculated that flattening of surface asperities was a likely phenomena, in a study investigating the dependence of the frictional response of articular cartilage on interstitial fluid pressurisation (Ateshian *et al.*, 2003). Katta *et al.* used a cartilage pin sliding against a cartilage plate experimental configuration to test healthy and GAG deficient cartilage. It was found that at nominal stress levels greater than 2 MPa, the GAG deficient samples had lost more than 60% of their initial thickness and failed to recover completely when soaked in PBS (Katta *et al.*, 2008b). The large deformations can be attributed to the reduction in compressive stiffness caused by a loss of GAG's (Katta *et al.*, 2008d). Despite the large deformations of GAG deficient cartilage, there was no increase in Ra values after testing and the Ra values were lower than for native cartilage plates. Katta *et al.* postulated that the during deformation of this cartilage with lower stiffness, smoothening of the cartilage surfaces may have occurred during the test (Katta *et al.*, 2008b).

A stronger correlation (R^2 = 0.8302) was found between the tibial plateau surface roughness and contact stress (Figure 3-12), in comparison to the condyle surface roughness. It is not fully understood why a better correlation was found between tibial surface roughness and contact stress. However, it must be noted that only four groups were included in this comparison. It does not include any data from the AC-vs-SSFP group, which had the single phase steel in the articulation and for which elevated contact stress and friction were observed, resulting in greater cartilage degradation.

It is evident that although the coefficient of friction and contact stress give a good indication of cartilage degradation, the complex biphasic tribology of cartilage make it difficult to accurately predict the effect of the changes in the tribological conditions on the subsequent degradation and wear of cartilage. It has long been recognized that cartilage has evolved to accommodate the hydrostatic stresses across the natural synovial joint and healthy synovial joints have low coefficient of friction. Also, as mentioned previously, it has been demonstrated in tribology that there is not always a strong relationship between the coefficient of friction and wear (Forster and Fisher, 1996; Pickard *et al.*, 1998b; Katta *et al.*, 2007; Katta *et al.*, 2008c). However, cartilage is no ordinary engineering material. While cartilage is designed to withstand large hydrostatic pressure, the nature of its biphasic composite structure provides only low resistance to shear stress, and thus it is possible that the degradation and wear of cartilage may be dependent on the friction shear stress, the product of frictional coefficient and contact stress. An excellent correlation (R^2=0.9487) was found between

wear and friction shear stress, as shown in Figure 3-14. This relationship was much stronger than that between wear and frictional coefficient or wear and contact stress. The correlation (R^2=0.668) between the Ra value of the condyles and friction shear stress is shown in Figure 3-16, only slightly stronger than that between the Ra value of the condyles and contact stress. Under applied loads there may be some flattening of surface asperities, which would mean that the measured surface roughness value would be lower than otherwise expected. This theory was proposed previously (Ateshian *et al.*, 2003). When examining the relationship between the tibial plateau surface roughness and friction shear stress (Figure 3-17), excellent agreement was found (R^2=0.9536). In this case, however, all articulating materials were biphasic in nature – either cartilage-on-cartilage or cartilage-on-meniscus. As discussed already, the single-phase nature of stainless steel results in elevated friction and wear, in comparison to the biphasic cartilage-on-cartilage articulation, tested at the same loading and stress conditions.

During many of the friction experiments, a small but steady rise in friction was found over the duration of the test, as shown in Figure 3-1 and Figure 3-2. The AC-vs-AC+meniscus group had the lowest average peak contact stress of all the groups, which was 2.8 MPa at an applied PL of 250 N. In a previous pin-on-plate study, performed at lower contact stress, no such rise in friction was found at up to 8 hours (Northwood and Fisher, 2007). This indicated that the higher, more physiological levels of contact stress used in this study may have caused some increase in friction, with the breakdown of cartilage constituents such as proteoglycan or collagen structure and/or the depletion of fluid load support. This theory is supported by the findings of the histological assessment of the cartilage sections, after friction testing. Following H&E and Sirius red staining of tibial cartilage sections from the AC-vs-AC+meniscus group, some disruption or breakdown of the histoarchitecture was evident (Figure 3-18 (f)) and (Figure 3-20 (d)), as well as GAG depletion (Figure 3-22 (d)) following Alcian blue staining. The breakdown of cartilage constituents was considerably more evident in the AC-vs-AC_meniscectomy group. Considerable disruption to both the condyle and tibial sections was obvious after H&E staining (Figure 3-19 (a-h)), Sirius red staining illustrated collagen disruption, gaps in the collagen architecture and tearing of collagen (Figure 3-21 (a-f)) and GAG depletion was apparent following alcian blue staining (Figure 3-23 (b, d-f)). This evidence of cartilage matrix breakdown which occurred during friction testing, particularly when the meniscus was removed, suggests that a

breakdown of fluid load support began during the tests, which resulted in an increase in solid-to-solid contact and a steady rise in friction. As discussed earlier, the breakdown of fluid support would have occurred to a greater extent in the AC-vs-AC_meniscectomy group, due to the smaller contact areas and larger contact stresses and this was also supported by the histological findings, in which the tissue disruption was markedly more severe for the AC-vs-AC_meniscectomy group.

3.5 Conclusions

This study is the first tribological simulation of the medial compartmental knee and has many advantages over simple geometry configurations. More physiologically relevant contact stresses and motion were applied, the geometry was that of the natural situation and the important biomechanical structure that is the meniscus was included. A tribological simulation of this scale can be used to examine the effects of any potential intervention for osteoarthritis of the knee such as lubricants, meniscectomy repair or cartilage defect repair.

The current study has demonstrated the direct elevation of the coefficient of friction and contact, immediate surface fibrillation, biomechanical wear and permanent deformation of cartilage upon removal of the meniscus. An important finding in this study was that although coefficient of friction gave a good indication of cartilage degradation, a stronger relationship was observed between wear and friction shear stress. Under the current test conditions, conducted for one hour, when friction shear stress levels were less than 0.5 MPa, surface degradation was prevented. It is recommended that friction shear stress be considered in all future tribological studies of articular cartilage.

This study further supports retaining the meniscus whenever possible in knee joint surgery and presents for the first time an *in vitro* model simulation system to investigate the tribological effects of meniscectomy and meniscus repair and regeneration. This model can now be applied to a wide range of interventions, which are used to repair or regenerate the meniscus.

Overall, this study supported our hypothesis that removal of the meniscus substantially diminished the biphasic lubrication mechanism leading to rapid surface damage wear and permanent deformation, at physiological load levels.

Chapter 4. Effect of Conformity of Tibial Hemiarthroplasty Prostheses

4.1 Introduction

The treatment of knee OA in the young and active patient poses a difficult problem. OA is a progressive, irreversible disease which normally requires surgical intervention. As discussed in detail in Section 1.8, commonly performed procedures such as TKA and UKA often compromise the results of future procedures and revisions, due to the fact that removing a large amount of bone stock is required. Alternative, more conservative interventions are required for the younger and more active patient, which preserve more bone stock, delaying the need for a UKA or TKA. Alternatives to UKA and TKA include hemiarthroplasty and knee spacer technology. However, degradation of the opposing femoral cartilage and onset of osteoarthritis in other compartments have been common causes of hemiarthroplasty failure to date, in the knee (Emerson and Potter, 1985; Scott *et al.*, 1985; Springer *et al.*, 2006), and the hip (D'Arcy and Devas, 1976; Amstutz *et al.*, 1994).

In the design of a hemiarthroplasty it is crucial to understand the tribology of the natural joint as well as the hemiarthroplasty bearing. Unlike normal engineering bearing mechanisms, those of synovial joints operate under a highly complex lubrication regime. Biphasic lubrication plays an important role, as well as conventional engineering hydrodynamic and boundary surface lubrication mechanisms. The wear and degradation of the biomaterial/cartilage interface is very important in the development of hemiarthroplasties. Numerous studies have been carried out to investigate the wear of cartilage against itself and against different biomaterials. These experiments have mainly been simple geometry pin-on-plate (PoP) or sphere-on-disc geometries (SoD) (Katta *et al.*, 2007; Freeman *et al.*, 2000; Northwood and Fisher, 2007; Northwood *et al.*, 2007). In order to develop a hemiarthroplasty it is important to gain an in-depth understanding of how this implant would function tribologically in the natural joint. Simple PoP and SoD experimental set-ups give a good comparison of friction and wear using different materials, but there are a number of important questions they cannot answer, related to key tribological and biomechanical system variables, but which are crucially important in clinical application:

Firstly, how much wear and degradation would a biomaterial implant impose on the opposing cartilage surface, a significant problem clinically (Emerson and Potter, 1985; Scott *et al.*, 1985; Springer *et al.*, 2006; D'Arcy and Devas, 1976; Amstutz *et al.*, 1994)? Secondly, how will the implant perform under physiological loads and motions? Finally, what are the effects of contact stress and tribology when using different implant geometries?

4.1.1 Hypothesis and Aims of the Study

In the complex biomechanics of healthy synovial joints, the meniscus fills the joint space, adding conformity to the joint, distributing the forces across the joint onto a larger area of articular cartilage, hence reducing contact stress (Kettlekamp and Jacobs, 1972; Seedhom *et al.*, 1974; Walker and Erkman, 1975; Krause *et al.*, 1976; Seedhom and Hargreaves, 1979b). Therefore, it was hypothesised that if the geometry of hemiarthroplasty or spacer bearings was based on the tibia and meniscus together, rather than simply the tibial plateau geometry (Scott *et al.*, 1985; Springer *et al.*, 2006), contact stresses would be decreased, resulting in reduced wear, and superior longevity.

The aim of the investigation described in this chapter, was to study and compare the tribological response of the intact medial compartment knee and a hemiarthroplasty-replaced medial compartmental knee, under physiologically relevant, dynamic loading and motion. Hemiarthroplasty bearings of different conformities were tested to examine the effect of conformity on contact stress and subsequently friction and degradation of cartilage.

4.2 Materials and Methods

Medial femoral condyles were harvested from bovine knees, as described in Section 2.2 and they were set-up in jigs for the friction simulator as described in Section 2.4. To simulate hemiarthroplasty stainless steel counterfaces were used. The effect of conformity of hemiarthroplasty bearings, on contact stress, friction and wear, was examined by replacing the tibial plateau with stainless steel plates of varying conformity. These plates were screwed into a jig for the friction simulator as shown in Figure 4-1(a). A stainless steel flat plate and stainless steel conforming plates with radii of 100 mm and 50 mm, were used as shown in Figure 4-1(b). The stainless

steel plates were polished and the surface roughness (Ra value) was measured to be 0.009 μm.

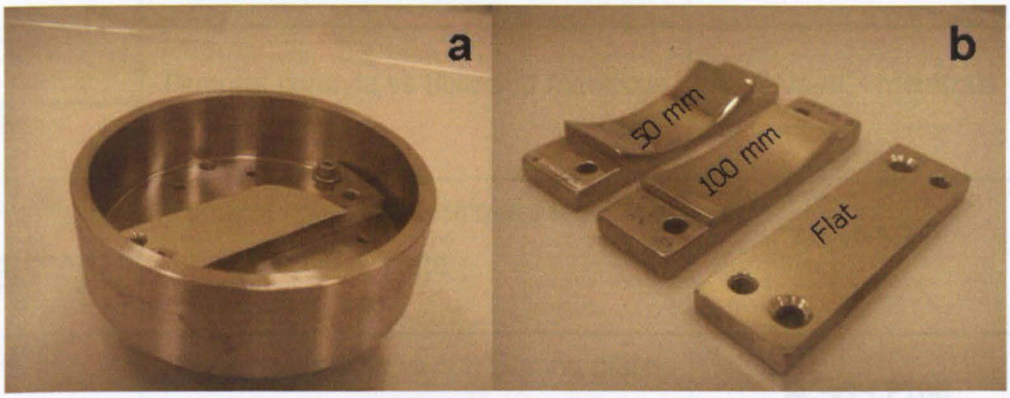

Figure 4-1: Stainless steel (SS) plates (a) Flat SS plate screwed into tibial specimen holder (b) Different geometries of SS plates.

The pendulum friction simulator was used to apply a dynamic axial force, as described in Section 2.5. Two levels of loading were used, a physiologically relevant load, based on Simon's calculations of bovine knee joints load (Simon, 1970) and a reduced level of loading to examine the effects of reduced contact stress. The higher dynamic load ranged between 66 N during swing phase to a maximum peak load of just over 1,000 N during stance. The lower dynamic load ranged between 16 N during swing phase to a peak load of 250 N during stance.

There were eight test groups performed for this study as outlined in Table 4-1. The negative control group for this study, was the simulation of the natural medial compartment – AC-vs-AC+meniscus. The positive control group was the worst-case hemiarthroplasty simulation - the femoral condyle articulating with a flat stainless steel plate. The effect of conformity of tibial bearings was investigated by using the two stainless steel plates of radii 100 mm and 50 mm.

For each test set six specimens were tested. Tests were conducted for 3,600 cycles at 1 Hz, equivalent to one hour of walking. Following testing in the friction simulator, specimens were allowed to recover for 24 hours in PBS solution before making silicon rubber replicas of each condyle and tibial surface for surface roughness measurements (Section 2.8). Then specimens were stored in PBS solution and frozen at -20°C until MRI scanning.

Load (N)	Bearing	Acronym
1,000	Femoral condyle vs tibia and meniscus	AC-vs-AC+meniscus
250		
1,000	Femoral condyle vs stainless steel flat plate	AC-vs-SSFP
250		
1,000	Femoral condyle vs conforming plate (R=100 mm)	AC-vs-CP100
250		
1,000	Femoral condyle vs conforming plate (R=50 mm)	AC-vs-CP50
250		

Table 4-1: Eight test groups used in the hemiarthroplasty conformity study. The table shows the four different bearings used in this study, the loads they were tested at and the acronym used to describe each throughout this chapter. The AC-vs-AC+meniscus group formed the negative control and the AC-vs-SSFP group formed the positive control group.

Throughout Section 4.3 results were analysed using single factor ANOVA, the findings of which are displayed in the figure legends. Where individual differences between group means were discussed throughout the text, the T-method was used.

4.3 Results

4.3.1 Friction Measurements

The coefficient of friction for each set of six specimens, tested over 3,600 cycles, at a PL of 250 N is shown in Figure 4-2. The coefficient of friction was highest for the SSFP, ranging between 0.06 and 0.11. Increasing the conformity of stainless steel plates, resulted in reduced frictional coefficients, for the SSCP100 and SSCP50, respectively. The SSCP100 group and, in particular, the SSCP50 group, had a similar frictional response to the negative control, the AC-vs-AC+meniscus group. The coefficient of friction for the AC-vs-SSCP100 group ranged between 0.03 and 0.06,

for the AC-vs-SSCP50 group it ranged between 0.02 and 0.04 and for the AC-vs-AC+meniscus it ranged between 0.01 and 0.03.

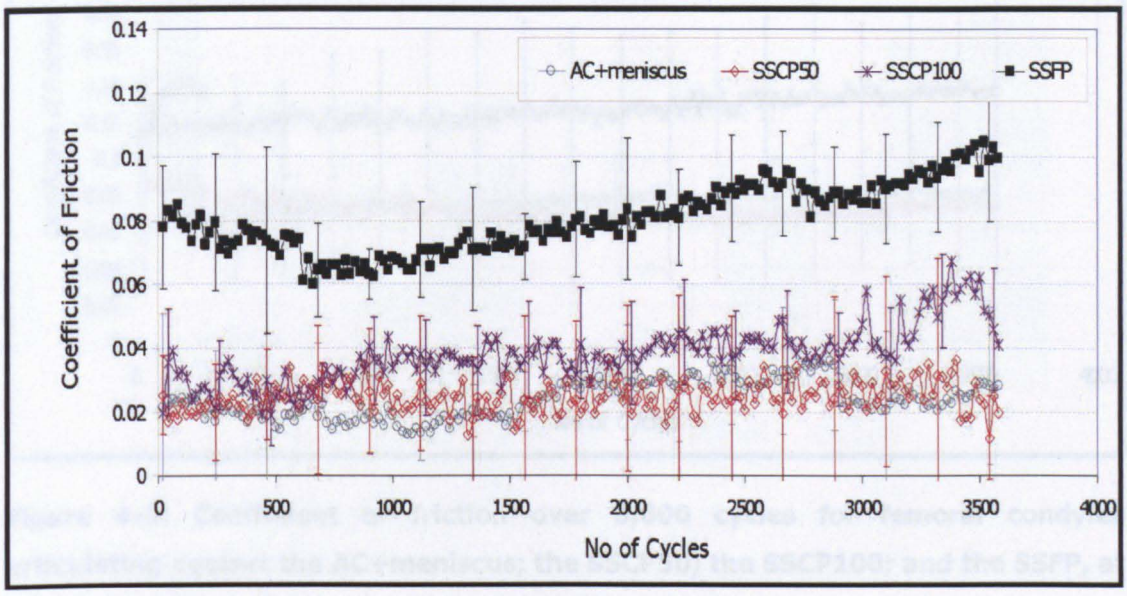

Figure 4-2: Coefficient of friction over 3,600 cycles for femoral condyles articulating against the tibia and meniscus; the SSCP50; the SSCP100; and the SSFP, at an applied peak load of 250 N. Data presented as mean (n=6) ± 95% confidence intervals.

When the bearings were tested at the higher, physiologically relevant, PL of 1,000 N the frictional coefficients were elevated for all bearings in comparison to the reduced level of loading, as shown in Figure 4-3. As described in Chapter 3, the SSFP group displayed catastrophic wear of cartilage through to the underlying bone and the test was discontinued after 300 cycles. Similar to the lower PL, the frictional coefficients decreased for all bearings, with increasing conformity. The coefficient of friction for the SSCP100 group ranged between 0.11 and 0.14, of similar magnitude to the SSFP group but the test ran successfully for the full 3,600 cycles. The coefficient of friction for the AC-vs-SSCP50 was similar to that for the AC-vs-AC+meniscus group, ranging between 0.06 and 0.08.

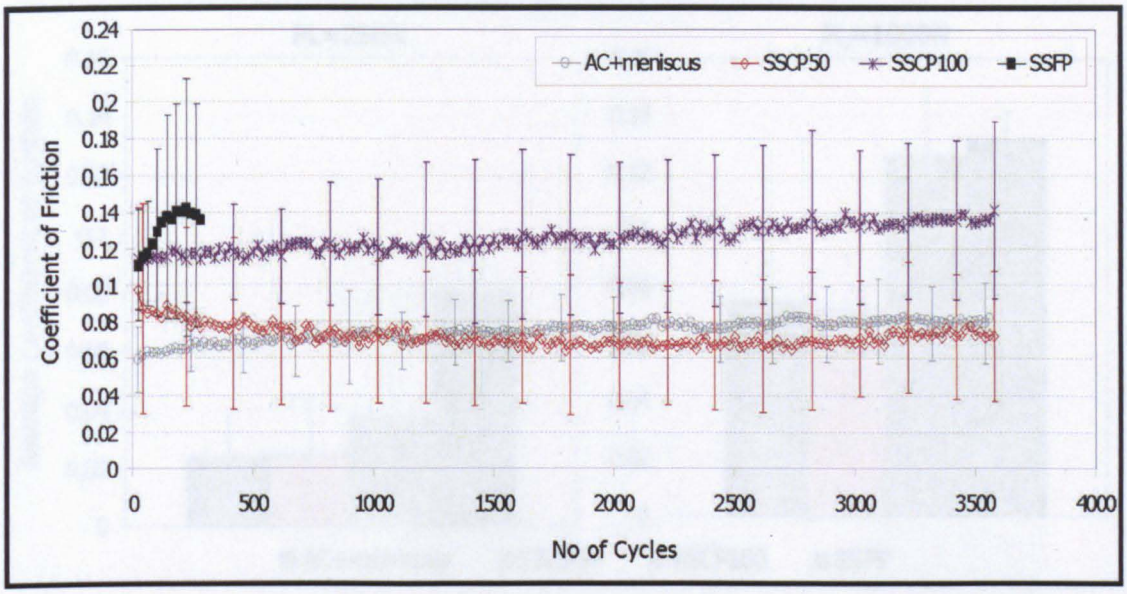

Figure 4-3: Coefficient of friction over 3,600 cycles for femoral condyles articulating against the AC+meniscus; the SSCP50; the SSCP100; and the SSFP, at an applied peak load of 1,000 N. Data presented as mean (n=6) ± 95% confidence intervals.

The average coefficient of friction for each bearing, at applied PL's of 250 N and 1,000 N is shown in Figure 4-4, which shows clearly the increasing coefficient of friction as the conformity of the bearings was decreased, although, there was no statistical difference (ns; ANOVA + T-test) between the AC-vs-SSCP50 and the AC-vs-SSCP100 groups at the lower level of loading. The coefficient of friction for the AC-vs-SSFP group was statistically higher than all of the other groups at the lower level of loading ($p<0.01$; ANOVA + T-test), however, at the higher level of loading there was no statistical difference (ns; ANOVA + T-test) between the flat plate and the AC-vs-SSCP100 group. At both levels of applied load there was no statistical difference between the frictional responses of the AC-vs-SSCP50 and the AC-vs-AC+meniscus groups (ns; ANOVA + T-test).

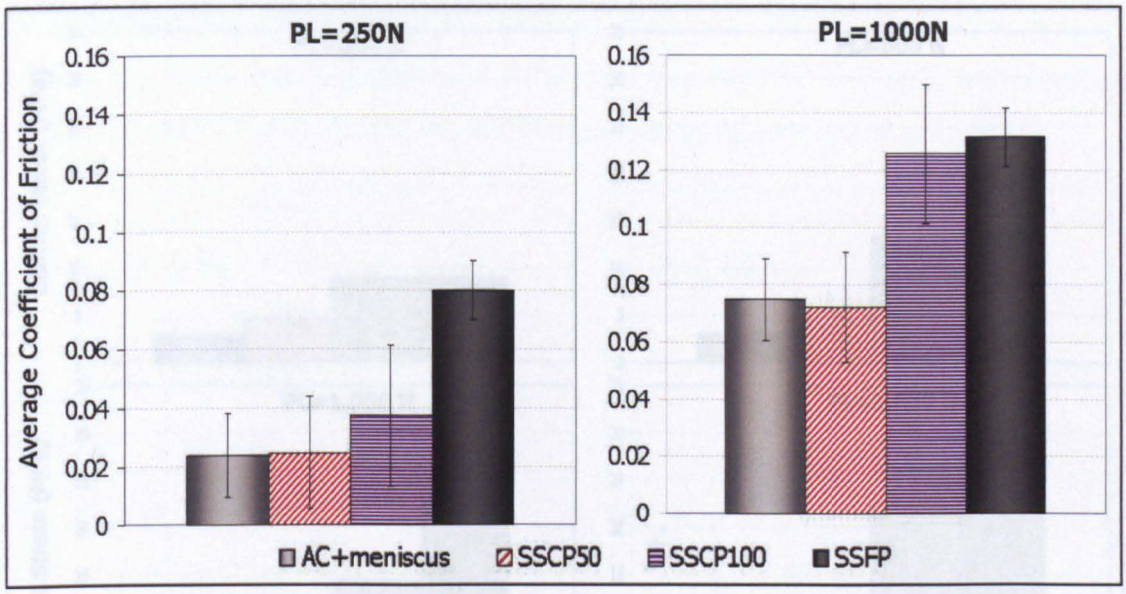

Figure 4-4: Average coefficient of friction for the four bearings, at applied peak loads of 250 N and 1,000 N. Data presented as mean (n=6) ± 95% confidence intervals.

The average peak contact stress was measured for each bearing as described in Section 2.7, at four different levels of applied load and the results are shown in Figure 4-5. Increasing contact stresses were observed with increasing load. The AC-vs-AC+meniscus group showed the lowest contact stress, even at an applied PL of 1,500 N, the peak contact stress was only 6.4 MPa. For the three stainless steel bearings the contact stress increased with decreasing conformity, particularly at the higher levels of loading. At the lower levels of loading (250 N and 500 N) there was no statistical difference (ns; ANOVA + T-test) between the contact stress for the AC-vs-SSCP100 group and the AC-vs-SSFP group. Otherwise, there was a statistical difference ($p<0.01$; ANOVA + T-test) between the contact stresses measured for the 50 mm, 100 mm and flat plate designs, at each load. Although the frictional response of the AC-vs-AC+meniscus group and AC-vs-SSCP50 were similar, the contact stresses measured for the AC-vs-SSCP50 group were statistically higher ($p<0.01$; ANOVA + T-test), at each load.

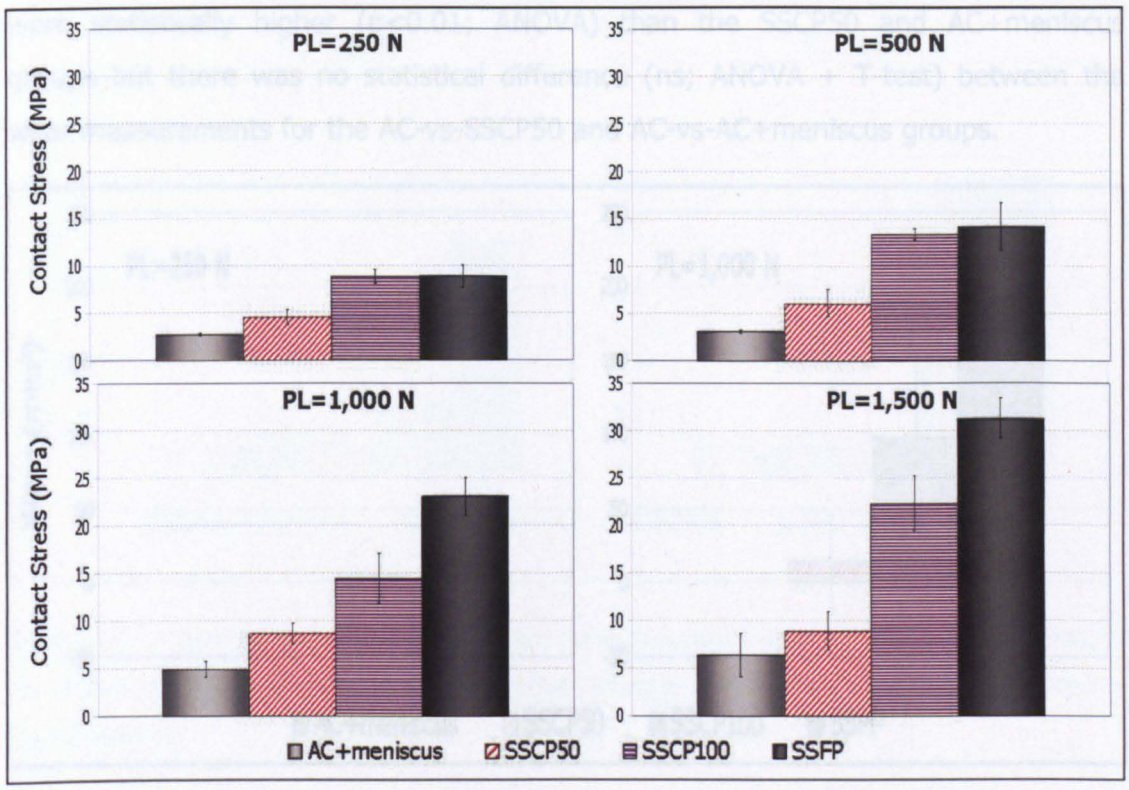

Figure 4-5: Peak contact stress measured between the articulating surfaces, at four levels of applied load. Data presented as mean (n=6) ± 95% confidence intervals.

4.3.2 Wear Analysis

Following friction testing the femoral condyles scanned in the μMRI scanner to a 78μm in plane pixel resolution, and the images were analysed as described in Section 2.9.1. As described in Chapter 3, there was no wear detected on the negative control specimens at either level of loading, nor was there any detectable wear on the condyles articulating with the SSCP50 at low load. Only one out of the six specimens articulating with the SSCP100 displayed surface fibrillation, and the wear was measured to be 31.32 mm^3 for that condyle and the average wear for the group was calculated to be 5.22 mm^3. All condyles articulating with the SSFP displayed surface damage and this was measured to be 46 mm^3. At the higher level of loading, two of the six condyles from the AC-vs-SSCP50 group had visible surface damage, and the average wear for the group was 13.96 mm^3. All six specimens articulating with the SSCP100 and SSFP at the high load had surface damage, which was measured to be 98.8 mm^3 and 190 mm^3, respectively. At both levels of loading the wear volumes for the SSFP group were statistically higher than for any of the other groups ($p<0.01$; ANOVA + T-test). Similarly the wear measurements for the AC-vs-SSCP100 group

were statistically higher ($p<0.01$; ANOVA) than the SSCP50 and AC+meniscus groups but there was no statistical difference (ns; ANOVA + T-test) between the wear measurements for the AC-vs-SSCP50 and AC-vs-AC+meniscus groups.

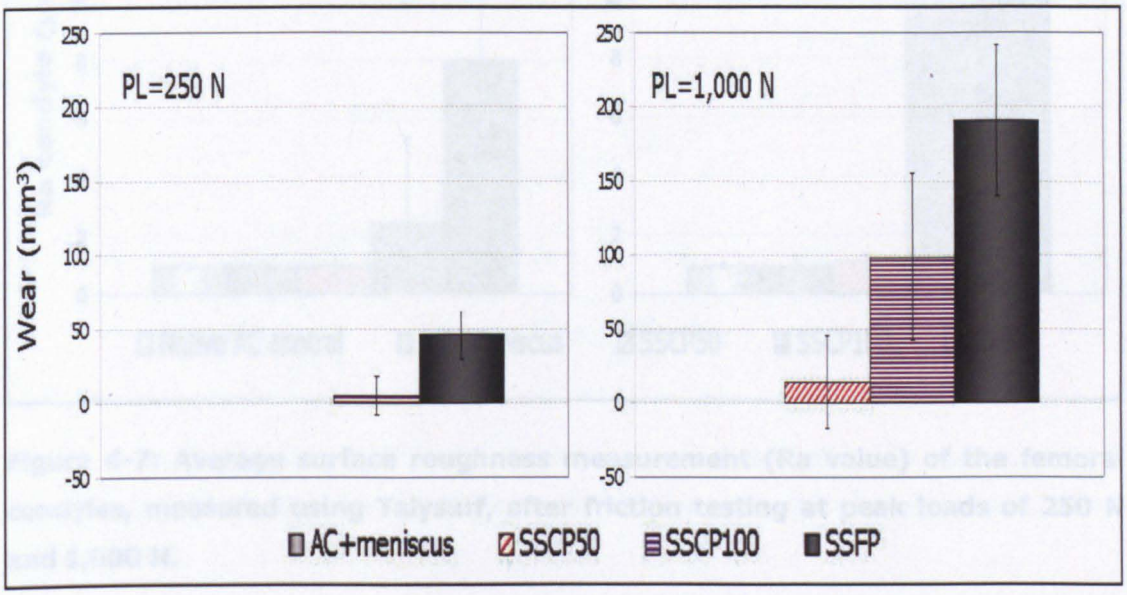

Figure 4-6: Average volume of cartilage removed from the femoral condyles. There was no wear detectable on the condyles from the negative control group at either load or on the condyles articulating with SSCP50 at low load.

The surface roughness (Ra value) was measured using silicon rubber replicas of the cartilage surface on the femoral condyles, as described in Section 2.8. There was no statistical difference (ns; ANOVA + T-test) between the Ra values for the AC-vs-AC+meniscus, the AC-vs-SSCP50 and the native cartilage control groups, at either the high or low levels of loading. At the applied PL of 250 N, the Ra value for the AC-vs-SSCP100 group was higher at 2.4 μm although not statistically different from the control group, but the Ra value from the AC-vs-SSFP group was statistically higher ($p<0.01$; ANOVA + T-test), at 8 μm. At the physiological PL of 1,000 N, the Ra values of the condyles from the AC-vs-SSCP100 and AC-vs-SSFP groups, were similar, approximately 10 μm, and not statistically different (ns; ANOVA + T-test) from each other, but statistically higher than all of the other groups ($p<0.01$; ANOVA + T-test).

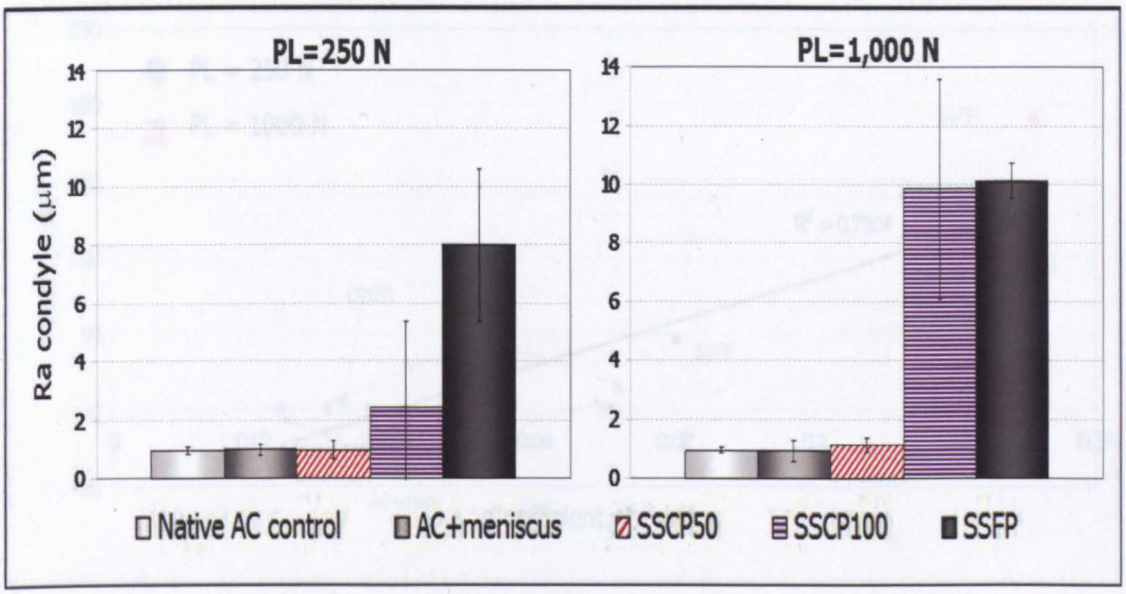

Figure 4-7: Average surface roughness measurement (Ra value) of the femoral condyles, measured using Talysurf, after friction testing at peak loads of 250 N and 1,000 N.

4.3.3 Relationships Between Different Tribological Conditions

The correlation (R^2 = 0.7904) between wear on the femoral condyles and the coefficient of friction is shown in Figure 4-8, where good agreement was found. However, in some situations this relationship did not apply, for example, the there was no significant difference (ns; ANOVA + T-test) between coefficients of friction for the AC-vs-SSFP and AC-vs-SSCP100 groups at the PL of 1,000 N (0.132 and 0.126), but there was almost twice as much wear on the condyles from the AC-vs-SSFP group.

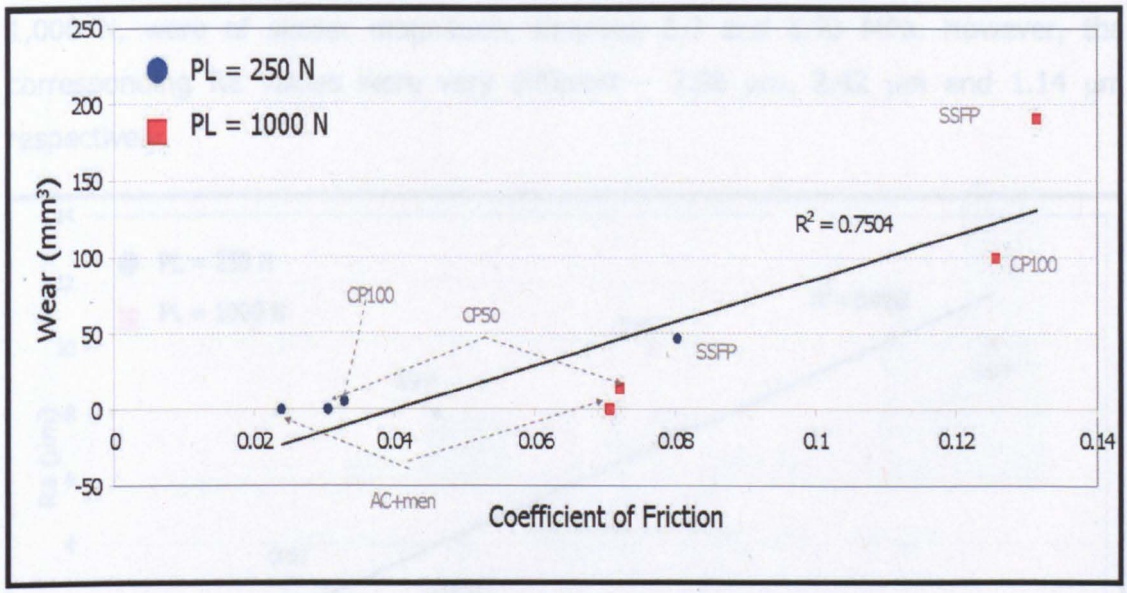

Figure 4-8: Correlation (R^2=0.7904) between volume of wear measured on femoral condyles and the coefficient of friction. Results presented are mean values (n=6).

Excellent agreement (R^2=0.9295) was found between the wear volume and contact stress in this study, as shown in Figure 4-9.

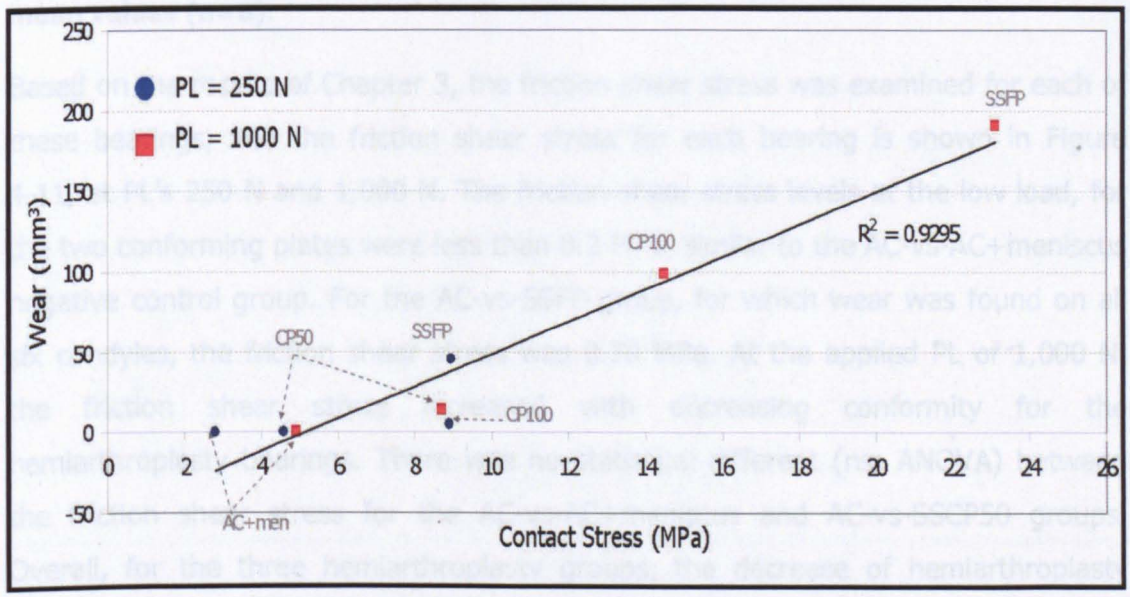

Figure 4-9: Correlation (R^2=0.9295) between volume of wear measured on femoral condyles and the measured peak contact stress. Results presented are mean values (n=6).

The relationship (R^2=0.6992) between the Ra values and contact stress was not as strong as for wear volume and contact stress. The contact stresses for the AC-vs-SSFP and AC-vs-SSCP100 at a PL of 250 N and for the AC-vs-SSCP50 at a PL of

1,000 N, were of similar magnitude, between 8.7 and 8.93 MPa. However, the corresponding Ra values were very different – 7.98 μm, 2.42 μm and 1.14 μm respectively.

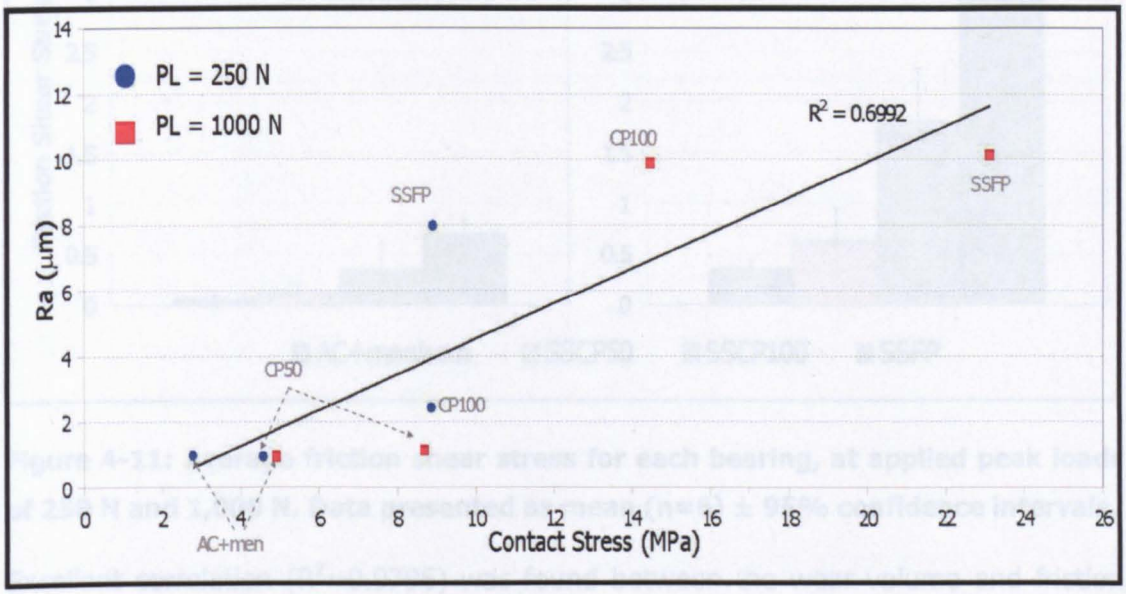

Figure 4-10: Correlation (R^2=0.6992) between the measured Ra value on the femoral condyles and the measured peak contact stress. Results presented are mean values (n=6).

Based on the results of Chapter 3, the friction shear stress was examined for each of these bearings, and the friction shear stress for each bearing is shown in Figure 4-11, at PL's 250 N and 1,000 N. The friction shear stress levels at the low load, for the two conforming plates were less than 0.2 MPa, similar to the AC-vs-AC+meniscus negative control group. For the AC-vs-SSFP group, for which wear was found on all six condyles, the friction shear stress was 0.70 MPa. At the applied PL of 1,000 N, the friction shear stress increased with decreasing conformity for the hemiarthroplasty bearings. There was no statistical different (ns; ANOVA) between the friction shear stress for the AC-vs-AC+meniscus and AC-vs-SSCP50 groups. Overall, for the three hemiarthroplasty groups, the decrease of hemiarthroplasty conformity resulted in a significant increase ($p<0.01$; ANOVA + T-test) in friction shear stress. The T-method was used to test for individual differences between the means of all of the groups.

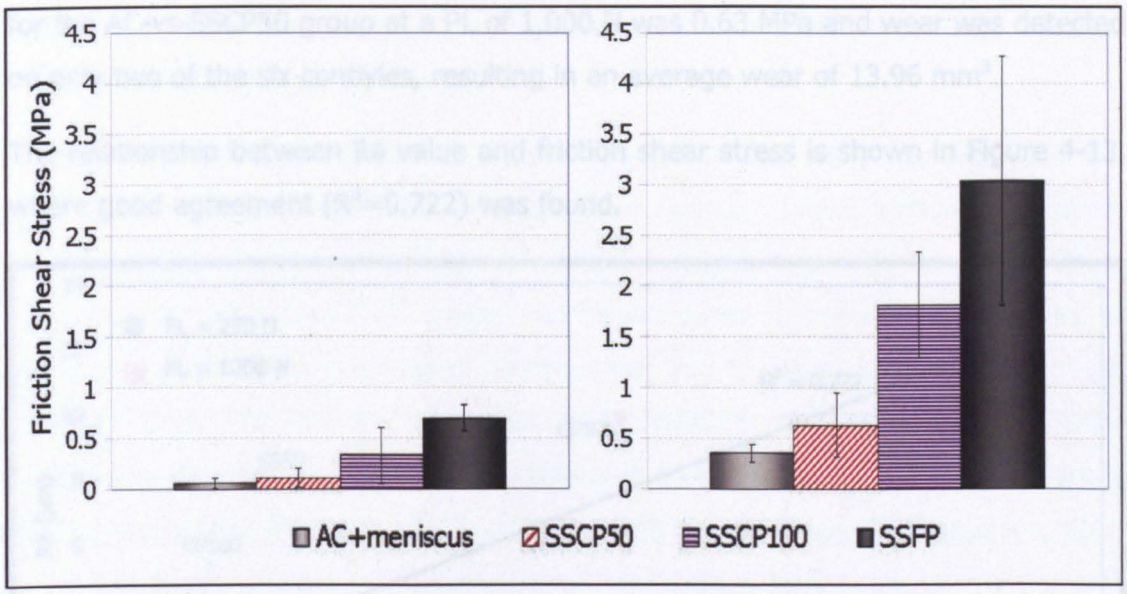

Figure 4-11: Average friction shear stress for each bearing, at applied peak loads of 250 N and 1,000 N. Data presented as mean (n=6) ± 95% confidence intervals.

Excellent correlation (R^2=0.9796) was found between the wear volume and friction shear stress, as shown in Figure 4-12.

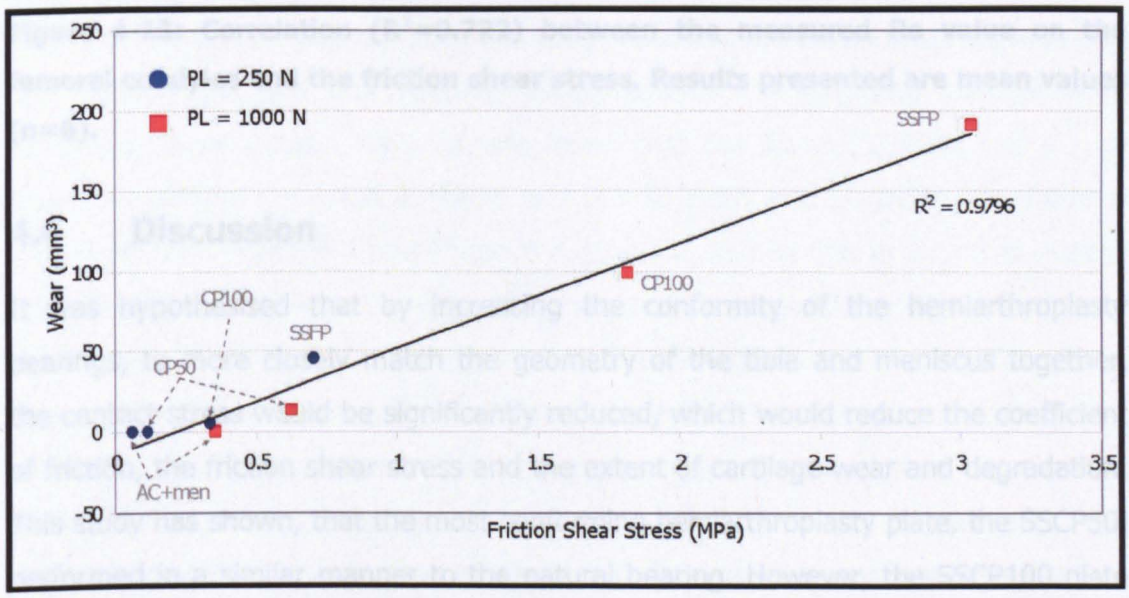

Figure 4-12: Correlation (R^2=0.9796) between volume of wear measured on femoral condyles and the friction shear stress. Results presented are mean values (n=6).

Generally, wear was found on femoral condyles when the level of friction shear stress was greater than 0.63 MPa. However, the average friction shear stress for the AC-vs-SSCP100 group at a PL of 250 N was 0.33 MPa and wear was detected on only one condyle, resulting in an average wear of 5.22 mm^3. Secondly, the average wear

for the AC-vs-SSCP50 group at a PL of 1,000 N was 0.63 MPa and wear was detected on only two of the six condyles, resulting in an average wear of 13.96 mm^3.

The relationship between Ra value and friction shear stress is shown in Figure 4-13, where good agreement (R^2=0.722) was found.

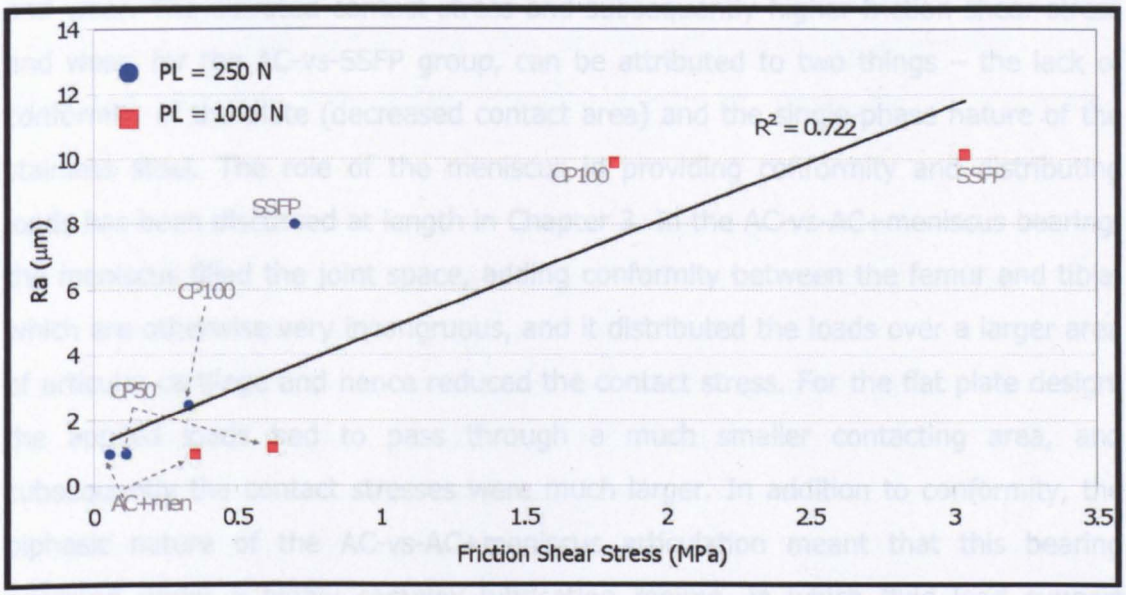

Figure 4-13: Correlation (R^2=0.722) between the measured Ra value on the femoral condyles and the friction shear stress. Results presented are mean values (n=6).

4.4 Discussion

It was hypothesised that by increasing the conformity of the hemiarthroplasty bearings, to more closely match the geometry of the tibia and meniscus together, the contact stress would be significantly reduced, which would reduce the coefficient of friction, the friction shear stress and the extent of cartilage wear and degradation. This study has shown, that the most conforming hemiarthroplasty plate, the SSCP50, performed in a similar manner to the natural bearing. However, the SSCP100 plate and SSFP plate designs led to a direct elevation of frictional coefficient, contact stress, friction shear stress and immediate surface fibrillation of the cartilage, direct biomechanical wear and permanent deformation. It should be noted at this point, that there would be a limit to the degree of conformity which would be acceptable biomechanically in the knee, to maintain the large range of motion of the joint. However, this dramatic short term tribological impact of reduced conformity on

increased coefficient of friction, contact stress and friction shear stress, has not been previously reported.

There was a remarkable difference between the tribological performances of the two control bearings, in terms of frictional coefficient, contact stress, friction shear stress and wear. The elevated contact stress and subsequently higher friction shear stress and wear, for the AC-vs-SSFP group, can be attributed to two things – the lack of conformity of the plate (decreased contact area) and the single-phase nature of the stainless steel. The role of the meniscus in providing conformity and distributing loads has been discussed at length in Chapter 3. In the AC-vs-AC+meniscus bearing, the meniscus filled the joint space, adding conformity between the femur and tibia, which are otherwise very incongruous, and it distributed the loads over a larger area of articular cartilage and hence reduced the contact stress. For the flat plate design, the applied loads had to pass through a much smaller contacting area, and subsequently the contact stresses were much larger. In addition to conformity, the biphasic nature of the AC-vs-AC+meniscus articulation meant that this bearing operated under a highly complex lubrication regime, in which fluid load support played an important role, meaning the solid phase experienced a smaller proportion of the total load and the frictional forces between the opposing surfaces were minimised (Mow *et al.*, 1980). It was found that the AC-vs-SSCP100 had a high frictional coefficient of 0.126 at the PL of 1,000 N, which was of similar magnitude to the AC-vs-SSFP Figure 4-3 and Figure 4-4. It is well known that in a natural healthy joint, the friction between the articulating surfaces is largely dependent on the solid phase interactions and the shearing between the surfaces, and whilst the fluid phase load support is maintained, the coefficient of friction remains very low. However, when a single phase material is introduced to the joint, a portion of the cartilage surface becomes constantly loaded against this biomaterial and rehydration of the tissue does not occur, resulting in diminished fluid load support and the onset of wear. The rise in the coefficient of friction due to diminished fluid phase load support has been widely reported for cartilage against metal articulations, using small scale pin on plate experiments (Forster and Fisher, 1996; Forster and Fisher, 1999; Kumar *et al.*, 2001; Basalo *et al.*, 2005; Krishnan *et al.*, 2005; Northwood *et al.*, 2007; Northwood and Fisher, 2007). In the two studies by Northwood *et al.*, the frictional response of cartilage against cartilage was also examined, in which fluid load support was maintained for up to eight hours of sliding and no rise in friction was observed.

It should be noted, that care is warranted when making a comparison between these previous studies and the current study, as the tribological conditions of these small scale experiments and the current natural joint simulation have many differences. The dependencies of contact stress, frictional coefficient and friction shear stress on the wear and degradation of cartilage may be different under the different tribological conditions applied and they are probably primarily dependent on the degree of cartilage rehydration possible under any given set of tribological conditions.

Despite the high frictional response of the AC-vs-SSCP100 group, changing the radius of the tibial hemiarthroplasty bearings did have a considerable effect on the contact stress, friction shear stress and wear. The increased conformity of this bearing meant contact stress was reduced to 14.48 MPa and the friction shear stress was 1.82 MPa, in comparison to 23.11 MPa (contact stress) and 3.04 MPa (friction shear stress) for the AC-vs-SSFP. Although wear was found on all condyles from the AC-vs-SSCP100 group (99 mm^3), it was less severe than the wear on the condyles from the AC-vs-SSFP group (191 mm^3). Although the frictional responses of these two bearings were similar, importantly, the contact stress, the friction shear stress and the degradation of the cartilage, were greatly reduced by increasing the conformity of the bearing.

Increasing the conformity to a 50 mm plate, resulted in a statistically significant ($p<0.01$; ANOVA) reduced contact stress, friction and degradation of cartilage, in comparison to the 100 mm plate and the flat plate designs. At the physiological PL of 1,000 N the coefficient of friction was 0.072 and contact stress was reduced to 8.70 MPa, resulting in a low friction shear stress of 0.63 MPa. Wear was only detected on two of the six condyles and the average wear for the group was 14 mm^3. Although the frictional response of the AC-vs-SSCP50 group was similar to that of the AC-vs-AC+meniscus, the lower contact stress found for the natural bearing resulted in a lower friction shear stress of 0.35 MPa and no wear was detected on any of the negative control articulating surfaces.

In a study by Pickard *et al.* the coefficient of friction levels of articular cartilage sliding on a stainless steel counterface, at short loading times, were found to be lower when the contact stress was increased from 2.0 MPa to 4.0 MPa (Pickard *et al.*, 1998b). Similarly Ateshian *et al.* found that friction levels decreased with increasing applied loads, for cartilage sliding on a glass plate (Ateshian *et al.*, 2003). In a third

study, an increase in contact stress reduced the friction levels by 35% between articulating cartilage surfaces (Katta *et al.*, 2007). Ateshian *et al.* proposed that these lower levels of friction could be attributed to the flattening of surface asperities of articulating cartilage samples under load (Ateshian *et al.*, 2003). Another possible explanation is that under applied loads, boundary lubricant molecules capable of enhancing friction properties are exuded into the contact region between the articulating surfaces. Lewis and McCutcheon demonstrated that the amount of fluid exuded from a cartilage surface increased with applied load, by pressing a glass platen covered in filter paper (to soak the fluid) on cartilage. When physiologically relevant levels of stress were applied, the amount of fluid exuded was sufficient enough to form a layer, 15 – 30 μm in thickness, over the contact region (Lewis and McCutchen, 1959). These phenomena may offer some explanation for the findings of the current study, in which very similar levels of frictional coefficient were found at different levels of stress, for the AC-vs-SSFP and AC-vs-SSCP100 and for the AC-vs-SSCP50 and the AC-vs-AC+meniscus. Considering the flat and 100 mm plates, for example, the levels of friction were similar, but the contact stress was over 1.5 times greater for the flat design and twice as much wear was found on the condyles. This may have been caused by a greater extent of asperity flattering under the larger applied stress, artificially reducing the coefficient of friction, or the larger applied stress may have caused a greater amount of boundary lubricants to be squeezed into the contact region of the AC-vs-SSFP articulation. Of course, it may also be a combination of the two.

Likewise, the coefficient of friction was of similar magnitude for the AC-vs-SSCP50 and AC-vs-AC+meniscus groups , despite the fact that contact stress was 1.75 times greater for 50 mm hemiarthroplasty bearing and the friction shear stress was 0.63 MPa, resulting in detectable wear on two of the condyles from this group. It is possible that the larger stress for the AC-vs-SSCP50 group may have caused flattening of asperities or exudation of lubricants. However, the natural, biphasic materials on both sides of the AC-vs-AC+meniscus articulation would have contributed considerably to the excellent performance of this bearing. Fluid phase load support would have been maintained for longer, minimising wear.

Lowering the applied peak load to 250 N, in order to artificially reduce the contact stress, had the same effect as that seen in Chapter 3. The coefficient of friction, contact stress and friction shear stress were reduced in comparison to the higher

level of loading and as a result the wear found on the femoral condyles was considerably less at the lower level of loading.

A good correlation was found between frictional coefficient and wear volume (R^2 = 0.7904) in the current study. However, a much stronger relationship was found between contact stress and wear volume (R^2 = 0.9295). However, this relationship did not apply under all circumstances. At a PL of 250 N the contact stresses were between 8.89 - 8.93 MPa for the AC-vs-SSCP100 and AC-vs-SSFP groups, but the coefficients of friction were very different, at 0.033 and 0.080 respectively. It was shown in Chapter 3 that the friction shear stress was an important tribological condition and again in this study, excellent agreement was found between wear and friction shear stress (R^2 = 0.9773). The excellent correlations found between both, contact stress and wear, and friction shear stress and wear, highlight the importance of these parameters in design and surgical application as well as in future tribological investigations of cartilage. In this study, wear was only detected above 0.6 MPa of friction shear stress, apart from one condyle displaying mild wear from the AC-vs-SSCP100 group at low load. However, it was not possible to establish such a "wear threshold" based upon the coefficient of friction or contact stress alone. Friction shear stress it appears, can give a much better indication of cartilage degradation.

Krishnan *et al.* demonstrated a linear negative relationship, experimentally, between the coefficient of friction and interstitial fluid load support. (Krishnan *et al.*, 2004b). However, is it is quite likely that a stronger relationship would be observed between the friction shear stress and the interstitial fluid load support. A limitation of this study was that the interstitial fluid load support was measured from the base of the specimen and not at the articular surface where sliding friction occurs. Following this study, Carter *et al.* measured the time-dependent frictional response of cartilage plugs of different surface areas, articulating on glass, in unconfined creep under a constant applied stress. It was demonstrated that the time for the friction coefficient to reach equilibrium increased linearly with decreasing contact area of the plugs, due to a faster decrease in the fluid pressurisation in the smaller samples (Carter *et al.*, 2007). In the current study, a similar, more rapid decrease in the fluid pressurisation was found for the least conforming bearings, with the smaller contact regions. The results of this study suggest that tibial hemiarthroplasty bearings should closely match the conformity of the natural tibia and meniscus structure.

Based on the results of this study a parallel study was performed by Luo Yong, a visiting researcher from China. In this study, the same experimental procedures were employed but polyurethane flat plates were used as the tibial counterface, instead of stainless steel. The results of this study can be found in Appendix II. Three different types of polyurethane (PU) were used (Table I-i and Figure I-i). In order of decreasing hardness they were red PU (shore hardness = D55-60), yellow PU (shore hardness = A90-95) and natural PU (shore hardness = A60-65). Only the worst case scenario – the flat plate design – was considered in this study and the peak load of 1,000 N was applied.

The coefficient of friction for these PU plates was relatively high (Figure I-ii), similar to that for the AC-vs-SSFP group. However, the peak contact stresses (Figure I-iii) for these PU groups were much lower than for the SSFP. Following μMRI scanning after the friction experiments, the volume of cartilage wear was calculated – the wear volume of the red PU group was 86 mm^3, for which the friction shear stress was 2.65 MPa. However, for the other two PU groups, there was no detectable wear and the friction shear stress was low – less than 1 MPa. The results of this study have shown that even using the worst-case design (flat plate), PU displayed a superior tribological performance than stainless steel plates, as well displaying less wear and lower friction shear stress than the two conforming designs.

Considering both, the results of the current study investigating the effect of conformity, and the results of the parallel study investigating PU as a tibial counterface material, it was concluded that any tibial hemiarthroplasty design should consider the use of a conforming geometry, made from a softer counterface material, such as medical grade polyurethane with a shore hardness of between A60-A95.

4.5 Conclusions

This tribological simulation of the medial compartmental knee with a tibial hemiarthroplasty, has many advantages over the simple geometry experiments which have been used previously to examine the tribological response of cartilage articulating with potential hemiarthroplasty biomaterials. More physiologically relevant contact stresses and motion can be applied and the geometry is that of the natural situation. A tribological simulation of this scale can be used to examine the

effects many hemiarthroplasty design considerations, such as geometry and design and well as biomaterial choice.

These studies demonstrate, for the first time, an *in vitro* model simulation system to investigate the tribological effects of hemiarthroplasty and the effect of conformity of hemiarthroplasty bearings. The current study has demonstrated, an elevation of the coefficient of friction, contact stress and friction shear stress and the subsequent increase in cartilage wear and degradation, upon decreasing the conformity of hemiarthroplasty bearings. The findings from this study support the development of hemiarthroplasty prosthesis, using similar geometry to the tibia and meniscus together.

The high dependency of cartilage wear and degradation on the level of friction shear stress was demonstrated in this study. Wear was induced on two of the six condyles at a friction shear stress level of 0.62 MPa (AC-vs-SSCP50) but when the friction shear stress increased to 0.7 MPa (AC-vs-SSFP), wear was detected on all of the condyles. Therefore, it is presumable that at friction shear stress levels of between 0.62 and 0.7 MPa, wear was induced for this hemiarthroplasty simulation. It is recommended that friction shear stress be considered in all future tribological studies of articular cartilage.

On the whole, the results of this study supported the hypothesis that if the geometry of hemiarthroplasty or spacer bearings was based on the tibia and meniscus together, rather than simply the tibial plateau geometry, contact stresses would be decreased, resulting in reduced wear and superior longevity. In addition to a conforming geometry, the tibial counterface should be made from a softer, non-metallic material such as medical grade polyurethane.

Chapter 5. Cartilage Defect Repair

5.1 Introduction

Damage to the articular cartilage surface has been shown to initiate *in vitro* at contact pressures of 25 MPa, under single high impact loads (Buckwalter, 1996; Buckwalter, 2002). These high impact, one-time, loads can arise from a serious extreme sports injury or a severe road traffic accident. However, the surface integrity can also be disrupted at much lower levels of contact stress, if the loading is cyclic and continuous (Buckwalter, 1996). Such injuries have been shown to disrupt the surface integrity of cartilage and to result in surface fibrillations (Weightman *et al.*, 1973; Buckwalter, 2002). It can, however, be argued that repetitive loading should a positive effect on cartilage integrity and that cyclic loading stimulates chondrocytes and matrix synthesis. It is widely known that cruciate ligament and meniscal injuries, arising from accidents or sports, lead to early-onset cartilage damage and osteoarthritis.

There are varying types of osteochondral defect. The defect can include matrix and cell injuries, resulting in no visible damage to the overall mechanical structure. The defect can be in the form of a focal mechanical tear or flap, which does not extend to the underlying subchondral bone (Minas and Nehrer, 1997; Newman, 1998; Buckwalter, 2002). Finally, osteochondral defects can extend to the subchondral bone, which leads to clot formation and an active inflammatory response (Minas and Nehrer, 1997; Newman, 1998; Buckwalter, 2002). In any case, when these localised cartilage defects occur, whatever the initiating factor and however severe, there are three main surgical interventions commonly used.

Firstly, abrasion and microfracture techniques penetrate the subchondral bone, stimulating an inflammatory response and vascular repair at the base of the defect. These treatments are of relatively low cost and can be performed arthroscopically. The resulting repair fibrocartilage, however, does not possess the mechanical and biochemical properties of articular cartilage and it has been shown to deteriorate over time (Minas and Nehrer, 1997; Newman, 1998; Gross, 2003).

Secondly, mosaicplasty (otherwise known as autologous osteochondral transplantation) which was described in Section 1.7.5, is advantageous in terms of the host response and cell survival rates. However, the limited supply of autogenous tissue and the necessity of matching surface topography and geometry, means that there are

limitations to the process (Minas and Nehrer, 1997; Newman *et al.*, 1998; Hangody *et al.*, 2001; Gross, 2003). Of course, another important concern is donor site morbidity.

The final procedure used to fill osteochondral defects is autologous chondrocyte implantation (ACI), described in Section 1.7.4, which involves harvesting the patients chondrocytes, growing them in culture for several weeks and finally reimplanting them and sealing them with a periosteum flap (also harvested from the patient) (Minas and Nehrer, 1997; Newman, 1998; Hangody *et al.*, 2001; Bentley *et al.*, 2003; Clar *et al.*, 2005). The associated drawbacks with ACI include the need for two operations and that the cell culture requires specialist knowledge and equipment, the availability of which is not widespread. These factors result in ACI being relatively far more expensive than microfracture or autologous osteochondral transplantation.

Overall, although success has been reported with these techniques (Hangody *et al.*, 2001; Bentley *et al.*, 2003; Clar *et al.*, 2005), they are not without their disadvantages: the deterioration of microfracture-induced fibrocartilage over time (Minas and Nehrer, 1997; Newman, 1998; Gross, 2003); the difficulties of ACI, in terms of matching the surface topography and geometry of the donor site and implant site (Minas and Nehrer, 1997; Newman *et al.*, 1998; Hangody *et al.*, 2001; Gross, 2003); as well as the reported deterioration of mosaicplasty over time (Bentley *et al.*, 2003). These factors highlight the fact that perhaps there is a better solution, until these techniques can be improved upon. Several animal studies have been conducted to investigate the potential of synthetic biomaterials for cartilage defect repair (Chang *et al.*, 1997; Chang *et al.*, 1998a; Chang *et al.*, 1998b; Kawalec *et al.*, 1998; Ushio *et al.*, 2003; Custers *et al.*, 2007a).

Therefore, the aim of this study was to investigate the tribological response of the medial compartmental knee, in its natural healthy state and with various biomaterial plugs implanted into the femoral condyle, to fill osteochondral defects, in an *in vitro* experimental simulation.

5.2 Materials and Methods

Pins of 10 mm diameter and 10 mm in depth were used to replace osteochondral defects in the femoral condyle, to simulate cartilage defect repair and to examine the effects of different substitute materials on the friction and wear, in the medial compartmental knee model.

5.2.1 Stainless Steel Pins

As a positive control stainless steel pins were used to fill osteochondral defects in the femoral condyle. Pins were 10 mm in diameter and 10 mm in height (Figure 5-1). The pins had a 40 mm radius on the upper surface, to match that of the femoral condyles which ranged between 38 mm and 42 mm, in the anterior-posterior direction.

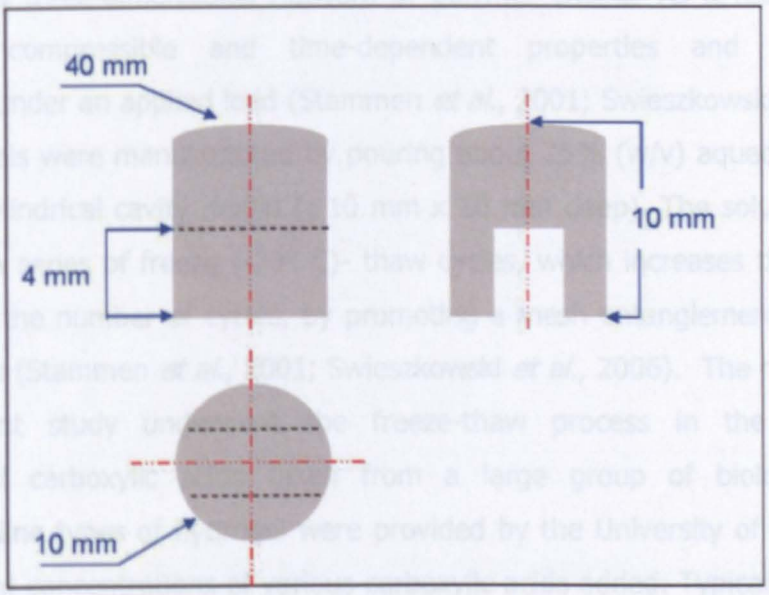

Figure 5-1: Stainless steel pins were used as osteochondral substitutes. Pins were 10 mm in diameter, 10 mm in height and they had a 4 mm key to facilitate cement fixation.

Before testing the upper radius and surface roughness of the pins were measured using a stylus profilometer, a Talysurf 5 model from Taylor Hobson, UK which was described in Section 2.8. Two perpendicular traces were taken across the surface of each pin.

	Radius	Surface Roughness (Ra)
Mean (n=6)	39.18 mm	0.0146 μm
±95% confidence interval	± 1.02 mm	± 0.0036 μm

Table 5-1: Surface properties of osteochondral substitute stainless steel pins, measured using stylus profilometry. Results presented as mean ± 95% confidence interval

5.2.2 Hydrogel Pins

Cyrostructured poly(vinyl alcohol) hydrogels were tested as osteochondral substitute materials. The hydrogel materials were manufactured at the Faculty of Materials Engineering, Warsaw University of Technology, Poland (Swieszkowski *et al.*, 2006). Like all natural and synthetic hydrogels, these poly(vinyl alcohol) hydrogels retain water within a three-dimensional network of polymer chains. As a result they have non-linear, incompressible and time-dependent properties and exhibit large deformations under an applied load (Stammen *et al.*, 2001; Swieszkowski *et al.*, 2006). These hydrogels were manufactured by pouring about 25% (w/v) aqueous solution of PVA, into a cylindrical cavity mould (ϕ 10 mm x 10 mm deep). The solution was then subjected to a series of freeze (-20° C)- thaw cycles, which increases the mechanical strength with the number of cycles, by promoting a mesh entanglement between the PVA molecules (Stammen *et al.*, 2001; Swieszkowski *et al.*, 2006). The hydrogels used in the current study underwent the freeze-thaw process in the presence of multifunctional carboxylic acids taken from a large group of biologically active compounds. Nine types of hydrogel were provided by the University of Warsaw, each with a different concentrations of various carboxylic acids added. Typical hydrogels are shown below in Figure 5-2 and the composition of each hydrogel is shown in Table 5-2.

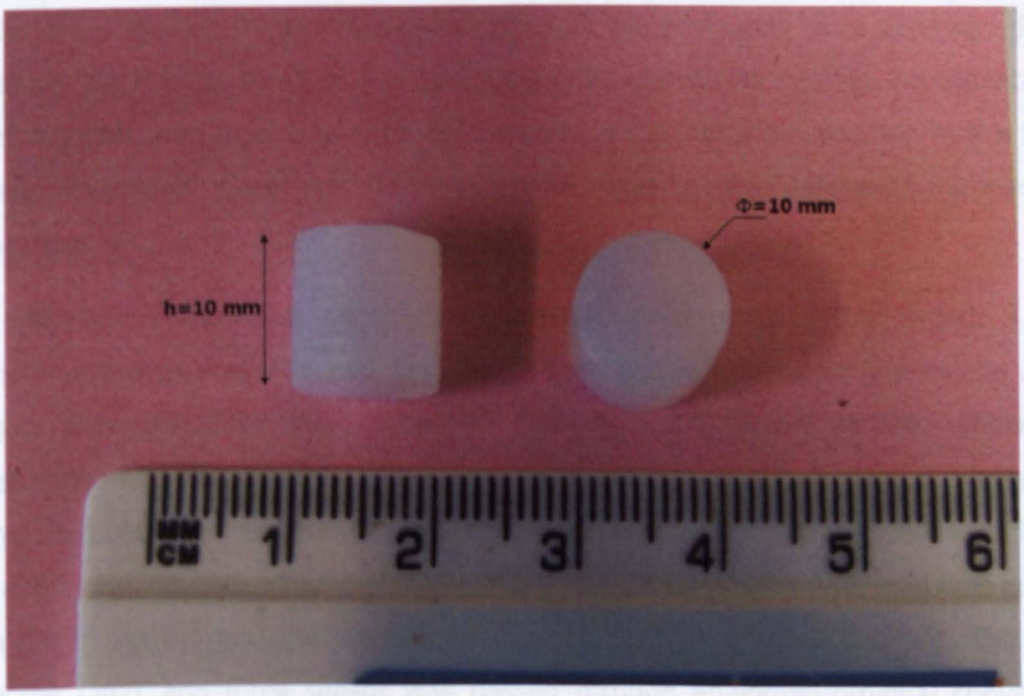

Figure 5-2: Poly (vinyl alcohol) hydrogels.

Hydrogel Code	Composition
HGEL_1	25% PVA(1)
HGEL_2	25% PVA(1) + 3% Adipic acid
HGEL_3	25% PVA(1) + 3% Citric acid
HGEL_4	25% PVA(1) + 3% Fumaric acid
HGEL_5	25% PVA(1) + 3% Gluconic acid
HGEL_6	25% PVA(1) + 3% Maleic acid
HGEL_7	25% PVA(1) + 5% Adipic acid
HGEL_8	25% PVA(2)
HGEL_9	25% PVA(1) + 5% Citric acid

Table 5-2: Composition of cryostructured poly(vinyl alcohol) hydrogels

5.2.3 Indentation Test for Hydrogel Deformation Properties

It was not feasible to use all of the hydrogels in the medial compartmental knee joint simulation, therefore some material properties of the hydrogels were determined and based on the results, three of the hydrogels were chosen for testing. An indentation apparatus was used to examine the deformation of the materials, coupled with a finite element simulation of the indentation test, which was used to determine the material properties.

The indentation apparatus consisted of a shaft, onto which a flat ended, 3 mm diameter indentor was attached (on the bottom end). At the top end of the shaft weights were added to apply a desired load. An LVDT (linear variable differential transformer) was also attached to the top end of the shaft to monitor the displacement of the shaft. At the lower end of the shaft a piezo-electric force transducer was fitted, just above the indentor attachment. The movement of the shaft under load was guided by a linear bearing and the speed was controlled by an oil-filled dashpot. The data from the LVDT and force sensor was passed through analogue-to-digital converters and acquired at a frequency of 5 Hz.

The calibration procedure for the indentation rig, as well as some representative results of a calibration can be found in Appendix III.

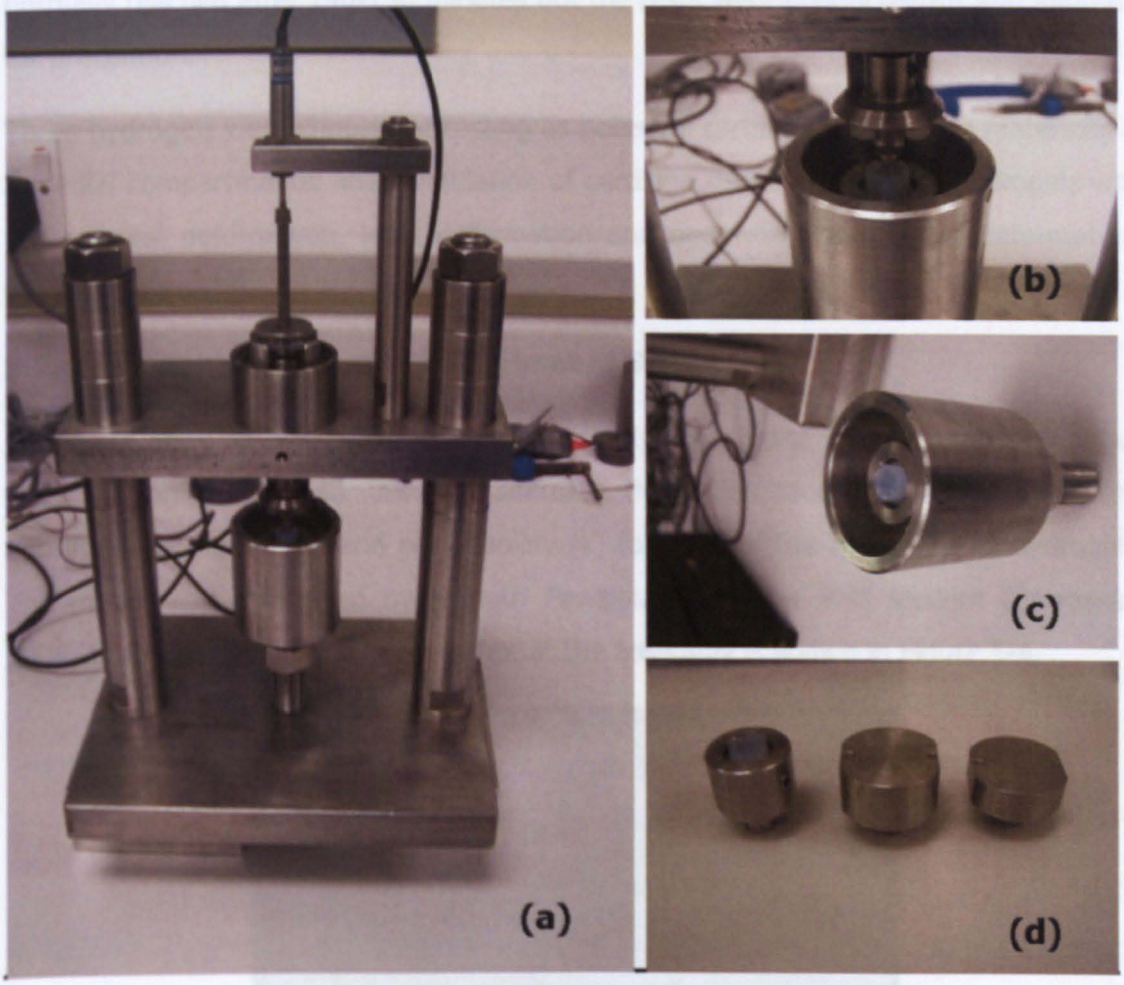

Figure 5-3: The indentation rig. (a) Indentation rig under operation. (b) Close up of hydrogel during an indentation test (c) Hydrogel in collet, inside specimen holder. (d) Collet and flat mountings (used for testing plates or flat samples), all of which fit in the specimen holder.

The specimen holder was specially designed so that it was height adjustable. It could be screwed onto the base of the indentation apparatus and when a suitable height was located, a locking nut at the bottom prevented shaking or movement during the test. The top end of the sample holder was like an open bath, with a hole at the centre of its base (Figure 5-3 (c)), into which a collet was mounted. The test specimens were secured inside the collet. When the test specimen was in the correct position for starting the test, the bath was filled with distilled water, to keep the specimens hydrated for the duration of the test.

Deformation of the hydrogel pins was recorded continuously at a sampling frequency of 5 Hz until the specimens reached their equilibrium deformation. Equilibrium was normally reached after 140-150 minutes but the tests were conducted for 200 minutes, for precaution.

Three hydrogels were chosen for testing as potential cartilage substitution materials, in a medial compartmental knee simulation of cartilage defect repair. The hydrogels with the greatest deformation, least deformation and one with intermediate deformation, were chosen.

5.2.4 Indentation Test - Finite Element Simulation

A two dimensional axisymmetric poroelastic (biphasic) finite element model (Abaqus CAE, version 6.7-1) was used to simulate the indentation tests and derive the aggregate modulus (Ha) and permeability (k) for each of the three chosen hydrogels. The model was developed by Sainath Pawaskar, a fellow PhD student (Pawaskar, 2006; Katta *et al.*, 2007). A screen shot of the assembly is shown in Figure 5-4.

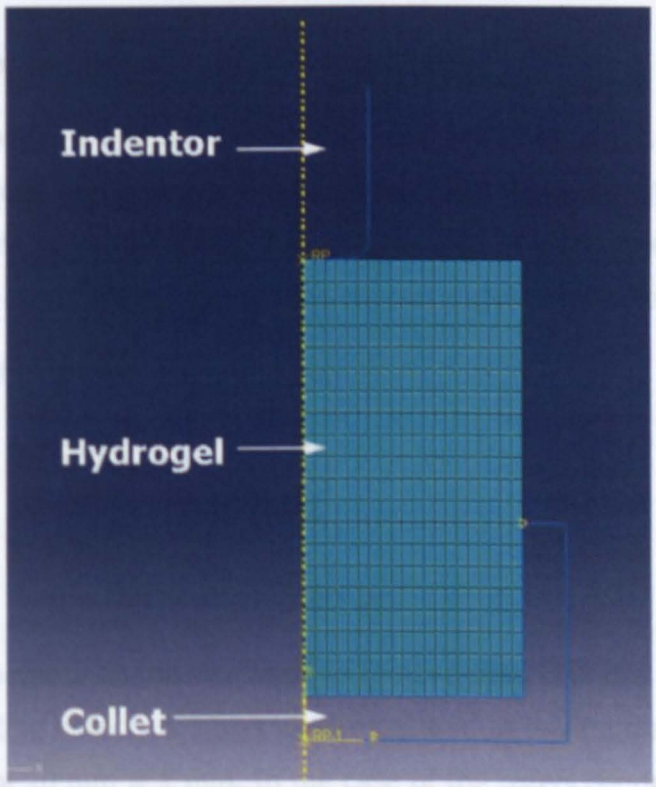

Figure 5-4: Axisymmetric poroelastic biphasic finite element model

The ϕ10 mm by 10 mm long uni-material hydrogel pin was modelled with 400 4-node axisymmetric quadrilateral, bilinear displacement, and bilinear pore pressure elements (CAX4RP). A maximum compressibility was assumed such that the Poisson's ratio of

the solid phase of each hydrogel was equal to 0.0 and a void ratio of 4.0 was selected, to model the hydrogel with a water content of 80%. The indentor and collet were modelled as analytically rigid with no permeability which meant that the contact face between the indentor and hydrogel was an impermeable boundary. A mesh sensitivity check on the predicted results was performed, the results of which can be seen in Appendix IV.

Whenever the metallic indentor and collet were in contact with the hydrogel surface, no fluid flow surface conditions were imposed and the remaining hydrogel surfaces had free flow conditions imposed. Load was applied via a ramp condition for two seconds and the deformation of the hydrogel was modelled for 200 minutes.

A Matlab program was used to match the computational deformation curve with the experimental. Initially the user selected reasonable aggregate modulus and permeability values for the hydrogel and then the Matlab program made alterations to these values, iteratively, until the two curves were within a reasonable standard error (<5%).

5.2.5 Specimen Preparation and Test Set-up

Medial femoral condyles and tibial plateaus were harvested from bovine knees, as described in Sections 2.2 and 2.3, respectively. They were mounted in jigs for the friction simulator as described in Section 2.4. However, before mounting the femoral condyle, a 10 mm defect was created in the contact region and either the:

- osteochondral pin was left in position
- defect was left blank
- defect was filled with a hydrogel pin
- defect was filled with a stainless steel pin

A drill with a diameter of 9 mm was used to remove osteochondral pins to a depth of 10 mm. The resulting defects or holes were measured to have a diameter of 10 ± 0.2 mm and a depth of 10 mm ± 1 mm. In the case of the osteochondral pin, the pin was not removed, merely cut 10 mm deep. The purpose of these osteochondral pins was to examine the effect of a cut in the cartilage surface on the biphasic properties, and in particular, to examine what effect this inevitable disruption to the biphasic fluid load support had on the overall tribological performance. In a second experimental group,

a 9 mm defect was tested as a blank hole. In the final four groups, the defect was filled with either a hydrogel (three hydrogels were used, with slightly different material properties) or a stainless steel pin, which had diameters of 10 mm.

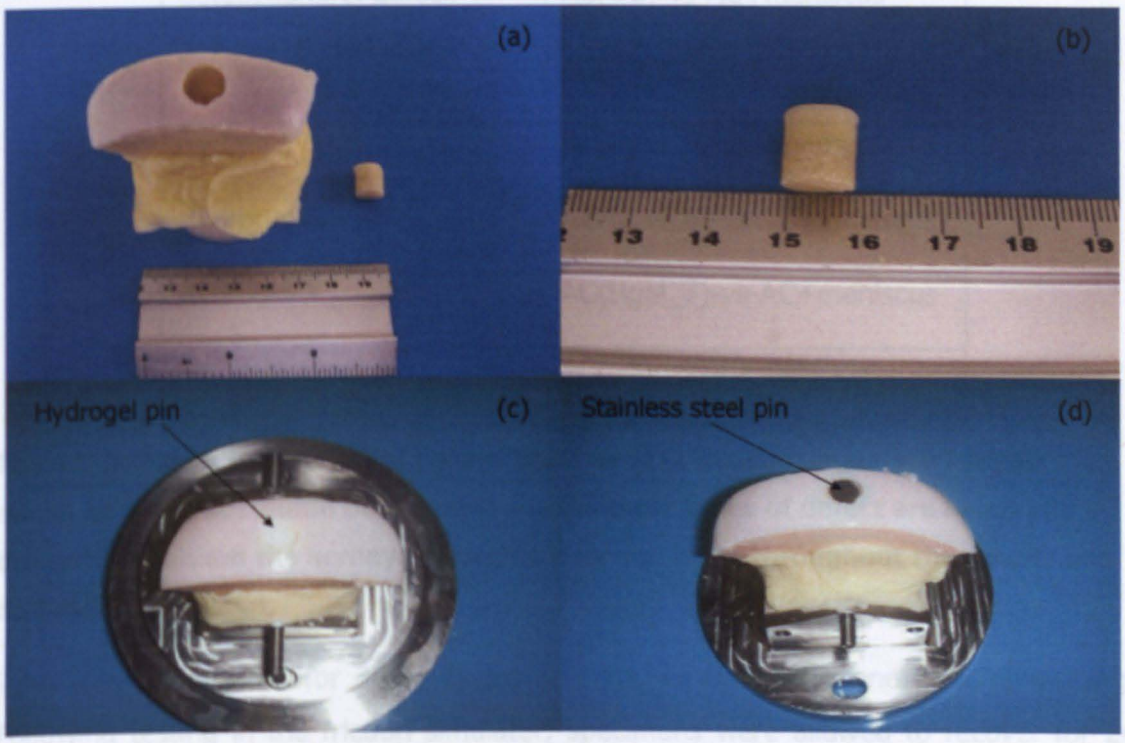

Figure 5-5: Osteochondral Defects. (a) an osteochondral defect has been removed from the contact region of condyle; (b) a 9 mm osteochondral plug; (c) a hydrogel pin fixed in a defect site and (d) a stainless steel pin fixed in a defect site.

There were seven experimental groups used in this study. The negative control group was a fully intact femoral condyle articulating with an intact tibial plateau and meniscus. In each of the other groups, the femoral condyle had an osteochondral defect and articulated with an intact tibial plateau and meniscus. The type of defect in each group, and its corresponding acronym used throughout the results and discussion, is shown in Table 5-3. For each test group six specimens were tested, except for each of the hydrogel groups, as only three samples of each hydrogel were available. In this study, only one level of loading was used, the higher and physiological level of loading, for which the peak load was 1,000 N.

Type of Defect	Acronym
No defect: healthy condyle	AC-vs-AC+meniscus
Osteochondral defect	AC(OC)-vs-AC+meniscus
Blank defect	AC(Blank)-vs-AC+meniscus
Hydrogel 5	AC(Hgel_5)-vs-AC+meniscus
Hydrogel 6	AC(Hgel_6)-vs-AC+meniscus
Hydrogel 7	AC(Hgel_7)-vs-AC+meniscus
Stainless Steel pin	AC(SS)-vs-AC+meniscus

Table 5-3: Seven experimental groups were used in the cartilage defect repair study. In the first column of the table the different types of defect are listed and in the second column the acronyms used to describe them throughout the results and discussion are listed.

Tests were conducted for 3,600 cycles at 1 Hz, equivalent to one hour of walking. Following testing in the friction simulator, specimens were allowed to recover for 24 hours in PBS solution before making silicon rubber replicas of each condyle and tibial surface for surface roughness measurements (Section 2.8). Due to the location of the defect on the condyle, at the centre of the contact region, surface roughness measurements could not be taken across the whole surface. Two profiles were taken either side of the defect, as shown in Figure 5-6.

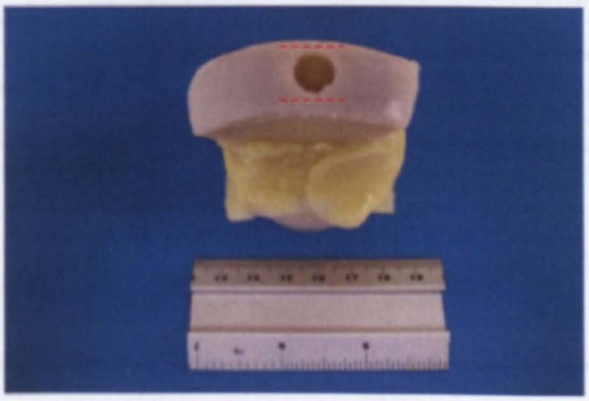

Figure 5-6: Surface roughness measurements were taken either side of the defect site on the femoral condyle. The red dotted lines indicate typical paths of the stylus profilometer.

Following the casting with silicon rubber, the specimens were stored in PBS solution and frozen at -20°C until MRI scanning and sectioning for histology. Histological sections were taken from either side of the defect site, along the same region that the surface roughness measurements were taken. The histological stains used were H&E, Sirius red and Alcian blue, as described in Section 2.10.

Throughout Section 5.3 results were analysed using single factor ANOVA. Individual differences between group means, discussed throughout the text, were obtained using the T-method.

5.3 Results

5.3.1 Determination of Hydrogel Material Properties

Indentation tests were performed on the nine types of hydrogels specimens. The deformation against loading time was plotted for each, as shown in Figure 5-7. It was decided to use three different hydrogels in the cartilage defect repair study using the medial compartmental knee simulation. Based on the indentation results, the hydrogels with the greatest deformation (Hgel_6), least deformation (Hgel_5) and one with intermediate deformation (Hgel_7) were selected. The deformation curves of the chosen hydrogels are shown in bold colours in Figure 5-7.

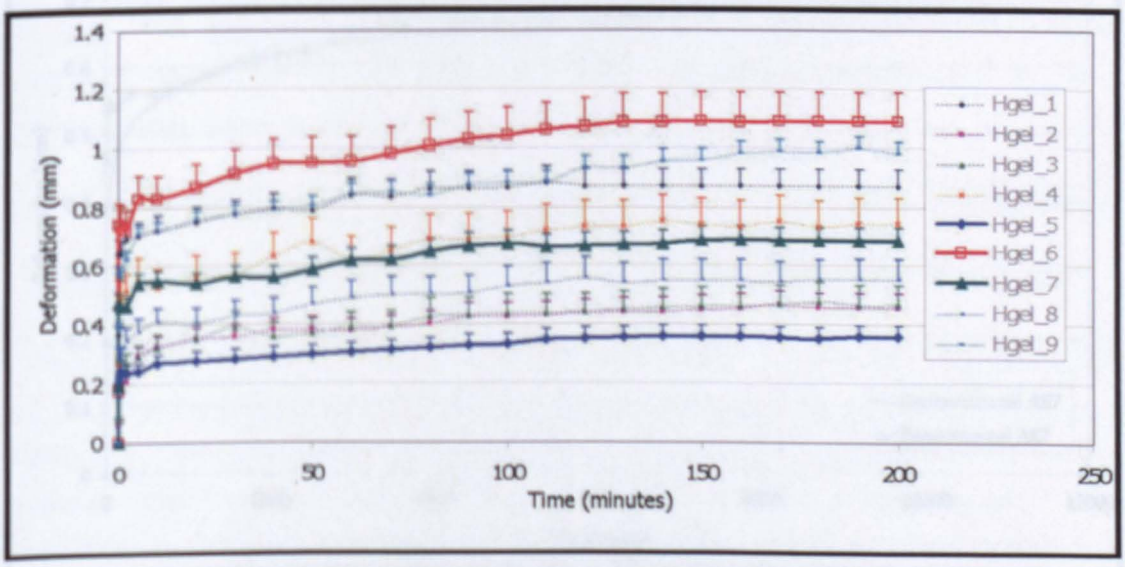

Figure 5-7: Deformation against loading time for the nine hydrogels tested in the indentation rig. Results presented as mean (n=3) + 95% confidence intervals.

The deformation curves of the three selected hydrogels, were compared with those from the computational experiment, described in Section 5.2.4. The two deformation

curves for each hydrogel are shown in Figure 5-8, Figure 5-9 and Figure 5-10, in order of increasing deformation. The biphasic material properties for each hydrogel, shown in Table 5-4, were derived using the Matlab program.

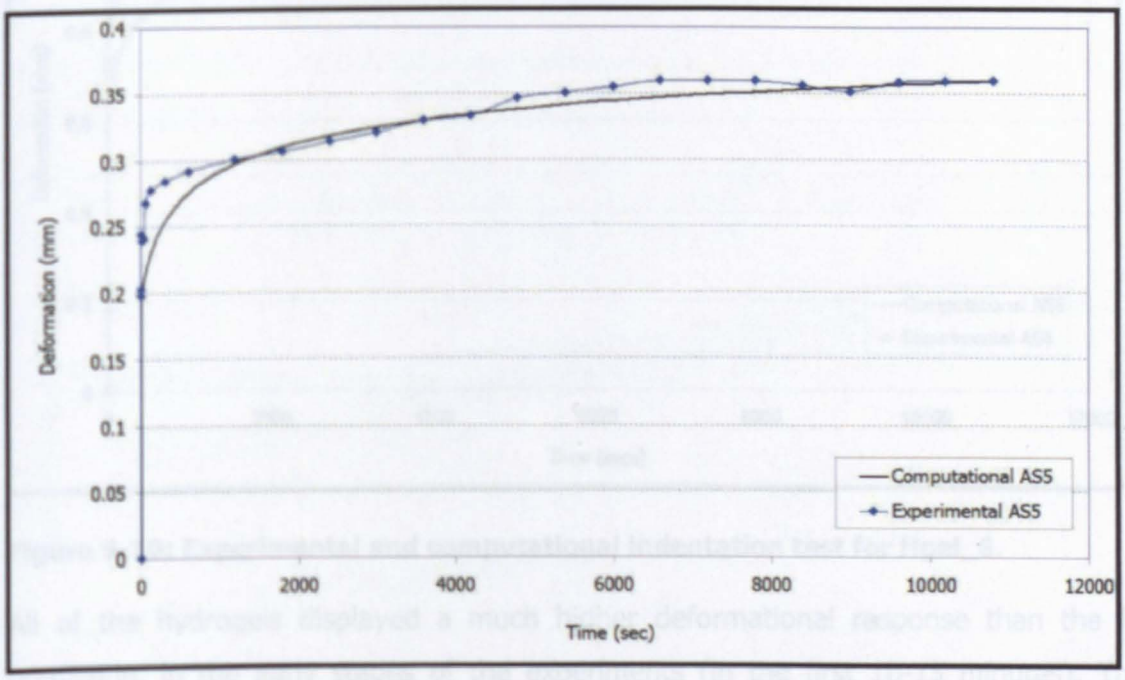

Figure 5-8: Experimental and computational indentation test for Hgel_5.

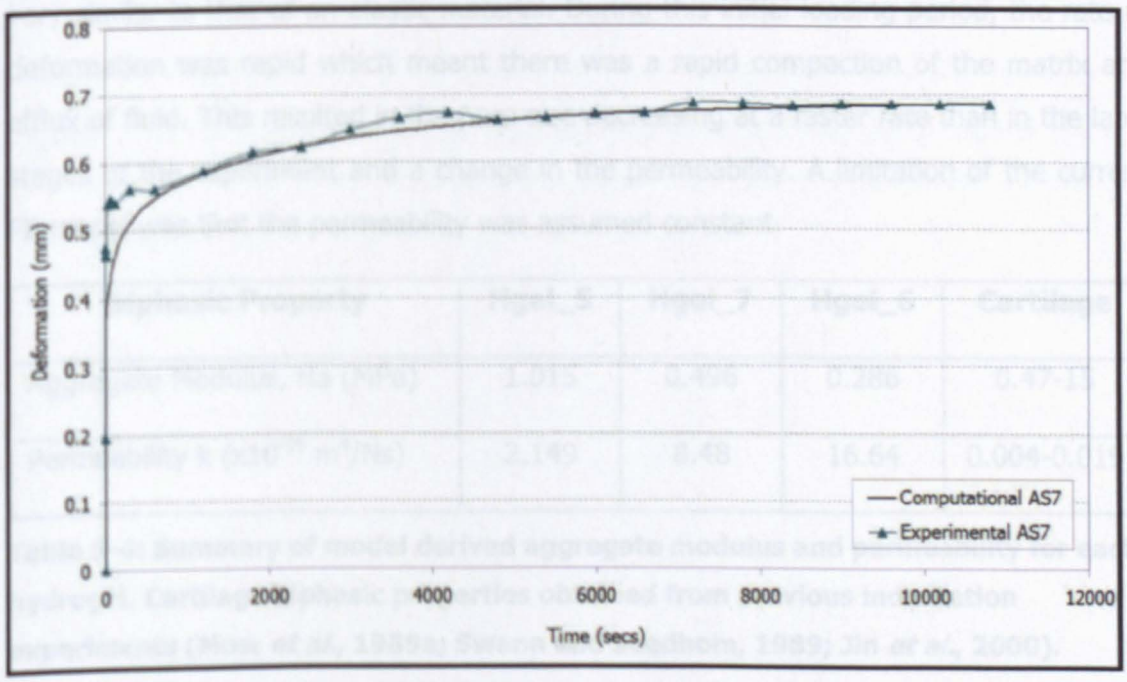

Figure 5-9: Experimental and computational indentation test for Hgel_7.

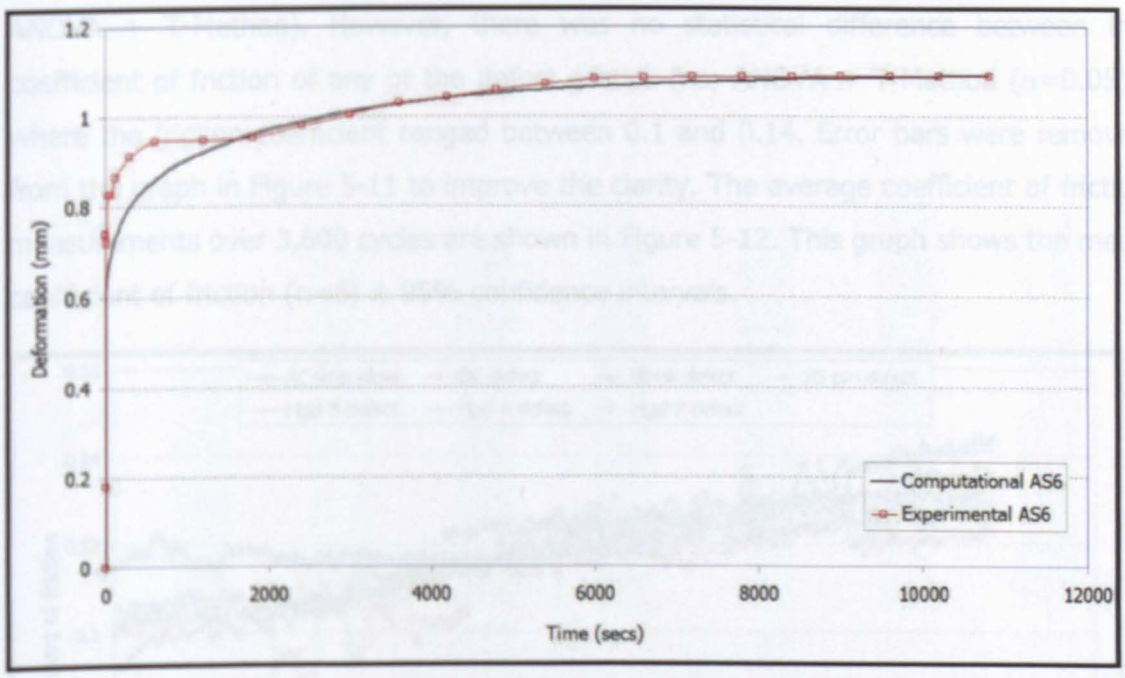

Figure 5-10: Experimental and computational indentation test for Hgel_6.

All of the hydrogels displayed a much higher deformational response than the FE prediction, in the early stages of the experiments (in the first 10-15 minutes). This suggested that there were some errors in the biphasic properties as the FE curve was very similar to that of an elastic material. During this initial loading period, the rate of deformation was rapid which meant there was a rapid compaction of the matrix and efflux of fluid. This resulted in the pore size decreasing at a faster rate than in the later stages of the experiment and a change in the permeability. A limitation of the current FE model was that the permeability was assumed constant.

Biphasic Property	Hgel_5	Hgel_7	Hgel_6	Cartilage
Aggregate Modulus, Ha (MPa)	1.015	0.496	0.286	0.47-15
Permeability k ($x10^{-15}$ m^4/Ns)	2.149	8.48	16.64	0.004-0.019

Table 5-4: Summary of model derived aggregate modulus and permeability for each hydrogel. Cartilage biphasic properties obtained from previous indentation experiments (Mow *et al.*, 1989a; Swann and Seedhom, 1989; Jin *et al.*, 2000).

5.3.2 Friction Measurements

The coefficient of friction against loading time for the seven groups is shown in Figure 5-11. For the AC-vs-AC+meniscus group, the coefficient of friction ranged between 0.06 and 0.08, which was statistically lower than all of the defect groups ($p<0.01$;

ANOVA + T-Method). However, there was no statistical difference between the coefficient of friction of any of the defect groups (ns; ANOVA + T-Method (α=0.05)), where the friction coefficient ranged between 0.1 and 0.14. Error bars were removed from the graph in Figure 5-11 to improve the clarity. The average coefficient of friction measurements over 3,600 cycles are shown in Figure 5-12. This graph shows the mean coefficient of friction (n=6) ± 95% confidence intervals.

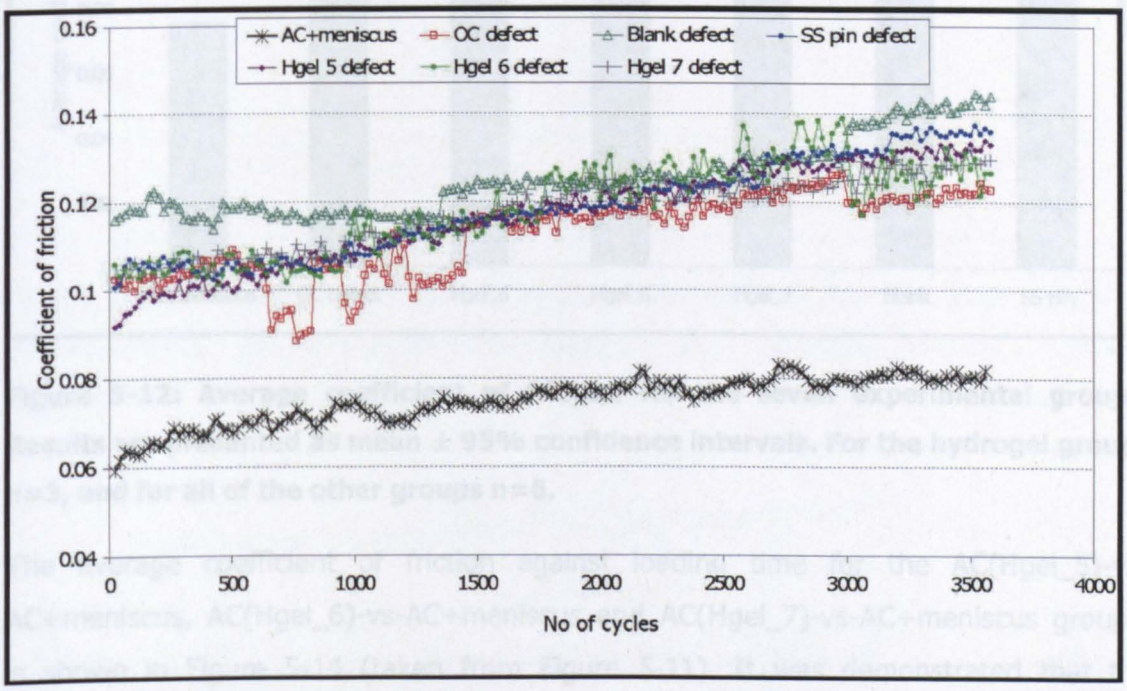

Figure 5-11: Coefficient of friction against time for the seven experimental groups. The mean of each group is presented. Error bars were omitted for clarity. For hydrogel groups (n=3) and for all other groups (n=6).

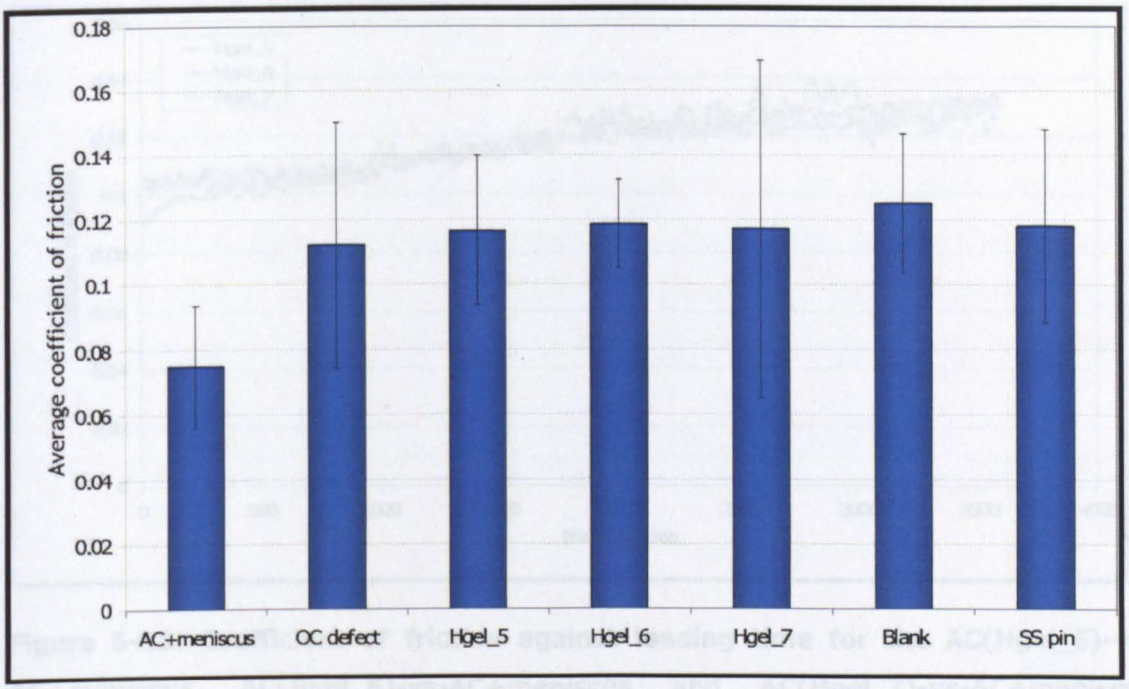

Figure 5-12: Average coefficient of friction for the seven experimental groups. Results are presented as mean ± 95% confidence intervals. For the hydrogel groups n=3, and for all of the other groups n=6.

The average coefficient of friction against loading time for the AC(Hgel_5)-vs-AC+meniscus, AC(Hgel_6)-vs-AC+meniscus and AC(Hgel_7)-vs-AC+meniscus groups, is shown in Figure 5-14 (taken from Figure 5-11). It was demonstrated that the addition of 3% gluconic acid, 3% maleic acid and 5% adipic acid, to hydrogels 5, 6 and 7 respectively, had no influence on the frictional response, as there was no statistical difference (ns; ANOVA; T-Method) in the frictional coefficient for any of the three groups.

The coefficient of friction for each of the specimens of each hydrogel defect group is shown in Figure 5-14. Most of the specimens had a coefficient of friction ranging between 0.1 and 0.14. One specimen, from the AC(Hgel_7)-vs-AC+meniscus group, performed with a lower coefficient of friction, similar to the AC-vs-AC+meniscus negative control. However, another specimen from the Hgel_7 defect group performed with a much higher coefficient of friction, ranging between 0.16 and 0.18. This variation is difficult to explain. Although the hydrogels were implanted flush with the surface, during the experiment, when loaded, they may have been proud or deep, causing variations in the frictional coefficient.

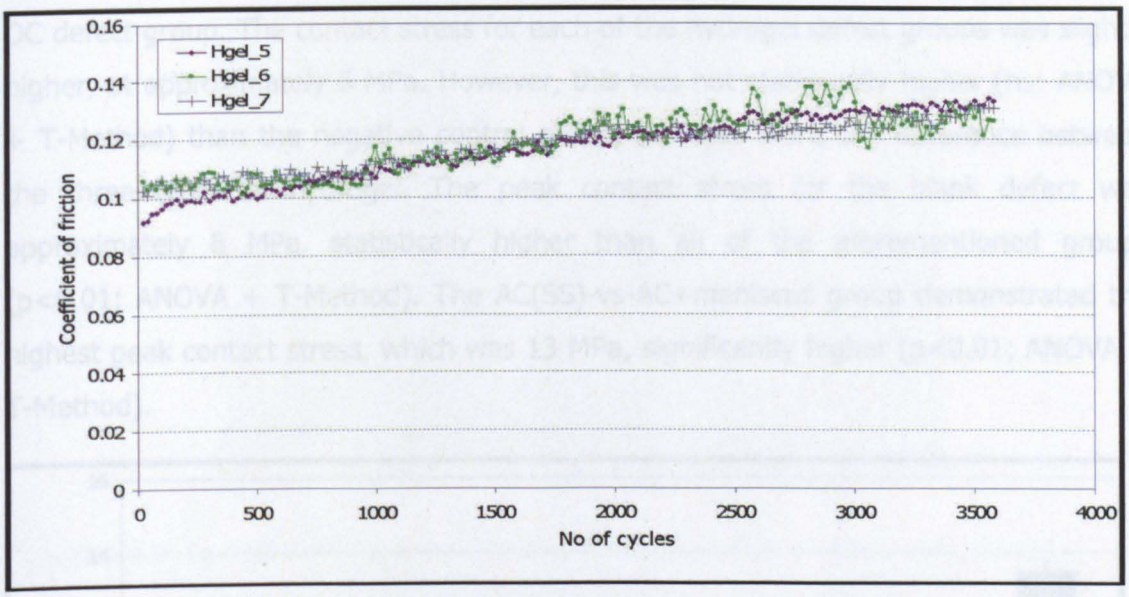

Figure 5-13: Coefficient of friction against loading time for the AC(Hgel_5)-vs-AC+meniscus, AC(Hgel_6)-vs-AC+meniscus and AC(Hgel_7)-vs-AC+meniscus groups. Error bars omitted for clarity. The mean (n=3) of each group is displayed.

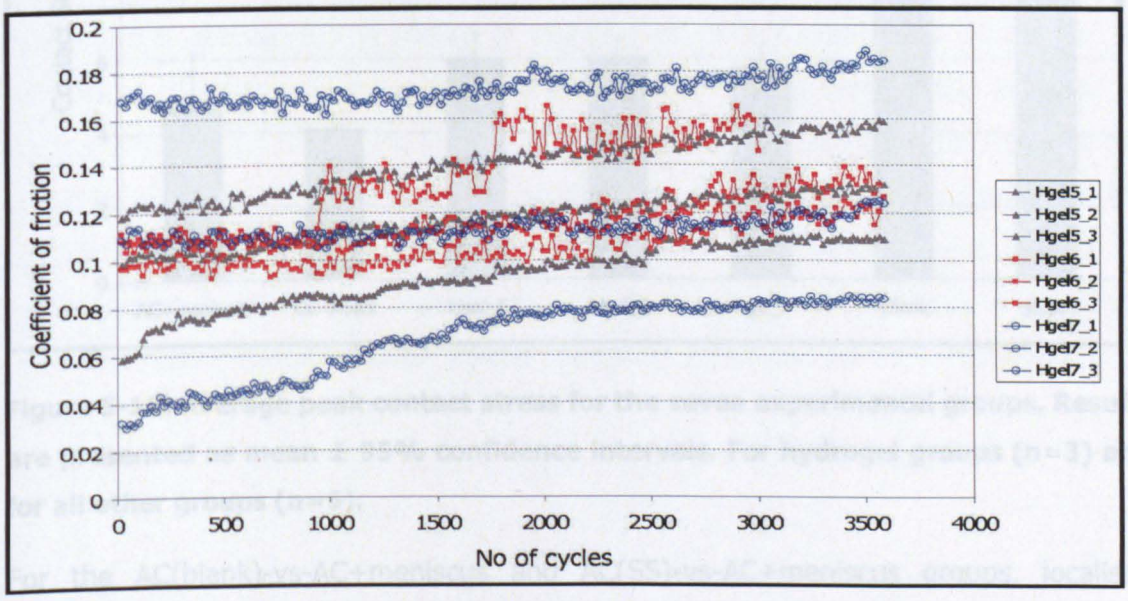

Figure 5-14: Coefficient of friction against time for the nine hydrogel defect specimens. The multifunctional carboxylic acids, which were added to the hydrogels, did not have any influence on the frictional properties, for example, Hgel_7 displayed the lowest frictional coefficient, as well as the highest.

The contact stress for each of the seven groups is shown in Figure 5-15. There was no statistical difference (ns; ANOVA + T-Method) between the contact stress for the AC-vs-AC+meniscus and the AC(OC)-vs-AC+meniscus groups, where the peak contact stress was between 4 and 5 MPa. This can be explained by the fact that the surface materials and geometries were the same, with just a cut in the articular surface of the

OC defect group. The contact stress for each of the hydrogel defect groups was slightly higher, at approximately 6 MPa. However, this was not statistically higher (ns; ANOVA + T-Method) than the negative control group, nor was there any difference between the three types of hydrogel. The peak contact stress for the blank defect was approximately 8 MPa, statistically higher than all of the aforementioned groups ($p<0.01$; ANOVA + T-Method). The AC(SS)-vs-AC+meniscus group demonstrated the highest peak contact stress, which was 13 MPa, significantly higher ($p<0.01$; ANOVA + T-Method).

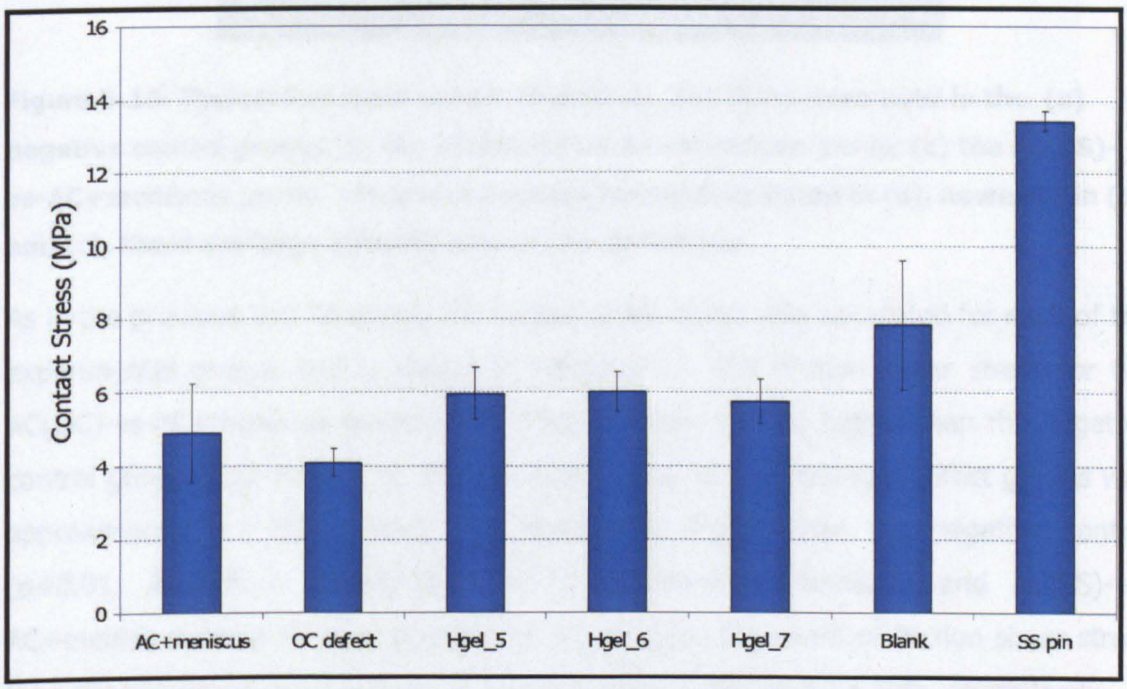

Figure 5-15: Average peak contact stress for the seven experimental groups. Results are presented as mean ± 95% confidence intervals. For hydrogel groups (n=3) and for all other groups (n=6).

For the AC(blank)-vs-AC+meniscus and AC(SS)-vs-AC+meniscus groups, localised areas of larger contact stress were observed around the defect site. A comparison of typical Fuji film strips from the negative control group and these two defect groups is shown in Figure 5-16. There were some localised increases in contact stress around the defect for the hydrogel groups, but to a much lesser extent.

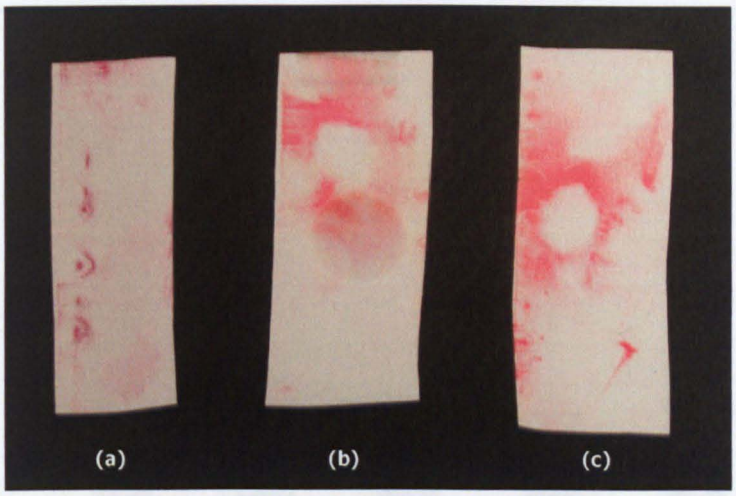

Figure 5-16: Typical Fuji films used in this study. Fuji films were used in the (a) negative control group; (b) the AC(blank)-vs-AC+meniscus group; (c) the AC(SS)-vs-AC+meniscus group. The stress appears evenly distributed in (a), however, in (b) and (c), there are large stresses around the defect site.

As in the previous two Chapters, the friction shear stress was calculated for each of the experimental groups and is shown in Figure 5-17. The friction shear stress for the AC(OC)-vs-AC+meniscus group (0.46 MPa) was only slightly higher than the negative control group (0.37 MPa). The friction shear stress for the hydrogel defect groups was approximately 0.7 MPA, which was statistically higher than the negative control ($p<0.01$; ANOVA + T-method). The AC(blank)-vs-AC+meniscus and AC(SS)-vs-AC+meniscus demonstrated significantly higher ($p<0.01$) levels of friction shear stress than the aforementioned groups, at approximately 1 MPa and 1.6 MPa, respectively.

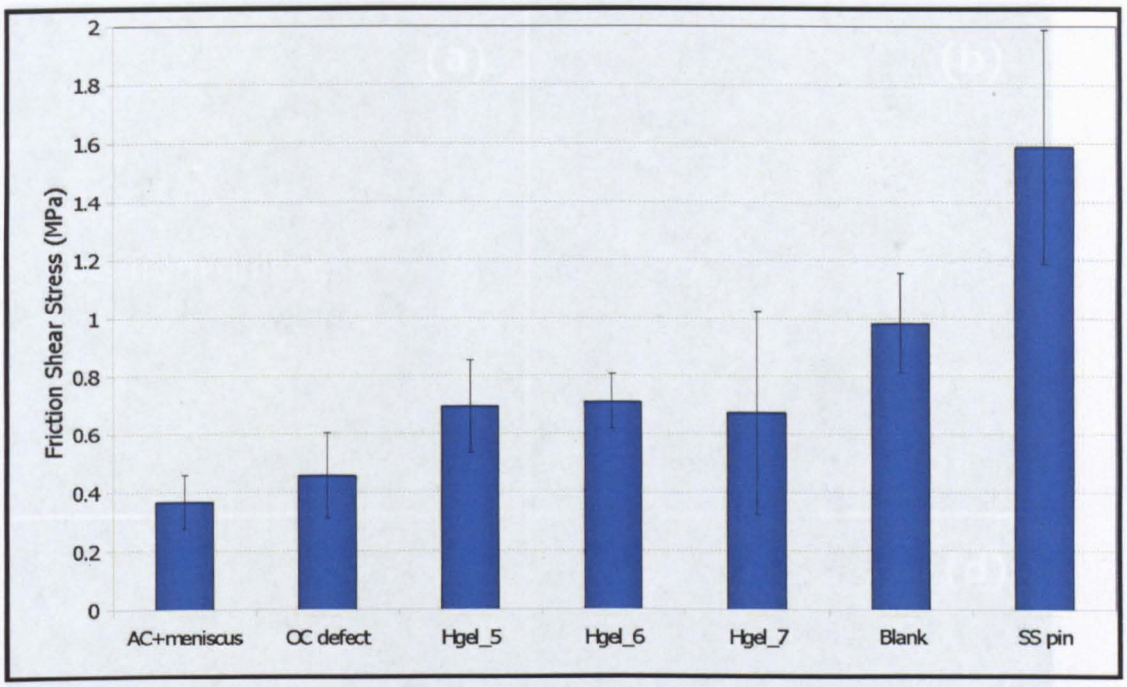

Figure 5-17: Average friction shear stress for the seven experimental groups. Results are presented as mean ± 95% confidence intervals. For hydrogel groups (n=3) and for all other groups (n=6).

5.3.3 Wear characterisation

All of the femoral condyles, with the exception of those from the AC(SS)-vs-AC+meniscus group, were scanned in the μMRI scanner. The stainless steel pins could not be removed from the condyles easily due to the cement fixation, therefore, these specimens were unsuitable for the scanner. Of the specimens which were scanned, there did not appear to be any damaged cartilage or loss of cartilage, on either side of the defect. As a result, wear was not characterised volumetrically for this study.

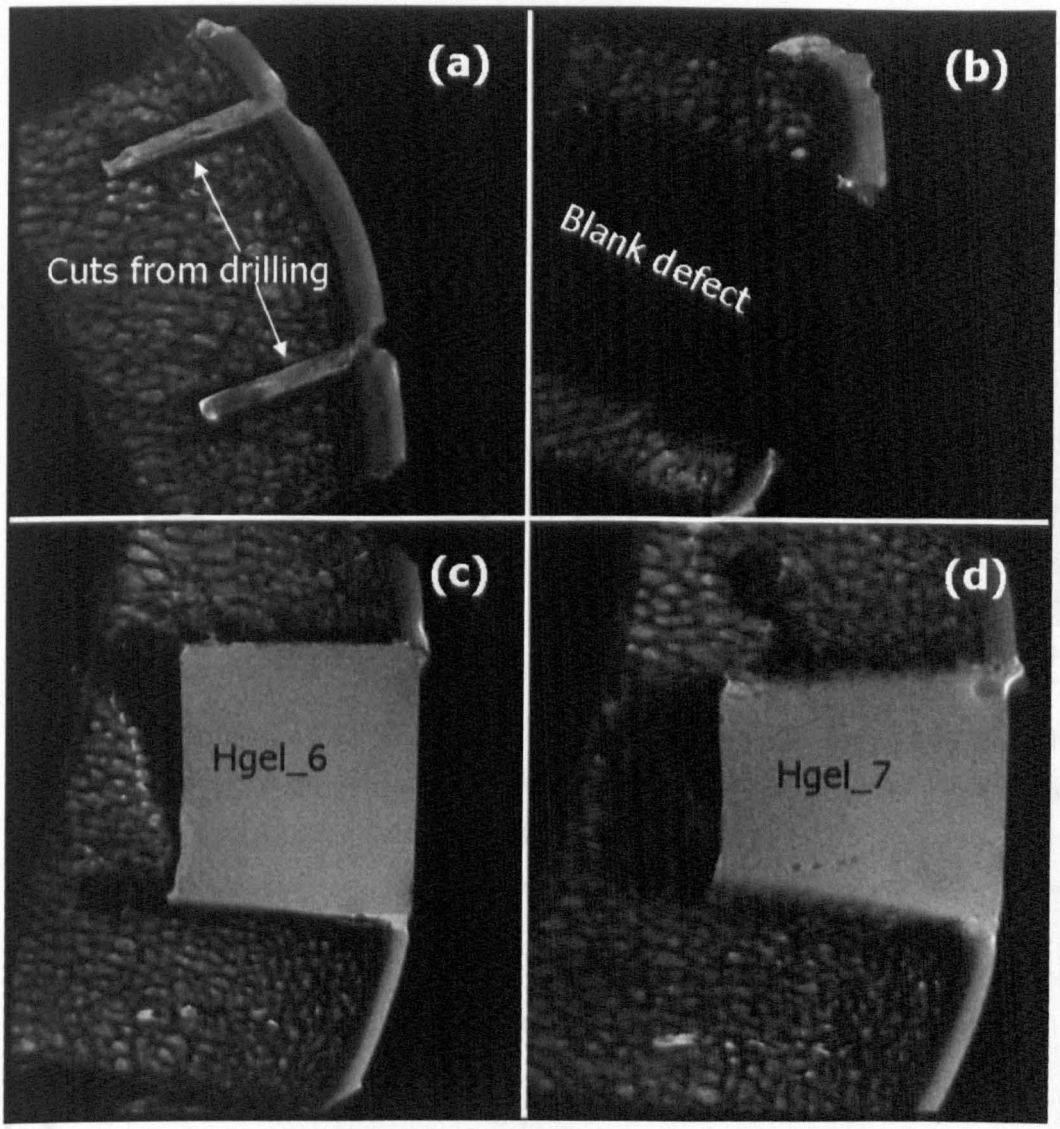

Figure 5-18: Representative μMRI images of the femoral condyles following friction testing. (a) OC defect (b) blank defect (c&d) hydrogel defects.

The Ra values for the femoral condyles, measured either side of the defect are shown in Figure 5-19, for each of the seven groups. All of the defect groups had a slightly higher Ra value than the AC-vs-AC+meniscus group, however, none were statistically higher (ns; ANOVA + T-Method). There was poor correlation found between the friction shear stress and the Ra values of the femoral condyles, as shown in Figure 5-20.

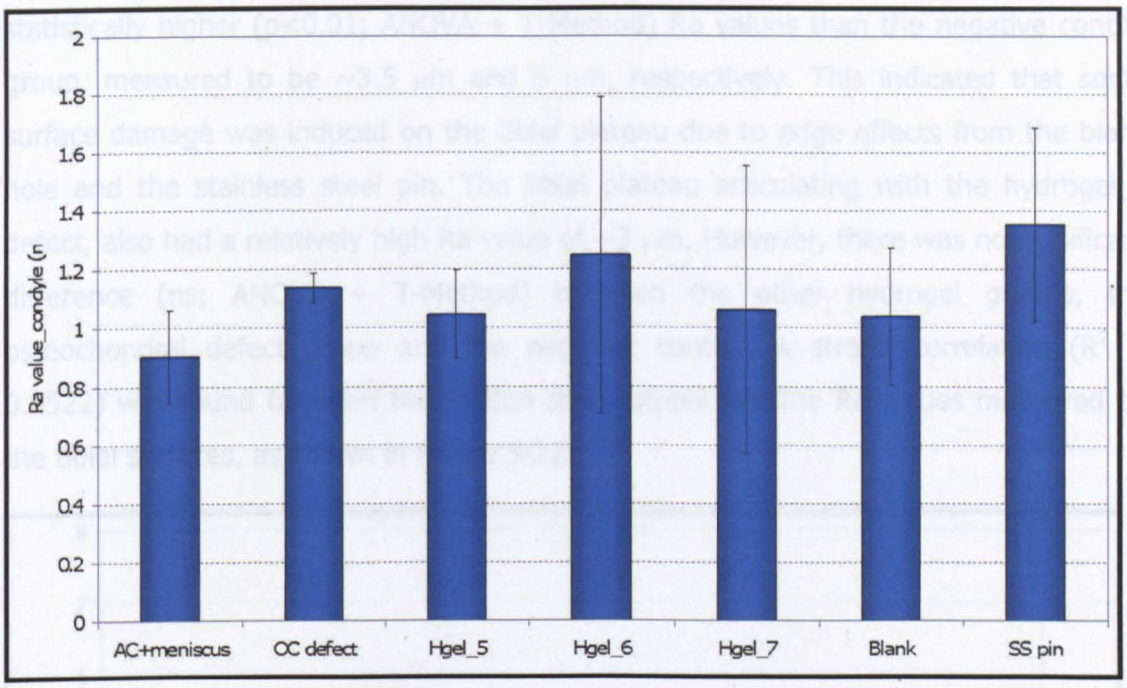

Figure 5-19: Average Ra value of the femoral condyles for the seven experimental groups. Results are presented as mean ± 95% confidence intervals. For hydrogel groups (n=3) and for all other groups (n=6).

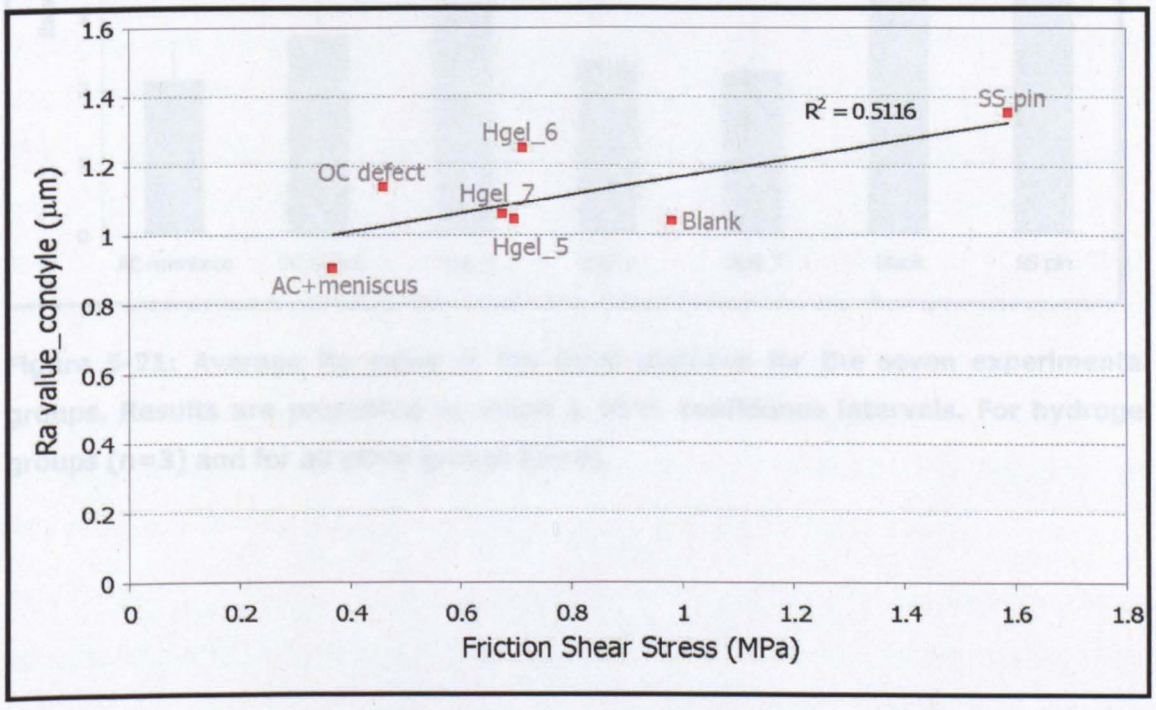

Figure 5-20: Correlation (R^2=0.5116) between the friction shear stress and the Ra values measured for the femoral condyles. Results presented are mean values (n=3 for hydrogels and n=6 for all other groups).

The Ra values measured for the tibial plateaus of the seven groups are shown in Figure 5-21. The AC(blank)-vs-AC+meniscus and AC(SS)-vs-AC+meniscus groups had

statistically higher ($p<0.01$; ANOVA + T-Method) Ra values than the negative control group, measured to be ~3.5 μm and 5 μm, respectively. This indicated that some surface damage was induced on the tibial plateau due to edge effects from the blank hole and the stainless steel pin. The tibial plateau articulating with the hydrogel_5 defect, also had a relatively high Ra value of ~3 μm. However, there was no significant difference (ns; ANOVA + T-Method) between the other hydrogel groups, the osteochondral defect group and the negative control. A strong correlation (R^2 = 0.8522) was found between the friction shear stress and the Ra values measured on the tibial surfaces, as shown in Figure 5-22.

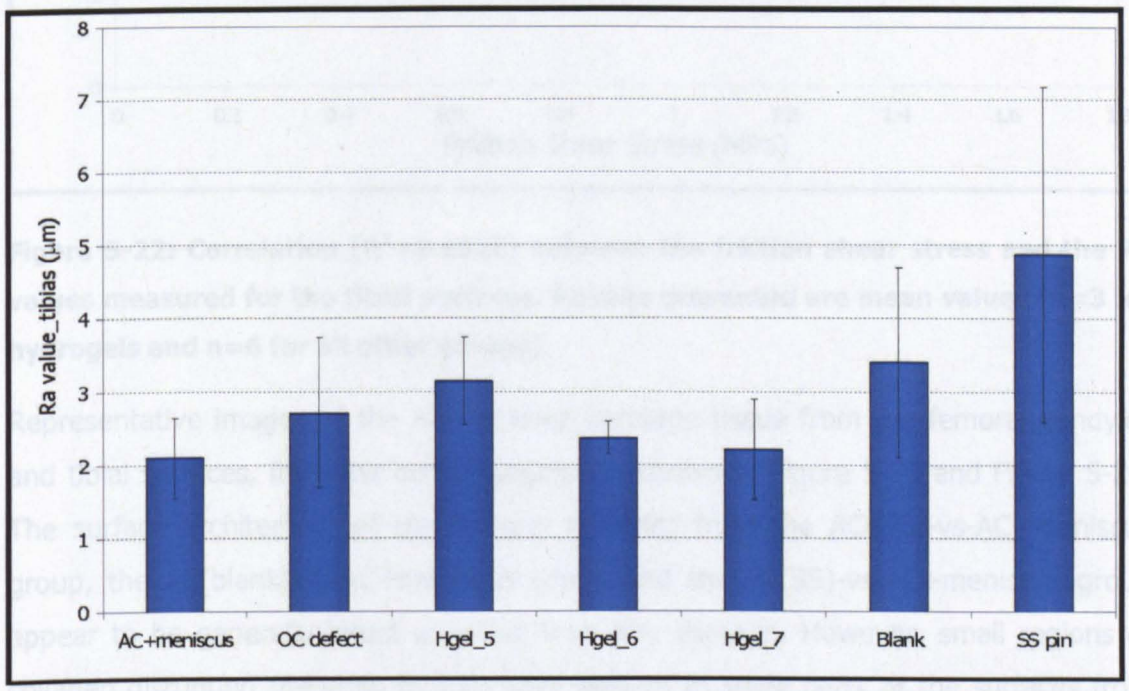

Figure 5-21: Average Ra value of the tibial plateaus for the seven experimental groups. Results are presented as mean ± 95% confidence intervals. For hydrogel groups (n=3) and for all other groups (n=6).

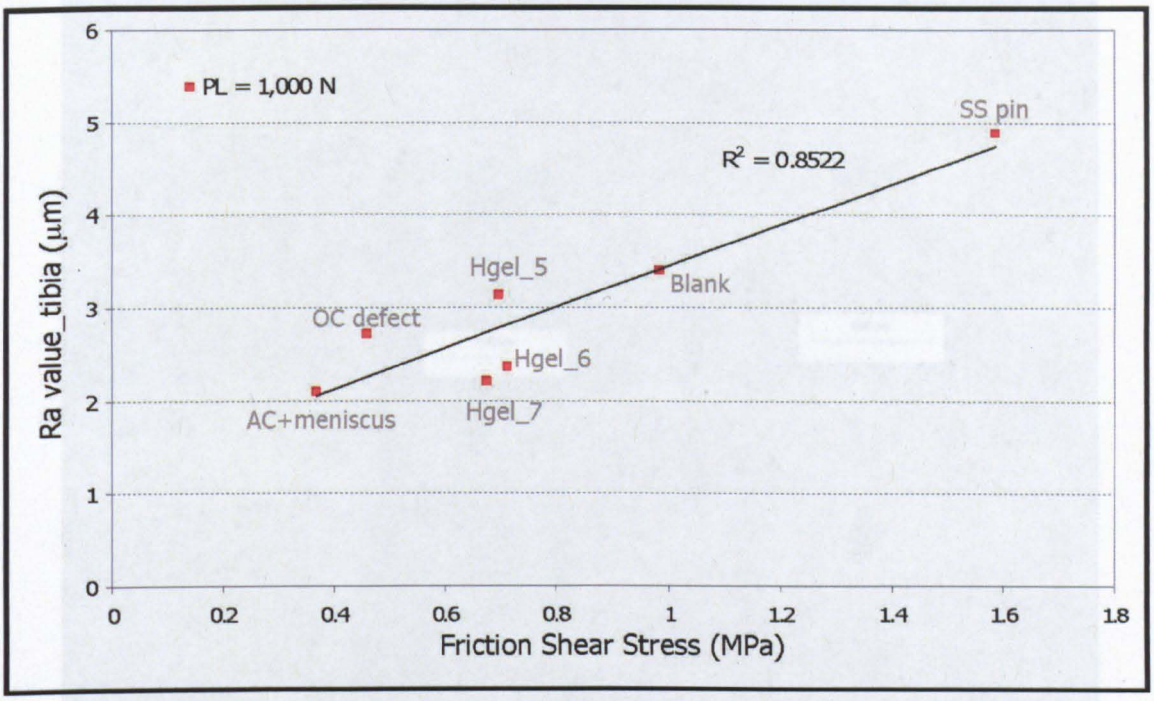

Figure 5-22: Correlation (R^2=0.8522) between the friction shear stress and the Ra values measured for the tibial surfaces. Results presented are mean values (n=3 for hydrogels and n=6 for all other groups).

Representative images of the H&E stained cartilage tissue from the femoral condyles and tibial surfaces, from the defect groups are shown in Figure 5-23 and Figure 5-24. The surface architecture of the femoral condyles from the AC(OC)-vs-AC+meniscus group, the AC(blank)-vs-AC+meniscus group and the AC(SS)-vs-AC+meniscus group appear to be generally intact and free from any damage. However, small regions of collagen disruption (denoted by CD) were evident in some parts of the surfaces from the AC(blank)-vs-AC+meniscus and the AC(SS)-vs-AC+meniscus groups (Figure 5-23 (c & e)). There appeared to be increased collagen disruption along the tibial surfaces, in comparison to the condyles for the AC(OC)-vs-AC+meniscus, the AC(blank)-vs-AC+meniscus and the AC(SS)-vs-AC+meniscus (Figure 5-23 (b, d, f & h)).

The surface architecture of the condyles and tibial plateaus for the hydrogel defect groups, appeared to have less collagen disruption and in most cases the collagen layer was visible along the surface (Figure 5-24 (a-d,f,h)). However, in some cases this layer had been completely removed from the femoral condyle (Figure 5-24 (e & g)) and some disruption to the collagen network was evident on one of the tibial plateaus (Figure 5-24 (f)).

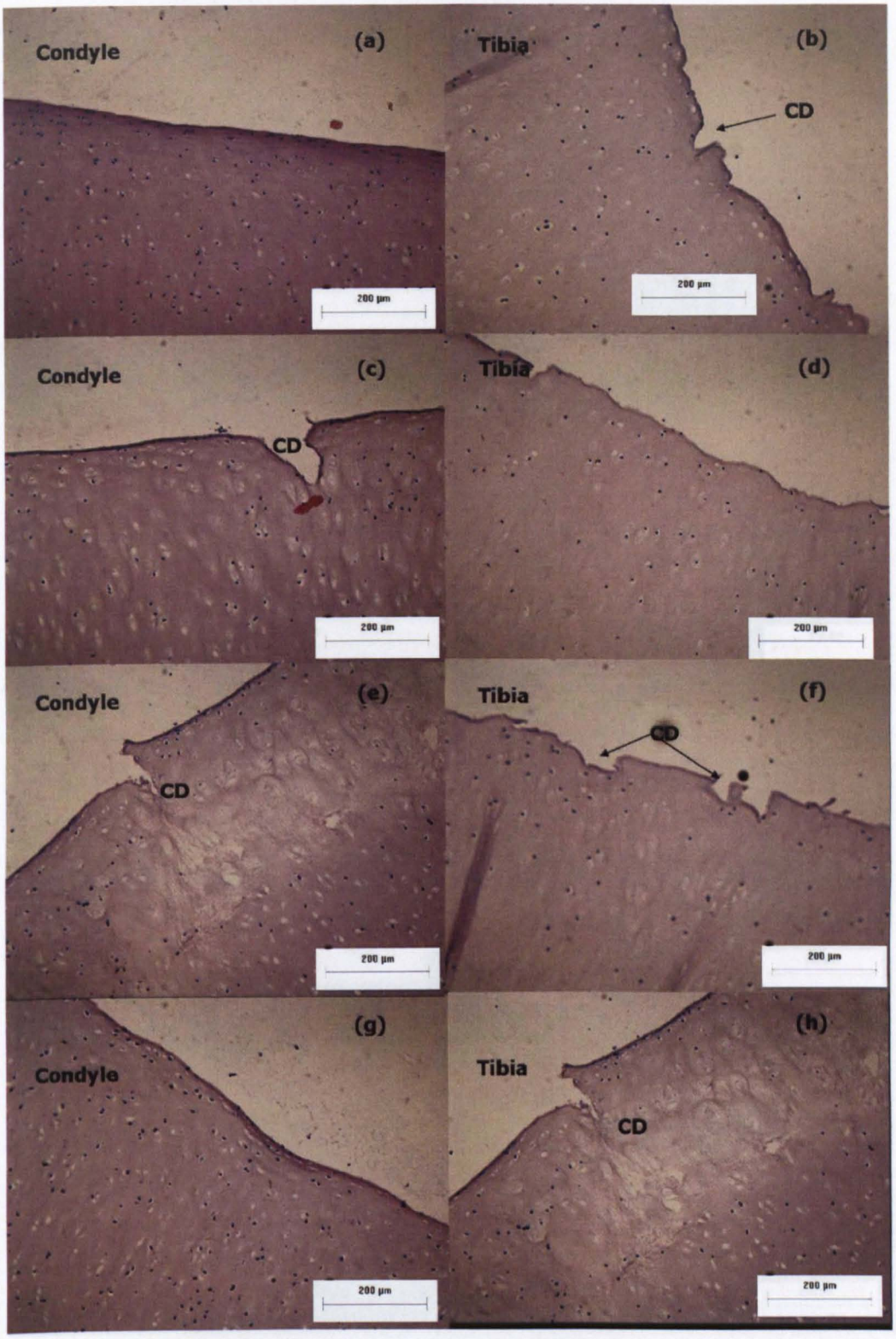

Figure 5-23: H&E stained cartilage from the cartilage defect repair study. All images were taken at x100 mag. Images (a&b) are from the AC(OC)-vs-AC+meniscus group; (c&d) are from the AC(blank)-vs-AC+meniscus group and (e-h) are from the AC(SS)-vs-AC+meniscus group.

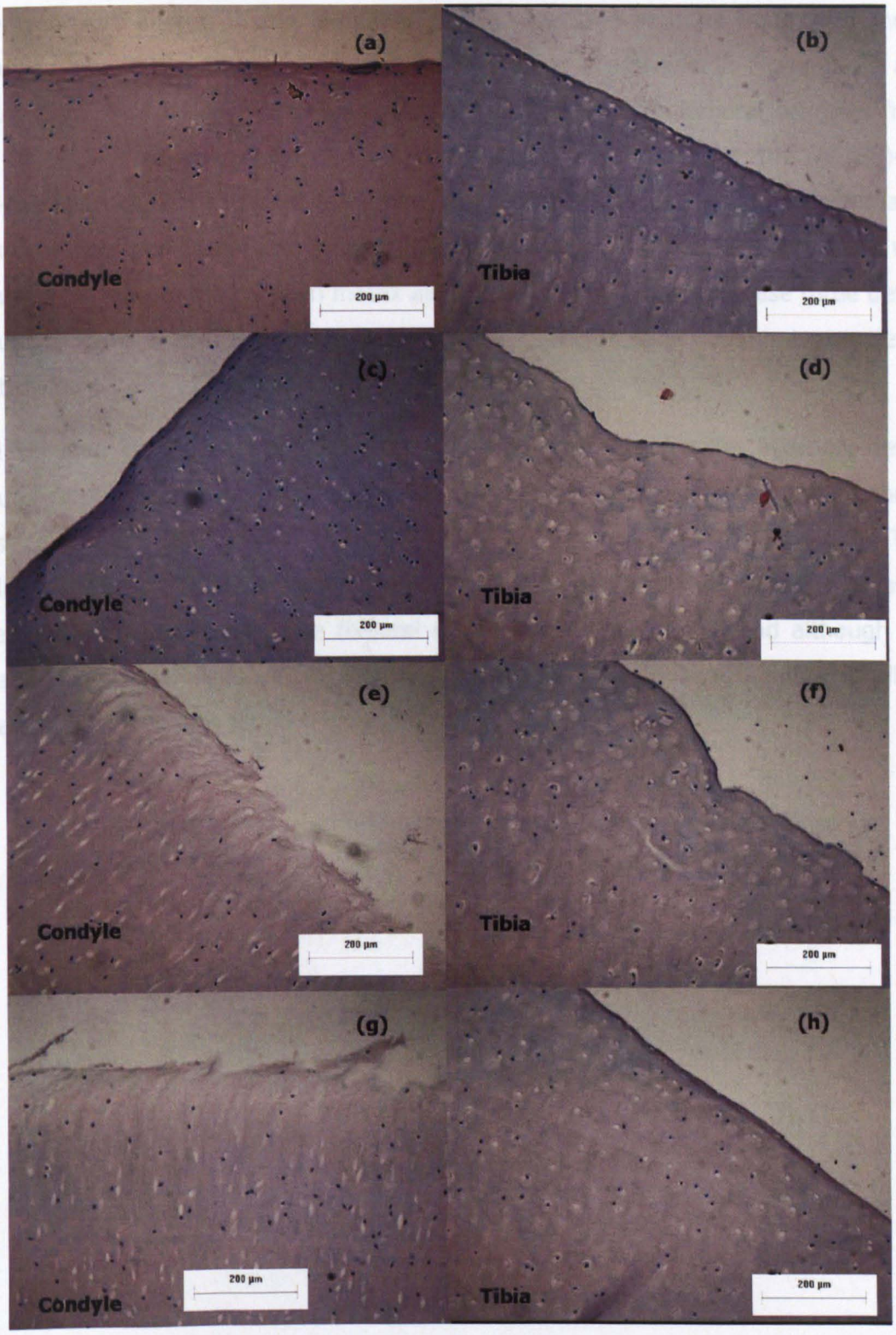

Figure 5-24: H&E stained cartilage from the cartilage defect repair study. All images were taken at x100 mag. Images (a-d) are from the AC(Hgel_5)-vs-AC+meniscus group; (e&f) are from the AC(Hgel_6)-vs-AC+meniscus group and (g&h) are from the AC(Hgel_7)-vs-AC+meniscus group.

Representative images of the Sirius red stained cartilage sections from the femoral condyles and tibial surfaces, from the defect groups are shown in Figure 5-25 and Figure 5-26. The collagen structure along the surfaces of the femoral condyles from the AC(OC)-vs-AC+meniscus, the AC(blank)-vs-AC+meniscus and the AC(SS)-vs-AC+meniscus groups appeared to be have been disrupted, although the collagen layer was present either side of any damage (Figure 5-25 (a, c, e & g)). Similarly, there was localised damage to the collagen matrix along the tibial surfaces, for these three defect groups (Figure 5-25 (b, d, f & h)), but the collagen layer was not completely destroyed.

The collagen structure of the condyles and tibial plateaus for the hydrogel defect groups, appeared to have less collagen disruption than the other defect groups and in most cases the collagen layer was visible along the surface (Figure 5-26 (a-d,f)). This finding was consistent with that of the H&E staining. Again, in one case the collagen layer was very depleted on the femoral condyle (Figure 5-26 (e)) and although the collagen layer was visible along the surfaces of the tibial plateaus, minor localised collagen disruption was found (Figure 5-24 (f)).

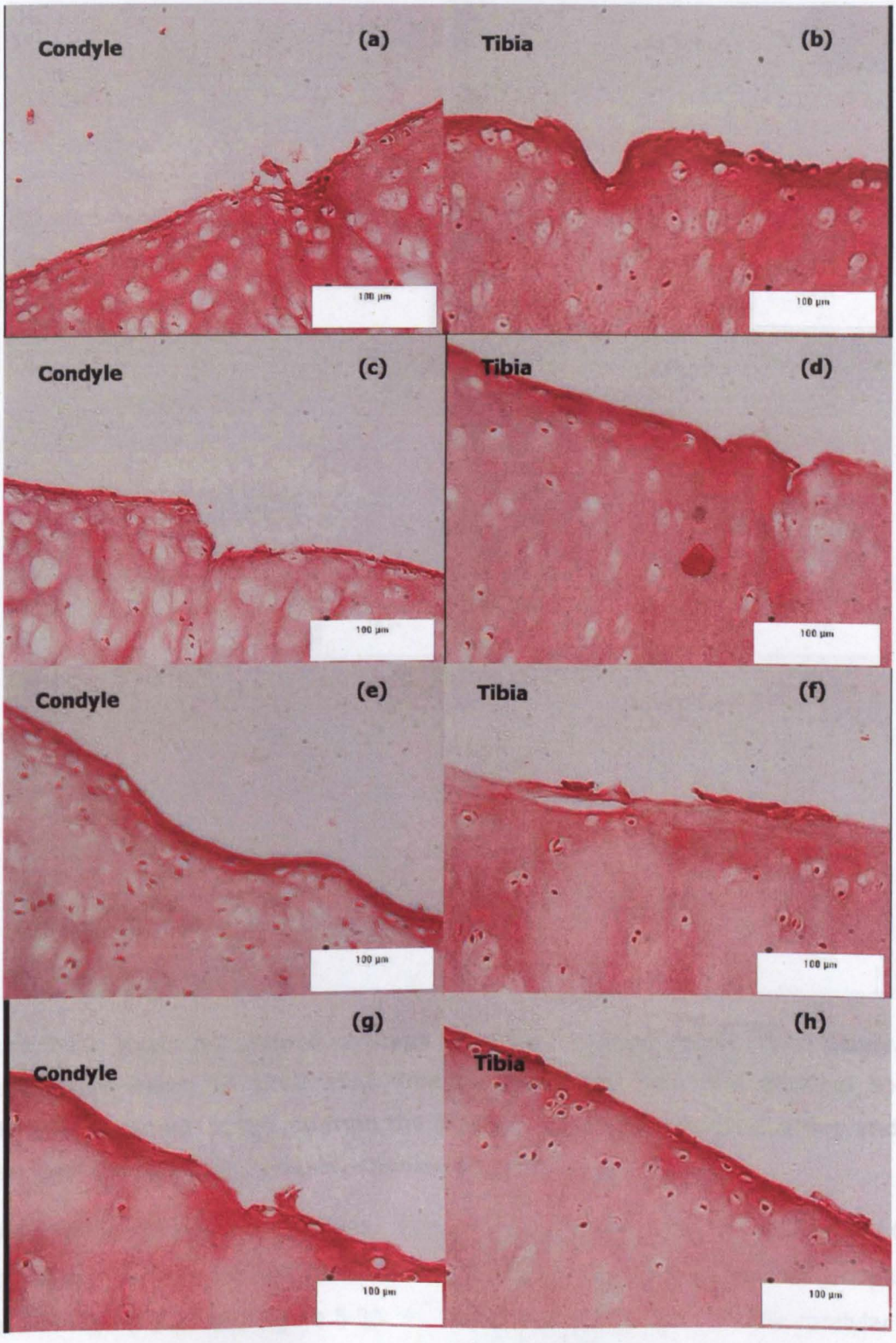

Figure 5-25: Sirius red stained cartilage from the cartilage defect repair study. All images were taken at x200 mag. Images (a&b) are from the AC(OC)-vs-AC+meniscus group; (c&d) are from the AC(blank)-vs-AC+meniscus group and (e-h) are from the AC(SS)-vs-AC+meniscus group.

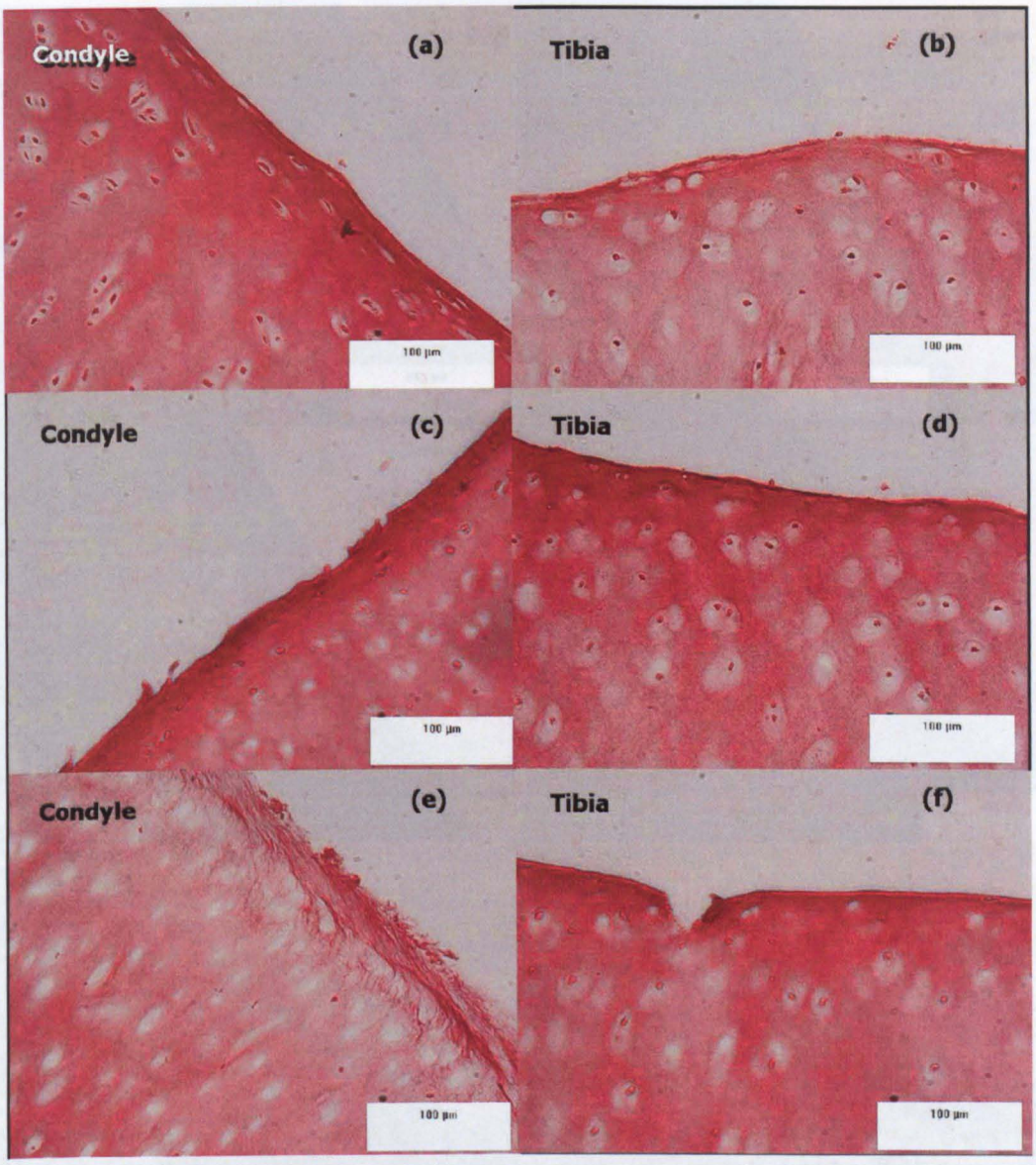

Figure 5-26: Sirius red stained cartilage from the cartilage defect repair study. All images were taken at x100 mag. Images (a&b) are from the AC(Hgel_5)-vs-AC+meniscus group; (c&d) are from the AC(Hgel_6)-vs-AC+meniscus group and (e-f) are from the AC(Hgel_7)-vs-AC+meniscus group.

Representative images of sections, stained with Alcian blue to show the GAG distribution, from the femoral condyles and tibial surfaces from the defect groups are shown in Figure 5-27 and Figure 5-28. For all defect groups, both for the condylar and tibial sections, the blue colouration was patchy and faded in parts, indicating regions of GAG depletion.

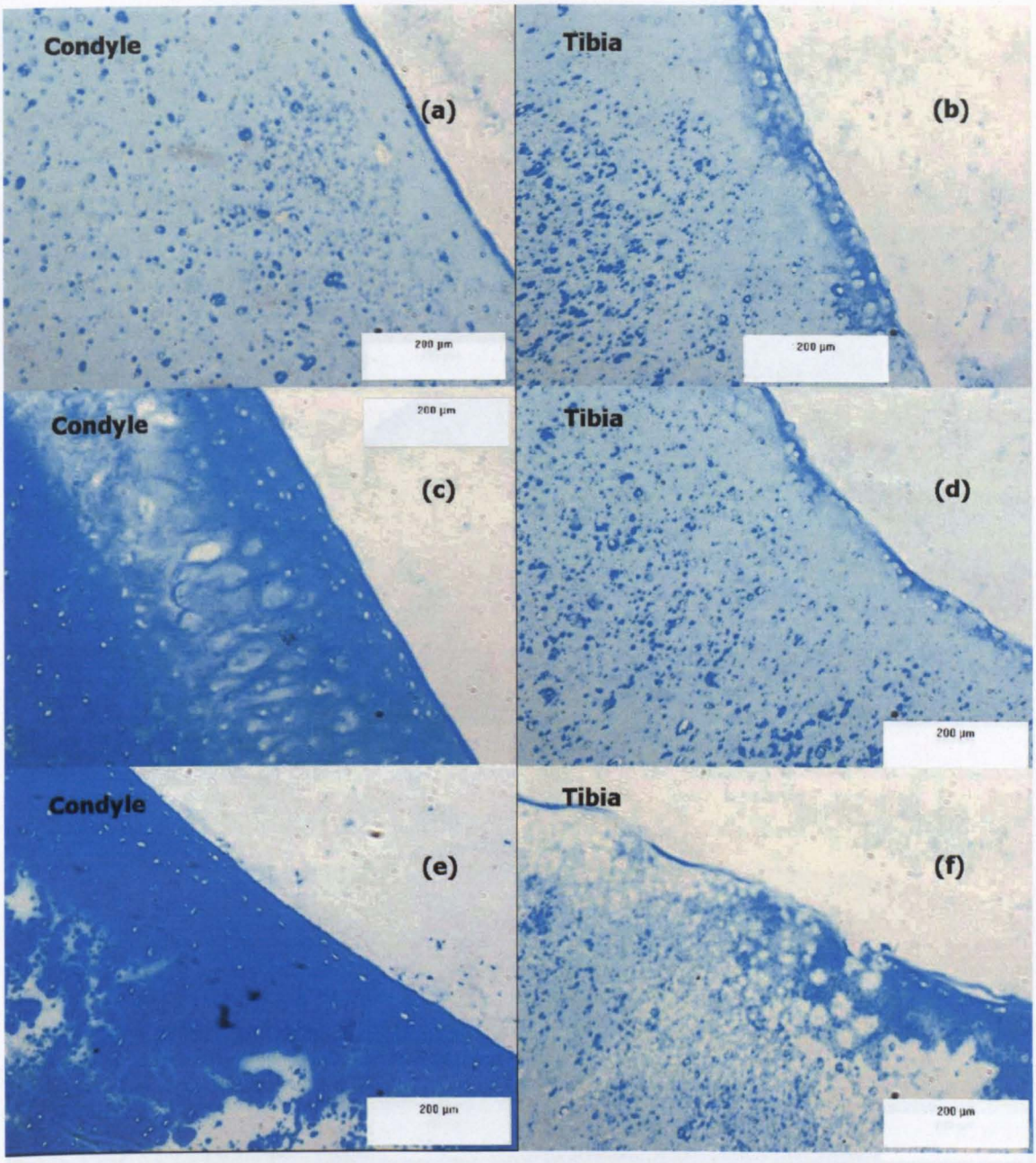

Figure 5-27: Alcian blue stained cartilage from the cartilage defect repair study. All images were taken at x100 mag. Images (a&b) are from the AC(OC)-vs-AC+meniscus group; (c&d) are from the AC(blank)-vs-AC+meniscus group and (e&f) are from the AC(SS)-vs-AC+meniscus group.

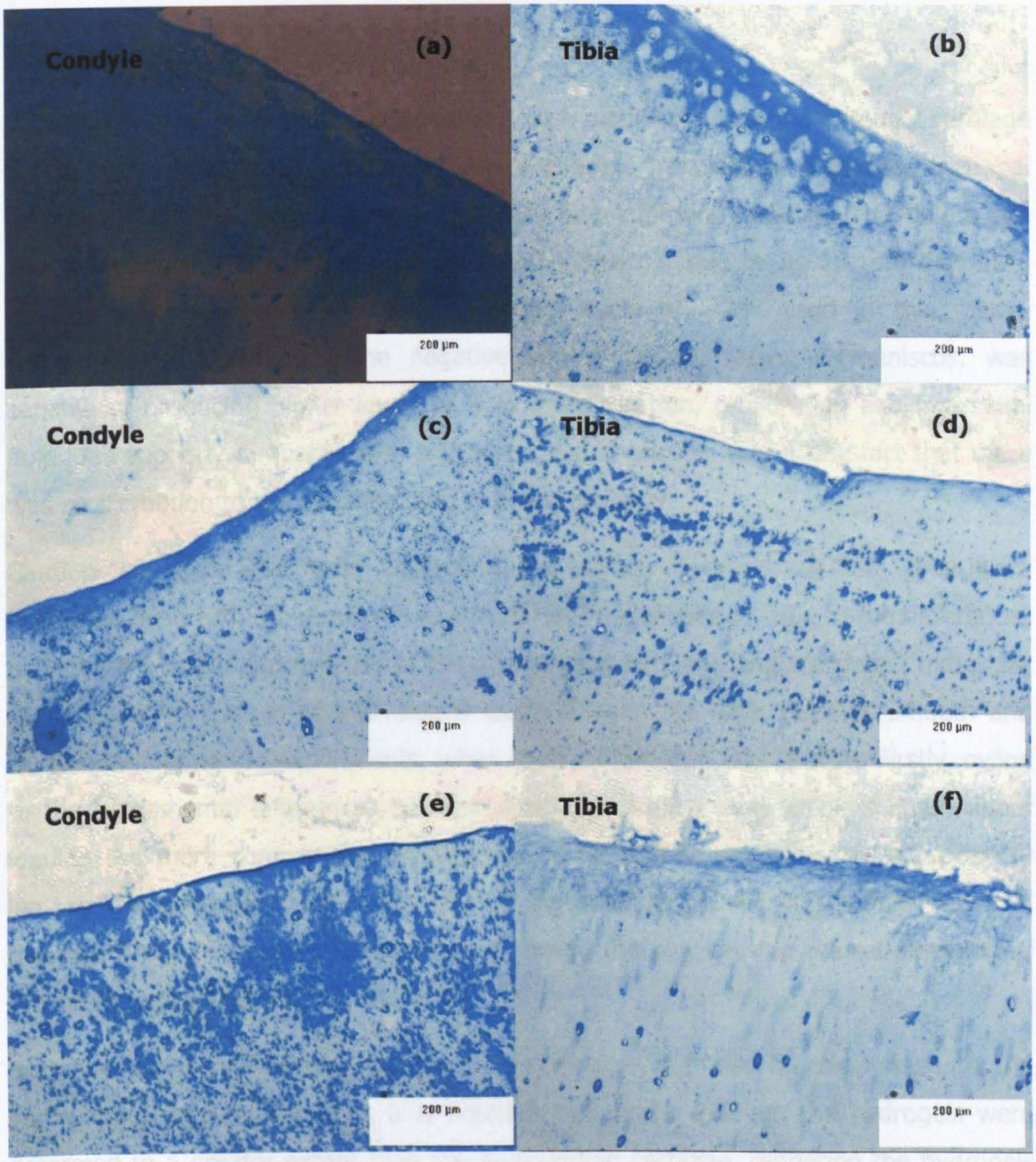

Figure 5-28: Alcian blue stained cartilage from the cartilage defect repair study. All images were taken at x100 mag. Images (a&b) are from the AC(Hgel_5)-vs-AC+meniscus group; (c&d) are from the AC(Hgel_6)-vs-AC+meniscus group and (e-f) are from the AC(Hgel_7)-vs-AC+meniscus group.

5.4 Discussion

Variation in experimental contact geometry, as a result of implanting potential cartilage defect repair biomaterials into the femoral condyle, resulted in a greater frictional response, than that demonstrated for a fully intact femoral condyle. The defect site was in continued contact with the tibia and meniscus, due to its 10 mm diameter, coupled with the truncated flexion-extension cycle of ~25° used in this medial compartmental simulation. The negative control group, AC-vs-AC+meniscus, was capable of producing higher levels of fluid pressurisation, rehydration and interstitial fluid load support, compared with any of the defect groups, due to the fact that there was no disruption to the cartilage structure and integrity.

Caution was exercised while implanting the defect materials, so that they were implanted flush with the surrounding articular surface. However, due to the differences between the material properties of the surrounding cartilage and the defect materials, the articulating surface of the femoral condyle, may not have been as smooth and conforming during the experiments, when the dynamic load was applied. Firstly, owing to the fundamental differences between articular cartilage and stainless steel, under loading the more compressive cartilage would deform to a greater extent, possibly leaving the stainless steel proud of the surrounding tissue. This would result in localised areas of elevated contact stress around the pin, causing a local elevation of the coefficient of friction.

Secondly, as the hydrogels had lower compressive stiffness in comparison to the surrounding articular cartilage, it is possible that under loading, the hydrogels were deformed to a greater extent than the surrounding cartilage, rendering the hydrogels in a deep position relative to the surrounding tissue. In this case, edge loading would have caused local increases in contact stress and coefficient of friction. Of course, this edge loading effect is also postulated to have occurred with the AC(blank)-vs-AC+meniscus group also.

Northwood conducted a small scale tribological study of cartilage defect repair, which involved a cartilage pin reciprocating (unidirectional) on a cartilage plate with a 6 mm diameter defect. A stainless steel pin or a hydrogel pin was used to fill the defect. Initially, the frictional coefficient was low, similar to the negative control of a cartilage pin reciprocating on a cartilage plate (no defect), but over time the friction started to rise, which was not observed for the negative control (Northwood, 2007). This

indicated that there was a continued reduction in the fluid load support over time. However, Northwood's tests were conducted at a much lower (8 times lower than the lowest contact stress found measured in the current study) level of contact stress of 0.5 MPa. It is possible that the much higher levels of contact stress used in the current study, caused a more rapid decrease of the interstitial fluid pressurisation.

The fact that the defect was continuously loaded and in contact with the tibia and meniscus, can explain the higher coefficient of friction. An increase in friction has been shown in previous studies to occur as a result of a loss of fluid load support and increased direct solid to solid contact, due to the unique biphasic nature of articular cartilage (Forster and Fisher, 1996; Northwood and Fisher, 2007). The continuous contact between the defect and the tibial surface may have increased this direct solid to solid contact. Furthermore, our studies and others (Forster and Fisher, 1996; Krishnan *et al.*, 2004b; Carter *et al.*, 2007; Katta *et al.*, 2007; Northwood *et al.*, 2007) have shown the importance of the level of contact stress and the nature of the loading cycle, particularly the loading-unloading cycle, and the ability of AC to rehydrate during unloading (Bell *et al.*, 2006). In particular, if the defects were in a proud or deep position relative to the surrounding tissue, larger localised contact stresses would have resulted in a more rapid decrease of the biphasic fluid load support, and subsequently, an increase in the coefficient of friction, the friction shear stress and the degradation of AC. The limited flexion-extension motion of 25°, resulting in a shorter stroke length, may have further limited the rehydration of the cartilage tissue, in comparison to that which occurs *in vivo,* causing a rise in frictional coefficient. Previous studies have shown how a shorter stroke length results in decreased fluid load support and increased friction (Bell *et al.*, 2006; Caligaris and Ateshian, 2008).

However, it was surprising that the coefficient of friction for the AC(OC)-vs-AC+meniscus group was so high in comparison to the negative control, particularly in the early stages of the experiments, as there was no difference in the contact materials and the contact geometry was in effect, the same. One would have expected that the initial coefficient of friction would have been approximately 0.06, as for the negative control, with a more rapid increase over the duration of the test, due to a more rapid decrease in the fluid load support as a result of the cut in the surface.

It was not surprising to find that there was no statistical difference between the Ra values of the femoral condyles or that there was not a strong correlation between the Ra values and friction shear stress, for the negative control group and the six defect

groups. The counterface surfaces (tibia and meniscus) were composed of the same materials and had the same geometry. Furthermore, if stainless steel or hydrogel defects developed a proud position in comparison to the surrounding cartilage tissue under loading, the pin would have borne a higher proportion of the load acting through the joint, shielding the cartilage from part of, or all of the loading.

However, for the tibial surfaces significant differences in the Ra values were observed and a strong correlation was found between the tibial Ra values and friction shear stress. The Ra values of the tibial surfaces articulating with the stainless steel defect (4.9 μm), were markedly higher than all of the other groups. As mentioned previously, when discussing the coefficient of friction, if the cartilage deformed around the stainless steel pin under load, rendering the pin in a relatively proud position, the change in geometry would result in increased levels of abrasive wear as the harder stainless steel material contacted the opposing surface. The Ra values for the tibial surfaces articulating with the blank defect (3.4 μm), were lower than for those articulating with the steel defect, but statistically higher than all of other groups. The disruption to the normally rounded and smooth geometry of the condyle with the presence of a 10 mm hole, would have caused localised edge loading. It was postulated that these edge effects resulted in increased levels of abrasive wear, which caused an increase in the surface roughness. The Ra values of the tibial surfaces articulating with the hydrogels were higher than the Ra value of the negative control group, although not statistically higher. The slight increase in the Ra value, may have been caused by a similar mechanism to that in the blank defects. The hydrogels, being more deformable than the cartilage surrounding them, may have sat in a deep position under load and edge loading effects may have resulted in wear and thus the increase in the Ra value.

The results of the histological assessment of the condyle and tibial cartilage were quite consistent with the surface topography measurements. When examining the histoarchitecture and in particular, collagen structure, with H&E and Sirius red staining, the condyle sections from the defect groups appeared to be generally, intact. Only very small (10 μm - 20 μm in length) disruptions to the collagen layer, were observed along the surface. However, in some of the condylar sections from the hydrogel defects, the collagen layer appeared to be almost completely diminished. This could have been as a result of excessive loading of the cartilage surfaces, due to increased deformation of the hydrogels, relative to the cartilage under loading. In general, although the collagen

layer was present in the tibial sections of all defect groups, there appeared to be more collagen disruption, than to the condylar sections. This increased disruption was as a result of the constant contact between the tibial cartilage and the defect on the opposing surface.

It was shown in Chapter 3 and Chapter 4 that there was a strong relationship between the friction shear stress and the wear of articular cartilage. In the current study however, the volume of cartilage wear was not quantified. However, the friction shear stress for the various defect groups increased with increasing changes in material and geometry. For example, there was no statistical difference between the friction shear stress for the negative control group and OC defect group, which was expected as there was no change to the articulating materials or to the geometries of the bearing. The friction shear stress increased to approximately 0.7 MPa when hydrogels were used as the defect material and there was no statistical difference between any of the hydrogel defects. Although biphasic materials, the compressive stiffness of the hydrogels was inferior to those of cartilage, which resulted in changes to the conformity of the condylar surface, resulting in localised increases in contact stress and coefficient of friction and thus the increase in friction shear stress. When a blank defect was used the friction shear stress increased to 0.97 MPa. Leaving the defect blank with a hole, increased the changes to the condylar geometry. Finally the highest friction shear stress was found for the stainless steel pin defect, where it reached 1.59 MPa. This elevation in friction shear stress can be attributed to two things: the use of a single phase material, rather than a biphasic, which was discussed in depth in Chapter 4; as well as the lack of deformation of the steel pin, in comparison to the surrounding cartilage.

The findings of this study suggest that biphasic materials should be considered over single phase materials such as stainless steel, as cartilage substitution materials. However, while PVA hydrogels possess 75% - 80% water content, similar to articular cartilage, an ongoing barrier to their use in load-bearing orthopaedic applications over the past two decades, has been their lack of sufficient mechanical properties to withstand the severe loading conditions imposed on articular joint surface (Corkhill *et al.*, 1990; Anseth *et al.*, 1996; Stammen *et al.*, 2001). The freeze-thaw process used in the manufacture of these hydrogels is one method used in an attempt to enhance the mechanical properties for load bearing orthopaedic application (Swieszkowski *et al.*, 2006). Other techniques include the use of cross-linking agents such as gluteraldehyde

or the introduction of composite materials such as rubber or glass (Stammen *et al.*, 2001). Clearly hydrogels for orthopaedic applications must possess similar mechanical properties to articular cartilage.

Hydrogels have the potential to mimic many of the important characteristics of articular cartilage, such as the biphasic fluid load support, low wear and shock absorption. However, another important consideration in the design of osteochondral substitute materials is the greater stiffness of the underlying bone, relative to articular cartilage. Cartilage is only 1-2 mm thick but the hydrogel pins used in the current study were 10 mm thick. The use of a thinner hydrogel layer, on a stiffer porous substrate, such as a fibre mesh or porous metal, would enhance the mechanical properties of the implant, reduce deformation and the resulting increase in localised contact stress, while still maintaining the biphasic fluid load support, low wear and shock absorbing properties. In Northwood's *in vitro* investigation of potential osteochondral substitution materials, the hydrogels used had a PMMA substrate (Northwood, 2007), which may have limited the deformation of the hydrogels, relative to the surrounding cartilage tissue.

Previous animal studies have been conducted to investigate the use of composite osteochondral devices (CODs), which comprised of PVA-hydrogels acting as artificial cartilage and a titanium fibre mesh acting as a porous artificial bone (Chang *et al.*, 1997; Chang *et al.*, 1998a; Ushio *et al.*, 2003). In the three studies the COD's were used for partial hemiarthroplasty of canine femoral heads and after periods of between 24-52 weeks, excellent osseointegration through the open pore structure and preservation of the opposing acetabular cartilage were observed. The COD devices were found to perform considerably better than control implants made from single phase materials – UHMWPE and alumina ceramics (Ushio *et al.*, 2003) and alumina and titanium (Chang *et al.*, 1998a). Other studies in animal models have investigated the use of single phase materials for cartilage defect repair. Kawalec implanted plug-like implants made from pyrolytic carbon and cobalt chromium alloy, into canine femoral condyles (Kawalec *et al.*, 1998) and Custers implanted cobalt chromium and oxidised zirconium plugs into rabbit condyles (Custers *et al.*, 2007b). In both of these studies extensive damage to the opposing tibial surface was observed, after only four weeks (Custers *et al.*, 2007b).

A limitation of the current study was that the volumetric wear on the tibial counterface could not be quantified, as this was the surface on which most damage occurred, due to the constant contact with the defect. However, high levels of friction shear stress

were found for the stainless steel defect group and it was shown in Chapters 3 and 4, that the friction shear stress correlated exceptionally well with the wear of articular cartilage. The high levels of friction shear stress and increased Ra values found, coupled with the damage to the opposing tibial surfaces observed in the aforementioned animal studies of defect repair with metallic plugs, indicates that metallic or single phase materials should not be considered as cartilage defect repair biomaterials.

The hydrogel materials showed more promising results, the friction shear stress was only slightly higher than the negative control and there was less tibial damage than with the stainless steel or blank defects. However, improving the mechanical strength of hydrogels is an important consideration. In the design of a hydrogel defect repair implant, it is also important to regard the cartilage and bone as a composite structure and attempt to mimic the underlying bone properties, as well as the articular cartilage.

5.5 Conclusions

This study was the first anatomical, *in vitro* tribological experimental simulation of cartilage defect repair in the medial compartmental knee. It has many advantages over the simple geometry experiments which have been used previously to examine the tribological response of cartilage articulating with potential osteochondral substitution biomaterials. The contact stresses and motions applied mimic those in the natural situation. This tribological simulation has the potential to examine the effects many cartilage defect repair designs, for example composite osteochondral devices.

This study has demonstrated for the first time an elevation in the coefficient of friction, relative to the negative control, irrespective of the type of defect repair used. The damage to the opposing (tibial) surfaces, appeared to be independent of the frictional coefficient. However, the contact stresses and friction shear stresses found, indicated that biphasic biomaterials should be considered for cartilage defect repair and that single phase, metallic materials are not suitable, due to the high friction shear stress and the damage observed on the opposing tibial surface.

The concept of cartilage defect repair is an attractive therapeutic intervention for young and active patients suffering from knee joint OA. In the current study, the biphasic cartilage substitute materials demonstrated lower levels of friction shear stress, which was shown in Chapters 3 and 4 to reduce volumetric wear of cartilage. Therefore, biphasic materials should be utilised in order to maintain fluid load support for a longer period of time. In the design of such defect repair implants, the compressive stiffness of these biphasic materials should be an important consideration. The inclusion of a stiffer substrate or porous material to mimic the material properties of bone should be investigated, in a tribological simulation.

Chapter 6. Overall Discussion and Future Objectives

Understanding the tribological characteristics of the cartilage-cartilage and cartilage-biomaterial interface is vital for the development of more satisfactory, and more conservative therapies for worn and damaged synovial joints. Today, the clinical demand for joint replacement and joint repair is on the rise and the reasons are multi-factorial. Our aging population, the increased number of road traffic accidents and the ever growing popularity of extreme sports, are just a few of the reasons why osteoarthritis sufferers are getting younger and younger. Of course the younger and more active the patient, the higher the likelihood is of multiple surgeries throughout their lifetime. Therefore, there is a huge clinical demand for less invasive treatment options, to delay the need for total joint arthroplasty and the inevitable revision arthroplasty.

Research into the biomechanical and tribological behaviour of articular cartilage has been a rapidly developing field over the past two decades. The majority of investigations into the tribological behaviour of cartilage have been in the form of small scale *in vitro* PoP and SoD experiments (Forster and Fisher, 1996; Pickard *et al.*, 1998a; Pickard *et al.*, 1998b; Freeman *et al.*, 2000; Ateshian *et al.*, 2003; Park *et al.*, 2003; Krishnan *et al.*, 2004b; Krishnan *et al.*, 2005; Bell *et al.*, 2006; Katta *et al.*, 2007; Northwood *et al.*, 2007; Northwood and Fisher, 2007; Katta *et al.*, 2008b). These studies have enhanced our understanding of the tribological characteristics of articular cartilage, by allowing precise control over the tribological conditions. The properties of cartilage-cartilage articulations can be compared with cartilage biomaterial (known engineering materials) articulations, which could be potential hemiarthroplasty or defect repair materials. The small size of the tests allows easy and simple evaluation of lubricants, biochemical degradation assays and variation of the cartilage make up, such as water and GAG content.

However, the geometries of these articulations do not mimic anatomical components. The oscillation of only one surface and the unnatural geometry of a cartilage pin increases the surface area and the fluid exudation away from the contact zone. These experiments are usually limited to contact stresses which are much lower than those experienced in a natural joint. Due to the simple geometry, increasing the contact stress to a physiological level, tends to result in edge loading effects which lead to abrasive wear. In most cases, only static loads can be applied, which means

the cartilage (pin) is constantly loaded and this limits the rehydration of the cartilage tissue. Therefore, the next step in terms of the development methods for the preclinical testing of therapeutic interventions, was to move towards partial or full condylar *in vitro* models which would allow the use of anatomical geometries as well as more physiologically relevant loads and motion. The first objective of this project was to develop an experimental simulation of the natural medial compartmental knee joint, with physiologically relevant loads and motions. The development of this novel anatomical simulation allowed the investigation of three potential therapies for damaged or diseased synovial joints: meniscectomy, hemiarthroplasty and cartilage defect repair. This novel *in vitro* simulation which has been developed to examine cartilage friction and wear, could be applied to any therapeutic intervention for the degenerative knee, such as meniscus replacements, various designs of uni- and hemi-arthroplasty, therapeutic lubricants and tissue engineered substitutes. This will have an impact on future treatments for knee joint degeneration and could potentially increase the availability and efficacy of solutions in the clinical community and improve patient care in the long-term.

The study investigating the tribological response of meniscectomy, described in Chapter 3, has shown for the first time, the direct elevation of contact stress, the coefficient of friction, friction shear stress and subsequently the wear and degradation of cartilage, in an *in vitro* tribological model. Although, the importance of the meniscus is widely known clinically, this experimental study demonstrated its importance in both providing conformity and load-bearing. The added conformity in the negative control group, meant that the contact areas were increased and the peak contact stresses were reduced. Furthermore, the meniscus is known to absorb over 50% of the load acting through the joint, by absorbing the loads from the concave femoral condyle and distributing them over the flatter tibial surface. In this study, when the meniscus was removed, the large knee joint loads, had to pass through the very incongruous surfaces of the condyle and tibia, which increased the contact stresses by approximately 350%. The study demonstrated how the reduction in contact areas, increased contact stresses resulted in a more rapid breakdown of the biphasic fluid load support. This resulted in an increase in direct solid-solid contact, causing an increase in the coefficient of friction. However, the meniscectomised bearing did display a superior tribological performance to the flat tibial hemiarthroplasty made from stainless steel (positive control), despite the fact

that the contact stresses for these two bearings were similar, particularly at the lower level of loading. This showed that by using a biphasic-vs-biphasic articulation, that the fluid load support is maintained for a longer period of time, than in a biphasic-vs-single-phasic articulation. Due to the more rapid decrease of biphasic fluid load support, the stainless steel hemiarthroplasty experienced increased solid-solid contact, which explained the higher frictional coefficients and friction shear stress for this bearing.

The investigation of the effect of the conformity of tibial hemiarthroplasty bearings was described in Chapter 4. The comparison of two different hemiarthroplasty materials was investigated by Luo Yong, the results of which are shown in Appendix II. It is widely accepted that in a natural healthy joint, the friction between the articulating surfaces is largely dependent on the solid phase interactions and the shearing between the surfaces, and whilst the fluid phase load support is maintained, the coefficient of friction remains very low. However, when a single phase material is introduced to the joint, a portion of the cartilage surface becomes constantly loaded against this biomaterial and rehydration of the tissue does not occur, resulting in diminished fluid load support and the onset of wear. The rise in the coefficient of friction due to diminished fluid phase load support has been widely reported for cartilage against metal articulations, using small scale pin on plate experiments (Forster and Fisher, 1996; Forster and Fisher, 1999; Kumar *et al.*, 2001; Basalo *et al.*, 2005; Krishnan *et al.*, 2005; Northwood *et al.*, 2007; Northwood and Fisher, 2007). However, this study aimed to reduce the solid-solid interactions by reducing the contact stress in the articulation, with the use of conforming bearings, which closely matched the conformity of the natural knee. This study has demonstrated that the use of more conforming bearings, resulted in reduced contact stress, friction and friction shear stress, particularly for the most conforming bearing which had a radius of curvature of 50 mm. The reduced stress and friction shear stress resulted in decreased levels of wear when measured with Talysurf profilometry (Ra value) and when quantified volumetrically from μMRI scans. Overall, this study demonstrated for the first time, the immediate decrease in contact stress, coefficient of friction and friction shear stress, upon increasing the conformity of the tibial hemiarthroplasty bearings. The increased contact area and decreased contact stress, provided by the conforming bearings, resulted in maintenance of the biphasic fluid load support for a longer duration. This limited the solid-solid interactions, which reduced the friction,

friction shear stress and the wear of the cartilage. The parallel study performed using polyurethane instead of stainless steel, showed that more compliant materials had a superior tribological performance and can increase the duration of biphasic fluid load support, reducing friction and wear.

The investigation of cartilage defect repair, in the medial compartmental knee joint was described in Chapter 5. This study investigated a stainless steel and hydrogels as potential osteochondral substitute materials. Osteochondral plugs (from the same condyle) and blank defects were also investigated. This study demonstrated elevated coefficients of friction, due to the disruption to the cartilage matrix, irrespective of the type of defect used. The cut through the cartilage surface, resulted in a rapid breakdown of the biphasic fluid load support, causing elevated friction. However, the healthy intact medial compartment (AC-vs-AC+meniscus) produced higher levels of fluid pressurisation, re-hydration and interstitial fluid load support compared to the models with defects. There was no significant differences between the frictional coefficients for any of the defect groups. This result demonstrated no connection with the wear (Ra values) measured. The stainless steel defect induced more surface abrasive wear on the opposing tibia, than any other group. The Ra values for the blank defect were also higher than for the hydrogel defect and osteochondral defect groups, due to edge loading effects. This interdependence between frictional coefficient and wear measurements was also demonstrated by Northwood, in a pin on plate experimental investigation of cartilage defect repair (Northwood, 2007). However, the friction shear stress in this study, was found to increase with increasing changes in geometry (to the condyle) and defect material. Although a limitation of this study was that the volumetric wear on the tibial surfaces could not be quantified, it was shown in Chapters 3 and 4, that friction shear stress correlated excellently with the volume of cartilage lost during tesing. Based on this finding, the results of this study indicated that only biphasic materials such as hydrogels should be considered as osteochondral substitute materials, bearing in mind that the mechanical strength of such materials is an important consideration.

In all three studies, the importance of the role of biphasic fluid load support in the outstanding lubrication properties of cartilage was demonstrated. Different tribological conditions caused a more rapid decrease of the interstitial fluid pressurisation and the biphasic fluid load support. Removal of the meniscus, the reduction of knee joint conformity (through meniscectomy or flat design

hemiarthroplasties), the introduction of a non-biphasic material or the disruption of the normal joint geometry, were the various factors which caused a more rapid decrease in fluid pressurisation, and biphasic fluid load support. This resulted in increased direct solid-solid contact and an increase in frictional coefficient, friction shear stress and the degeneration of cartilage.

It was evident throughout the three studies that although the coefficient of friction and contact stress gave a good indication of cartilage degradation, the complex biphasic tribology of cartilage made it difficult to accurately predict the effect of the changes in the tribological conditions, on the subsequent degradation and wear of cartilage. Many previous tribological studies of cartilage have demonstrated that a strong relationship between the coefficient of friction and wear of cartilage, is not found under all tribological test conditions (Forster and Fisher, 1996; Pickard *et al.*, 1998b; Katta *et al.*, 2007; Katta *et al.*, 2008c). While cartilage is designed to withstand large hydrostatic pressure, the nature of its biphasic composite structure provides only low resistance to shear stress, and it was demonstrated in the current study that the degradation and wear of cartilage was highly dependent on the friction shear stress. When the wear data from the studies examining the effects of meniscectomy, hemiarthroplasty conformity and hemiarthroplasty material was compared with the friction shear stress data, excellent agreement was found (R^2=0.8422), despite the various geometries, materials and levels of contact stress used. A plot of this relationship is shown in Figure 6-1. However, when the frictional coefficient and wear data were compared from these three studies, there was a very poor correlation (R^2=0.226) found. The choice of material appeared to have an impact. For example, at similar levels of coefficient of friction (0.07-0.08), the wear found on the condyles articulating with the SSFP (45 mm^3) and the AC+meniscus (0 mm^3) were very different. At the higher end of the coefficient of friction spectrum (COF > 0.12), severe wear was found on the condyles articulating with the SSCP100 (98 mm^3) and SSFP (193 mm^3) but no wear was found on those articulating with the natural PU and yellow PU.

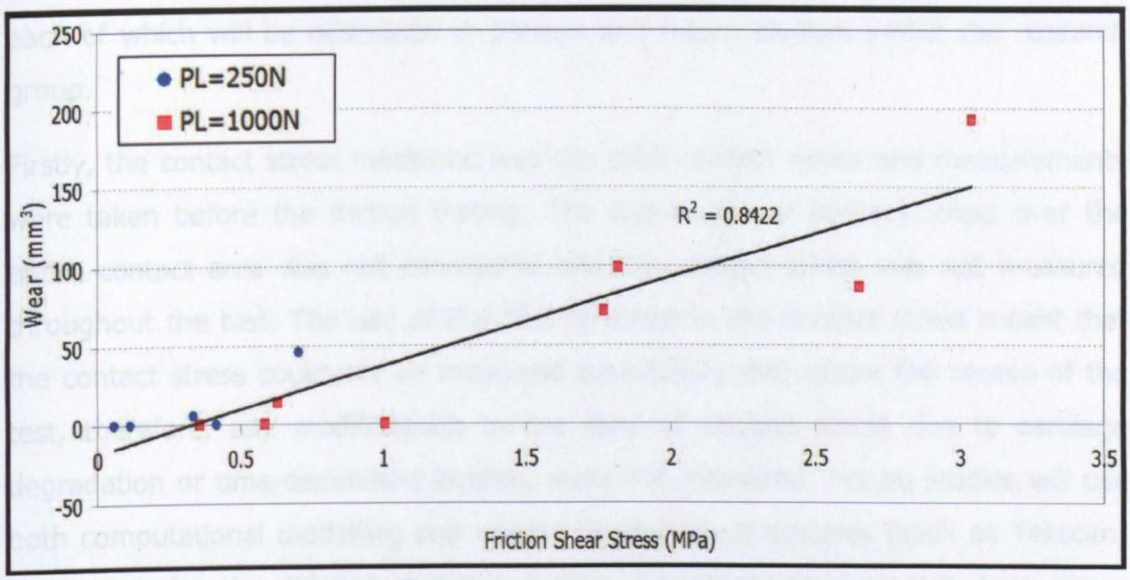

Figure 6-1: Excellent correlation was found between wear and friction shear stress when the data from three studies was combined: the meniscectomy study, the hemiarthroplasty conformity study and the hemiarthroplasty material study. Results presented are mean values (n=3 for hydrogels and n=6 for all other groups).

The author is not aware of any previous cartilage tribological studies, in which the dependency of cartilage wear on the friction shear stress has been reported. The current studies have demonstrated for the first time an exceptional correlation between friction shear stress and the wear and degradation of cartilage under the current tribological conditions, even though a range of geometries, materials and levels of contact stress were applied. It is recommended that friction shear stress should be an important consideration in future studies examining the friction, wear and lubrication of cartilage-cartilage and cartilage-biomaterial articulations.

The work described in this thesis provides new insights into cartilage tribology and the scope for future investigations using the medial compartmental knee joint simulation is vast. This experimental model can be used to investigate any potential knee joint intervention such as meniscus substitutions, therapeutic lubricants, new implant designs such as unicompartmental arthroplasties, hemiarthroplasties, osteochondral/chondral implants and tissue engineered substitutes. One current study is examining the effect of different types of meniscal tear on the tribological response of the medial compartment. There were a few limitations associated with these *in vitro* studies in their current form relating to the experimental methods,

each of which will be addressed in present and future studies, within the research group.

Firstly, the contact stress measured was the peak contact stress and measurements were taken before the friction testing. The distribution of contact stress over the entire contact area was not considered and the contact stress was not measured throughout the test. The use of Fuji film to measure the contact stress meant that the contact stress could not be measured periodically throughout the course of the test, therefore, any modifications to the level of contact stress due to cartilage degradation or time-dependent loading, were not measured. Future studies will use both computational modelling and on-line measurement systems (such as Tekscan) to characterise the detailed spatial and time-dependent pressure and shear stress distribution.

The piezoelectric transducer mechanism used to measure the coefficient of friction, measured the global friction between the contacting surfaces. It is likely that there were localised regions of higher friction in some cases, particularly for the cartilage defect repair bearings.

In the current study, the limited flexion-extension motion of 25°, resulting in a shorter stroke length, may have limited the rehydration of the cartilage tissue, in comparison to that which occurs *in vivo*, causing a higher frictional coefficient. Previous studies have shown how a shorter stroke length results in decreased fluid load support and increased friction (Bell *et al.*, 2006; Caligaris and Ateshian, 2008). A further limitation was the use of a single compartment and a truncated femoral condyle. A shift in the loading distribution between the two condyles due to meniscectomy or unicompartmental hemiarthroplasty, was not considered in the current study. Clinically, the un-operated compartment has been shown to take a larger proportion of the total joint load following meniscectomy (Ihn *et al.*, 1993). However, as the loading was not reduced for the meniscectomised compartment in the current study, the author feels that the worst case scenario was investigated. Future simulations will be advanced to include full gait, multi-axis kinematics and motions and whole natural joints, which were not included in this study due to limitations of the current pendulum friction simulator. Such simulations will allow the investigation of changes in the loading and pressure (using Tekscan) distributions, as well as the exploration of more complicated therapeutic interventions, such as uni-

and bi-compartmental meniscectomy and uni- and bi-compartmental hemiarthroplasty.

Three forms of damage have been identified in this study: surface fibrillation; permanent deformation associated with loss of matrix material and water; and permanent displacement of matrix material. We have not to date been able to quantify the contributions to permanent deformation, but it is recommended that analysis of matrix elements in the lubricant be carried out in the future.

Methodologies are under development to quantify the volumetric wear of cartilage on the tibia and the meniscus, using μMRI scans. The imaging probe of the scanner was 30 mm in diameter, meaning the tibia and meniscus were too large. Trimming them to size would have required clamping the contact region, inducing deformation. This was avoidable with the femoral condyle as the cemented portion was easily clamped. Secondly, a more complex program would be required to re-fit the original surface of the incongruous tibia. It may be useful in future investigations to use a porcine knee joint. In this case, the femur, tibia and meniscus could be scanned pre- and post-friction testing and subtraction techniques could be used to calculate the wear volumes.

Notwithstanding the aforementioned limitations, significant advances were made in the research field of cartilage and synovial joint tribology, with the use of an anatomically and physiologically relevant *in vitro* simulation. The use of this advanced simulation including the challenging geometries and loading and motions of the natural knee, has provided new information and exciting prospects for the future work in the field. The most important conclusions of this thesis are listed below.

6.1 Conclusions

A novel tribological simulation of the natural medial compartmental knee was developed and used to investigate the tribological response of different cartilage substitution/replacement therapies. With increasing changes in the tribological conditions from those of the natural joint, this unique simulation demonstrated successfully the depletion of interstitial fluid pressurisation and fluid load support, causing an increase in contact stress, friction shear stress and cartilage degradation. A novel method was developed to quantify cartilage wear, volumetrically, with the

use of high resolution μMRI scans. This proved to be a very useful technique and the scope for future analysis of cartilage with μMRI is immense.

The effect of removing the meniscus was shown to cause a more rapid decrease in the fluid load support, than the conforming intact joint. This resulted in higher levels of frictional coefficient, contact stress, friction shear stress, and cartilage degradation. The smaller contact areas as a result of the incongruous articulation of the femur and tibia, meant that the fluid load support was depleted at a faster rate, the degree of solid-solid contact was increased, which caused elevated friction. This study showed for the first time in an *in vitro* system, the importance of the meniscus, in terms of joint congruency and stabilisation and load bearing and distribution. However, the meniscectomised bearing, although non-conforming, had a superior tribological response to the flat stainless steel plate, which indicates that the nature of the biphasic materials, meant that fluid load support was maintained for longer. Overall, this study supports retaining the meniscus whenever possible.

Conforming hemiarthroplasty bearings should always be considered over flat or non conforming designs. It was demonstrated that decreasing the conformity of the hemi design, resulted in elevation of the coefficient of friction, contact stress and friction shear stress with a resulting increase in cartilage wear. Considering the parallel study using polyurethane, although only flat designs were used, the more compliant material displayed a superior tribological performance to stainless steel. This study supports the use of hemiarthroplasty, for young and active patients, with the use of conforming designs with a compliant material such as medical grade polyurethane.

Cartilage defect repair, using biphasic materials, was shown to be a potential treatment option for young and active patients. It is advantageous over current clinical treatments as it involves just a single operation, the defect site can be completely filled in and the defect is synthetic meaning there are no donor site morbidity complications. However, material choice is an important consideration. Biphasic materials should be considered, provided that they possess sufficient stiffness and are not very deformable relative to the surrounding cartilage. However, single phase biomaterials such as stainless steel, are not recommended for cartilage defect repair, based on the results of this study.

An important finding of the current study was that the wear and degradation of cartilage was highly dependent on friction shear stress, the product of coefficient of

friction and contact stress. A strong relationship was found between wear and friction shear stress, irrespective of the various materials, geometries and levels of stress used. It is recommended that this new and unique relationship is considered in all future tribological studies of cartilage. Finally, this project has provided further insight into the complex tribological regime associated with articular cartilage and synovial joints.

Appendix I

Lubrication film thickness prediction

The fluid film thickness was predicted for the worst case scenario – the femoral condyle articulating on a flat stainless steel plate, based on a study by Jin *et al.,* in which the transient lubrication in knee prosthesis with compliant layers, was considered (Jin *et al.*, 1998). Fluid film predictions including the meniscus would be very complex and have not been reported before.

A simple ellipsoid on a plane configuration was used to represent the medial compartmental hemiarthroplasty. It is convenient and acceptable to represent certain synovial joints, like the ankle (Medley *et al.*, 1984; Dowson and Jin, 1986) and the knee, with a cylinder or ellipsoid in articulation with a plane, configuration. A schematic representation of the model is shown in Figure I-i. For fluid film prediction in the current study, using this model, the cartilage is modelled as the compliant layer (Figure I-i) attached to the rigid substrate (bone) underneath. The ellipsoid (steel) is modelled as a rigid body. This assumption of modelling the cartilage layer on a rigid bone substrate (rather than on the rigid ellipsoid (bone)) is valid as the contacting geometries and material properties are maintained.

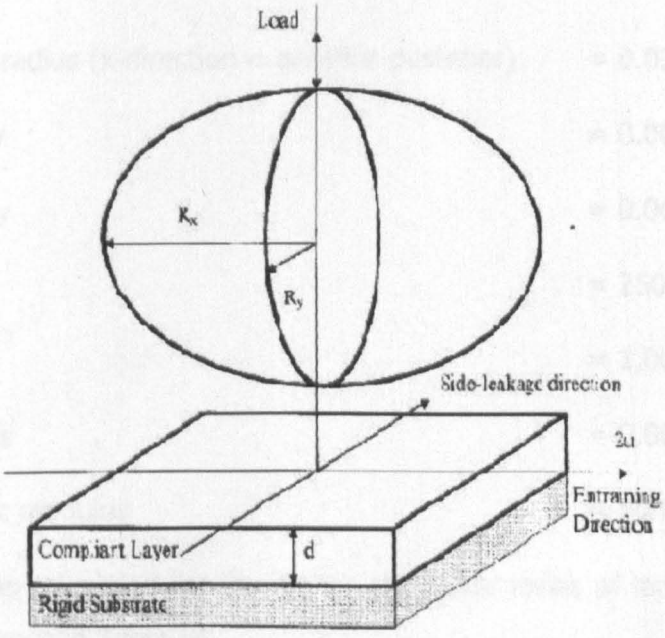

Figure I-i: A schematic ellipsoid-on-plane model for transient lubrication analysis in knee prosthesis with compliant layers. Image taken from (Jin *et al.*, 1998). The

articular cartilage is the compliant layer and the bone and stainless steel are modelled as rigid bodies.

The compliant (cartilage) layer was assumed to have a uniform thickness and to be linear elastic and with a Poisson's ratio of 0.4. The lubricant was assumed to be Newtonian, isoviscous and incompressible. The two levels of loading (250 N and 1,000 N) from the laboratory experiments were examined separately. Due to the dynamic nature of the loading cycle a combined elastic modulus of 50 MPa was reasonable. Under the current dynamic conditions, interstitial fluid pressurisation results in a greater stiffness than under a static conditions. Additionally, in previous studies, a range of values for Young's modulus have been determined. Higginson and Snaith tested their specimens in confined oscillating compression and found the value of Young's modulus to range between 50 - 150 MPa (Higginson and Snaith, 1979). However, Johnson *et al.* estimated the value of Young's modulus to range between 10 - 20 MPa, when testing specimens in unconfined compression (Johnson *et al.*, 1977). Thus a representative elastic modulus of 50 MPa was chosen for the current analysis.

The formula for minimum film thickness (h), for a layered surface, used was:

$$h = (1.25)R_x\left(\eta u / E_{eq}R_x\right)^{0.52}\left(W / E_{eq}R_x^{\,2}\right)^{-0.16}\left(d / R_x\right)^{0.37}$$

where,

R_x = femoral condyle radius (x-direction = anterior-posterior) = 0.038 m

η = lubricant viscosity = 0.001 Pa s

u = entraining velocity = 0.0076 m s^{-1}

W = Load (low) = 250 N

(high) = 1,000 N

d = cartilage thickness = 0.0014 m

E_{eq} = combined elastic modulus = 50 MPa

The film thickness was calculated for the higher and lower levels of loading used in and the results are shown in Table I-i.

Load (N)	250	1,000
Film thickness, h (μm)	0.27	0.22

Table I-i: Results of the film thickness prediction for the two levels of applied load.

The combined surface roughness (Ra) for the cartilage condyle and stainless steel plate was 0.96 μm, which is greater than the maximum fluid film thickness value calculated, therefore, it was reasonable to assume that all the friction studies presented, acted within a mixed or boundary lubrication regime. However, it is also important to consider the effect of micro-elastohydrodynamic smoothening (Dowson and Jin, 1986). Localised contact pressures have the ability to "smooth" the relatively rough cartilage surface, as they pass through the loaded region. The deformation of the surfaces reduces the film pressure and thus increases the fluid entrainment and film thickness. Although, smoothening may enhance the fluid film regime, the stroke length used in the current simulation was only 7.8 mm and therefore, would not allow complete replenishment of the fluid film during each cycle. Therefore, it is reasonable to say that biphasic and mixed lubrication regimes, were the dominant lubrication regimes in the current study.

Appendix II

Effect of Material of Tibial Hemiarthroplasty Materials

The effect of using three grades of polyurethane as a tibial hemiarthroplasty bearings was investigated in a parallel study, conducted by Luo Yong, a visiting PhD student from the Institute of Tribology and Reliability Engineering in the China University of Mining and Technology. Three different types of polyurethane with different modulii were chosen to articulate against articular cartilage. The red polyurethane was the hardest and the yellow and natural polyurethanes were softer. The shore hardness for each is shown in Table I-I and a photograph of the three of the plates used is shown in Figure I-i. For each combination, 6 samples were used

Materials	Shore hardness
PU Natural	A60-65
PU Yellow	A90-95
PU Red	D55-60

Table II-i: The shore hardness of the three polyurethane plates used in the study.

Figure II-i: Three polyurethane plates used in the study – red, natural and yellow.

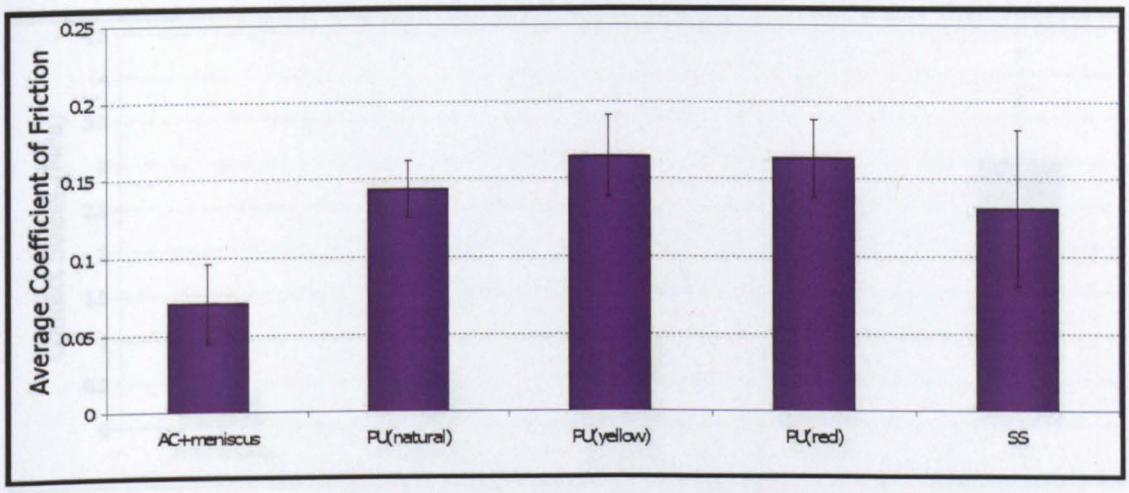

Figure II-ii: Average coefficient of friction for the negative control (AC-vs-AC+meniscus), the three polyurethane plates (natural, red and yellow) and the positive control (AC-vs-SSFP). Results presented as mean ± 95% confidence intervals.

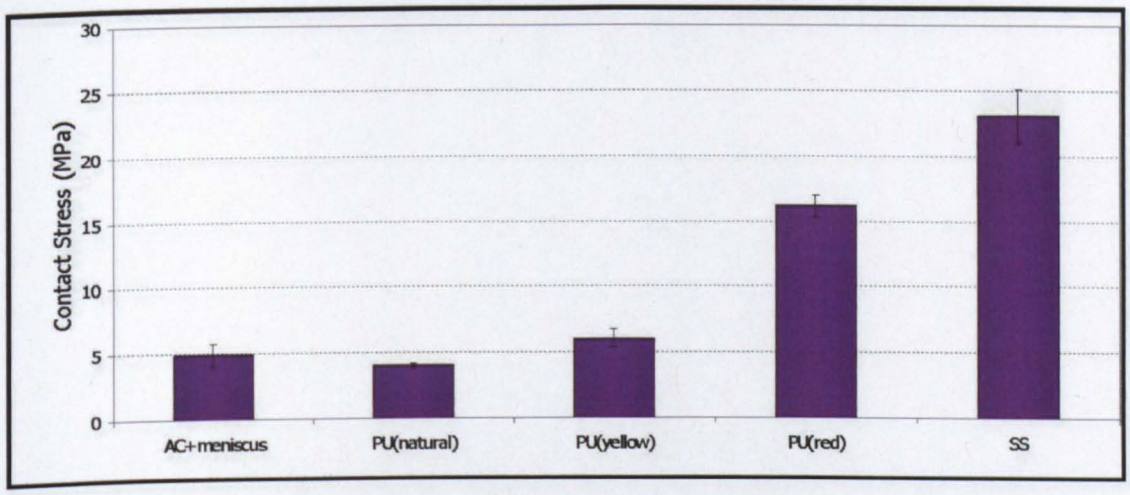

Figure II-iii: Average peak contact stress for the negative control (AC-vs-AC+meniscus), the three polyurethane plates (natural, red and yellow) and the positive control (AC-vs-SSFP). Results presented as mean ± 95% confidence intervals.

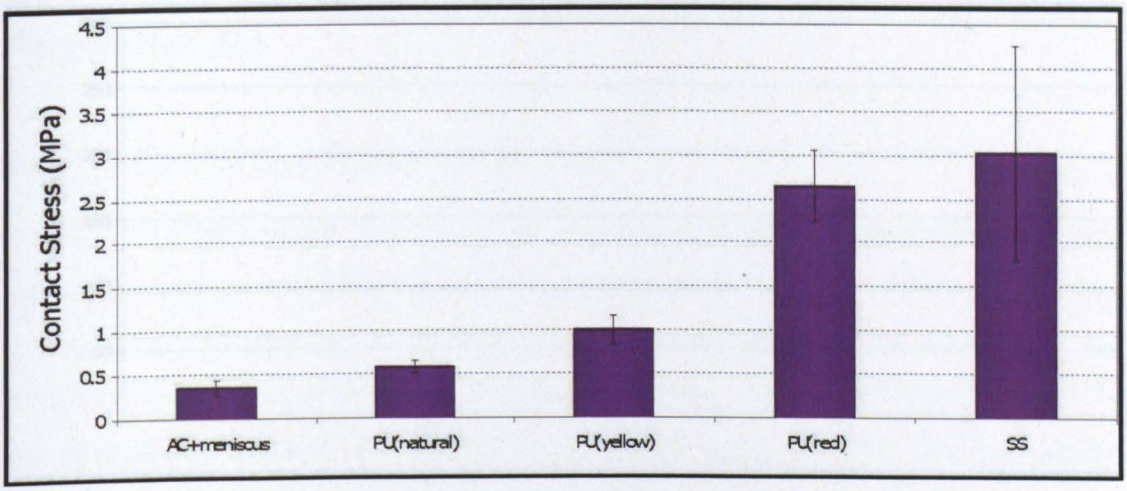

Figure II-iv: Average friction shear stress for the negative control (AC-vs-AC+meniscus), the three polyurethane plates (natural, red and yellow) and the positive control (AC-vs-SSFP). Results presented as mean ± 95% confidence intervals.

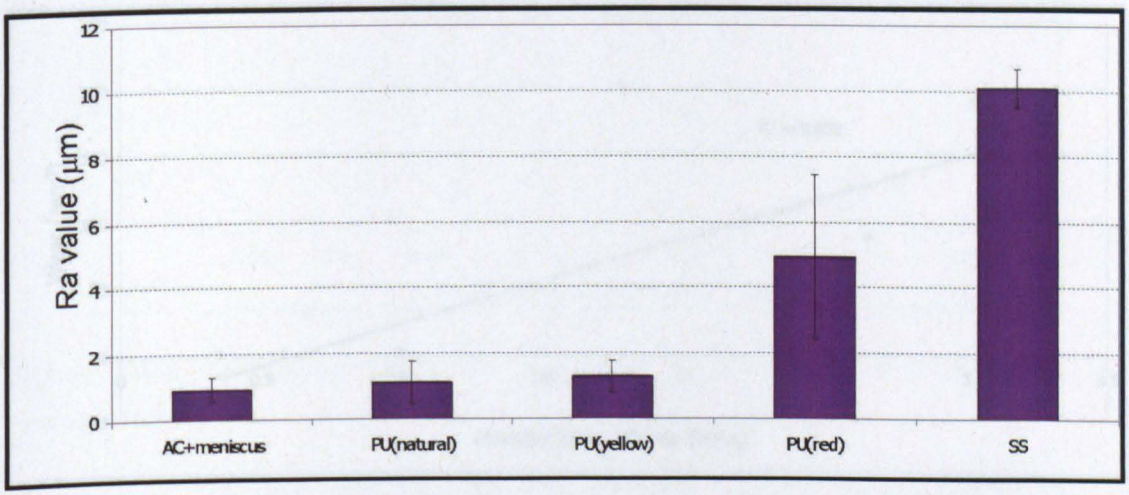

Figure II-v: Average Ra value for the femoral condyles from the negative control (AC-vs-AC+meniscus), the three polyurethane plates (natural, red and yellow) and the positive control (AC-vs-SSFP). Results presented as mean ± 95% confidence intervals.

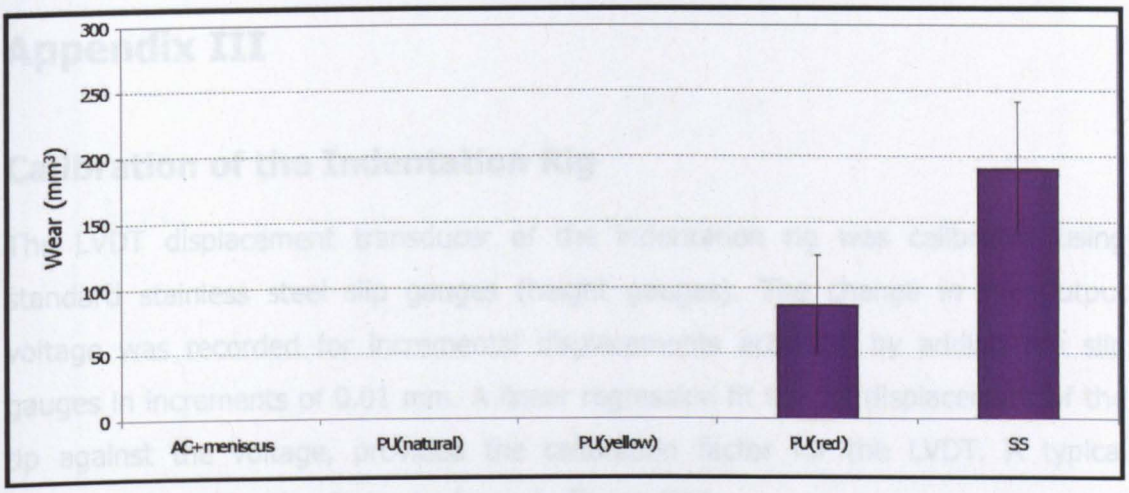

Figure II-vi: Average wear measured from the μMRI scans of the femoral condyles from the negative control (AC-vs-AC+meniscus), the three polyurethane plates (natural, red and yellow) and the positive control (AC-vs-SSFP). Results presented as mean ± 95% confidence intervals.

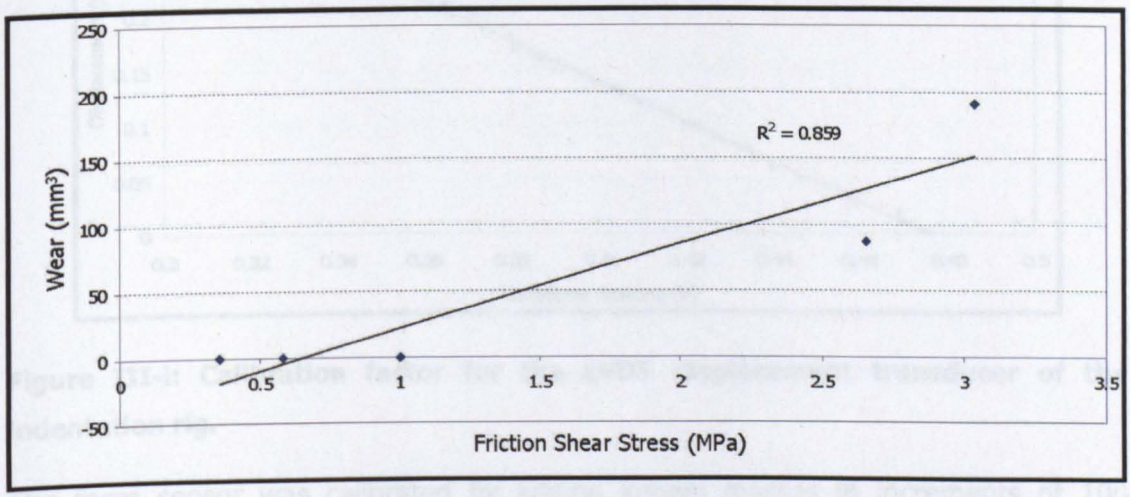

Figure II-vii: A good correlation (R^2 = 0.859) was found between the volumetric wear and the friction shear stress.

Appendix III

Calibration of the Indentation Rig

The LVDT displacement transducer of the indentation rig was calibrated using standard stainless steel slip gauges (height gauges). The change in the output voltage was recorded for incremental displacements achieved by adding the slip gauges in increments of 0.01 mm. A linear regression fit for the displacement of the tip against the voltage, provided the calibration factor for the LVDT. A typical example of a calibration factor is shown in Figure III-i.

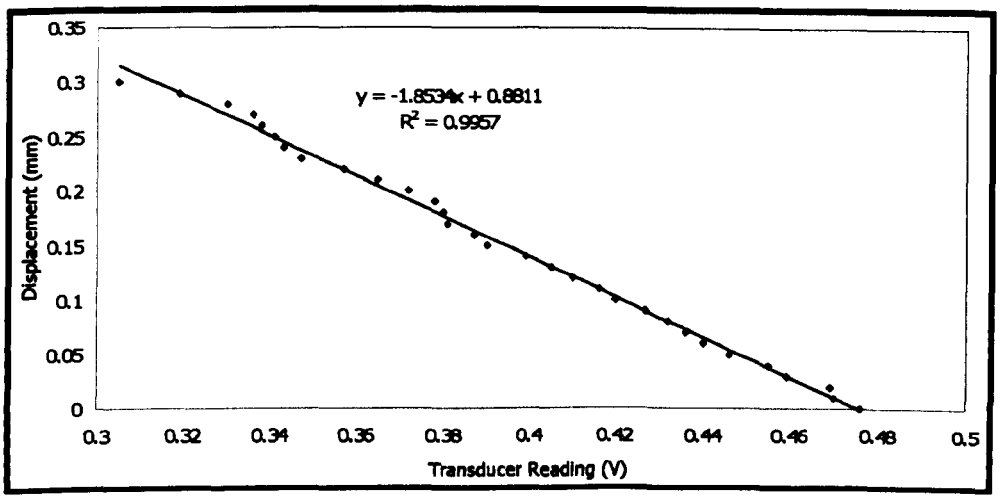

Figure III-i: Calibration factor for the LVDT displacement transducer of the indentation rig.

The force sensor was calibrated by adding known masses in increments of 100 grams and recording the changes in the voltage reading from the force sensor. A linear regression fit between the contact stress applied and the output voltage provided the calibration factor for the force sensor. A typical example of a force sensor calibration is shown in Figure III-ii.

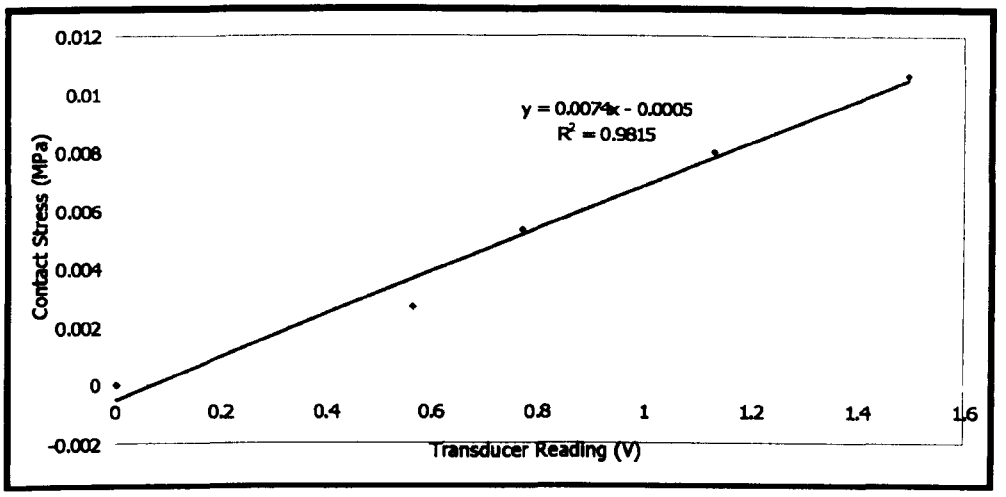

Figure III-ii: Calibration factor for the force sensor of the indentation rig.

Appendix IV

Finite element mesh sensitivity analysis

A coarse mesh with 2,452 elements was used initially (Figure IV (a)). The mesh was subsequently reduced to 602 elements (b), 402 elements (c) and 202 elements (d). There was less than 2% error between the maximum Von Mises stress (red regions) for the meshes used in (a), (b) and (c). However, when the mesh was decreased to 202 elements the error increased to almost 8% and the edge of the indentor impinged on the hydrogel due to an insufficient mesh. Therefore, mesh (c) was used in the indentation computational analysis. A close-up screen shot of the indentor impinging on the hydrogel is shown in Figure IV-iii.

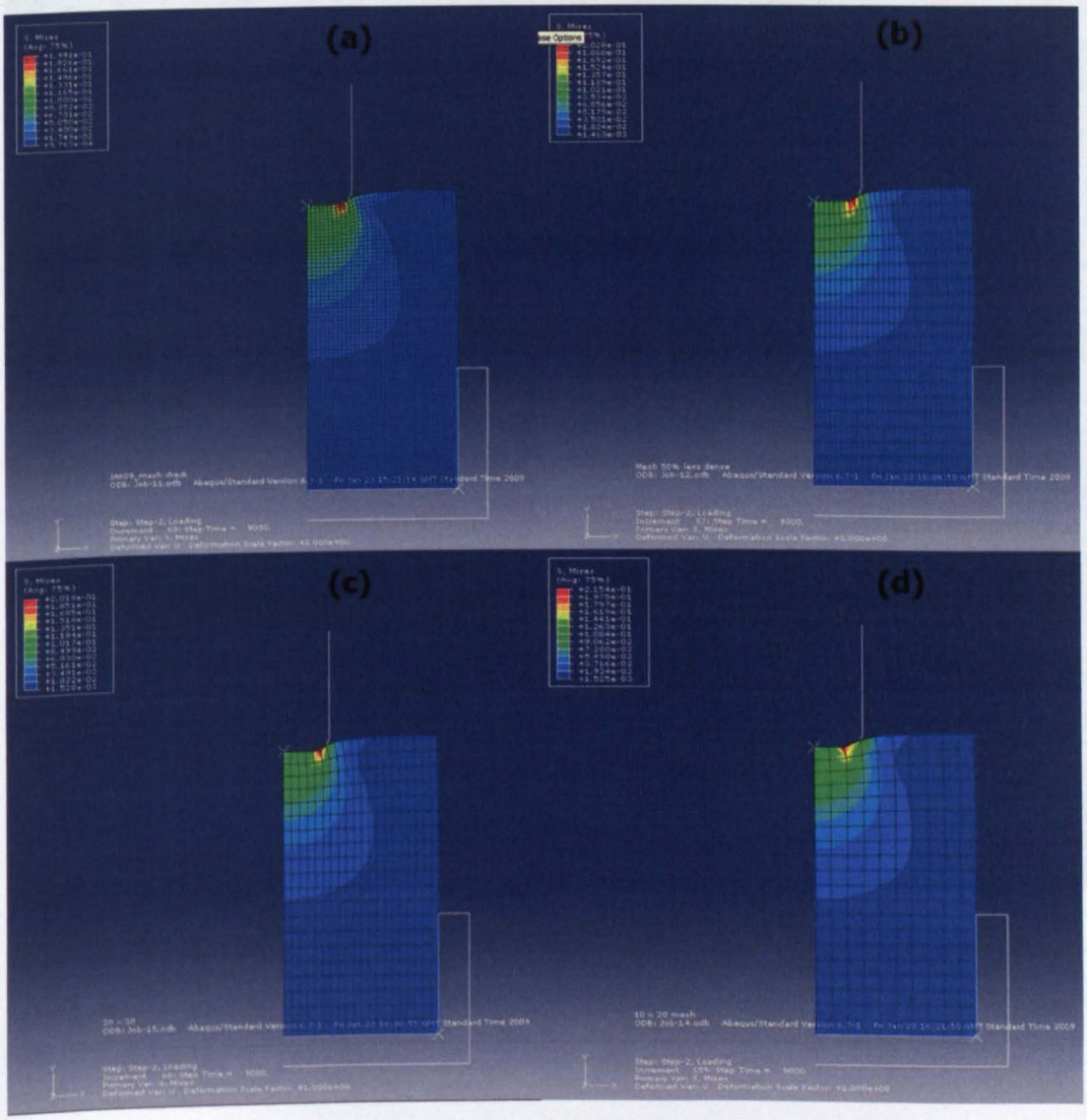

Figure IV-i: Maximum Von Mises stress (MPa) - mesh sensitivity analysis .

The maximum vertical displacement was examined in the mesh sensitivity analysis (Figure IV-ii), which was in agreement with the stress analysis. In this case, the blue colour indicates areas of maximum displacement, as the displacement was in the negative direction. There was less than 1% error between the maximum displacement when meshes (a), (b) and (c) were used. However, the error increased to ~4% when the mesh was reduced to 202 elements in (d), for which the indentor impinged on the hydrogel.

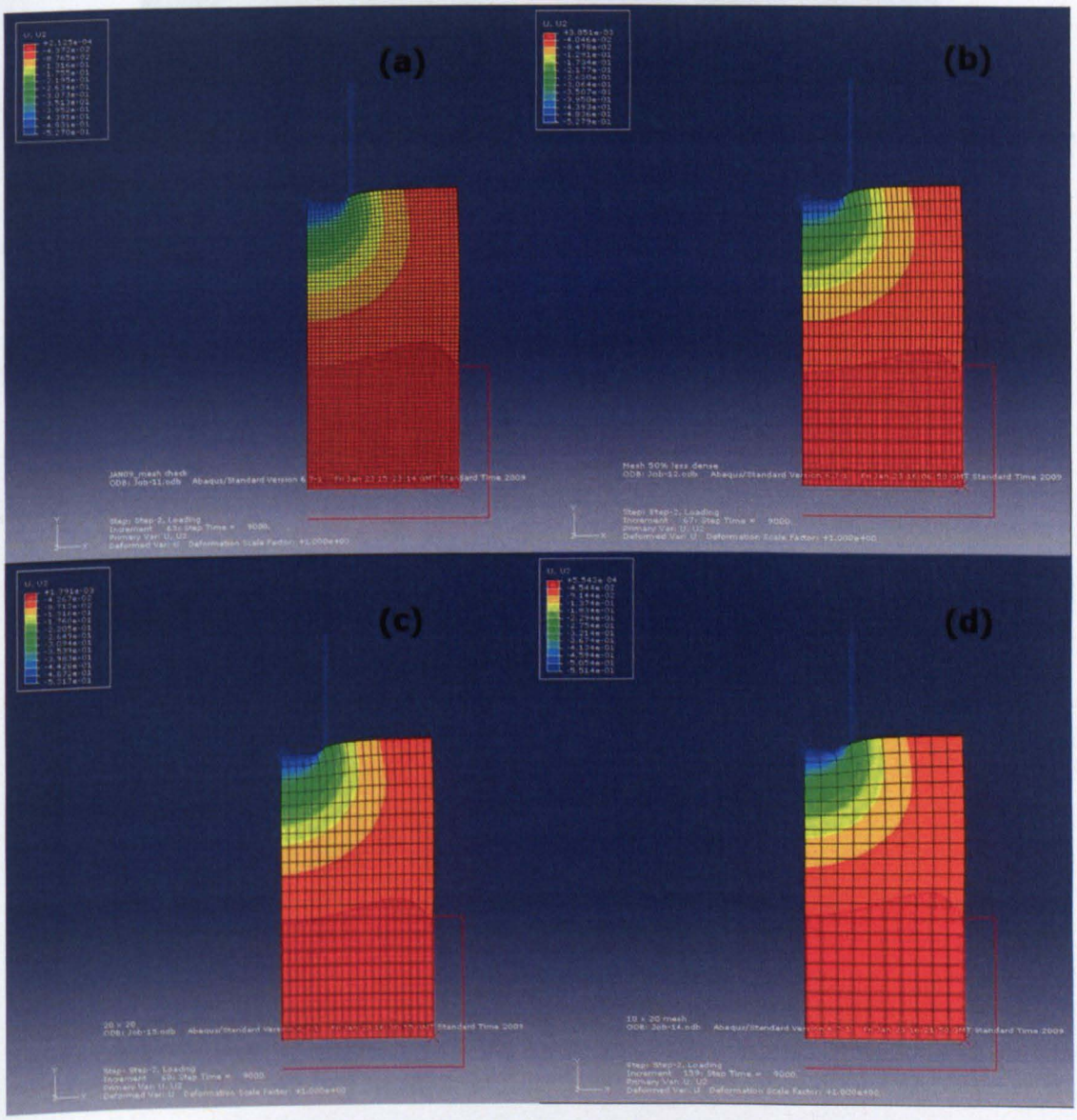

Figure IV-ii: Maximum vertical displacement (mm) - mesh sensitivity analysis .

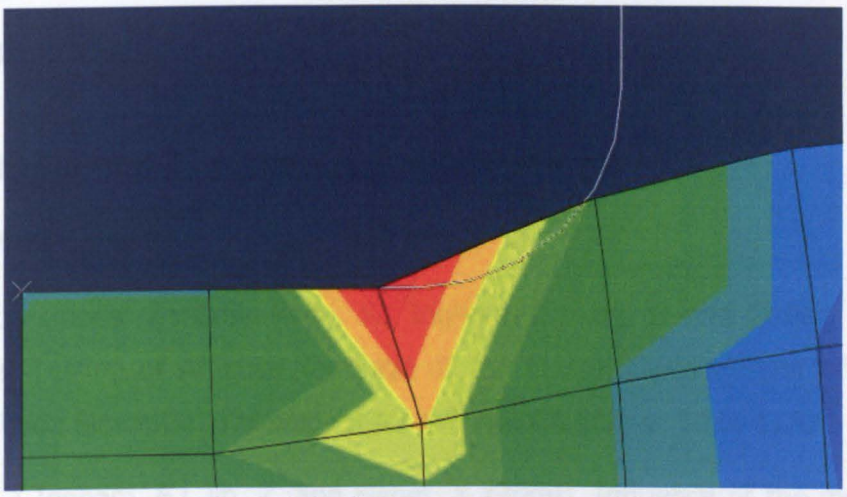

Figure IV-iii: A screen shot from Abaqus CAE showing where the indentor impinged on the hydrogel due to an insufficient mesh.

Appendix V

Publications and Conference Presentations

Journal Publications

McCann, L.; Udofia, I.; Graindorge, S.; Ingham, E.; Jin, Z. and Fisher, J. (2008). Tribological Testing of Articular Cartilage of the Medial Compartment of the Knee using a Friction Simulator. *Tribology International.* **41** (11) p: 1126-1133.

McCann, L.; Ingham, E.; Jin, Z. and Fisher, J. (2009). Influence of the meniscus on friction and degradation of cartilage in the natural knee joint. *Osteoarthritis and Cartilage.* Accepted and In Press

McCann L.; Ingham, E.; Jin, Z. and Fisher, J. (2009). An Investigation of Knee Hemiarthroplasty Designs on Contact Stress, Friction and Degradation of Articular Cartilage: A Tribological Study. *Journal of Biomechanics.* In Press.

Journal Publications to be submitted

Yong, L.; McCann, L.; Ingham, E.; Zhongmin J.; Shirong G. and Fisher, J. (2009). A medial compartmental knee, in vitro tribological simulation, of the effects of using polyurethane as a potential hemiarthroplasty material.

McCann, L.; Ingham, E.; Zhongmin, J.; Fisher, J. (2009). A novel *in vitro* simulation of cartilage defect repair in the medial compartmental knee, using synthetic biomaterials.

Conference Oral Presentations

34th Leeds-Lyon Symposium on Tribology (2007), Lyon, France;

International Cartilage Repair Society (2007), Warsaw, Poland;

World Congress of Biomaterials (2008), Amsterdam, The Netherlands;

British Orthopaedic Research Society (2008), Manchester, UK;

European Society of Biomechanics (2008), Lucerne.

Conference Poster Presentations

British Orthopaedic Research Society (2007), Dundee, UK;

Orthopaedic Research Society (2008), San Francisco, USA; and

The 2nd Annual Workshop on Imaging Based Measures of Osteoarthritis (2008), Boston, USA.

Orthopaedic Research Society (2009), Las Vegas, USA.

International Cartilage Repair Society (2009), Miami, USA.

References

Abdel-Hamid, M., Hussein, M. R., Ahmad, A. F. & Elgezawi, E. M., (2005). Enhancement of the repair of meniscal wounds in the red-white zone (middle third) by the injection of bone marrow cells in canine animal model. *International Journal of Experimental Pathology,* 86, 117-123.

Adams, C. S. & Horton, W. E., (1998). Chondrocyte apoptosis increases with age in the articular cartilage of adult animals. *Anat. Rec.,* 250, 418-425.

Agrawal, V. & Stinson, M., (2007). Arthroscopic grafting of greater tuberosity cyst and rotator cuff repair. *Arthroscopy - The Journal of Arthroscopic and Related Surgery,* 23.

Ahmed, A. M. & Burke, D. L., (1983). In vitro measurement of static pressure distribution in synovial joints, part I: Tibial surface of the knee. *J Biomech. Eng.,* 105, 216.

Amstutz, H. C., Grigoris, P., Safran, M. R., Grecula, M. J., Campbell, P. A. & Schmalzried, T. P., (1994). Precision-fit surface hemiarthroplasty for femoral head osteonecrosis. Long-term results. *J Bone Joint Surg Br,* 76, 423-427.

Anseth, K. S., Bowman, C. N. & Brannonpeppas, L., (1996). Mechanical properties of hydrogels and their experimental determination. *Biomaterials,* 17, 1647-1657.

Armstrong, C. G. & Mow, V. C., (1982). Variations in the intrinsic mechanical properties of human articular cartilage with age, degeneration, and water content. *J Bone Joint Surg Am,* 64, 88-94.

Arnoczky, S. P., (1990). Structure and Biology of Knee Meniscus. In: MOW, V. C., RATCLIFFE, A. & WOO, S. L.-Y. (Eds.) *Biomechanics of Diarthrodial Joints.* New York, Springer-Verlag.

Ateshian, G. A. & Mow, V. C., (2005). Friction, Lubrication and Wear of Articular Cartilage and Diarthrodial Joints. In: MOW, V. C. & HUISKES, R. (Eds.) *Basic Orthopaedic Biomechanics and Mechano-Biology.* Philadephia, Lippincott Williams and Wilkins.

Ateshian, G. A., Soltz, M. A., Mauck, R. L., Basalo, I. M., Hung, C. T. & Lai, W. M., (2003). The Role of Osmotic Pressure and Tension-Compression Nonlinearity in the Frictional Response of Articular Cartilage. *Transport in Porous Media,* 50, 5-33.

Bailie, A. G., Lewis, P. L., Brumby, S. A., Roy, S., Paterson, R. S. & Campbell, D. G., (2008). The unispacer knee implant - Early clinical results. *J Bone Joint Surg Br,* 90B, 446-450.

Baratz, M. E., Fu, F. H. & Mengato, R., (1986). Meniscal Tears - the Effect of Meniscectomy and of Repair on Intraarticular Contact Areas and Stress in the Human Knee - a Preliminary-Report. *American Journal of Sports Medicine,* 14, 270-275.

Basalo, I. M., Raj, D., Krishnan, R., Chen, F. H., Hung, C. T. & Ateshian, G. A., (2005). Effects of enzynamatic degradation on the frictional response of articular cartilage in stress relaxation. *J. Biomech,* 38, 1343-1349.

Bashir, A., Gray, M. L., Hartke, J. & Burstein, D., (1999). Nondestructive imaging of human cartilage glycosaminoglycan concentration by MRI. *Magnetic Resonance in Medicine,* 41, 857-865.

Bell, C. J., Ingham, E. & Fisher, J., (2006). Influence of hyaluronic acid on the time-dependent friction response of articular cartilage under different conditions. *J Eng Med,* 220, 23-31.

Benedek, T. G., (2006). A history of the understanding of cartilage. *Osteoarthritis and Cartilage,* 14, 203-209.

Bentley, G., Biant, L. C., Carrington, R. W. J., Akmal, M., Goldberg, A., Williams, A. M., Skinner, J. A. & Pringle, J., (2003). A prospective, randomised comparison of autologous chondrocyte implantation versus mosaicplasty for osteochondral defects in the knee. *J Bone Joint Surg Br,* 85B, 223-230.

Bergmann, G., Graichen, F. & Rohlmann, A., (1993). Hip-Joint Loading during Walking and Running, Measured in 2 Patients. *J Biomech,* 26, 969-990.

Beris, E. A., Lykissas, M. G., Papageorgiou, C. D. & Georgoulis, A. D., (2005). Advances in articular cartilage repair. *International Journal of Injury,* 365, 514-523.

Broom, N. D. & Silyn-Roberts, H., (1990). Collagen-collagen versus collagen-proteoglycan interactions in the determination of cartilage strength. *Arthritis Rheum.,* 33, 1512-1517.

Bruns, J., Kahrs, J., Kampen, J., Behrens, P. & Plitz, W., (1998). Autologous perichondral tissue for meniscal replacement. *J Bone Joint Surg Br,* 80B, 918-923.

Buckwalter, J. A., (1996). Evidence for overuse/overloading of joints in the genesis and progression of osteoarthritis. *Current Orthopaedics,* 10, 220-224.

Buckwalter, J. A., (1998). Articular cartilage: injuries and potential for healing. *J Orthop Sports Phys Ther,* 28, 192-202.

Buckwalter, J. A., (2002). Articular cartilage injuries. *Clinical Orthopaedics and Related Research,* 21-37.

Buckwalter, J. A., Martin, J. & Mankin, H., (2000). Synovial joint degeneration and the syndrome of osteoarthritis. *Instr Course Lect,* 49, 481-489.

Buckwalter, J. A. & Mow, V. C., (1992). Cartilage repair in osteoarthritis. *Osteoarthritis: Diagnosis and Management.* Philadelphia, Saunders.

Burke, D. L., Ahmed, A. H. & Miller, J., (1978). A Biomechanical study of partial and total medial meniscectomy. *Arthroscopy,* 13, 673.

Burstein, D. & Gray, M., (2003). New MRI techniques for imaging cartilage. *J Bone Joint Surg Am,* 85-A Suppl 2, 70-77.

Caligaris, M. & Ateshian, G. A., (2008). Effects of sustained interstitial fluid pressurization under migrating contact area, and boundary lubrication by synovial fluid, on cartilage friction. *Osteoarthritis and Cartilage,* 16, 1220-1227.

Carrington, J. L., (2004). Aging bone and cartilage: cross cutting tissues. *Biochemical and Biophysical Research Communications,* 328, 700-708.

Carter, M. J., Basalo, I. M. & Ateshian, G. A., (2007). The temporal response of the friction coefficient of articular cartilage depends on the contact area. *J Biomech,* 40, 3257-3260.

Chang, Y. S., Gu, H. O., Kobayashi, M. & Oka, M., (1998a). Comparison of bony ingrowth into an osteochondral defect and an artificial osteochondral composite device in load-bearing joints. *The Knee,* 5, 205-213.

Chang, Y. S., Gu, H. O., Kobayashi, M. & Oka, M., (1998b). Influence of various structure treatments on histological fixation of titanium implants. *J. Arthroplasty,* 13, 816-825.

Chang, Y. S., Oka, M., Gu, H. O., Kobayashi, M. & Toguchida, J., (1997). Histologic comparison of tibial articular surfaces against rigid materials and artificial articular cartilage. *J Biomed Material Res,* 37, 51-59.

Clar, C., Cummins, E., Mcintyre, L., Thomas, S., Lamb, J., Bain, L., Jobanputra, P. & Waugh, N., (2005). Clinical and cost-effectiveness of autologous chondrocyte implantation for cartilage defects in knee joints: systematic review and economic evaluation. *Health Technol Assess,* 9, iii-iv, ix-x, 1-82.

Cole, B. J., Carter, T. R. & Rodeo, S. A., (2002). Allograft meniscal transplantation - Background, techniques, and results. *J Bone Joint Surg Am,* 84A, 1236-1250.

Conaghan, P., (2006). Is MRI useful in osteoarthritis? *Best Practice & Research in Clinical Rheumatology,* 20, 57-68.

Corkhill, P. H., Trevett, A. S. & Tighe, B. J., (1990). The potential of hydrogels as synthetic articular cartilage. *Proc Inst Mech Eng [H],* 204, 147-155.

Custers, R. J., Dhert, W. J., Van Rijen, M. H., Verbout, A. J., Creemers, L. B. & Saris, D. B., (2007a). Articular damage caused by metal plugs in a rabbit model for treatment of localized cartilage defects. *Osteoarthritis and Cartilage,* 15, 937-945.

Custers, R. J. H., Dhert, W. J. A., Rijen, V. M. H. P. & Saris, D. B. F. (2007b) Treating localized cartilage defects wtih small metal plugs: an analysis biocompatibility and osseointegration. *53rd Annual Meeting of the Orthopaedic Research Society.*

D'arcy, J. & Devas, M., (1976). Treatment of fractures of the femoral neck by replacement with the Thompson prosthesis. *J Bone Joint Surg Br,* 58, 279-286.

Distefano, V. J., (1980). Function, post-traumatic sequelae and current concepts of management of knee meniscus injuries: a review article. *Clin Orthop,* 143.

Dorotka, R., Windberger, U., Macfelda, K., Bindreiter, U., Toma, C. & Nehrer, S., (2004). Repair of articular cartilage defects treated by microfracture and a three-dimensional collagen matrix. *Biomaterials,* 26, 3617-3629.

Dowson, D. & Jin, Z., (1986). Micro-elastohydrodynamic lubrication of synovial joints. *Eng Med.,* 15, 63-65.

Dowson, D. & Wright, V., (1981). Introduction to the Biomechanics of Joints and Joint Replacement,

Emerson, R. H. & Potter, T., (1985). The Use of the McKeever Metallic Hemiarthroplasty for Unicompartmental Arthritis. *Journal of Bone and Joint Surgery-American Volume,* 67A, 208-212.

Fairbank, T. J., (1948). Knee joint changes after meniscectomy. *J Bone Joint Surg Br,* 30-B, 664-670.

Falez, F. & Sciarretta, F. V., (2005). Treatment of osteochondral symptomatic defects of the knee with salucartilage. *J Bone Joint Surg,* 87-B, 202.

Filidoro, L., Dietrich, O., Weber, J., Rauch, E., Oerther, T., Wick, M., Reiser, M. F. & Glaser, C., (2005). High-resolution diffusion tensor imaging of human patellar cartilage: Feasibility and preliminary findings. *Magnetic Resonance in Medicine,* 53, 993-998.

Forsey, R. W., Fisher, J., Thompson, J., Stone, M. H., Bell, C. & Ingham, E., (2006). The effect of hyaluronic acid and phospholipid based lubricants on friction within a human cartilage damage model. *Biomaterials,* 27, 4581-4590.

Forster, H. & Fisher, J., (1996). The influence of loading time and lubricant on the friction of articular cartilage. *Proc. Inst. Mech. Eng.,* 210, 109-119.

Forster, H. & Fisher, J., (1999). The influence of continuous sliding and subsequent surface wear on the friction of articular cartilage. *Proc. Inst. Mech. Eng.,* 213, 329-345.

Freeman, M. E., Furey, M. J., Love, B. J. & Hamptom, J. M., (2000). Friction, wear and lubrication of hydrogels as synthetic articular cartilage. *Wear,* 241, 129-135.

Gong, J. P. & Osada, Y., (2002). Surface friction of polymer gels. *Progress in Polymer Science,* 27, 3-38.

Grad, S., Lee, R., Gorna, K., Gogolewski, S. & Wimmer, M. A., (2005). Surface motion upregulates superficial zone protein and hyaluronan production in chondrocyte seeded three-dimensional scaffolds. *Tissue Engineering* 11, 249-258.

Graindorge, S., Ferrandez, W., Ingham, E., Jin, Z., Twigg, P. & Fisher, J., (2006). The role of the surface amorphous layer of articular cartilage in joint lubrication. *Proc Inst Mech Eng [H],* 220, 597-607.

Graindorge, S., Ferrandez, W., Jin, Z., Ingham, E. & Fisher, J., (2005). The natural synovial joint: a finite element investigation of biphasic surface amorphous layer lubrication under dynamic loading conditions. *Proc Inst Mech Eng [J]: Engineering Tribology,* 220, 671-681.

Graindorge, S. & Stachowiak, G. W., (2000). Changes occurring in the surface morphology of articular cartilage during wear. *Wear,* 24, 143-150.

Gross, A. E., (2003). Cartilage resurfacing: filling defects. *J Arthroplasty,* 18, 14-7.

Gu, W. Y., Lai, W. M. & Mow, V. C., (1993). Transport of fluid and ions through a porous-permeable charged-hydrated tissue and streaming potential data on normal bovine articular cartilage. *J Biomech,* 26, 709-723.

Hallock, R. H. & Fell, B. M., (2003). Unicompartmental Tibial Hemiarthroplasty. Early Results of the Unispacer(TM) Knee. *Clinical Orthopaedics and Related Research,* 416, 154-163.

Hangody, L., Feczko, P., Bartha, L., Bodo, G. & Kish, G., (2001). Mosaicplasty for the treatment of articular defects of the knee and ankle. *Clinical Orthopaedics and Related Research,* S328-S336.

Hardingham, T. E., Muir, H., Kwan, M. K., Lai, W. M. & Mow, V. C., (1987). Viscoelastic properties of proteoglycan solutions with varying proportions present as aggregates. *J Orthop Res,* 5, 36-46.

Hashimoto, S., Ochs, R. L., Komiya, S. & Lotz, M., (1998). Chondrocyte-derived apoptotic bodies and calcification of articular cartilage. *Prot. Natl. Acad. Sci. USA,* 95, 3094-3099.

Hayes, W. C. & Mockros, L. F., (1971). Viscoelastic properties of human articular cartilage. *Journal of Applied Physiology,* 31, 562-568.

Helmer, K. G., Nair, G., Cannella, M. & Grigg, P., (2006). Water movement in tendon in response to a repeated static tensile load using one-dimensional magnetic resonance imaging. *J Biomech Eng,* 128, 733-741.

Hickery, M. S., Bayliss, M. T., Dudhis, J., Lewthwaite, J. C., Edwards, J. C. & Pitsillides, A. A., (2003). Age-related changes in the response of human articular cartilage to 1L-1alpha and transforming growth factor-beta (TGF-beta): chondrocytes exhibit a diminished sensitivity to TGF-beta. *J. Biol. Chem.,* 278, 53063-53071.

Higginson, G. R. & Snaith, J. E., (1979). The mechanical stiffness of articular cartilage in confined oscillating compression. *Engineering in Medicine,* 8, 11-14.

Hills, B. A. & Butler, B. D., (1984). Surfactants identified in synovial fluid and their ability to act as boundary lubricants. *Ann Rheum Dis,* 43, 641-648.

Hills, B. A. & Crawford, R. W., (2003). Normal and prosthetic synovial joints are lubricated by surface-active phospholipids. *J. Arthro,* 18, 499-505.

Holmes, M. H., Lai, W. M. & Mow, V. C., (1985). Singular Perturbation Analysis of the Nonlinear, Flow-Dependent Compressive Stress-Relaxation Behavior of Articular-Cartilage. *Journal of Biomechanical Engineering-Transactions of the Asme,* 107, 206-218.

Honner, R. & Thompson, R. C., (1971). Nutritional Pathways of Articular Cartilage - Autoradiographic Study in Rabbits Using S-35 Injected Intravenously. *J Bone Joint Surg Am,* A 53, 742-&.

Hoshino, A. & Wallace, W. A., (1987). Impact-Absorbing Properties of the Human Knee. *J Bone Joint Surg Br,* 69, 807-811.

Ihn, J. C., Kim, S. J. & Park, I. H., (1993). In-Vitro Study of Contact Area and Pressure Distribution in the Human Knee after Partial and Total Meniscectomy. *International Orthopaedics,* 17, 214-218.

Jay, G. D., (1992). Characterization of a Bovine Synovial-Fluid Lubricating Factor .1. Chemical, Surface-Activity and Lubricating Properties. *Connective Tissue Research,* 28, 71-88.

Jin, Z. M., Dowson, D., Fisher, J., Ohtsuki, N., Murakami, T., Higaki, H. & Moriyama, S., (1998). Prediction of transient lubricating film thickness in knee prostheses with compliant layers. *Proc Inst Mech Eng [H]: Engineering in Medicine,* 212, 157-164.

Jin, Z. M., Pickard, J. E., Forster, H., Ingham, E. & Fisher, J., (2000). Frictional behaviour of bovine articular cartilage. *Biorheology,* 37, 57-63.

Johnson, G. R., Dowson, D. & Wright, V., (1977). The elastic behaviour of articular cartilage under sinusoidally varying compressive stress. *International Journal of Mechanical Sciences,* 19, 301-308.

Johnson, R. J., Kettelka.Db, Clark, W. & Leaverto.P, (1974). Factors Affecting Late Results after Meniscectomy. *J Bone Joint Surg Am,* A 56, 719-729.

Jurvelin, J. S., Muller, D. J., Wong, M., Studer, D., Engel, A. & Hunziker, E. B., (1996). Surface and subsurface morphology of bovine humeral articular cartilage as assessed by atomic force and transmission electron microscopy. *J Struct Biol,* 117, 45-54.

Katta, J., Jin, Z., Ingham, E. & Fisher, J. (2008a) Chondroitin Sulphate - an effective joint lubricant? *16th Congress of European Society of Biomechanics.*

Katta, J., Jin, Z. M., Ingham, E. & Fisher, J., (2008b). Effect of nominal stress on the long term friction, deformation and wear of native and glycosaminoglycan deficient articular cartilage. *Osteoarthritis and Cartilage,* doi:10.1016/j.joca.2008.20.008.

Katta, J., Jin, Z. M., Ingham, E. & Fisher, J. (2008c) Friction and Wear of Native and GAG Deficient Articular Cartilage. *World Congress of Biomaterials.* Amsterdam.

Katta, J., Pawaskar, S. S., Jin, Z. M., Ingham, E. & Fisher, J., (2007). Effect of load variation on the friction properties of articular cartilage. *Proc Inst Mech Eng [J]: Engineering Tribology,* 221, 175-181.

Katta, J., Stapleton, T., Ingham, E., Jin, Z. M. & Fisher, J., (2008d). The effect of glycosaminoglycan depletion on the friction and deformation of articular cartilage. *Proc Inst Mech Eng [H]: Engineering in Medicine,* 222, 1-11.

Kawalec, J. S., Hetherington, V. J., Melillo, T. C. & Corbin, N., (1998). Evaluation of fibrocartilage regeneration and bone response at full-thickness cartilage defects in articulation with pyrolytic carbon or cobalt-chrome alloy hemiarthroplasties. *J Biomed Material Res,* 41, 534-540.

Kawamura, S., Lotito, K. & Rodeo, S. A., (2003). Biomechanics and healing response of the meniscus. *Operative Techniques in Sports Medicine,* 11, 68-76.

Kettlekamp, D. B. & Jacobs, A. W., (1972). Tibiofemoral contact areas - determination and implications. *J Bone Joint Surg Am,* 54, 349-356.

King, D., (1936). The function of semilunar cartilages. *Journal of Bone and Joint Surgery,* 18, 1069-1076.

Klompmaker, J., Jansen, H. W., Veth, R. P., Nielsen, H. K., Degroot, J. H., Pennings, A. J. & Kuijer, R., (1992). Meniscal repair by fibrocartilage? An experimental study in the dog. *J Orthop Res,* 10, 359-370.

Kobayashi, S., Yonekubo, S. & Kurogouchi, Y., (1995). Cryoscanning Electron-Microscopic Study of the Surface Amorphous Layer of Articular-Cartilage. *Journal of Anatomy,* 187, 429-444.

Kobayashi, S., Yonekubo, S. & Kurogouchi, Y., (1996). Cryoscanning electron microscopy of loaded articular cartilage with special reference to the surface amorphous layer. *Journal of Anatomy,* 188, 311-322.

Kohn, D., Wirth, C. J., Reiss, G., Plitz, W., Maschek, H., Erhardt, W. & Wulker, N., (1992). Medial meniscus replacement by a tendon autograft. Experiments in sheep. *J Bone Joint Surg Br,* 74, 910-917.

Krause, W. R., Pope, M. H. & Johnson, R. J., (1976). Mechanical changes in the knee after meniscectomy. *J. Bone Joint Surg,* 58A, 599-604.

Krishnan, R., Caligaris, M., Mauck, R. L., Hung, C. T., Costa, K. D. & Ateshian, G. A., (2004a). Removal of the superficial zone of bovine articular cartilage does not increase its frictional coefficient. *Osteoarthritis and Cartilage,* 12, 947-955.

Krishnan, R., Kopacz, M. & Ateshian, G. A., (2004b). Experimental verification of the role of interstitial fluid pressurization in cartilage lubrication. *J Orthop Res,* 22, 565-570.

Krishnan, R., Mariner, E. N. & Ateshian, G. A., (2005). Effect of dynamic loading on the frictional response of bovine articular cartilage. *J Biomech,* 38, 1665-1673.

Kumar, P., Oka, M., Toguchida, J., Kobayashi, M., Uchida, E., Nakamura, T. & Tanaka, K., (2001). Role of uppermost superficial surface layer of articular cartilage in the lubrication mechanism of joints. *Journal of Anatomy,* 199, 241-250.

Kwan, M. K., Wayne, J. S., Woo, S. L. Y., Field, F. P., Hoover, J. & Meyers, M., (1989). Histological and Biomechanical Assessment of Articular-Cartilage from Stored Osteochondral Shell Allografts. *J Orthop Res,* 7, 637-644.

Lai, W. M., Hou, J. S. & Mow, V. C., (1989a). Applicaton of triphasic theory to the study of transient behaviour of cartilage. *Adv. Bioeng. Trans.,* 15, 101-102.

Lai, W. M., Hou, J. S. & Mow, V. C., (1989b). Triphasic theory for articular cartilage swelling. *Proc. Biomech. Symp. Trans,* 98, 33-36.

Lai, W. M., Hou, J. S. & Mow, V. C., (1991). A triphasic theory for the swelling and deformation behaviours of articular cartilage. *Journal of Biomech. Eng.,* 113, 245-258.

Lai, W. M., Mow, V. C. & Roth, V., (1981). Effects of non-linear strain-dependent permeability and rate of compression on the stress behaviour of articular cartilage. *J Biomech. Eng.,* 103, 61-66.

Lange, J., Follack, N., Nowotny, T. & Merk, H., (2006). Results of SaluCartilage implantation for stage IV chondral defects in knee joint area. *Unfallchirurg,* 109, 193-199.

Lewis, P. R. & Mccutchen, C. W., (1959). Experimental Evidence for Weeping Lubrication in Mammalian Joints. *Nature,* 184, 1285.

Lipiello, L., Kaye, C., Neumata, T. & Mankin, H., (1985). *In Virto* metabolic response of articular cartilage segments to low levels of hydrostatic pressure. *Connective Tissue Response,* 13, 99-107.

Lipshitz, H., Etheredge, R. & Glimcher, M. J., (1975). *In Vitro* Wear of Articular-Cartilage. 1. Hydroxyproline, Hexosamine, and Amino-Acid Composition of Bovine Articular Cartilage as a Function of Depth from Surface; Hydroxyproline Content of Lubricant and Wear Debris as a Measure of Wear. *J Bone Joint Surg Am,* A 57, 527-534.

Lu, X. L., Sun, D. D. N., Guo, X. E., Chen, F. H., Lai, W. M. & Mow, V. C., (2004). Indentation determined mechanoelectrochemical properties and fixed charge density of articular cartilage. *Annals of Biomedical Engineering,* 32, 370-379.

Malinin, T. & Ouellette, E. A., (2000). Articular cartilage nutrition is mediated by subchondral bone: a long-term autograft study in baboons. *Osteoarthritis and Cartilage,* 8, 483-491.

Mankin, H. J. & Thrasher, A. Z., (1975). Water-Content and Binding in Normal and Osteoarthritic Human Cartilage. *J Bone Joint Surg Am,* A 57, 76-80.

Mazzucco, D., Scott, R. & Spector, M., (2004). Composition of joint fluid in patients undergoing total knee replacement and revision arthroplasty: correlation with flow properties. *Biomaterials,* 25, 4433-4445.

Mcalindon, T. E., Lavalley, M. P., Gulin, J. P. & Felson, D. T., (2000). Glucosamine and chondroitin for treatment of osteoarthritis - A systematic quality assessment and meta-analysis. *Jama-Journal of the American Medical Association,* 283, 1469-1475.

Mccutchen, C. W., (1959). Mechanism of animal joints: Sponge-hydrostatic and weeping bearings. *Nature,* 184, 1284-1285.

Mccutchen, C. W., (1962). The frictional properties of animal joints. *Wear,* 5, 1-17.

Mcdermott, I. D., Sharifi, F., Bull, A. M. J., Gupte, C. M., Thomas, R. W. & Amis, A. A., (2006). The consequences of meniscectomy. *J Bone Joint Surg Br,* 88-B, 1549-1556.

Mcgloughlin, T. M. & Kavanagh, A. G., (2000). Wear of ultra-high molecular weight polyethylene (UHMWPE) in total knee prostheses: a review of key influences. *Proc Inst Mech Eng [H]: Engineering in Medicine,* 214, 349-359.

Mckibbin, B. & Holdsworth, F. W., (1966). The Nutrition of Immature Joint Cartilage in the Lamb. *J Bone Joint Surg,* 48, 793-803.

Mcrobbie, D. W., Moore, E. A., Graves, M. J. & Prince, M. R., (2003). MRI From Picture to Proton, Cambridge University Press, Cambridge

Meder, R., De Visser, S. K., Bowden, J. C., Bostrom, T. & Pope, J. M., (2006). Diffusion tensor imaging of articular cartilage as a measure of tissue microstructure. *Osteoarthritis and Cartilage,* 14, 875-881.

Medley, J. B., Dowson, D. & Wright, V., (1984). Transient elastohydrodynamic lubrication models for the human ankle joint. *Engineering in Medicine,* 13, 137-151.

Meyer, C., Horas, U., Horbelt, R. & Schnettler, R., (2005). Dislocation of artificial cartilage (SaluCartilage). *Unfallchirurg,* 108, 163-6.

Minas, T. & Nehrer, S., (1997). Current concepts in the treatment of articular cartilage defects. *Orthopedics,* 20, 525-38.

Morita, Y., Tomita, N., Aoki, H., Sonobe, M., Wakitani, S., Tamada, Y., Suguro, T. & Ikeuchi, K., (2006). Frictional properties of regenerated cartilage in vitro. *J Biomech,* 39, 103-109.

Mosher, T. J. & Dardzinski, B. J., (2004). Cartilage MRI T2 relaxation time mapping: overview and applications. *Semin Musculoskelet Radiol,* 8, 355-368.

Mow, V. C. & Ateshian, G. A., (1997). Friction, lubrication and wear of diarthrodial joints. In: MOW, V. C. & HAYES, W. C. (Eds.) *Basic Orthopaedic Biomechanics.* New York, Raven press.

Mow, V. C., Gibbs, M. C., Lai, W. M., Zhu, W. B. & Athanasiou, K. A., (1989a). Biphasic indentation of articular cartilage-Part II. A numerical algorithm and an experimental study. *J Biomech,* 22, 853-861.

Mow, V. C., Gu, W. Y. & Chen, F. H., (2005). Structure and Function of Articular Cartilage and Meniscus. In: MOW, V. C. & HUISKES, R. (Eds.) *Basic Orthopaedic Biomechanics and Mechano-Biology.* 3rd ed. Philadelphia, Lippincott Williams and Wilkins.

Mow, V. C. & Hayes, W. C., (1997). Basic Orthopaedic Biomechanics., Lippincott-Raven,

Mow, V. C., Holmes, M. H. & Lai, W. M., (1984b). Fluid transport and mechanical properties of articular cartilage: a review. *J Biomech,* 17, 377-394.

Mow, V. C., Hou, J. S., Owens, J. M. & Ratcliffe, A., (1990). Biphasic and Quasilinear Viscoelastic Theories for Hydrated Soft Tissues. In: MOW, V. C., RATCLIFFE, A. & WOO, S. L.-Y. (Eds.) *Biomechanics of Diarthrodial Joints. Volume 1.* New York, Springer-Verlag.

Mow, V. C., Kuei, S. C. & Lai, W. M., (1980). Biphasic creep and stress relaxation of articular cartilage in compression: theory and experiments. *J. Biomech. Eng.,* 102, 73-84.

Mow, V. C., Mak, A. F., Lai, W. M., Rosenberg, L. C. & Tang, L. H., (1984a). Viscoelastic properties of proteoglycan subunits and aggregates in varying solution concentrations. *J Biomech,* 17, 325-338.

Mow, V. C., Ratcliffe, A. & Poole, A. R., (1992). Cartilage and diarthrodial joints as paradigms for hierarchial materials adn structures. *Biomaterials,* 13, 67-97.

Mow, V. C., Zhu, W., Lai, W. M., Hardingham, T. E., Hughes, C. & Muir, H., (1989b). The influence of link protein stabilization on the viscometric properties of proteoglycan aggregate solutions. *Biochim Biophys Acta,* 992, 201-208.

Murray, D. W., Goodfellow, J. W. & O'connor, J. J., (1998). Ten year survivorship study of Oxford medial unicompartmental arthroplasty. *J. Bone Joint Surg,* 80B, 983-989.

Nagura, T., O'dyrby, C., Alexander, E. J. & Andriacchi, T. P. (2001) Mechanical Loads on the Knee Joint During Deep Flexion. *Bioengineering Conference ASME 2001.*

Newman, A. P., (1998). Articular cartilage repair. *American Journal of Sports Medicine,* 26, 309-324.

Newman, J. H., (2000). Unicompartmental knee replacement. *The Knee,* 7, 63-70.

Newman, J. H., Ackroyd, C. E. & Shah, N. S., (1998). Unicompartmental or total knee replacement? The 5 year results of a prospective randomised trial of 102 osteoarthritic knees with unicompartmental arthritis. *J. Bone Joint Surg,* 80B, 862-865.

Nieminen, M. T., Toyras, J., Laasanen, M. S., Silvennoinen, J., Helminen, H. J. & Jurvelin, J. S., (2004). Prediction of biomechanical properties of articular cartilage with quantitative magnetic resonance imaging. *J Biomech,* 37, 321-328.

Nissi, M. J., Toyras, J., Laasanen, M. S., Rieppo, J., Saarakkala, S., Lappalainen, R., Jurvelin, J. S. & Nieminen, M. T., (2004). Proteoglycan and collagen sensitive MRI evaluation of normal and degenerated articular cartilage. *Journal of Orthopaedic Research,* 22, 557-564.

Noguchi, T., Yamamuro, T., Oka, M., Kotoura, Y., Hyon, S. H. & Ikada, Y., (1991). Poly(vinyl alcohol) hydrogel as an artificial articular cartilage: Evaluation of biocompatibility. *J. Appl. Biomater,* 2, 101-107.

Nordin, M. & Frankel, V. H., (2001). Basic Biomechanics of the Musculoskeletal system, Lippincott Williams & Wilkins, Philadelphia

Northwood, E. & Fisher, J., (2007). A multi-directional in vitro investigation into friction, damage and wear of innovative chondroplasty materials against articular cartilage. *J Clin Biomech,* 22, 834-842.

Northwood, E., Fisher, J. & Kowalski, R., (2007). Investigation of the friction and surface degradation of innovative chondroplasty materials against articular cartilage. *Proc Inst Mech Eng [H]: Engineering in Medicine,* 221, 263-279.

Northwood, E. J. (2007) Cartilage wear simulation models for surface and spacer hemiarthroplasty and tissue engineering. *School of Mechanical Engineering.* University of Leeds.

Oka, M., Ushio, K., Kumar, P., Ikeuchi, K., Hyon, S.-H., Nakamura, T. & Fujita, H., (2000). Development of artificial articular cartilage. *Instn Mech Engrs,* 214, 59-68.

Ozkaya, N. & Nordin, M., (1999). Fundamentals of biomechanics: equilibrium, motion and deformation, Springer, New York

Park, S., Costa, K. D. & Ateshian, G. A., (2004). Microscale frictional response of bovine articular cartilage from atomic force microscopy. *J Biomech,* 37, 1679-1687.

Park, S., Krishnan, R., Nicoll, S. B. & Ateshian, G. A., (2003). Cartilage interstitial fluid load support in unconfined compression. *J Biomech,* 36, 1785-1796.

Pawaskar, S. S. (2006) Contact mechanics modelling of articular cartilage and applications. *Institute of Medical and Biological Engineering, School of Mechanical Engineering.* Leeds, University of Leeds.

Pickard, J. E., Fisher, J., Ingham, E. & Egan, J., (1998a). Investigation into the effects of proteins and lipids on the frictional properties of articular cartilage. *Biomaterials,* 19, 1807-1812.

Pickard, J. E., Ingham, E., Egan, J. & Fisher, J., (1998b). Investigation into the effect of proteoglycan molecules on the tribological properties of cartilage joint tissues. *Proc Inst Mech Eng [H]: Engineering in Medicine,* 212, 177-182.

Pinals, R. S., (1992). Pharmacologic treatment of osteoarthritis. *Clinical Therarpy,* 14, 336-346.

Plainfosse, M., Hatton, P. V., Crawford, A., Jin, Z. M. & Fisher, J., (2007). Influence of the extracellular matrix on the frictional properties of tissue-engineered cartilage. *Biochem Soc Trans,* 35, 677-679.

Poole, C. A., Flint, M. H. & Beaumont, B. W., (1987). Chondrons in Cartilage - Ultrastructural Analysis of the Pericellular Microenvironment in Adult Human Articular Cartilages. *Journal of Orthopaedic Research,* 5, 509-522.

Proctor, C. S., Schmidt, M. B., Whipple, R. R., Kelly, M. A. & Mow, V. C., (1989). Material Properties of the Normal Medial Bovine Meniscus. *J Orthop Res,* 7, 771-782.

Radin, E. I., Swann, D. A. & Weisser, P. A., (1970). Separation of hyaluronate-free lubricating fraction from synovial fluid. *Nature,* 228.

Reinholz, G. G., Lu, L., Saris, D. B. F., Yaszemski, M. J. & O'driscoll, S. W., (2004). Animal models for cartilage reconstruction. *Biomaterials,* 25, 1511-1521.

Sarzi-Puttini, P., Cimmino, M. A., Scarpa, R., Caporali, R., Parazzini, F. & Zaninelli, A., (2005). Osteoarthritis: An overview of the disease and its treatment strategies. *Seminars in Arthritis and Rheumatism,* 35, 1-10.

Sasada, T., (2000). Lubrication of Human Joints. Nature of Joint Friction and "Surface Gel Hydration Lubrication". *Proc Ann Meeting Jap Soc Orthop Biomech,* 21, 17-22.

Sawae, Y., Matsumoto, K., Hor, M. & Murakami, T., (2000). Surface layer of articular cartilage observed by atomic force microscopy in liquid. Morphology and role in joint lubrication. *Proc Ann Meeting Jap Soc Orthop Biomech,* 21, 7-12.

Schmidt, B. M., Mow, V. C., Chun, L. E. & Eyre, D. R., (2005). Effects of proteoglycan extraction on the tensile behaviour of articular cartilage. *Journal of Orthopaedic Research,* 8, 353-363.

Schwarz, I. M. & Hills, B. A., (1998). Surface-active phospholipid as the lubricating component of lubricin. *Br. J. Rheum,* 37, 21-26.

Scott, R., Joyce, M. J., Ewald, F. C. & Thomas, W. H., (1985). McKeever metallic hemiarthroplasty of the knee in unicompartmental degenerative arthritis. Long-term clinical follow up and current indications. *J Bone Joint Surg,* 67, 203-207.

Seedhom, B. B., Dowson, D. & Wright, V., (1974). Functions of the menisci – a preliminary study. *J Bone Joint Surg Br,* 56-B, 381-387.

Seedhom, B. B. & Hargreaves, D. J., (1979a). Transmission of load in the knee joint with special reference to the role of the meniscus: part II. Experimental results, discussions and conclusions. *Engineering in Medicine,* 1979, 220-228.

Seedhom, B. B. & Hargreaves, D. J., (1979b). Transmission of the load in the knee joint with special reference to the role of the menisci Part II: experimental results, discussion and conclusions. *Engineering in Medicine,* 8, 220-228.

Simon, W. H., (1970). Scale Effects in Animal Joints. I. Articular Cartilage Thickness and Compressive Stress. *Arthritis and Rheum,* 13, 244-255.

Sisto, D. J. & Mitchell, I. L., (2005). Unispacer arthroplasty of the knee. *J Bone Joint Surg,* 87, 1706-1711.

Smith, G. D., Knutsen, G. & Richardson, J. B., (2005). A clinical review of cartilage repair techniques. *J Bone Joint Surg,* 87-B, 445-449.

Sokal, R. & Rohlf, J., (2005). Biometry, New York: W.H. Freeman

Sokoloff, L., (1969). Elasticity of Aging Cartilage. *Fed. Proc.,* 25, 1089-1095.

Soltz, M. A. & Ateshian, G. A., (1998). Experimental verification and theoretical prediction of cartilage interstitial fluid pressurization at an impermeable contact interface in confined compression. *J Biomech,* 31, 927-934.

Springer, B. D., Scott, R. D., Sah, A. P. & Carrington, R., (2006). McKeever hemiarthroplasty of the knee in patients less than sixty years old. *J Bone Joint Surg Am,* 88A, 366-371.

Stachowiak, G. P., Stachowiak, G. W. & Podsiadlo, P., (2006). Automated classification of articular cartilage surfaces based on surface texture. *Proc Inst Mech Eng [H]: Engineering in Medicine,* 220.

Stachowiak, G. W., Batchelor, A. W. & Griffiths, L. J., (1994). Friction and wear changes in synovial joints. *Wear,* 171, 135-142.

Stammen, J. A., Williams, S., Ku, D. N. & Guldberg, R. E., (2001). Mechanical properties of a novel PVA hydrogel in shear and unconfined compression. *Biomaterials,* 22, 799-806.

Swann, A. C. & Seedhom, B. B., (1989). Improved techniques for measuring the indentation and thickness of articular cartilage. *Proc Inst Mech Eng [H],* 203, 143-150.

Swann, D. A., Bloch, K. J., Swindell, D. & Shore, E., (1984). The Lubricating Activity of Human Synovial-Fluids. *Arthritis and Rheumatism,* 27, 552-556.

Swann, D. A., Hendren, R. B., Radin, E. L., Sotmann, S. L. & Duda, E. A., (1981). The lubricating activity of synovial fluid glycoproteins. *Arthritis and Rheum.,* 24, 22-30.

Swann, D. A., Silver, F. H., Slayter, H. S., Stafford, W. & Shore, E., (1985). The Molecular-Structure and Lubricating Activity of Lubricin Isolated from Bovine and Human Synovial-Fluids. *Biochemical Journal,* 225, 195-201.

Swieszkowski, W., Ku, D. N., Bersee, E. N. & Kurzydlowski, K. J., (2006). An elastic material for cartilage replacement in an arthritic shoulder joint. *Biomaterials,* 27, 1534-1541.

Szomor, Z. L., Martin, T. E., Bonar, F. & Murrell, G. A. C., (2000). The protective effects of meniscal transplantation on cartilage - An experimental study in sheep. *J Bone Joint Surg Am,* 82A, 80-88.

Temenoff, J. S. & Mikos, A. G., (2000). Review: tissue engineering for regeneration of articular cartilage. *Biomaterials,* 21, 431-440.

Trattnig, S., Mlynarik, V., Breitenseher, M., Huber, M., Zembsch, A., Rand, T. & Imhof, H., (1999). MRI visualization of proteoglycan depletion in articular cartilage via intravenous administration of Gd-DTPA. *Magnetic Resonance Imaging,* 17, 577-583.

Ushio, K., Oka, M., Hyon, S.-H., Yura, S., Toguchida, J. & Nakamura, T., (2003). Partial hemiarthroplasty for the treatment of osteonecrosis of the femoral head. An experimental study in the dog. *J. Bone Joint Surg,* 85-B, 922-930.

Waldman, S. D., Spiteri, C. G., Grynpas, M. D., Pilliar, R. M., Hong, J. & Kandel, R. A., (2003). Effect of Biomechanical conditioning on cartilaginous tissue formation in vitro. *J Bone Joint Surg Am,* 85, 101-105.

Walker, P. S. & Erkman, M. J., (1975). The role of the menisci in force transmission across the knee. *Clin Orthop Rel Res,* 109, 184-192.

Wang, A., Essner, A., Polineni, V. K., Stark, C. & Dumbleton, J. H., (1998). Lubrication and wear of ultra-high molecular weight polyethylene in total joint replacements. *Tribology International,* 31, 17-33.

Weightman, B., Freeman, M. A. R. & Swanson, S. A. V., (1973). Fatigue of Articular-Cartilage. *Nature,* 244, 303-304.

Woo, S. L.-Y. & Buckwalter, J. A. (1988) Injury and repair of the musculoskeletal soft tissues. *AAOS.* Illinois.

Woo, S. L., Simon, B. R., Kuei, S. C. & Akeson, W. H., (1980). Quasi-linear viscoelastic properties of normal articular cartilage. *J Biomech Eng,* 102, 85-90.

Wu, J. Z. & Herzog, W., (2002). Simulating the swelling and deformation behaviour in soft tissues using a convective thermal analogy. *Biomedical Engineering Online,* 1.

Zhu, W., Lai, W. M. & Mow, V. C., (1991). The density and strength of proteoglycan-proteoglycan interaction sites in concentrated solutions. *J Biomech,* 24, 1007-1018.

Zhu, W., Mow, V. C., Koob, T. J. & Eyre, D. R., (1993). Viscoelastic shear properties of articular cartilage and the effects of glycosidase treatments. *J Orthop Res,* 11, 771-781.